Design, Synthesis and Application of Novel Light-Activated Molecular Probes

DPhil Dissertation

Megan N. Stanton-Humphreys

Supervisor: Dr Stuart Conway

St Hugh's College

University Of Oxford

Design, Synthesis and Application of Novel Light-Activated Molecular Probes

Megan N. Stanton-Humphreys, Supervisor: Dr Stuart Conway

St Hughs College, University Of Oxford

Submitted for DPhil degree, Michaelmas 2010

Caged compounds are biologically active molecules that are rendered inert by masking an important functionality with a photolabile protecting, 'caging', group. The caging group can be removed by irradiation with light to reveal the active compound with restored pharmacological activity with high spatial and temporal control. This technology provides an ideal tool for the study of many chemical, physiological and biological systems.

This DPhil dissertation highlights several projects in which caging technology has been employed to address biological problems and questions. The first example of spatially controlled mitochondrial inactivation is reported - a tool for the study of the role of mitochondria in Ca^{2+} signalling. Caged TRPV1 agonists and antagonists have been developed to probe TRPV1, specifically the location of the agonist-binding site. T cell activation has been controlled with light as a tool to gain insight into the adaptive immune response. Caged sodium channel blockers have been investigated. Wavelength-orthogonal photolysis in a neuronal system has been demonstrated using the neurotransmitters glutamate and GABA - this represents a significant advancement in caging technology. This dissertation also includes investigations into the development of novel caging groups.

Declarations

I, Megan Stanton-Humphreys, hereby certify that this thesis, which is approximately 71 400 words in length, has been written by me, that it is the record of work carried out by me and that it has not been submitted in any previous application for a higher degree.

I was admitted as a research student in September 2007 and as a candidate for the degree of Doctor of Philosophy in October 2010; the higher study for which this is a record was carried out in the University of St Andrews in 2007, and the University of Oxford between 2008 and 2010.

Date Signature of candidate

I hereby certify that the candidate has fulfilled the conditions of the Regulations appropriate for the degree of Doctor of Philosophy in the University of Oxford and that the candidate is qualified to submit this thesis in application for that degree.

Date Signature of supervisor

In submitting this thesis to the University of Oxford we understand that we are giving permission for it to be made available for use in accordance with the regulations of the University Library for the time being in force, subject to any copyright vested in the work not being affected thereby. We also understand that the title and the abstract will be published, and that a copy of the work may be made and supplied to any *bona fide* library or research worker, that this thesis will be electronically accessible for personal or research use, and that the library has the right to migrate

this thesis into new electronic forms as required to ensure continued access to the thesis. We have obtained any third-party copyright permissions that may be required in order to allow such access and migration.

Acknowledgements

I would like to thank my supervisor, Dr Stuart Conway, for his direction and encouragement throughout my DPhil. I would like to thank him for always being available for questions, and being interested and enthusiastic about this project. I have learnt so much from him over the past three years.

Thank you to The Leverhulme Trust, which funded this project. Thank you to the University of St Andrews, St Hugh's College University of Oxford, The Overseas Research Scheme, the University of Oxford Chemistry Department and the Vice-Chancellors Fund for additional financial support.

Thank you to the analytical staff at the University of St Andrews, particularly Dr Tomas Lebl, Mrs Melanja Smith and Mrs Sylvia Williamson. Thank you to the analytical staff at the University of Oxford, particularly Miss Tina Jackson and Dr Barbara Odell.

It has been wonderful to collaborate with a number of research groups. Thank you to Dr Tom Brown, Dr Nigel Emptage, Prof. John McCarron, Dr Simon Milling, Prof. Leonard Khiroug and Prof. Rashid Giniatullin. Thank you to Craig McDougall for teaching me physics and enduring countless hours of photolysis experiments; and Dr Ruth Taylor for answering many biology questions.

I have really enjoyed working with a great group of chemists. Thanks to Tashfeen, our fabulous post-doc who helped me find my feet and patiently answered my questions and showed me how to work in a lab. Thanks to Neil for much chemistry advice. Huge thanks to Tom, who also made the trip down to Oxford, for making the lab as fun as it could be. Great to work with him despite his fumehood…

Thanks to the Fairbanks group who welcomed us into their lab at the University of Oxford. Thanks to Brendan, Tom, and the last man standing - Dan. I would not have learnt so much about the joy of cricket commentary without you! Thanks to John for all the tea and chats. Àine has been such a special friend over the past two years. I'm glad to have her as my fumehood neighbour. It was a pleasant surprise to work with Jess over the past year and I'm glad it will continue. I appreciate her support and friendship. Thanks to Kirsty for her company and friendship since the beginning, despite not working in the lab together for very long. Diane must be mentioned for introducing Lady Gaga to the lab. Thanks to Yulin for being my reliable stores partner.

I would like to thank my family for their confidence in me, and for their love and support. I miss them.

To Paul, my amazing husband who left everything in South Africa for me to pursue this DPhil. He is my best friend and biggest support. I want to sincerely thank him for his love, loyalty and ability to make me laugh.

Thank you to Jesus Christ, my Saviour and Lord. The more I learn about biological systems, the more I marvel at the complexity and beauty of what He has made. Thank you.

Psalm 19:1-4

The heavens declare the glory of God;
And the firmament shows His handiwork.
Day unto day utters speech,
And night unto night reveals knowledge.
There is no speech nor language
Where their voice is not heard.
Their line has gone out through all the earth,
And their words to the end of the world.

Table of Contents

List of Abbreviations

ADP	adenosine diphosphate
APC	allophycocyanin
ATP	adenosine triphosphate
BAPTA	1,2-bis(*o*-aminophenoxy)ethane-*N,N,N',N'*-tetraacetic acid
BCMACMOC	{7-[bis(carboxymethyl)amino]coumarin-4-yl}methoxycarbonyl
Bhc	6-bromo-4-diazomethyl-7-hydroxycoumarin
BHQ	8-bromo-7-hydroxyquinoline
c	concentration
C4MNB	α-carboxy-4-methoxy-2-nitrobenzyl
cAMP	cyclic adenosine monophosphate
CCCP	carbonyl cyanide 3-chlorophenylhydrazone
cDNA	complementary deoxyribonucleic acid
CDNI	4-carboxymethoxy-5,7-dinitroindolinyl
CFSE	carboxyfluorescein succinimidyl ester
cGMP	cyclic guanosine monophosphate
CNS	central nervous system
COSY	correlation spectroscopy
CPZN	capsazepine
DBU	1,8-diazabicyclo[5.4.0]undec-7-ene
DC	dendritic cell
DCC	*N,N'*-dicyclohexylcarbodiimide
DCU	dicyclohexylurea

DEACM	diethylaminocoumarin-4-yl
DIC	differential interference contrast
DIPEA	*N,N'*-diisopropylethylamine
DMAP	4-dimethylaminopyridine
DMF	*N,N*-dimethylformamide
DMNB	4,5-dimethoxynitrobenzyl
DMNPB	3-(4,5-dimethoxy-2-nitrophenyl)-2-butyl
DMPU	1,3-dimethyltetrahydro-2(1H)-pyrimidinone
DMNPE	4,5-dimethoxy-2-nitrophenyl
DNA	deoxyribonucleic acid
DNBOC	di(nitrobenzyl)oxycarbonyl
DNP	2,4-dinitrophenol
EDC·HCl	1-ethyl-3-(3-dimethylaminopropyl) carbodiimide hydrochloride
EDTA	ethylenediaminetetraacetic acid
EGTA	ethyleneglycoltetraacetic acid
EPSC	excitatory postsynaptic potential
ER	endoplasmic reticulum
ESPT	excited-state proton transfer
FCCP	carbonylcyanide 4-trifluromethoxy phenylhydrazone
FTIR	Fourier transform infrared spectroscopy
GC-MS	gas chromatography and mass spectrometry
Gfp	green fluorescent protein
GPCR	G-protein-coupled receptor
HBTU	*O*-benzotriazole-*N,N,N',N'*-tetramethyl-uronium-hexafluoro-

	phosphate
HMBC	heteronuclear multiple bond coherence
HOBT	hydroxybenzotriazole
HPA	4-hydroxyphenacyl
HSQC	hetronuclear single quantum coherence
IL	interleukin
InsP_3	*myo*-inositol 1,4,5-triphosphate
IPA	2-propanol
IR	infra red spectroscopy
ISC	intersystem crossing
KIE	kinetic isotope effect
LFP	laser flash photolysis
MCM	(7-methoxycoumarin-4-yl)methyl
MHC	major histocompatibility complex
MNI	methoxynitroindoline
MPA	4-methoxyphenacyl
NB	2-nitrobenzyl
NBOC	2-nitrobenzyloxycarbonyl
NBS	*N*-bromosuccinimide
NDBF	nitrodibenzofuran
N-DCAC	7-(dicarboxymethyl)-aminocoumarin
NMDA	N-methyl D-aspartate
NPE	1-(2-nitrophenyl)ethyl
NPEOC	2-(2-nitrophenyl)ethoxycarbonyl
NV	2-nitroveratryl

NVOC	6-nitroveratroyloxycarbonyl
OVA	ovalbumin
PG	protecting group
PIP2	phosphatidylinositol-4,5-bisphosphate
PM	propionyloxymethyl
rac	racemic
RNA	ribonucleic acid
ROC	receptor-operated channel
RT	room temperature
SOC	store-operated channel
TBABr	tetrabutylammonium bromide
TBAF	tetrabutylammonium fluoride
TBAI	tetrabutylammonium iodide
TBS	*tert*-butyldimethylsilane
TCR	T cell receptor
TEMPO	2,2,6,6-tetramethyl-piperidin-1-oxyl
TFA	trifluoroacetic acid
Th	T helper cell
THF	tetrahydrofuran
TIPS	triisopropylsilyl
TLC	thin layer chromatography
TMS	tetramethyl silane
VOC	voltage-operated channel
UV	ultraviolet
UV/Vis	ultraviolet and visable

Amino Acid Code

G	glycine	Gly
A	alanine	Ala
L	leucine	Leu
M	methionine	Met
F	phenylalanine	Phe
W	tryptophan	Trp
K	lysine	Lys
Q	glutamine	Gln
E	glutamic acid	Glu
S	serine	Ser
P	proline	Pro
V	valine	Val
I	isoleucine	Ile
C	cysteine	Cys
Y	tyrosine	Tyr
H	histidine	His
R	arginine	Arg
N	asparagine	Asn
D	aspartic acid	Asp
T	threonine	Thr

Chapter 1:

Introduction

1. Introduction

1.1. Background

The complexity and spatial and temporal organisation of biological systems provides a significant, often unmet, challenge to studying and understanding these systems. In order to study biological processes within individual cells and organisms, it is necessary that a particular aspect in a cell or organism can be manipulated selectively. Chemical and biochemical tools, such as inhibitors and activators, can be used to control intracellular pathways. Their influence on the action of cells and organisms can be observed in order to gain insight into cellular functioning. However, once the chemical tool enters the cell, control over its intracellular spatial distribution and duration of activity are lost.[1] A significant advancement in the study of biological systems has been the discovery and application of light-activated biologically significant molecules, whose activation can be spatiotemporally controlled. Since the first report of the photorelease of glycine from an inactive precursor by Barltrop *et al.*[2] in 1962, light-activated compounds have found numerous applications in biochemistry, cell biology, physiology and molecular biology.[3] This technology has employed light-activated signalling molecules and secondary messengers of every size, from Ca^{2+} to proteins.[3]

Covalently attaching a photolabile protecting group to the biologically active molecule of interest can render it temporarily inactive by masking the

functional group on the molecule that is responsible for its biological activity. This biologically inactive compound can be applied to the cell or organism of interest. Light can then be used as an external trigger to remove the photolabile protecting group and release the compound of interest, with restored biological activity, in a highly controlled manner.[3] Focused light allows for active compounds to be released with excellent spatial resolution (< 0.5 μm) and temporal control (μs to ms).[4] Therefore, photolabile protecting groups allow for the targeted, controlled, intracellular delivery of biologically active molecules in a non-disruptive manner, Figure 1.1. These 'light-activated' compounds are commonly referred to as 'caged' compounds. This term was coined by Hoffman and co-workers in a report describing the first synthesis of light-activated ATP and its application to the study of the Na^+-pump.[5] This terminology can be confusing as it suggests that the compound of interest is in a cage in the topological sense, such as inside a C_{60} molecule. However, this term has been used for over 30 years and is the one most commonly used in the literature in this field.

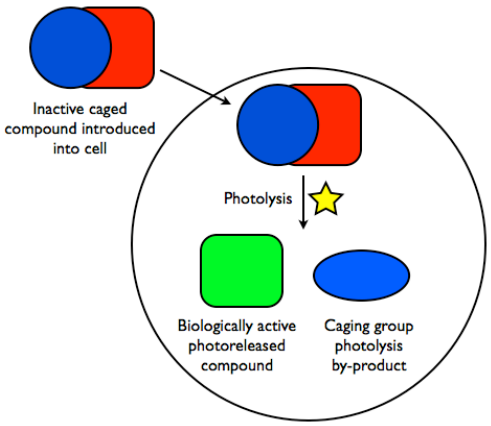

Figure 1.1. A cartoon representation of the photolysis of an inactive caged compound in a cell to release the biologically active compound of interest, now able to exert its affect on the cell, and the caging group photolysis by-product.

Photolabile protecting groups were first developed for use in organic synthesis. Barton[6] and Barltrop[2] conducted pioneering work in the use of light to evoke chemical reactions. These techniques possess many advantages over traditional chemical means. For example, additional chemical reagents are not required, resulting in photorelease being termed a 'traceless reagent process'.[7] This type of photodeprotection allows for the possibility of manipulating extremely sensitive molecules, which are incompatible with acids or bases - which would traditionally be used for deprotection steps.

By the 1970s, biologists had started to mention caged biologically active molecules. In 1977, Engels *et al.* synthesised a 2-nitrobenzyl-caged cyclic adenosine monophosphate (cAMP) derivative **1**, Figure 1.2.[8] This protection increased the membrane permeability of cAMP; the potential for light activation was not the main focus of the paper.[8] A year later, in 1978, Kaplan *et al.* reported the first synthesis and application of a biologically active caged

molecule. An adenosine triphosphate (ATP) derivative was caged with a 2-nitrobenzyl group **2**, Figure 1.2.[5] Kaplan *et al.* not only reported the synthesis of caged ATP, the application of this caged compound to a biological system was demonstrated. Na^+,K^+-ATPase, the enzyme responsible for active Na^+ and K^+ transport across membranes, was not able to hydrolyse the caged ATP **2**. However, upon irradiation photoreleased ATP was able to activate the pump. Early studies with caged ATP included observing single turnovers of the Na^+-pump.[9]

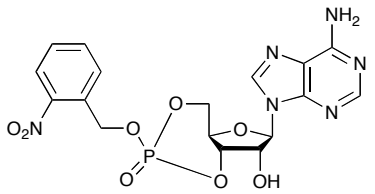

1

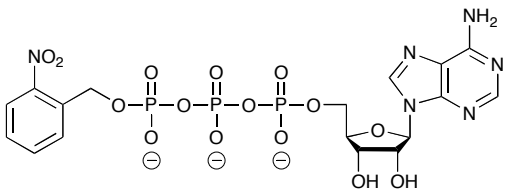

2

Figure 1.2. The first biologically significant caged compounds, a caged cyclic adenosine monophosphate (cAMP) derivative **1**[8] and a caged adenosine triphosphate (ATP) derivative **2**.[5]

1.2. Quantifying the Performance of Caged Compounds

Photolysis of a caged compound involves the absorption of a photon of light to form an excited, unstable intermediate species which is transformed to

generate the stable, photoreleased, biologically active compound. The absorbance of light by the caged compound; the probability that light absorption will result in photorelease; and the rate at which the excited intermediate is transformed to give the desired uncaged product, all contribute to the performance of a caged compound. These parameters are quantified by the extinction co-efficient (ε), quantum efficiency (Φ) and rate constant of photorelease (k_{rel}), respectively.[4]

The molar extinction co-efficient (ε) appears in Beer's Law ($A = \varepsilon.l.c$). It characterises the ability of a molecule to absorb a photon. Most caged compounds have ε between 10^3 and 10^4 $M^{-1}cm^{-1}$. The quantum efficiency (Φ) is the fraction of absorbed photons that result in photolysis. It is calculated as the ratio of the amount of product (uncaged) molecules formed to the amount of photons absorbed by the caged compound. It ranges from 0.01 to 0.2 for most caged compounds, which corresponds to 1% to 20% of absorbed photons triggering photorelease. The rate of photorelease is important for the study of fast biological responses such as receptor activation. The rate constant, k_{rel}, describes how rapidly the excited intermediate generates the uncaged, photoreleased product. It ranges from 10^2 to 10^7 sec^{-1} for most caged compounds. A larger value corresponds to more rapid photorelease.

1.3. The use of Caged Compounds in Biological Systems

The caged compound is delivered into the system under study using microinjection, membrane permeabilisation or perfusion from a patch pipette.

Photorelease of the biologically active molecule from its caged, inactive, form can be spatially and temporally confined so as to deliver the biologically active molecule in a specific location and concentration within a cellular environment. In order to employ a caged compound in a biological system, it must meet certain criteria. The following points have been adapted from Lester and Sheehan's criteria.[7,10] Both the caged compound and the caging group photolysis by-product must be biologically inert, at least for the timescale of the experiment. The caged compound, uncaged active compound and caging group photolysis by-product must be soluble in aqueous media at neutral pH. The caged compound must be stable to hydrolysis and enzymatic cleavage to ensure that any uncaging is exclusively as a result of photolysis of the caging group. Photolysis should ideally be clean, fast and occur with high quantum yield. Quantum yield (Φ) above 0.1 is desirable. For time-resolved work, the release rate of the biologically active compound must exceed that of the response investigated.[11] The excitation wavelength of the caged compound should be greater than 300 nm to prevent cellular damage due to high absorption of nucleotides and proteins in the wavelength region 250-300 nm. The caged compound should have a high extinction co-efficient (ε) at the excitation wavelength. The photolysis by-product should not absorb at the same wavelength as excitation to avoid acting as a light filter. The most commonly employed useful caging groups which meet most of these criteria are the 2-nitrobenzyl, benzoin and α-substituted acetophenone caging groups and their derivatives. These caging groups will be discussed in greater detail.

1.4. 2-Nitrobenzyl Caging Group

In 1966, Schofield and co-workers first reported the photorelease of benzoic acid from the 2-nitrobenzyl caging group, Scheme 1.1.[12] This work was conducted at the University of Oxford in the Dyson Perrins Laboratory. Only 17% benzoic acid **5** was obtained upon irradiation of the caged precursor **3**. This low yield was attributed to the reactivity of the photolysis by-product, nitrosobenzaldehyde **4**, which was converted into azobenzene-2,2'-dicarboxylic acid **6**. This chromophore acted as a light filter, competing with the caged compound for incident light. Phenyl α-substituted nitrobenzyl ester **7** yielded higher conversion to benzoic acid **5**, Scheme 1.1. This higher conversion was attributed to the reduced reactivity of the nitrosobenzophenone **8** photolysis by-product, so that a light-filtering azobenzene derivative was not observed.

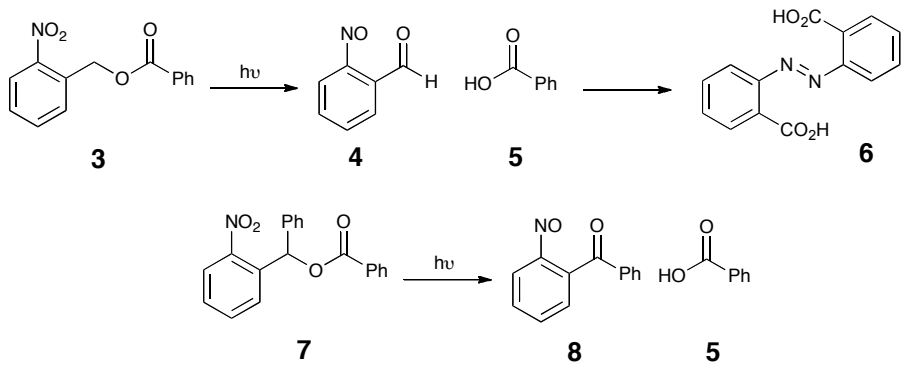

Scheme 1.1. Photorelease of benzoic acid **5** from the nitrobenzyl caged precursors. Photolysis of the nitrobenzyl ester **3** yielded benzoic acid **5** and nitrosobenzaldehyde **4**. Nitrosobenzaldehyde was subsequently converted into azobenzene-2,2'-dicarboxylic acid **6**, which competed with the caged precursor **3** for incident light. Photolysis of the phenyl α-substituted nitrobenzyl ester **7** yielded benzoic acid **5** and nitrosobenzophenone **8**.[12]

In the 1978 report by Hoffman and co-workers, inorganic phosphate and ATP were photoreleased from the 2-nitrobenzyl and α-substituted 1-(2-nitro)phenylethyl caging groups, Scheme 1.2.[5] The successful employment of a caged compound of biological significance in physiological medium opened the door for the application of caged compounds to a variety of biological systems.

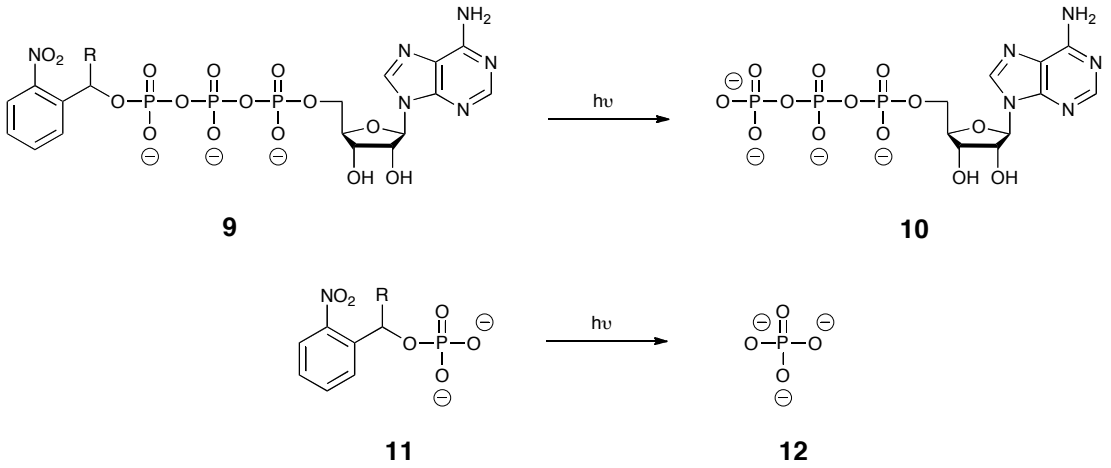

Scheme 1.2. Photorelease of ATP **10** and inorganic phosphate **12** from caged precursors (**9** and **11**). R = H, 2-nitrobenzyl caging group; R = CH_3, 1-(2-nitro)phenylethyl caging group.

A number of nitrobenzyl caging group derivatives have been developed, and used to cage carboxylic acids, alcohols and amines.[3,13] These include the 6-nitroveratroyloxycarbonyl (NVOC) **13**, nitrobenzyloxycarbonyl (NBOC) **14**, di(nitrobenzyl)oxycarbonyl (DNBOC) **15**, 4,5-dimethoxynitrobenzyl (DMNB) **16** and 2-nitrobenzyl (NB) groups, Figure 1.3. An interesting derivative, bis(2-nitrophenyl)ethanediol **17**, has been employed to cage ketones and aldehydes.[14] Methoxy substituents have been shown to increase the rate of photolysis of nitrobenzyl derivatives.[15] Photolysis yields the uncaged compound, nitrosobenzaldehyde and CO_2, if a carbonate linker is present.

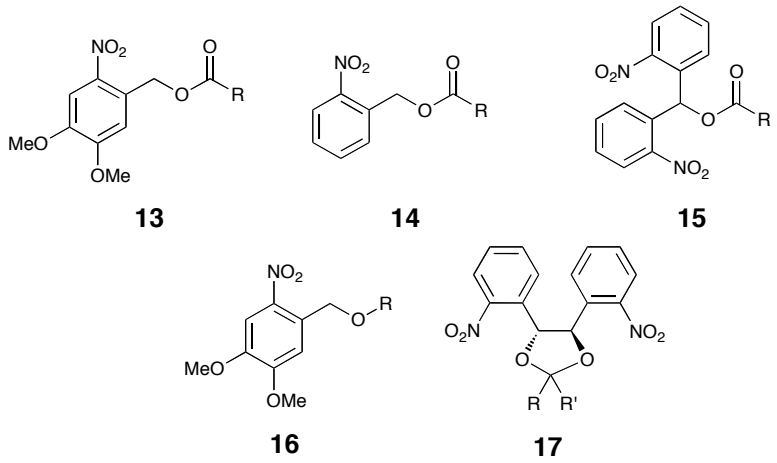

Figure 1.3. Derivatives of the 2-nitrobenzyl caging group include the 6-nitroveratroyloxycarbonyl (NVOC) **13**, nitrobenzyloxycarbonyl (NBOC) **14**, di(nitrobenzyl)oxycarbonyl (DNBOC) **15**, 4,5-dimethoxynitrobenzyl (DMNB) **16** and bis(2-nitrophenyl)ethanediol **17** groups.

The functional group to be protected can also be linked to the 2-nitrobenzyl group at the β position, Scheme 1.3.[15] In this case, a different photolysis by-product, nitrovinylbenzene **19**, is obtained. The 3-(4,5-dimethoxy-2-nitrophenyl)-2-butyl (DMNPB) ester derivative of this group has been employed to cage glutamate.[16]

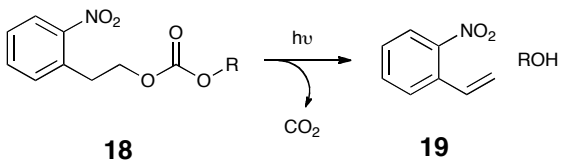

18 **19**

Scheme 1.3. Photolysis of the 2-(2-nitrophenyl)ethoxycarbonyl (NPEOC) group **18**.[15]

The excitation of the 2-nitrobenzyl chromophore leads to formation of a highly reactive diradical species **21**, Scheme 1.4. Upon absorption of a photon of light, a *n* to π* transition yields the singlet state, $S_1(n\pi^*)$, which decays by intersystem crossing to the triplet state diradical, $T_1(n\pi^*)$, from which subsequent steps in the photolysis pathway follow.[17] The 2-nitrobenzyl caging group photolysis mechanism is classified as a Norrish-type II[13,18] reaction because hydrogen abstraction from the γ-position, or intramolecular 1,5-H shift, occurs from the diradical **21** to yield the *aci*-nitro tautomer **22** as the primary photoproduct within 5 ps. Compound **22** has a pK_a of 4 and can be ionised to give the deprotonated state **23**. Cyclisation to the short-lived benzisoxazolidine **25** was observed by Il'ichev *et al*., Scheme 1.4 Pathway A.[19] Cyclisation proceeds irreversibly from the neutral nitronic acid **22**, but not from the deprotonated charged state **23**. This observation implies specific acid catalysis for the decay of the *aci*-nitro intermediate **22** of 2-nitrobenzyl derivatives.[11] However, the subsequent ring opening and elimination reactions are catalysed by general base. The acetal intermediate **26** is formed which yields the uncaged, photoreleased compound (ROH) and a nitrosoaldehyde photolysis by-product **4**.

However, Gaplovsky *et al.* reported that an additional pathway exists for 2-nitrobenzyl alcohols.[20] Primary *aci*-nitro photoproducts **22** react by two competing reaction paths. The primary *aci*-nitro tautomer **22** can form a nitroso hydrate **24** by transfer of the leaving (R) group, Scheme 1.4 Pathway B. Release of the uncaged compound (ROH) from **24** yields the nitrosoaldehyde photolysis by-product **4**. Which pathway is followed is strongly dependent on the reaction medium and pH. Pathway B prevails in aprotic solvents and aqueous acid or base, whereas pathway A dominates in neutral water. The rate-determining step depends on the nature of the leaving group, pH, temperature and solvent.

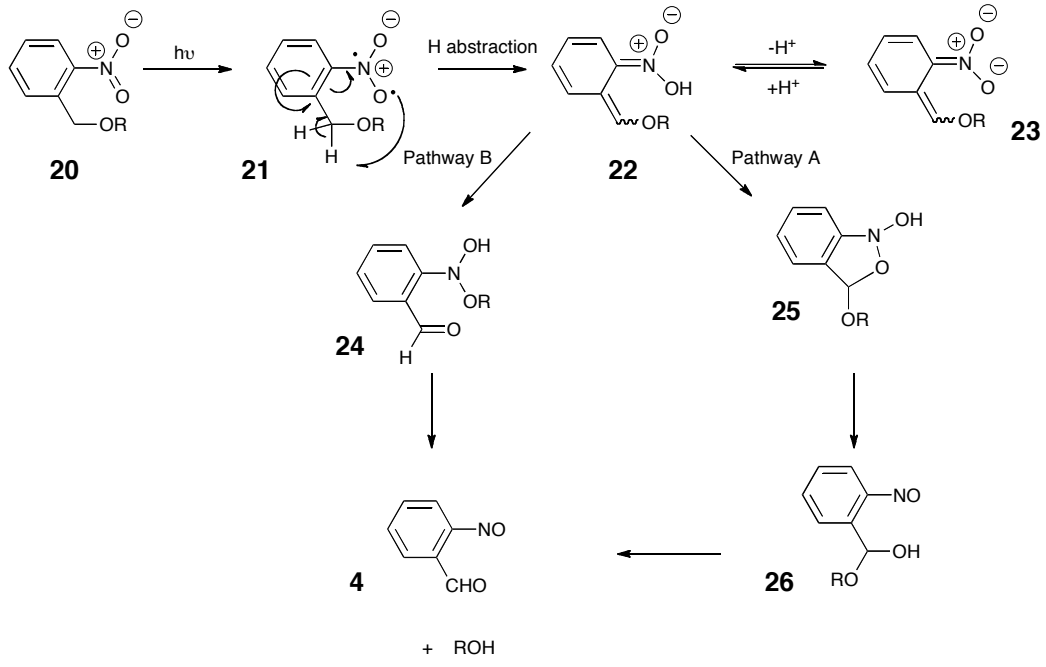

Scheme 1.4. The uncaging mechanism of the 2-nitrobenzyl caging group involves competing reaction pathways of the primary *aci*-nitro photoproduct **22**. Deprotonation of the neutral *aci*-nitro intermediate **22** to the unreactive charged species **23** is shown. R = leaving group.[11,19,20]

One disadvantage of the 2-nitrobenzyl group is that upon photolysis a nitrosoaldehyde by-product **4** is formed. This reactive compound is very electrophilic and hence likely to react with nucleophiles found in proteins and other biomolecules, potentially causing damage to the biological system under investigation. In short-term *in vitro* studies, this by-product is not a significant problem as the cellular damage caused is unlikely to manifest itself in the timescale of the experiments. However, this group is likely to cause problems in longer-term *in vitro* studies, and also in any *in vivo* studies or photodynamic therapy applications. In order to avoid forming the potentially harmful nitrosoaldehyde as a photolysis by-product, modifications of the nitrobenzyl caging group have been developed. As mentioned above, α-substituted nitrobenzyl caging groups yield a less reactive nitrosoketone photolysis by-product, for example **8** (Scheme 1.1). An interesting alternative solution to this problem was reported by Pirrung *et al*.[21] The 2-nitrobenzyl group was modified to form **27**, which traps the nitroso photolysis by-product in an intramolecular hetero Diels-Alder reaction to yield a benign product **28**, Scheme 1.5.[21]

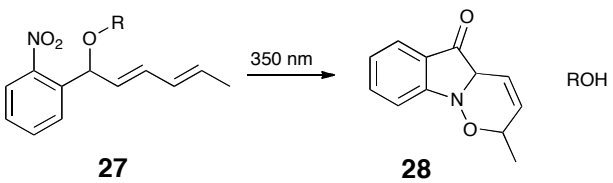

27 **28**

Scheme 1.5. Modified nitrobenzyl group **27** which traps the nitroso photolysis by-product in an intramolecular hetero Diels-Alder reaction. R = benzyl, *n*-hexyl.[21]

The number of studies that employ some variation of the 2-nitrobenzyl group testify to its applicability and usefulness.[3] Photolysis of this group is unaffected by modest changes in temperature and media, occurs with high quantum efficiencies (Φ = 0.1-0.6), and is activated by wavelengths longer than 300 nm. However, photorelease is limited to the millisecond to second time frame. The rate constant, k_{rel} , ranges from 1 to 10^3 sec^{-1}.[22] Therefore, this group has not been useful for the study of rapid biochemical events in which the event being studied, for example enzyme hydrolysis, is more rapid than the rate of photorelease of the biologically active compound of interest.

1.5. Benzoin Caging Group

In 1964, Sheehan and Wilson demonstrated that benzoin acetate (desyl acetate) undergoes photolytic cyclisation to 2-phenylbenzofuran with release of acetic acid.[23] In a subsequent study, unsymmetrical benzoin acetates, substituted on the non-conjugated ring, were photolysed. It was found that the *meta*-methoxy substituent **29**, Figure 1.4, enhanced the yield of the reaction.[24] Near quantitative release of acetic acid and very high quantum yield (Φ = 0.64) confirm that this caging group is suitable for protecting carboxylic acids. However, the *para*-methoxy substituent **30** decreased the yield. Interestingly, photolysis of the *meta*-methoxy substituent **29** was not quenched by neat piperylene, which is a triplet quencher, suggesting a singlet excited state. However, the *para*-methoxy substituent **30** was unreactive in a 1 M solution of piperylene, suggesting a triplet excited state.[24]

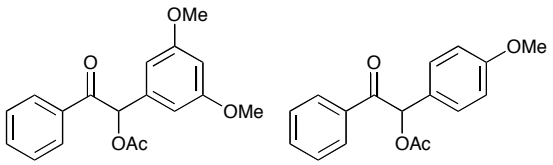

29 **30**

Figure 1.4. 3',5'-Methoxybenzoin acetate **29** and 4'-methoxybenzoin acetate **30**.

Givens and Matuszewski demonstrated the applicability of the benzoin group as a phosphate caging group, Scheme 1.6.[25] These photolysis reactions were quenched with piperylene and naphthalene triplet quenchers. This result indicated triplet-state reactivity.[25] Extremely fast photolysis rates (k_{rel} > 10^8 sec^{-1})[26] made this group attractive for intracellular release of biologically active compounds to study rapid biochemical events.

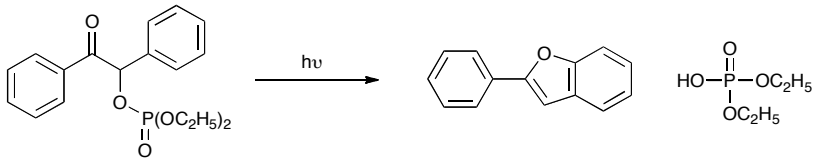

31 **32** **33**

Scheme 1.6. Photolysis of benzoin diethyl phosphate **31** yields the rearranged photolysis by-product, 2-phenylbenzofuran **32**, and the phosphate ester **33**.[25]

Apparently contradicting mechanistic experimental data suggests that different reaction pathways operate, depending on the substituents, solvent and leaving group.[13] A mechanistic study by Pirrung *et al.* on the photolysis of 3',5'-dimethoxybenzoin esters supports an excited singlet state undergoing C-R bond heterolysis to give an ion pair directly, Scheme 1.7.[27] A general

feature of the R group is that it must be acidic, suggesting that R^- is generated in the photolysis mechanism. The electron-donating methoxy groups in the *meta*-position stabilise the singlet excited state of the benzylic cation **35** more than in the *para*-position, the opposite of ground state behaviour. This observation is in accordance with the work of Zimmerman and Sandel on the photochemical *meta*-effect.[28] They investigated photo-solvolysis of substituted benzyl acetates and observed that electron-donating groups at the *meta*-position were more effective in promoting excited state solvolysis than in the *para*-position. Pirrung *et al.* observed cyclisation of the α-ketocation **35** to the 2-phenylbenzofuran precursor **36**, followed by deprotonation to obtain the final photolysis by-product **37**. This study proposed that the rate-limiting step is the deprotonation of **36**.[27]

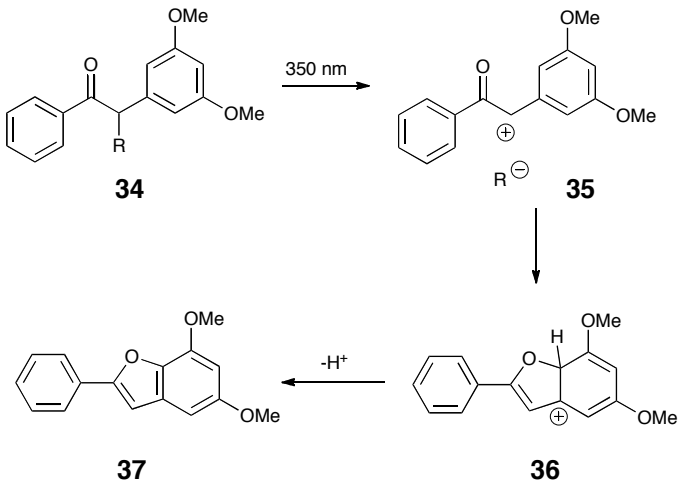

Scheme 1.7. Proposed photolysis mechanism of the 3',5'-dimethoxybenzoin caging group **34** to yield the photolysis by-product 2-phenylbenzofuran **37**. R represents the leaving group.[27]

High quantum yields, rapid rates of photorelease and an inert benzofuran photolysis by-product are significant advantages of the benzoin caging group compared with the nitrobenzyl caging group. However, there are limitations. Low solubility in aqueous buffer and hydrolytic instability can be a problem. The caging group has a stereogenic centre and caging a chiral biologically active compound raises the issue of diastereomeric mixtures if racemic benzoin is used.[13] The photolysis by-product absorbs in the same wavelength range as the parent caged compound. It can, therefore, act as a light filter, potentially reducing photolytic efficiency.[11]

1.6. Phenacyl Caging Group

1.6.1. Methoxyphenacyl Caging Group

In 1973, Sheehan *et al.* demonstrated the photocleavage reaction of the 4-methoxyphenacyl (MPA) caging group **38**, a chemically simpler version of the benzoin chromophore.[29] 4-Methoxyacetophenone **42** and the released carboxylic acid **43** were obtained. The mechanism proposed by Sheehan is of β-homolytic cleavage to yield the α-keto radical **40**, Scheme 1.8. Subsequent hydrogen abstraction from the solvent, dioxane in this study, yields the photoreduced by-product, 4-methoxyacetophenone **42**. Benzophenone quenched the reaction completely, providing evidence that the reaction proceeds through a long-lived triplet state, having a lifetime longer than 10^{-10} s.[29] This phenacyl photocleavage reaction was applied to many amino acids and peptides.[29] Epstein *et al.* applied the 4-methoxyphenacyl ester to

the caging of phosphates.[30] He proposed the same homolytic photolysis mechanism as Sheehan, Scheme 1.8.

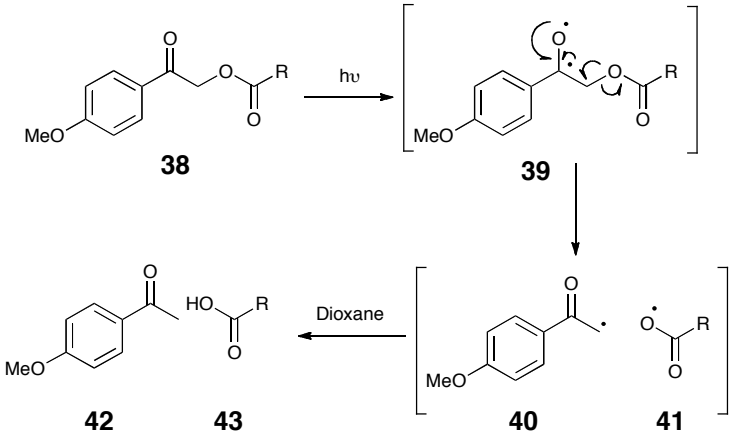

Scheme 1.8. Proposed photolysis mechanism of the 4-methoxyphenacyl caging group **38** to yield photoreduced 4-methoxyacetophenone **42**.[29]

When the photolysis of a 4-methoxyphenacyl caged phosphate was carried out in *tert*-butyl alcohol, a poor hydrogen-atom donor, Givens and co-workers observed that the major photolysis product was the rearranged *tert*-butyl 4-methoxyphenylacetate **47**, Scheme 1.9.[31] This product was proposed to form as a result of a heterolytic photolysis cleavage mechanism. This result highlights the effect of solvent, not only on the rate and kinetics of photolysis, but also on the actual photolysis pathway and mechanism. In addition, leaving groups with greater nucleophilicity (e.g. phosphate over acetate) tend to favour this heterolysis mechanism.[31]

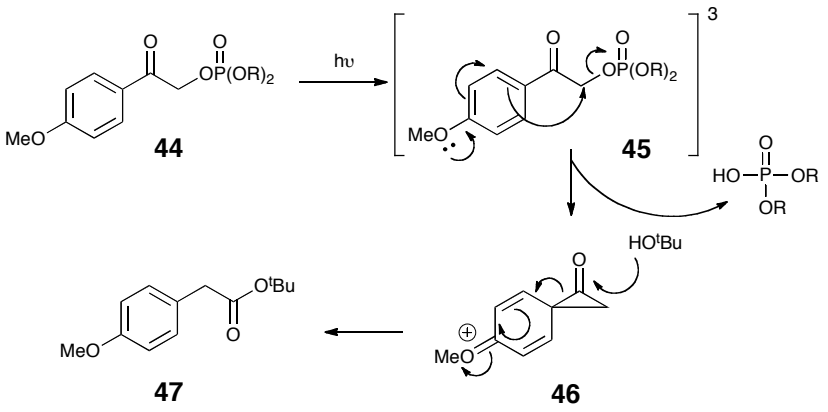

Scheme 1.9. Proposed photolysis mechanism of 4-methoxyphenacyl caged phosphate **44** when irradiated at 366 nm in *tert*-butyl alcohol. The major photolysis product was the rearranged *tert*-butyl 4-methoxyphenylacetate **47**.[31,32]

This rearrangement (Scheme 1.9) is consistent with a report by Anderson and Reese[32] in 1962, who observed a photo-induced rearrangement which involved aryl participation for irradiation of 4-methoxy- and 4-hydroxyphenacyl chloride. Ethyl 4-methoxyphenylacetate and ethyl 4-hydroxyphenylacetate respectively were isolated when photolysis was performed in ethanol. This type of rearrangement is similar to that illustrated in Scheme 1.9, except that ethanol was the nucleophile which opened the spiroketone intermediate **46**. In the absence of *para* electron-donating groups on the aromatic ring, such as phenacyl chloride, irradiation resulted in the photoreduction product (acetophenone) exclusively.

1.6.2. Hydroxyphenacyl Caging Group

Givens and Park subsequently developed the 4-hydroxyphenacyl (HPA) caging group and used it to photorelease ATP with an efficiency (Φ) of 0.37.[33] A year later, in 1997, it was demonstrated to be an efficient caging group for excitatory amino acids and peptides.[34] The rate constant of photorelease, ~ 10^7 s^{-1}, is several orders of magnitude faster than the nitrobenzyl group.[22] The 4-hydroxyphenacyl caging group has greater solubility in aqueous media than the 4-methoxyphenacyl and benzoin caging groups, making it more applicable to biological systems. Unlike the nitrobenzyl and benzoin cages, hypochromic (blue) shift of UV absorption upon photolysis to 4-hydroxyphenylacetic acid **54** (Scheme 1.10) results in a 'transparent' by-product which does not interfere with the UV absorbance of the caging group.[33] In contrast to the complex photochemistry of the 4-methoxyphenacyl caging group, discussed above, the 4-hydroxyphenacyl caging group is converted exclusively to 4-hydroxyphenylacetic acid **54** at 300 nm.[22] Despite a clear and consistent observation of the photolysis by-product from this caging group, there has been debate over the photolysis mechanism. Givens and Park proposed a photo-Favorskii rearrangement in which the primary photochemical step is triplet homolysis to a radical pair (**50** and **41**), that then undergoes fast electron transfer to an ion pair (**51** and **52**), Scheme 1.10.[22] Electron donation from the oxygen lone pair of the hydroxyl group into the ring, to quench the carbocation α to the carbonyl, results in a spiroketone intermediate **53**. This intermediate is trapped with water (or other nucleophilic

solvent) to yield the carboxylic acid photolysis by-product **54**. The observation that sodium 2-naphthalenesulfonate successfully quenched photolysis provided evidence for involvement of a triplet state.[22]

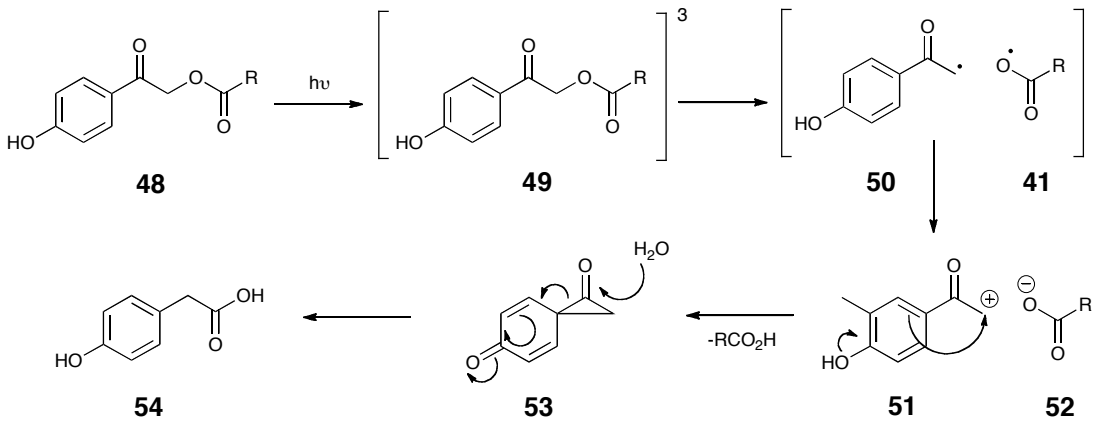

Scheme 1.10. Proposed photolysis mechanism of the 4-hydroxyphenacyl caging group **48**.[22] R = alkyl chain.

Zhang *et al.*[35] instead proposed that the primary photochemical step from the singlet excited state **56** is excited-state proton transfer (ESPT), in which there is formal intramolecular proton transfer from the phenolic proton to the carbonyl oxygen of the ketone (which is closer to the ring), mediated by solvent water, Scheme 1.11. This generates a reactive *para*-quinone methide phototautomer **57**, which releases the carboxylic acid with concerted rearrangement to a spiroketone intermediate **53**, Scheme 1.11. This intermediate is opened with water to obtain 4-hydroxyphenylacetic acid **54**.[35] The dependence of the quantum yield on the solvent pH, with reduced photolysis observed at higher pH, was used to support this mechanism. It was rationalised that if the phenol hydroxy group was already deprotonated (at

higher pH), ESPT could not occur, resulting in reduced quantum efficiency. It was observed that the triplet quenchers, sodium sorbate, *trans*-piperylene and 1,3-cyclohexadiene, did not significantly decrease the photolysis yield. It was concluded that this is inconsistent with an acetophenone triplet state and, therefore, a singlet excited state was proposed.[35]

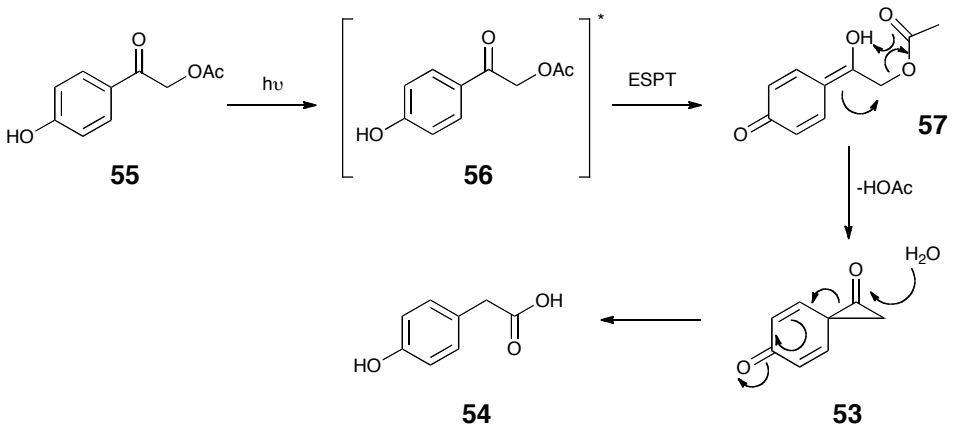

Scheme 1.11. Alternative proposed photolysis mechanism of the 4-hydroxyphenacyl caging group.[35]

In response to the report by Zhang *et al*.[35], Givens and co-workers demonstrated that photorelease of diethyl phosphate from 4-hydroxyphenacyl diethyl phosphate in neutral aqueous media did proceed *via* a short-lived triplet state with a lifetime of 0.4 ns in 1:1 acetonitrile and water.[36] UV/Vis spectra of transients obtained by nanosecond laser flash photolysis (LFP), and pump-probe spectroscopy were some of the techniques employed in this study.

In 2008, Givens *et al.* subsequently reported observation of a triplet biradical **59**, as well as a new side product, 4-hydroxybenzyl alcohol **61**, at high water concentrations, Scheme 1.12.[37] This by-product is formed by decarbonylation of the spiroketone intermediate **53**, and provides evidence for its existence, as it has never actually been detected despite being proposed by Anderson and Reese in 1962.[32,37]

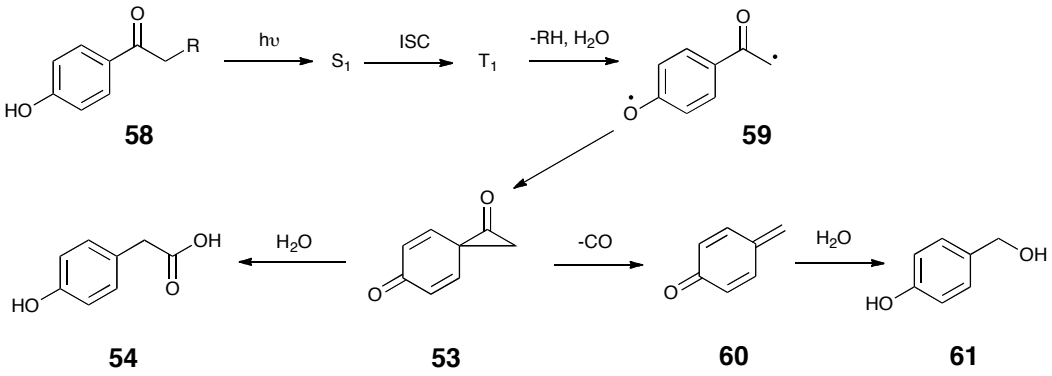

Scheme 1.12. Most recent proposed photolysis mechanism of the 4-hydroxyphenacyl caging group. A new side product, 4-hydroxybenzyl alcohol **61**, was observed. R = diethyl phosphate, tosylate, mesylate.[37]

1.7. Other Common Caging Groups

1.7.1. The Coumarinyl Group

In 1984, Givens and Matuszewski reported the photorelease of phosphates from the (7-methoxycoumarin-4-yl)methyl (MCM) caging group **62**, Scheme 1.13.[25] Irradiation of the MCM caging group in aqueous media leads to release of the protected compound and formation of the corresponding hydroxymethyl coumarin **63**. A photosolvolysis S_N1 mechanism involving

heterolysis from the singlet-excited state to form an ion pair, which is quenched by the solvent, has been proposed.[11,38]

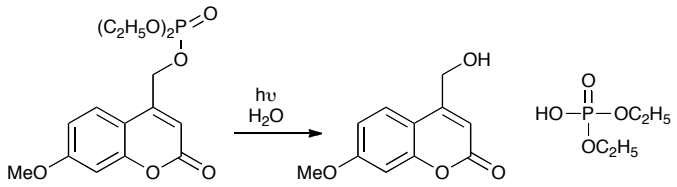

62 **63** **33**

Scheme 1.13. The first report of the coumarinyl caging group. Photolysis of MCM-caged diethyl phosphate **62** in aqueous medium released diethyl phosphate **33** and a hydroxymethyl coumarin photolysis by-product **63**.[25]

Appending charged or polar moieties to the aromatic ring of the coumarinyl caging group increases its water-solubility. This caging group, and variations thereof, have been used to cage phosphate, alcohol, carboxylic acid, carbonyl, thiol and amine functionalities.[39] The photorelease of cyclic nucleoside monophosphate derivatives (cAMP and cGMP) from MCM-caged precursors has been demonstrated *in vitro* in a mammalian cell line expressing the cyclic nucleotide-gated ion channel.[38] Furuta *et al.* first reported that a significant property of this caging group is its relatively high two-photon excitation cross-section which makes it suitable for two-photon excitation.[40] Two-photon excitation will be discussed in greater detail later in this chapter.

1.7.2. 1-Acyl-7-nitroindolines

Amit *et al.* reported a new light-sensitive amide in 1976.[41] Irradiation of substituted 1-acyl-7-nitroindolines **64** in organic solvents yielded the free carboxylic acid and nitroindoline **66** photolysis by-product, Scheme 1.14. Corrie and co-workers employed a derivative of this group to cage glutamate, in which X = CH_2CO_2Me.[42] However, in aqueous solution, Corrie and co-workers observed that nitrosoindoline **65** was the major photolysis by-product, not nitroindoline **66**. This result suggests that this photolysis mechanism is significantly solvent-dependent. The proposed photolysis mechanism involves the transfer of the acyl group to the neighbouring nitro substituent.

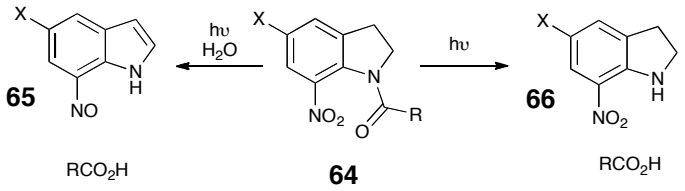

Scheme 1.14. Photolysis of substituted 1-acyl-7-nitroindolines **64** yields the free carboxylic acid and either nitroindoline **66** or nitrosoindoline **65**, depending on solvent. X = Br, NO_2, CH_2CO_2Me, OMe.[41,42]

1.7.3. The Cinnamyl Ester Group

Olefins isomerise upon irradiation with UV-light. This property has been exploited in the design of a cinnamyl ester caging group used to acylate and, therefore, inactivate an enzyme. Turner *et al.* reported that acylation of the

active-site serine of α-thrombin renders the enzyme inactive.[43] Photoisomerisation of the cinnamyl-caged enzyme **67** brings the ester bond in close proximity to the *ortho*-hydroxyl group. This internal hydroxyl nucleophile attacks the carbonyl group resulting in lactonisation and enzyme deacylation and, therefore, enzyme activation, Scheme 1.15.[43] This caging group is interesting because it allows for fluorescence reporting. Photolysis yields the fluorescent coumarin photolysis by-product **69** which can be used as a reporter to quantify photorelease and, therefore, active compound delivery.[44] Using two-photon photolysis, uncaging and excitation of the reporter can be achieved using the same excitation source at 750 nm.

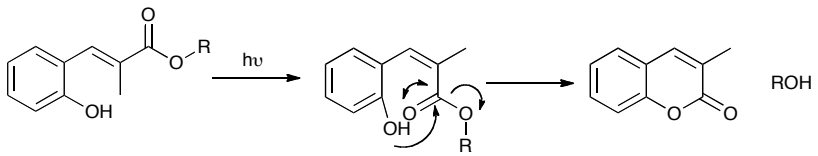

67 **68** **69**

Scheme 1.15. Photolysis of the cinnamyl ester caging group **67** yields the free active enzyme (ROH) and the coumarin photolysis by-product **69**. R = Biologically active compound, e.g. an enzyme.[43]

1.7.4. The Quinoline Group

The 8-bromo-7-hydroxyquinoline (BHQ) caging group **70** (Scheme 1.16) was first reported in 2002 by Dore and Fedoryak.[45] It was first described as a carboxylic acid cage[45] but later reported to release phosphates and diols.[46] The major advantages of BHQ are its high quantum efficiency of one-photon

photolysis, increased solubility in aqueous buffers, and its photolysis efficiency using two-photon excitation. A photosolvolysis S_N1 mechanism involving heterolysis of the benzylic C-O bond from the singlet-excited state has been proposed.[46]

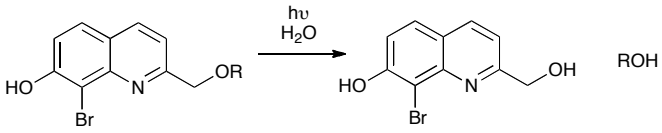

70 **71**

Scheme 1.16. Photolysis of the BHQ caging group **70** yields the uncaged compound (ROH) and the starting BHQ cage **71**. R = Biologically active compound.[45]

1.8. Two-Photon Photolysis

The wavelengths employed in single-photon photolysis, in the near ultra-violet (UV) range of the electromagnetic spectrum, can be absorbed by nucleotides and proteins, causing photodamage to the biological material. In 1990, Denk *et al.* demonstrated a means of overcoming this problem using two-photon excitation.[47] It was reported that using lower energy photons with wavelengths in the range of 640 nm to 700 nm, faster photolysis with stronger focusing, in smaller volumes could be achieved. This was demonstrated using 1-(2-nitro)phenylethyl caged ATP **9** (Scheme 1.2).[47]

Two-photon absorption is the simultaneous absorption of two photons by the same molecule. The main difference between one- and two-photon absorption is that the simultaneous absorption of two photons results in absorption being dependent on the square of the irradiation intensity, while one-photon absorption is linearly dependent on intensity.[48] Most of the applications of two-photon absorption are as a result of this intensity dependence. Using femto-second pulses, with high peak power, and small spot sizes gives high irradiation intensity in a very small volume. Uncaging occurs preferentially at the focus of the longer wavelength (IR) laser beam, allowing for accurate penetration into tissue samples and greater spatial control of active compound release. One-photon photolysis allows for uncaging to occur above and below the focal plane, whereas two-photon photolysis occurs only at the focal plane, illustrated by the excitation volume, Figure 1.5. In addition to the advantage of

greater uncaging resolution, reaching an excited state using photons of half the energy (twice the wavelength) compared with one-photon absorption is particularly attractive to the biological application of caging technology as cellular damage can be minimised.

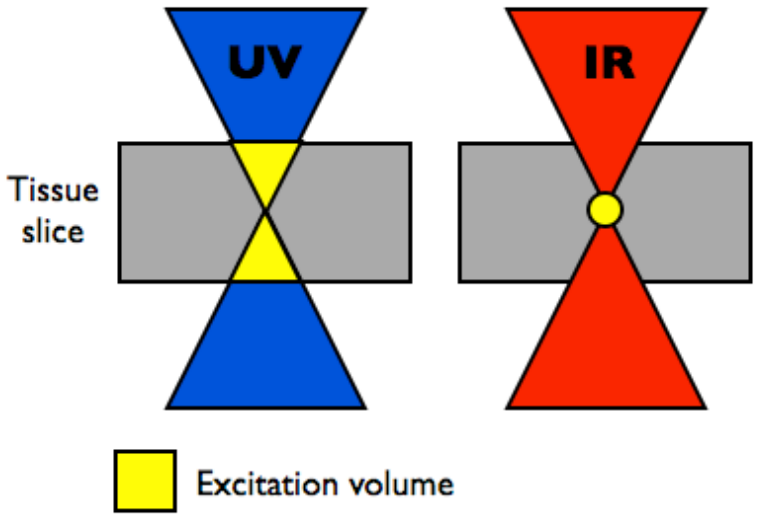

Figure 1.5. Due to the intensity dependence of two-photon absorbance, uncaging occurs only at the focal plane, unlike single-photon photolysis - which occurs above and below the focal plane. Two-photon photolysis, therefore, offers greater uncaging spatial resolution than single-photon photolysis.

Figure 1.6 is a photograph taken by Craig McDougall at the School of Physics and Astronomy, University of St Andrews.[49] It shows the difference between single-photon excitation of fluorescence (top beam); a Bessel beam which does not diffract as it propagates (middle beam); and two-photon excitation of fluorescence (bottom spot). This photograph beautifully illustrates the superior spatial resolution of two-photon excitation (and, therefore, uncaging)

compared with one-photon excitation. The two-photon excitation volume is a small dot while the one-photon excitation volume is a diffuse band.

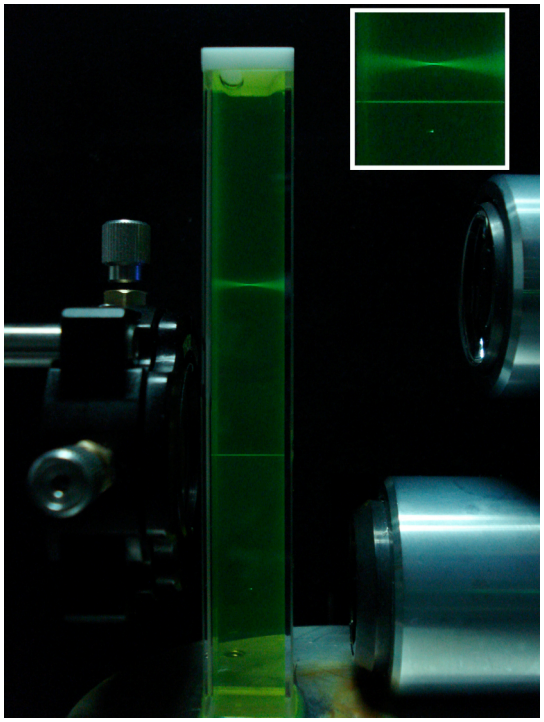

Figure 1.6. A photograph taken by Craig McDougall at the School of Physics and Astronomy, University of St Andrews. It shows the difference between single-photon excitation of fluorescence (top beam); a Bessel beam which does not diffract as it propagates (middle beam); and two-photon excitation of fluorescence (bottom spot). These beams are clearly represented in the right-hand box.[49]

The two-photon cross-section (δ) is a quantitative measure of the probability of two-photon absorption. It has units of $cm^4.s.photon^{-1}$ and 10^{-50} $cm^4.s.photon^{-1}$ is called a Göppert-Mayer (GM). This unit is named after Maria Göppert-Mayer who first theoretically analysed the simultaneous absorption of two photons by the same molecule in the 1930s.[48] The two-photon action

cross-section is usually measured, which is the product of the two-photon cross-section and the quantum efficiency of photolysis ($\delta.\Phi$).

The caging groups that have been developed for single-photon photolysis generally exhibit very low two-photon photolytic efficiency. For example, the two-photon cross-section of the DMNB caging group is approximately 0.01 GM within the 700-750 nm range.[50] For efficient two-photon photolysis of a caging group in a biological system, a two-photon cross-section of 3 GM and above is ideal.[51] Some chemical modifications to the traditional caging groups have improved their two-photon sensitivity. The nitrodibenzofuran (NDBF) chromophore **72**, Figure 1.7, based on the 2-nitrobenzyl skeleton, was reported by Ellis-Davies and co-workers in 2006.[52] NDBF-caged ethyleneglycoltetraacetic acid (EGTA), the Ca^{2+} chelator, was observed to have a two-photon cross-section of ~ 0.6 GM. Two-photon photolysis of NDBF-EGTA induced localised Ca^{2+} release from the sarcoplasmic reticulum of cardiac myocytes.[52] Aujard *et al.* evaluated the 2-nitrobenzyl skeleton for the design of caging groups with red-shifted absorption to improve two-photon absorbance.[50] Conjugated electron-donating substituents were appended to the nitrobenzyl aromatic ring, for example **73**, Figure 1.7. Different conjugated paths between the electron-donating and withdrawing groups were introduced. Enhancing conjugation did result in red-shifted absorption and improvement of two-photon absorbance. Two-photon cross-sections up to 0.05 GM were observed.[50] However the quantum yields remained low, between 0.1 and 1%.

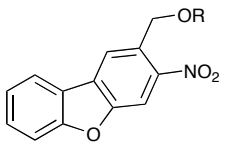

72

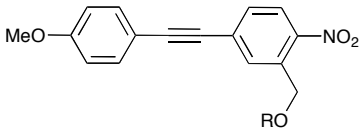

73

Figure 1.7. The nitrodibenzofuran chromophore **72** employed by Ellis-Davies and co-workers to cage EGTA,[52] and the π-extended nitrobenzyl derivative, the (5-((4-methoxyphenyl)ethynyl)-2-nitrophenyl) caging group **73**, developed by Aujard *et al.*[50]

Extending the work of Aujard *et al*., Gug *et al.* recently caged glutamate with a π-extended nitrobenzyl derivative, the 3-(2-propyl)-4'-methoxy-4-nitrobiphenyl caging group **74**, Figure 1.8. A high two-photon uncaging cross-section was reported, $\delta.\Phi$ = 0.45 GM at 800 nm.[53]

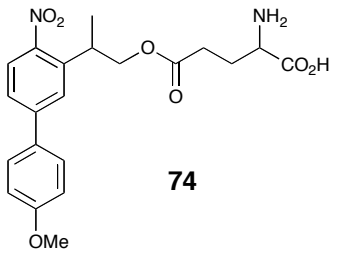

74

Figure 1.8. Glutamate caged with a π-extended nitrobenzyl derivative, the 3-(2-propyl)-4'-methoxy-4-nitrobiphenyl caging group **74**.[53]

1.9. Biological Applications of Caged Compounds

1.9.1. Caged Ca^{2+}

Considering the importance of Ca^{2+} as a secondary messenger, it is not surprising that Ca^{2+} dynamics have been explored using 'caged' Ca^{2+}. Since Ca^{2+} itself cannot be caged, it is instead sequestered by a chelator that changes from high Ca^{2+} affinity to low Ca^{2+} affinity upon photolysis. Therefore, Ca^{2+} concentrations can be locally altered with high temporal and spatial resolution. In 1988, Ellis-Davies and Kaplan reported 4,5-dimethoxynitrobenzyl-caged EDTA, called DM-nitrophen **75**, Scheme 1.17.[54] The dissociation constant changes from 5 nM to several mM upon photolysis at pH 7.2, resulting in a local increase in Ca^{2+} concentration at the site of photolysis. However, a limitation of DM-nitrophen **75** is that it also binds Mg^{2+}, complicating the interpretation of biological results from Ca^{2+} release. A number of caged Ca^{2+} chelators have been developed and applied to a number of biological systems.[3]

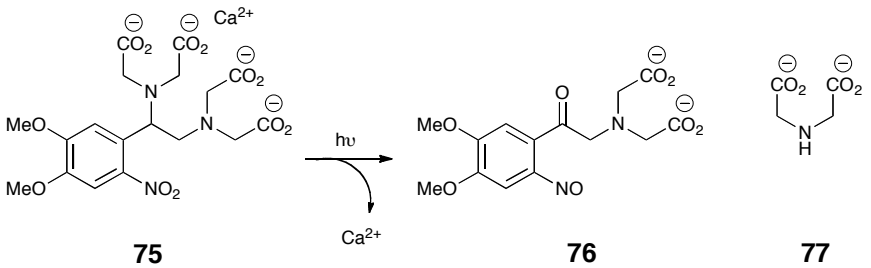

75 **76** **77**

Scheme 1.17. Photolysis of the DM-nitrophen-Ca^{2+} complex **75** results in the release of Ca^{2+}.[54]

1,2-Bis(*o*-aminophenoxy)ethane-*N,N,N',N'*-tetraacetic acid (BAPTA) is a known Ca^{2+}-selective chelator. Caged Ca^{2+} buffers, for example diazo-BAPTA **78** (Scheme 1.18), which sequester Ca^{2+} after photolysis have been developed. These compounds allow for a decrease in Ca^{2+} concentration following irradiation, Scheme 1.18.[55] Photochemical rearrangement of the diazoacetyl group of diazo-BAPTA **78** converts it into an electron-donating carboxymethyl group **79**. A 30-fold increase in Ca^{2+} affinity upon photolysis was observed.[55]

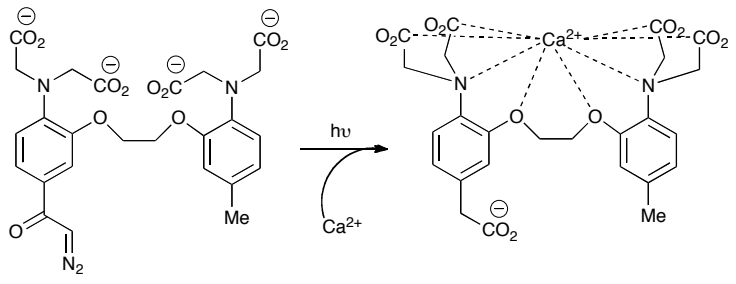

78 **79**

Scheme 1.18. Photolysis of diazo-BAPTA **78** results in the sequestering of Ca^{2+} by the uncaged product BAPTA **79**.[55]

An interesting example, in which two different kinds of caged Ca^{2+} chelators were employed to finely control Ca^{2+} concentrations *in vivo*, was reported by Gomez and Spitzer.[56] Growth cones at the tips of neurons migrate through the developing nervous system and guide axons to appropriate target regions. The effect of Ca^{2+} on growth cone motility was investigated. Photolysis of diazo-BAPTA **78**, and the resulting Ca^{2+} concentration suppression, accelerated axon extension. However, photolysis of nitrobenzyl-caged EGTA, and the resulting release of Ca^{2+}, slowed axon growth. This study demonstrated that Ca^{2+} transients control axon growth in the developing *Xenopus* spinal cord.[56]

1.9.2. Caged Neurotransmitters

Caged-glutamate is the most extensively studied and employed compound in the field of caging technology.[3] As discussed in greater detail in Chapter 6, glutamate is the major excitatory neurotransmitter in the mammalian central nervous system. Methoxynitroindolino (MNI)-glutamate **80**, Figure 1.9, was developed by Matsuzaki *et al.* in 2001.[57] MNI-glutamate was reported to have a two-photon cross-section of 0.06 GM, sufficient for two-photon photolysis in a biological system. Using cultured hippocampal neurons, two-photon photolysis of glutamate was achieved with spatiotemporal resolution similar to that of presynaptic terminals. This remarkable resolution allowed for activation of individual dendritic spines. This allowed for glutamate receptors along dendrites of CA1 pyramidal neurons to be mapped.[57]

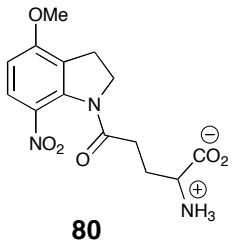

80

Figure 1.9. MNI-caged glutamate **80** employed in two-photon photolysis studies *in vitro*.[57]

1.9.3. Caged Ins*P*$_3$

Caged *myo*-inositol 1,4,5-triphosphate (Ins*P*$_3$) is another biologically significant light-activated small molecule which is widely used in cell biology.[58] Ins*P*$_3$ binds to the Ins*P*$_3$ receptor on the endoplasmic reticulum, triggering release of Ca^{2+} and an increase in cytosolic free Ca^{2+}. In 1987, Walker *et al.* first reported the application of 1-(2-nitrophenyl)ethyl (NPE) esters of Ins*P*$_3$ **81**, Figure 1.10, (caged as a mixture at the 4 and 5 position phosphate groups) to skeletal and smooth muscle cells.[59] Photorelease of Ins*P*$_3$ from the caged inactive precursor induced full contraction in both muscle types. This result provided strong evidence for the hypothesis that Ins*P*$_3$ is a second messenger in the regulation of muscle contraction.[59]

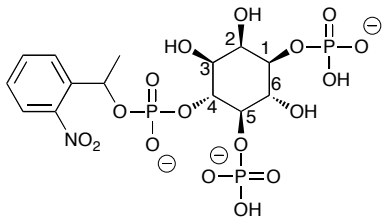

81

Figure 1.10. NPE-caged InsP_3 **81** employed by Walker *et al.* to investigate the role of InsP_3 in muscle contraction.[59]

Li *et al.* developed a membrane-permeant DMNB-caged InsP_3 ester **82** (Scheme 1.19). This compound allowed for exogenous InsP_3 to be delivered into populations of unpermeabilised cells with spatial and temporal control.[60] The caged, membrane-permeant ester **82** diffuses into cells where hydrolysis of the propionyloxymethyl (PM) ester by non-selective esterases yields the inactive, caged, charged InsP_3 derivative **83**, Scheme 1.19. This trapped membrane-impermeant caged compound does not activate the InsP_3 receptor. Upon UV illumination, the caged InsP_3 analogue **84** is photoreleased, Scheme 1.19. Spikes of cytosolic free Ca^{2+} were observed. In activated T cells, it was observed that photorelease of the InsP_3 analogue **84** stimulated gene expression *via* the nuclear factor. Repetitive UV flashes elicited more gene expression than one sustained flash. This result suggests that Ca^{2+} spike frequency can optimise gene expression.[60]

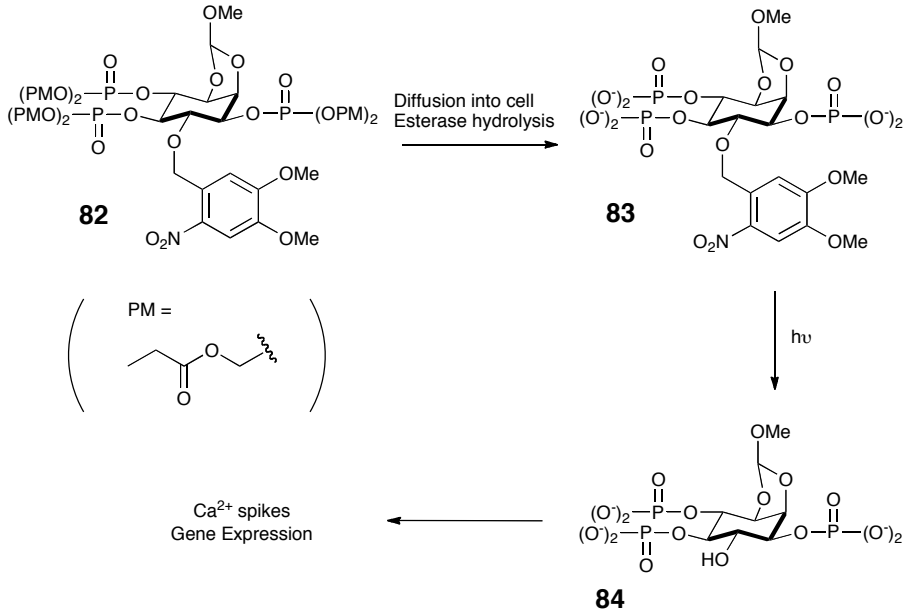

Scheme 1.19. The DMNB-caged, membrane-permeant InsP_3 derivative **82** diffuses into cells. Hydrolysis of the propionyloxymethyl ester by non-selective esterases yields the inactive, caged, charged InsP_3 derivative **83**. Upon UV illumination, photorelease of the InsP_3 analogue **84** elicits spikes of cytosolic free Ca^{2+} and gene expression.[60]

1.9.4. Caged Nucleic Acids - Controlling Gene Expression

Nucleic acids are the cell's information storage device. They regulate fundamental biological processes including gene transcription and protein translation. Caged nucleic acids have allowed for the control of gene expression with high spatial and temporal resolution.[58] This control of gene expression has been used to study the embryonic development of the fruitfly, albino frog and zebrafish.[61] The zebrafish is the ideal model for caged-molecule applications, since it develops *ex utero* and has sufficient transparency during embryogenesis.

Ando *et al.* randomly modified the phosphate backbone of green fluorescent protein (*Gfp*) mRNA with the 6-bromo-4-diazomethyl-7-hydroxycoumarin (Bhc) caging group **85**, Figure 1.11.[62] Approximately 30 Bhc groups bound to the phosphate backbone per kilobase of RNA sequence. It was demonstrated that Bhc-caged *Gfp* mRNA had reduced translational activity *in vitro*. Upon irradiation with UV light, partial recovery of translational activity was observed.

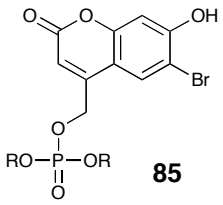

85

Figure 1.11. Phosphate group of an RNA backbone caged with the Bhc caging group. R = RNA chain.[62]

This newly-developed technology was applied to the caging of the mRNA encoding the transcription factor Engrailed2a (eng2a). Zebrafish embryos injected with Bhc-caged eng2a mRNA appeared to develop normally in the dark. However, exposure to 365 nm light caused the loss of the eyes, and development of the midbrain with deletion of the forebrain. This result suggests that this factor regulates cell fate choice in the developing central nervous system.[62]

1.9.5. Caged Peptides and Proteins

In comparison to the overwhelming number of reports describing the synthesis and application of caged low molecular weight compounds to biological systems, there are fewer reports of caged proteins. Proteins are more difficult handle, manipulate and characterise than small molecules.[63] However, caged proteins offer the exciting possibility of manipulating complex cellular events.

Caged peptides can be prepared from caged amino acids using solid-phase peptide synthesis.[58] Photo-controlled cell adhesion was demonstrated by Petersen *et al.* using the caged peptide RGD.[64] RGD (Arg-Gly-Asp) is a cell-adhesive peptide which promotes integrin-mediated cell adhesion. It was caged with a 3-(4,5-dimethoxy-2-nitrophenyl)-2-butyl ester (DMNPB) caging group on the carboxylic acid side chain of the aspartic acid residue **86**, Scheme 1.20. No cell adhesion was observed onto the caged peptide. However, after irradiation cell adhesion was observed, Scheme 1.20.[64]

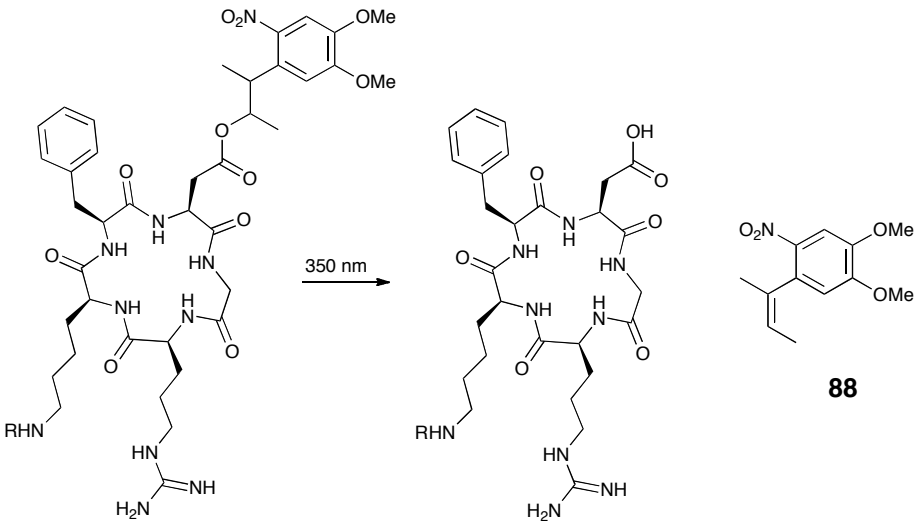

Scheme 1.20. Photolysis of DMNPB-caged RGD **86** yields the cell-adhesive, active state **87**. R = linker to silica surface.[64]

Unlike caged small molecules and peptides, caged proteins cannot be synthesised using uniform chemistry.[58] The simplest method for statistically modifying a protein is by employing the reactivity of functional groups of amino acid side chains.[3] Caging groups can be attached to these sites. For example, cysteine residues of proteins and sulfhydryl groups of cages can be coupled. Schultz and co-workers demonstrated that caged amino acids could be incorporated into proteins in a site-directed manner using a nonsense-codon and a corresponding tRNA loaded with a caged amino acid. Using this technology 2-nitrobenzyl-caged cysteine was incorporated into proteins in yeast.[65]

An example of the application of caged proteins to manipulate enzyme function was reported by Endo *et al.*[66] The DMNB caging group was used to

cage lysine. This modified amino acid was incorporated into a specific site (Lys132) in the salt-bridge network in the dimer interface of the *Bam*HI mutant restriction endonuclease. The activity of the photo-functionalised *Bam*HI mutant was suppressed. However, irradiation at 365 nm at 0 °C for 20 minutes resulted in the recovery of enzyme activity.[66] Therefore, direct photochemical control of enzymatic activity was demonstrated. The authors proposed that this technology could be applied to other proteins to control their structure and function.

Having recognised that caged proteins would be especially useful in signal transduction research, Bayley and co-workers caged the catalytic subunit of protein kinase A.[67] It was first confirmed that the catalytic subunit of protein kinase A could be activated by thiophosphorylation at Thr-197. This modified protein was caged with 4-hydroxyphenacyl bromide. The caged protein **89** (Scheme 1.21) exhibited 17-fold reduced catalytic activity. Upon irradiation with UV light (280-370 nm), a 15-fold increase in catalytic activity was observed. This result is consistent with approximately 85% yield of the uncaged, active protein **90**, Scheme 1.21.[67]

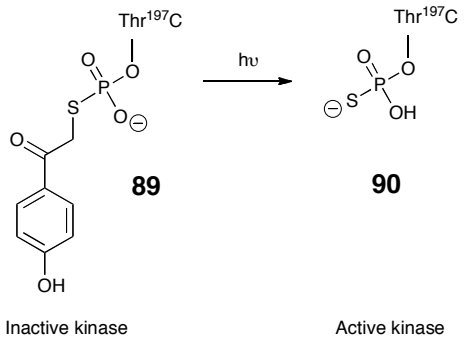

Scheme 1.21. Photolysis of the 4-hydroxyphenacyl-caged thiophosphorylated protein kinase A catalytic subunit **89**.[67] C = catalytic subunit.

1.10. Conclusion

The use of caged compounds to answer biological questions has been successfully demonstrated in many reports. However, this is an exciting field which still has problems to overcome, which will require collaborations between physicists, chemists and biologists. Physicists contribute to the development of better laser sources with the appropriate requirements for application to a biological system of interest. Chemists have the challenge of designing new generations of caged compounds with specific properties required for a biological system of interest. For example, larger two-photon cross-section and greater aqueous solubility are desirable; membrane-permeability or impermeability may be required. Biologists provide insight into which biological questions are important and how these questions can be addressed using the tools developed by physicists and chemists.

This DPhil dissertation highlights several projects in which caging technology has been applied to address biological problems and questions. Each 'Results and Discussion' chapter begins with an introduction to the specific biological system of interest and the aims and hypotheses for the synthesis and application of caged compounds to that system.

1.11. Specific Project Aims

The design, synthesis, and application of novel caged mitochondrial uncouplers to achieve spatially and temporally controlled mitochondrial inactivation in intact cells.

The design and synthesis of caged TRPV1 agonists and antagonists as tools to probe the TRPV1 receptor. It was aimed to design and synthesise TRPV1 agonists with reduced membrane permeability as tools to establish the location of the TRPV1 agonist-binding site.

It was aimed to synthesise nitroindoline-caged glutamate and incorporate it into an antigenic peptide to allow for control over T-cell activation in order to gain insight into adaptive immune responses.

The design and synthesis of caged local anaesthetics, lidocaine and QX-314, to achieve control over Na^+-channel activation.

It was aimed to develop novel caging groups with improved photolysis characteristics.

Wavelength-orthogonal photolysis of caged neurotransmitters was a significant aim to improve the current available caging technology.

In order to achieve greater control over photolysis, it was proposed that pH-dependent caging groups be designed and synthesised.

Chapter 2:

Results and Discussion - Caged AG10

2. Caged AG10: new tools for spatially predefined mitochondrial uncoupling

2.1. Introduction and Aims

The aim of this project was to design and synthesise caged molecular probes to investigate the role of mitochondria in Ca^{2+} signalling. It was aimed to employ caged mitochondrial uncouplers to selectively inhibit mitochondria in intact native cells with spatial and temporal control.

Ca^{2+} is a ubiquitous and highly versatile intracellular signalling molecule.[68] It is able to regulate a diverse range of cellular functions and processes because the Ca^{2+} signalling mechanism is versatile in terms of speed, amplitude and spatio-temporal patterning.[68,69] For example, in smooth muscle, intracellular Ca^{2+} is able to control and coordinate several diverse cellular activities including cell division, growth, metabolism, contraction and cell death.[70] The Ca^{2+} signalling network consists of four functional units - a signal triggers Ca^{2+}-mobilising signals; 'ON' mechanisms are activated, increasing cytoplasmic Ca^{2+} concentration; Ca^{2+}-sensitive processes are stimulated; and 'OFF' mechanisms restore resting state Ca^{2+} levels.[68] An extracellular stimulus generates Ca^{2+} mobilising signals. Cells generate Ca^{2+} signals by employing both internal and external sources of Ca^{2+}. The endoplasmic reticulum (ER) houses the internal Ca^{2+} store. Release of Ca^{2+} from the ER is

controlled by various channels. These channels include the inositol-1,4,5-triphosphate receptor (InsP_3R), and ryanodine receptor (RYR) families, located on the ER membrane.[68] The Ca^{2+} mobilising signals result in the activation of 'ON' mechanisms, which results in an increase in the intracellular concentration of Ca^{2+} from 100 nM to approximately 1000 nM. This increase in Ca^{2+} concentration is due to Ca^{2+} influx across the plasma membrane or release from intracellular stores through various channels. These channels include store-operated channels (SOCs), voltage-operated channels (VOCs) and receptor-operated channels (ROCs). The increase in intracellular Ca^{2+} concentration results in the stimulation of Ca^{2+}-sensitive processes and the subsequent triggering of specific cellular pathways. Ca^{2+}-sensitive processes include contraction, fertilisation, membrane excitability, secretion, metabolism, proliferation and apoptosis. 'OFF' mechanisms, which include pumps and exchangers, restore Ca^{2+} to its resting concentration.

Despite this basic summary of the Ca^{2+} signalling toolkit, the changes in the cytoplasmic Ca^{2+} concentration are spatially and temporally complex.[70] Of particular significance is the cell's ability to localise Ca^{2+} signals to certain regions by creating high local concentrations of Ca^{2+}, called microdomains, which are different from the cytoplasmic average. This localisation enables cellular activities, such as ion channel and transcription factor activation, to be controlled from discrete regions. For example, regulated exocytosis can occur at one site within the cell without interfering with Ca^{2+}-dependent physiological processes that take place at a different cellular location.[71] Locally-derived Ca^{2+} signals are as a result of the close proximity of organelles, such as

mitochondria and ER, and their ability to regulate local Ca^{2+} concentrations. This control over local Ca^{2+} concentrations is achieved due to the brief open time of ion channels, localisation of Ca^{2+} by buffering and the clustering of ion channels.[70]

Mitochondria were initially recognised for their ability to produce ATP *via* oxidative phosphorylation. However, they are also major regulators of vascular smooth muscle Ca^{2+} microdomains.[70] They accumulate, store and release Ca^{2+} and thereby alter the spatio-temporal pattern of Ca^{2+} gradients.[72] Interestingly, mitochondria are simultaneously integrated in the regulation of ion channels and Ca^{2+} transporters, oxygen radical production, metabolite recycling and intracellular redox potential.[73]

Mitochondrial Ca^{2+} uptake occurs *via* the Ca^{2+}-selective uniporter in the inner mitochondrial membrane, which is driven by the electrical potential ($\Delta\Psi_m$ of -150 to -180 mV) across the inner mitochondrial membrane.[72] Ca^{2+} efflux occurs *via* a Na^+(or H^+)-Ca^{2+} antiporter mechanism in which Ca^{2+} efflux proceeds at a constant rate, unaffected by increases in mitochondrial Ca^{2+} concentration.[72] During rapid rises in cytoplasmic Ca^{2+} concentration, mitochondria tend to accumulate Ca^{2+} and only release it slowly back into the cytosol.[74] Mitochondria accumulate Ca^{2+} during a range of Ca^{2+} signalling events, from muscle contraction to fertilisation.[70]

It is established that mitochondria play an important role in development of microdomains. However, much of what is understood of the role of

mitochondria in regulating Ca^{2+} signalling has been inferred from pharmacological approaches in which mitochondrial activity is inhibited throughout the entire cell. Such approaches lack spatial discrimination and have been unable to determine how the local activity of mitochondria controls Ca^{2+} signals in small regions and how these microdomains control signals throughout the cell. Such a study would require the selective activation or inhibition of mitochondria in subcellular regions of the intact, native cell. It was hypothesised that caging technology could be employed for such a study. The spatio-temporally controlled photolytic release of a mitochondrial inhibitor would allow for the inhibition of a sub-population of mitochondria in an intact cell.

A protonophore is a compound with an extensive conjugated π-orbital system and an acidic proton. Such molecules can dissipate proton and charge gradients across biological membranes by cycling across them as either the protonated acid or deprotonated conjugate base. This results in an increase of proton conductance, which, in mitochondria, uncouples proton gradient formation from ATP production and causes the electrical potential across the inner mitochondrial membrane, $\Delta\Psi_m$, to collapse. Protonophores such as carbonyl cyanide 3-chlorophenylhydrazone (CCCP) **91**, carbonylcyanide 4-trifluoromethoxy phenylhydrazone (FCCP) **92** and 2,4-dinitrophenol (DNP) **93** (Figure 2.1) are commonly used to dissipate $\Delta\Psi_m$ and thus inhibit mitochondrial functions, such as Ca^{2+} uptake.

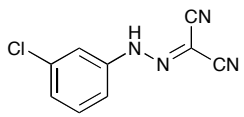

91

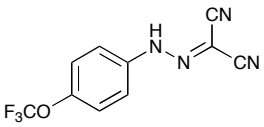

92

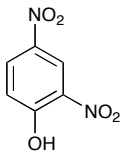

93

Figure 2.1. Protonophores commonly used to dissipate $\Delta\Psi_m$ - carbonyl cyanide 3-chlorophenylhydrazone (CCCP) **91**, carbonylcyanide 4-trifluoromethoxy phenylhydrazone (FCCP) **92** and 2,4-dinitrophenol (DNP) **93**.

The tyrphostin AG10 **94** (Figure 2.2) is a mitochondrial uncoupler[75] which acts as a protonophore causing an increase in the rate of oxygen consumption and 90% reduced cellular ATP concentration by uncoupling the oxidative phosphorylation pathway from ATP production.

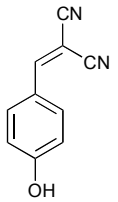

94

Figure 2.2. The mitochondrial uncoupler AG10 **94**.[75]

It was proposed that one approach to study how mitochondria acting in localised regions control the global Ca^{2+} signalling of the cell is to photolyse a caged protonophore. It was envisaged that photolysis of caged-AG10 in small, restricted regions of the cell could be used to achieve spatially predefined

mitochondrial coupling, in which only mitochondrial activity at the site of photolysis is inhibited.

2.2. Synthesis of Caged-AG10 Derivatives

AG10 was caged with a DMNB caging group in the presence and absence of a carbonate linker. The caging group was coupled to the phenolic position of AG10 as this is the functional group which is essential for its biological activity as a proton "shuttle" in order to dissipate $\Delta\Psi_m$.

The first step towards the synthesis of DMNB-caged AG10 **98** (Scheme 2.1) was the *O*-alkylation of 4-hydroxybenzaldehyde **96** with 3,4-dimethoxy-2-nitrobenzyl bromide **95** using DMF and K_2CO_3 at 40 °C to afford the DMNB-benzaldehyde derivative **97** in a reasonable yield. Condensation of DMNB-caged benzaldehyde **97** with malononitrile in a Knoevenagel-like condensation reaction proceeded smoothly and the desired product **98** was obtained in modest yield, Scheme 2.1. The synthesis of DMNB-caged AG10 directly from AG10 **94** was not possible. This may be because free AG10 is not a good enough nucleophile to react with DMNB bromide **95**. As 4-hydroxybenzaldehyde **96** has a less extensive conjugated π-system than AG10 **94**, it was envisaged that this compound would be sufficiently nucleophilic to react with DMNB bromide **95**. This proved to be the case and the synthesis of DMNB-caged benzaldehyde **97** was achieved as discussed.

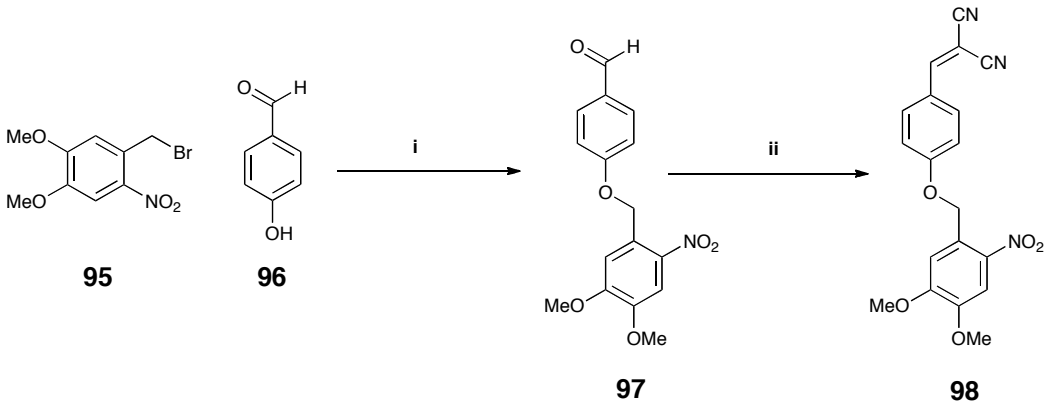

Scheme 2.1. Syntheses of DMNB-caged AG10 **98**. *Reagents and conditions:* i. DMNB bromide, DMF, K_2CO_3, 40 °C, 83%; ii. $CH_2(CN)_2$, piperidine, EtOH, reflux, 50%.

The addition of a carbonate linker between the biologically active compound and the caging group can alter the wavelengths at which the compound absorbs.[76] This linker may allow for photolysis at a biologically less damaging (longer) wavelength or an improved quantum yield.[13] Therefore, it was decided to synthesise the DMNB-caged AG10 derivative with a carbonate linker **99**. In order to incorporate the carbonate linker, 4-hydroxybenzaldehyde **96** was reacted with malononitrile in another Knoevenagel-like condensation reaction to form free AG10 **94**, Scheme 2.2. This product was reacted with 4,5-dimethoxy-2-nitrobenzyl chloroformate in the presence of 3.0 equivalents of triethylamine to obtain DMNB-carbonate (CDMNB)-caged AG10 **99** in modest yield.

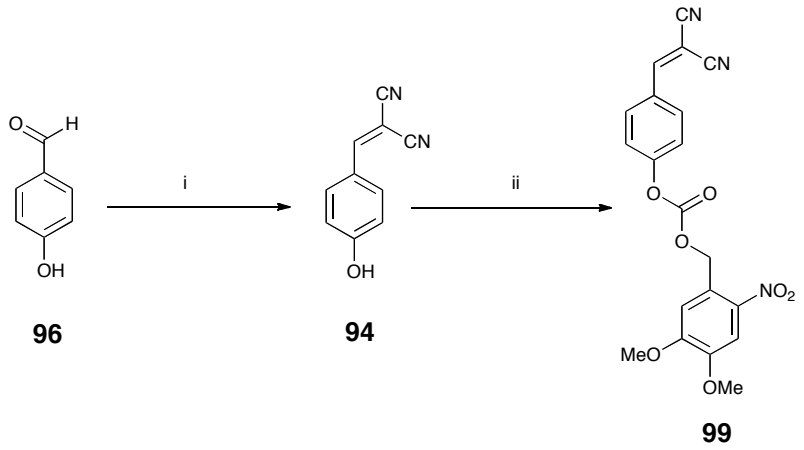

96 **94** **99**

Scheme 2.2. Syntheses of DMNB carbonate-caged AG10 **99**. *Reagents and conditions*: i. $CH_2(CN)_2$, piperidine, EtOH, reflux, 82%; ii. DMNB chloroformate, NEt_3, THF, RT, 37%.

2.3. UV/Vis Spectra of Caged AG10 Derivatives

UV-Vis absorption spectra were obtained to provide an indication of which wavelengths were most likely to evoke successful photolysis. Two peaks were observed in the UV/Vis spectrum of AG10 **94** (0.1 mM in methanol) (Figure 2.3), one with λ_{max} of 353 nm and a second with λ_{max} of 423 nm. It was speculated that this second peak might be as a result of a small amount of deprotonated AG10 in the methanol solution. To test this hypothesis, the UV/Vis spectrum of AG10 was obtained in both acidic (0.1 mM in methanol, HCl added to attain apparent pH 2) and basic (0.1 mM in methanol, DBU added to attain apparent pH 12) conditions (Figure 2.3). It was observed that under acidic conditions the peak at 423 nm completely disappeared and only the peak at 353 nm, with an extinction co-efficient (ε) of 33915 $L.mol^{-1}.cm^{-1}$, was present. Conversely, under basic conditions the peak at 353 nm

completely disappeared and a peak at 416 nm was present. These results seem to confirm the hypothesis that the peak at 423 nm is due to deprotonated AG10.

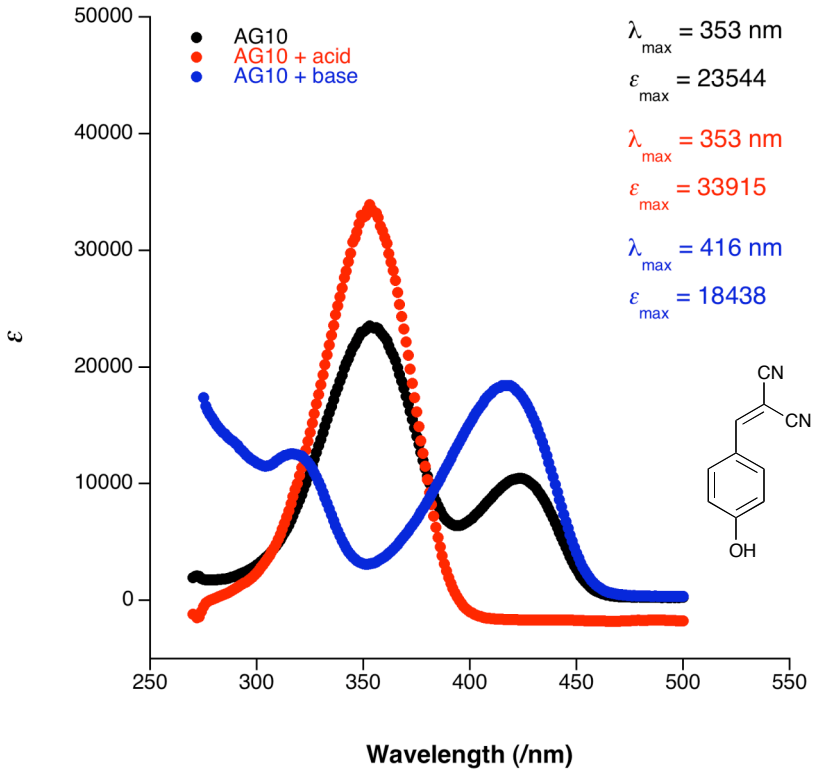

Figure 2.3. AG10 **94** UV/Vis spectrum (0.1 mM in MeOH) (black), AG10 UV/Vis spectrum (0.1 mM in MeOH, HCl added to attain apparent pH 2) (red), AG10 UV/Vis spectrum (0.1 mM in MeOH, DBU added to attain apparent pH 12) (blue). ε = extinction co-efficient, $L.mol^{-1}.cm^{-1}$.

DMNB-caged AG10 **98** (0.1 mM in DMSO) was observed to have λ_{max} of 351 nm and an extinction co-efficient (ε) of 43803 $L.mol^{-1}.cm^{-1}$. CDMNB-caged AG10 **99** (0.1 mM in DMSO) had λ_{max} of 316 nm and an extinction co-efficient (ε) of 12057 $L.mol^{-1}.cm^{-1}$, Figure 2.4. The lower extinction co-efficient

of CDMNB-caged AG10 **99** suggests that its photolysis may be less efficient than DMNB-AG10 **98**, because its absorption is not as strong.

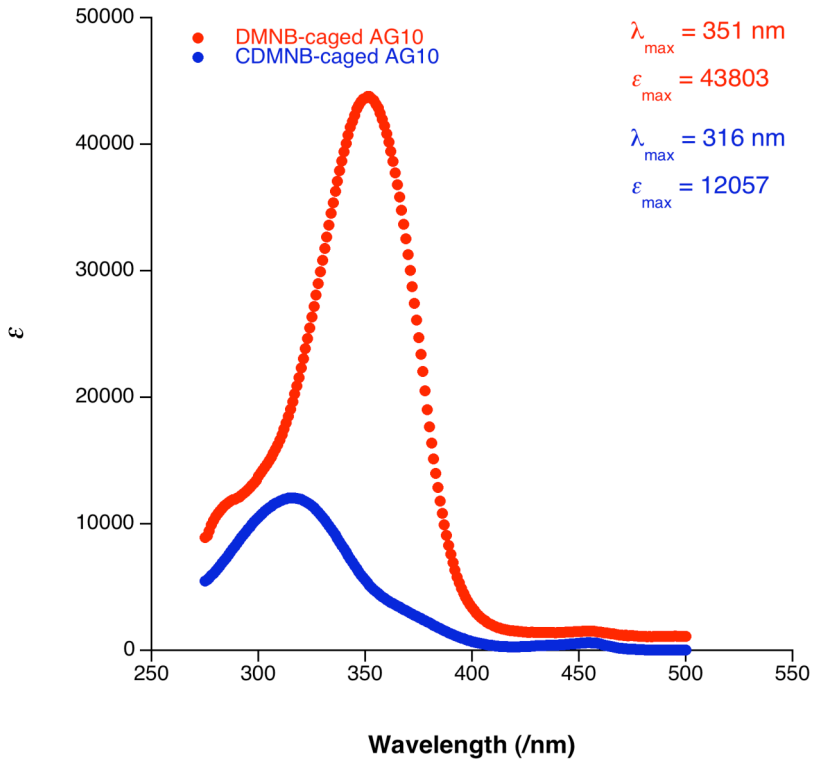

Figure 2.4. DMNB-caged AG10 **98** UV/Vis spectrum (0.1 mM in DMSO) (red); CDMNB-caged AG10 **99** UV/Vis spectrum (0.1 mM in DMSO) (blue). ε = extinction co-efficient, $L.mol^{-1}.cm^{-1}$.

2.4. Photolysis Studies of the Caged AG10 Derivatives

Photolysis of the caged AG10 derivatives was carried out with the assistance of our collaborators at the School of Physics and Astronomy, University of St Andrews, Craig McDougall and Dr Tom A. Brown. Please refer to the General Experimental Section for details of experimental procedures.

A 3 mM solution of each caged compound in DMSO was prepared. Care was taken to protect the solutions from exposure to background UV irradiation. During photolysis experiments, aliquots (1 mL) of the solution were placed into UV transmitting cuvettes and exposed to radiation from the given laser source for fixed time durations. A continuous wave (CW) laser diode provided light of 375 nm at powers of up to 8 mW. Other wavelengths were obtained using an optical parametric oscillator that was pumped at 355 nm by a frequency tripled Nd:YAG laser. After exposure to laser radiation the samples were analysed and photolysis quantified using ^{1}H NMR and HPLC. Quantification by ^{1}H NMR involved the addition of a known concentration of hexamethyldisiloxane standard to each photolysis sample. HPLC analysis was carried out using a Phenomenex, Gemini 5 µ C18 110A, 25.0 × 4.60 mm column and Gilson HPLC setup. The column was run using a gradient of water and acetonitrile with 0.05% trifluoroacetic acid. Quantification was achieved using previously measured calibration curves for AG10 **94**, DMNB-AG10 **98** and CDMNB-AG10 **99**.

2.4.1. Quantitative Photolysis of DMNB-Caged AG10 98

Before the caged compounds were used for *in vitro* studies, their photolysis characteristics were investigated. DMNB-caged AG10 **98** was irradiated at 355 nm, at 95 mJ of energy for 1, 2, 3, 4, and 5 minutes. As it is possible for a number of photolytic degradation products to form, it was important to establish that AG10 **94** was being formed during photolysis. A control sample, which was left on the bench for the duration of the experiment, but not

exposed to laser irradiation, was also analysed. The control sample did not contain any free AG10. It was found that the percentage of free AG10 **94** did increase over time while the percentage of caged material **98** decreased over time. Photolysis of the DMNB-caged AG10 derivative **98** for 5 minutes gave rise to 35% of the total material being AG10 when analysed by ^{1}H NMR and 46% of the total material being AG10 when analysed by HPLC, as shown in Figure 2.5. It is generally accepted that HPLC analysis is more sensitive that ^{1}H NMR analysis when quantitative data are required. More AG10 **94** (produced by photolysis) was detected by HPLC than was detected by ^{1}H NMR, and hence greater values for the percentage of AG10 present were observed. However, the general trends in amount of photolysis were similar for both methods of detection.

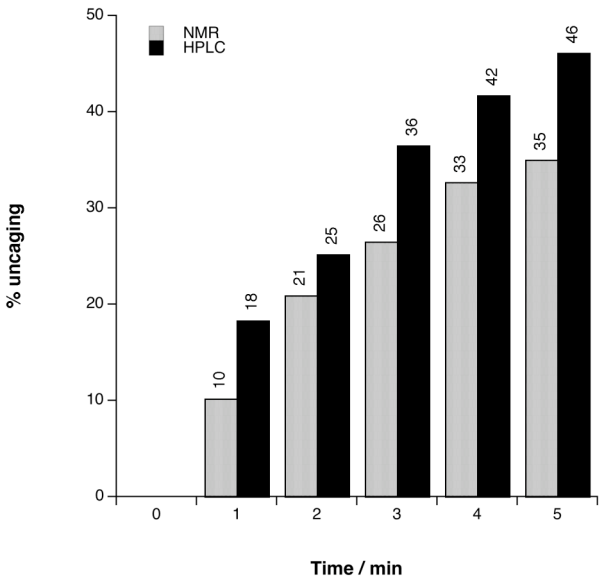

Figure 2.5. Quantification of the percentage of AG10 **94** present after photolysis of DMNB-caged AG10 **98**, following irradiation at 95 mJ, 355 nm in DMSO for 1, 2, 3, 4 and 5 minutes. Photolysis samples were analysed by ^{1}H NMR with hexamethyldisiloxane standard in CD_2Cl_2 (grey bars) and by HPLC (black bars).

The ^{1}H NMR spectra of the photolysis samples of DMNB-caged AG10 **98** after exposure to irradiation at 95 mJ, 355 nm in DMSO after 0, 1, 2, 3, 4 and 5 minutes are overlaid in Figure 2.6. The partial ^{1}H NMR spectrum labelled 'control' is that of a sample of DMNB-caged AG10 which was left on the bench for the duration of the experiment, but not exposed to laser irradiation. The partial ^{1}H NMR spectrum labelled 'AG10' is that of a synthetic sample of AG10 in the same solvent system as the photolysis sample. These spectra confirm that photolysis of DMNB-caged AG10 **98** led to the loss of caged AG10 and the appearance of free AG10 **94**. During photolysis, the appearance and growth of doublets at 7.82 and 6.88 ppm correspond to the release of AG10 from DMNB-caged AG10.

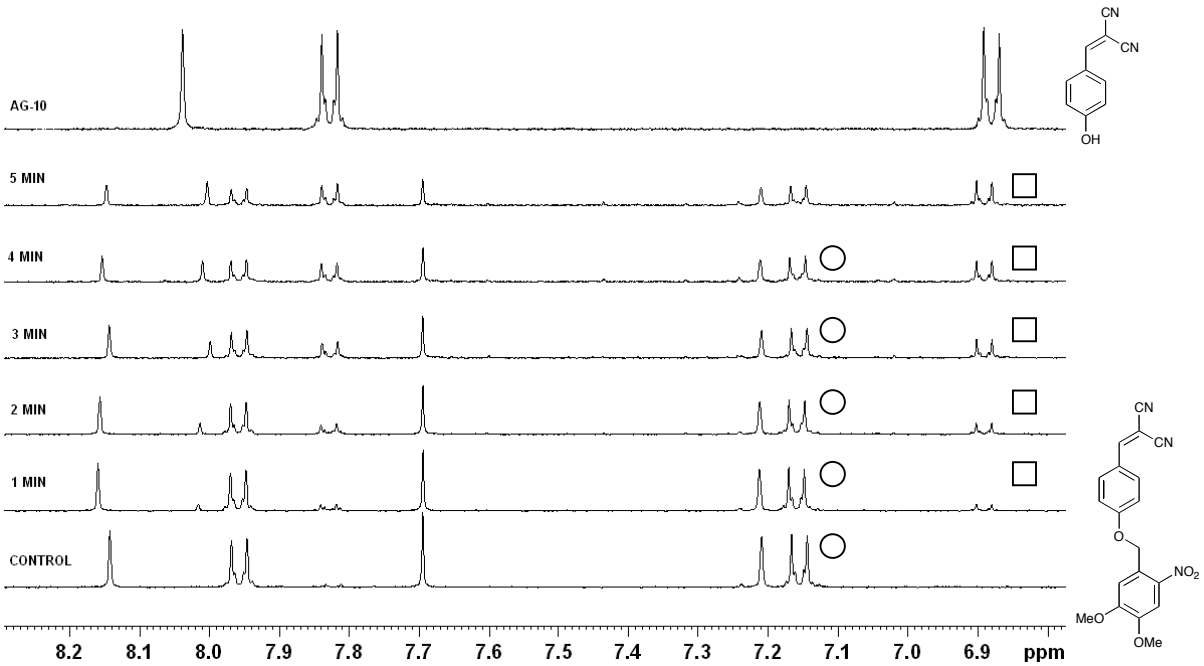

Figure 2.6. Partial 300 MHz ^{1}H NMR spectra of DMNB-caged AG10 **98** photolysed at 95 mJ, 355 nm in DMSO for 0, 1, 2, 3, 4 and 5 minutes. Hexamethyldisiloxane standard in CD_2Cl_2 was added to each sample after irradiation. Peaks corresponding to DMNB-caged AG10 **98** (○) diminished during the photolysis run. The aromatic peak at 6.89 ppm (□) from uncaged AG10 **94** was seen to appear and grow during the photolysis run. The control sample, in which the caged compound was not exposed to laser irradiation, did not possess any uncaged material. The top spectrum of pure AG10 with standard confirms that it was AG10 that was released during photolysis.

2.4.2. Quantitative Photolysis of CDMNB-Caged AG10 99

CDMNB-caged AG10 **99** was irradiated at 355 nm, 95 mJ for 1, 2, 3, 4, and 5 minutes. A control sample, which was left on the bench for the duration of the experiment, but not exposed to laser irradiation, was also analysed. The

control sample did not contain any free AG10. It was found that the percentage of free AG10 **94** did increase over time, however, not as much as during the photolysis of DMNB-caged AG10 **98**. Under the same conditions employed for photolysis of DMNB-AG10 **98**, photolysis of CDMNB-caged AG10 **99** for 5 minutes resulted in only 26% (^{1}H NMR) – 29% (HPLC) release of free AG10, as shown in Figure 2.7. Both methods used for the quantification of photolysis gave comparable results.

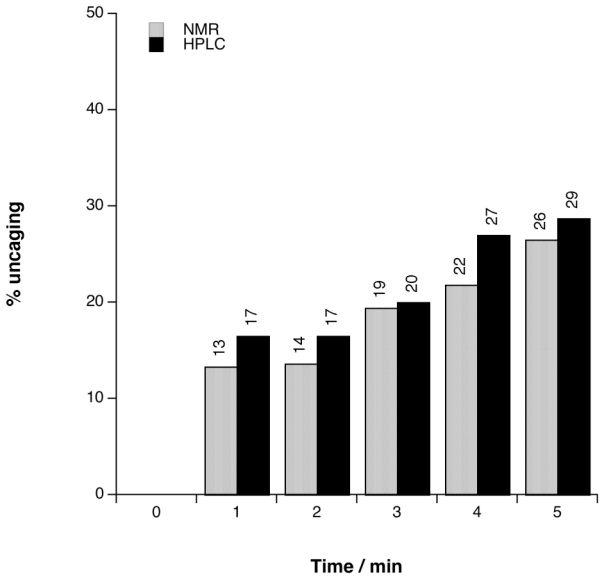

Figure 2.7. Quantification of the percentage of AG10 **94** present after photolysis of CDMNB-caged AG10 **99**, following irradiation at 95 mJ, 355 nm in DMSO for 1, 2, 3, 4 and 5 minutes. Photolysis samples were analysed by ^{1}H NMR with hexamethyldisiloxane standard in CD_2Cl_2 (grey bars) and by HPLC (black bars).

The ^{1}H NMR spectra of the photolysis samples of CDMNB-caged AG10 **99** after exposure to irradiation at 95 mJ, 355 nm in DMSO after 0, 1, 2, 3, 4 and 5 minutes are overlaid in Figure 2.8. These spectra confirm that photolysis of CDMNB-caged AG10 **99** led to the loss of caged AG10 and the appearance

of free AG10 **94**. During photolysis, the appearance and growth of doublets at 7.82 and 6.88 ppm correspond to the release of AG10 from CDMNB-caged AG10.

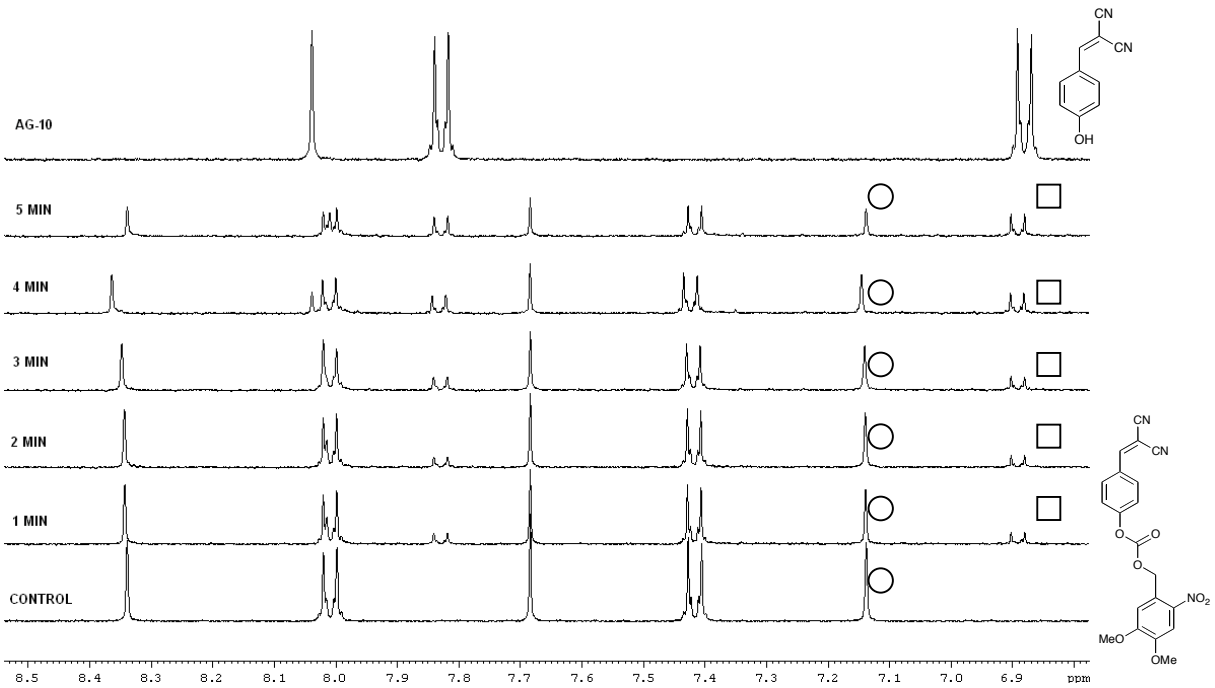

Figure 2.8. Partial 300 MHz ^{1}H NMR spectra of CDMNB-caged AG10 **99** photolysed at 95 mJ, 355 nm in DMSO for 0, 1, 2, 3, 4 and 5 minutes. Hexamethyldisiloxane standard in CD_2Cl_2 was added to each sample after irradiation. Peaks corresponding to CDMNB-caged AG10 **99** (○) diminished during the photolysis run. The aromatic peak at 6.89 ppm (□) from uncaged AG10 **94** was seen to appear and grow during the photolysis run. The top spectrum of pure AG10 with standard confirms that it was AG10 released during photolysis.

2.4.3. Determining Whether Heating Causes Uncaging

A 1 mL aliquot of a 3 mM solution of DMNB-AG10 **98** in DMSO was photolysed at 95 mJ for 5 minutes. The temperature was recorded at 1-minute intervals. It was found that the maximum temperature obtained during this time was 55 °C.

A fresh 1 mL aliquot of a 3 mM sample of DMNB-AG10 **98** in DMSO was heated at 65 °C for 5 minutes, covered in foil to prevent exposure to light. ^{1}H NMR analysis of the heated sample, using the hexamethyldisiloxane standard, confirmed that no uncaging had occurred. Only DMNB-caged AG10 **98** was detected.

2.5. Application of Caged AG10 to a Biological System

Biological evaluation of the caged AG10 compounds was carried out by our collaborators at the Department of Physiology and Pharmacology at the University of Strathclyde, Dr Susan Chalmers and Prof. John G. McCarron. Please refer to General Experimental Section for details of experimental procedures.

Firstly, it was necessary to confirm that AG10 **94** does act as an uncoupler and cause mitochondrial depolarisation. Freshly isolated colonic myocytes were loaded with the $\Delta\Psi_m$-sensitive fluorescent dye, tetramethylrhodamine, ethyl ester perchlorate (TMRE). TMRE is a lipophilic, cationic, fluorescent dye that accumulates within mitochondria according to their electrical potential ($\Delta\Psi_m$). $\Delta\Psi_m$ depolarisation decreases mitochondrial TMRE concentration, which results in a decrease in TMRE fluorescence. The observation that cells loaded with TMRE showed a loss of TMRE fluorescence upon addition of 100 μM AG10 **94** to the bathing solution, indicated that AG10 does act as an uncoupler resulting in mitochondrial depolarisation as reported,[75] as shown in Figure 2.9.

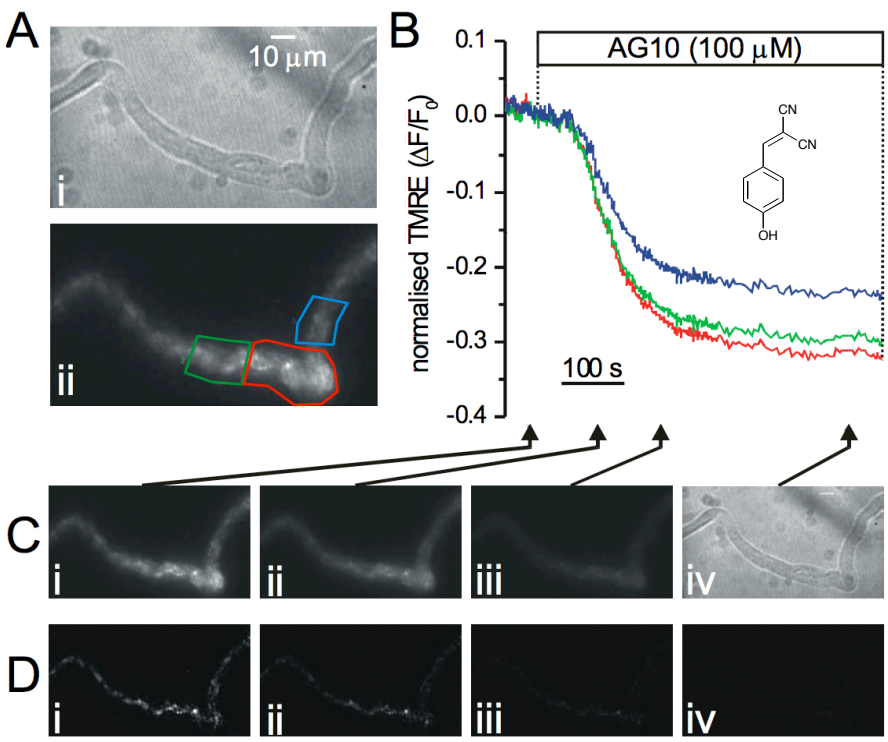

Figure 2.9. AG10 **94** rapidly causes mitochondrial depolarisation. Freshly isolated colonic myocytes (shown in brightfield, Ai) were loaded with the $\Delta\Psi_m$-sensitive fluorescent dye TMRE (10 nM, Aii). AG10 (100 μM, added to the bathing solution; B) caused a loss of TMRE fluorescence, indicating $\Delta\Psi_m$ depolarisation (regions shown in Aii are plotted in B). Example images of TMRE fluorescence are shown in panel Ci-iv. Panel D contains the same images as panel C but where mitochondrial fluorescence was enhanced by "top-hat" edge detection analysis.

Having observed the effect of free AG10 **94** *in vitro*, the caged AG10 derivatives were applied to the same cell line. DMNB-caged AG10 **98** was photolysed within isolated myocytes. DMNB-caged AG10 (25 μM) was introduced into the cytosol of freshly isolated colonic smooth muscle cells using the whole-cell patch clamp configuration. Photolysis of DMNB-caged AG10 **98** for 4 minutes resulted in $\Delta\Psi_m$ depolarisation, as indicated by the

localised loss of TMRE fluorescence, shown in Figure 2.10. What was significant was that the loss of TMRE fluorescence, and therefore $\Delta\Psi_m$ depolarisation, was only observed at the site of photolysis, even after 20 minutes. The fact that mitochondrial depolarisation did not spread throughout the cell suggests that the photoreleased AG10 **94** incorporates into nearby intracellular membranes, causing localised $\Delta\Psi_m$ depolarisation, and does not diffuse throughout the cell, presumably due to its hydrophobic nature.

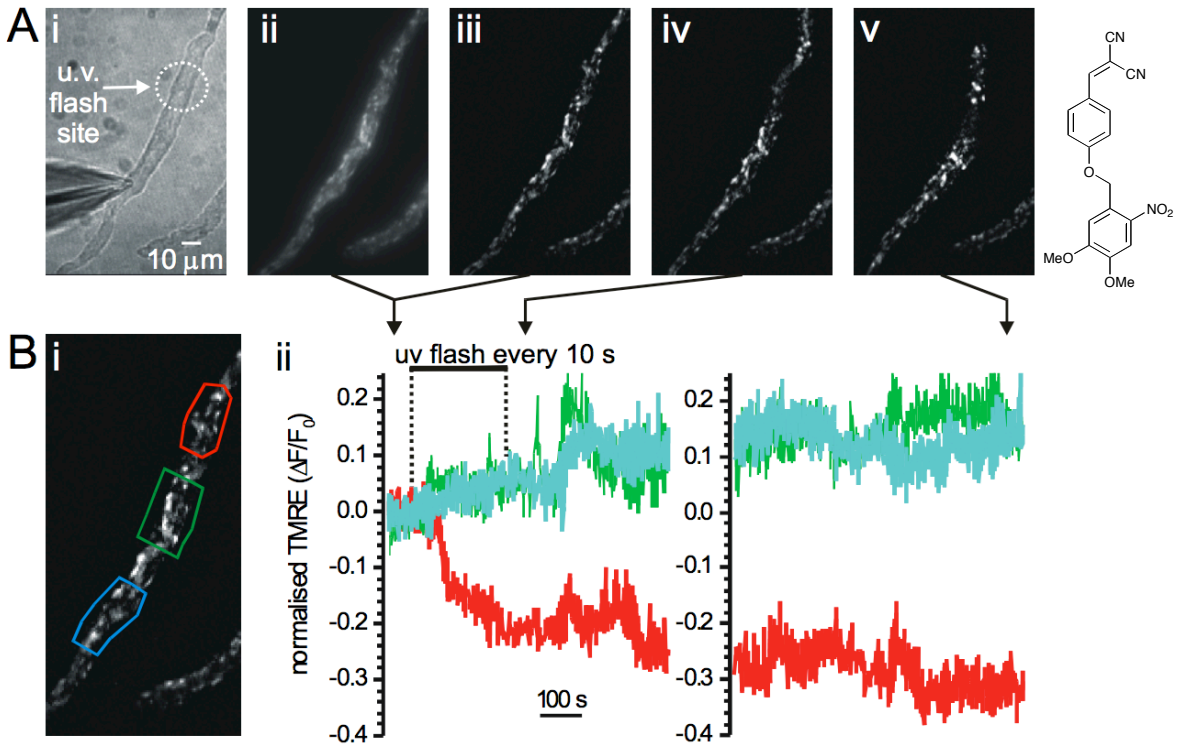

Figure 2.10. Localised mitochondrial depolarisation following photolytic release of AG10 **94** (from DMNB-caged AG10 **98**) in a small region of the cell. Isolated colonic myocytes were loaded with the $\Delta\Psi_m$-sensitive fluorophore TMRE (10 nM) then voltage-clamped in the whole-cell configuration. **Ai:** Brightfield image of a cell with the site of localised photolysis highlighted. TMRE fluorescence is predominantly localised to mitochondrial structures (**Aii**). **Aii-v:** TMRE fluorescence was reduced only in the region of photolytic release of AG10 **94** and did not spread throughout the cell over the following 20 minutes as shown by the dark region in **Av** only at the photolysis site. TMRE fluorescence actually increased in regions neighbouring the site of AG10 release (highlighted in red and blue), presumably due to dye relocation – TMRE moving out of the photolysed region and into the surrounding regions.

CDMNB-caged AG10 **99** was employed in a similar experiment. However, because this compound has greater solubility in DMSO and water than DMNB-caged AG10 **98**, a higher concentration of caged compound could be delivered into the myocytes (62 μM versus 25 μM for DMNB-caged AG10). For this reason, despite the presumed less efficient photolysis of this caged compound, more noticeable and rapid mitochondrial depolarisation was observed when this compound was photolysed within the cells, as shown in Figure 2.11. The 'flash site' is highlighted in red and only in this region was a loss of fluorescence (and therefore $\Delta\Psi_m$ depolarisation) observed over time.

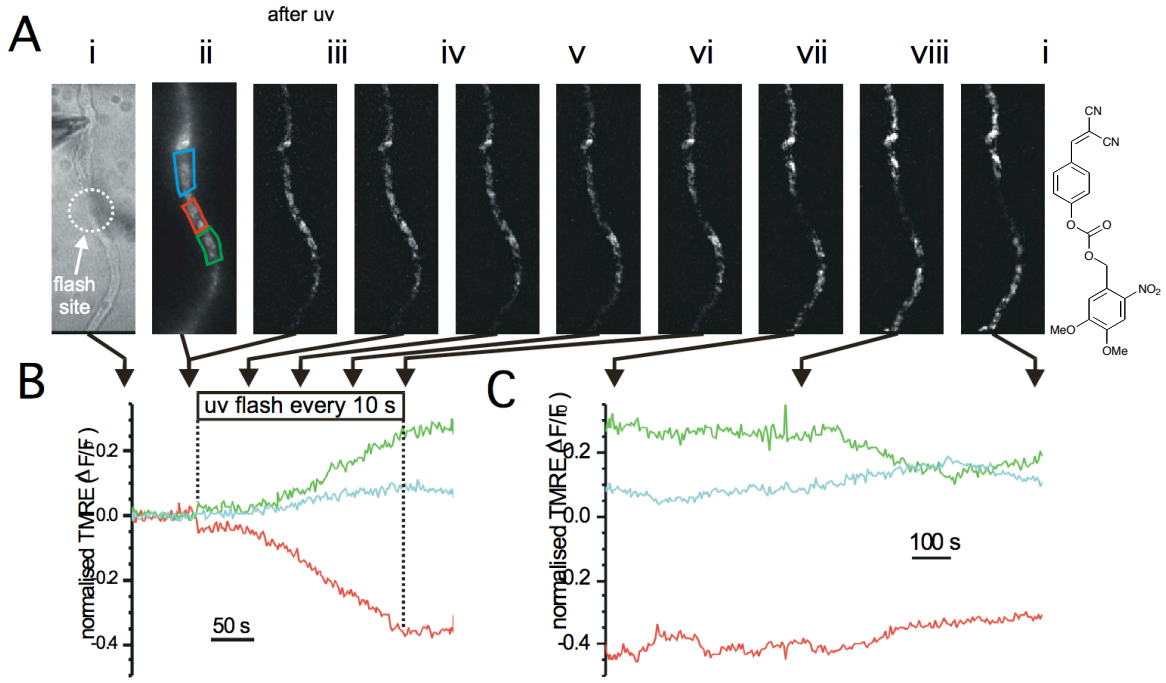

Figure 2.11. CDMNB-caged AG10 **99** was photolysed to evoke $\Delta\Psi_m$ depolarisation in a single smooth muscle cell. Isolated colonic myocytes were loaded with the $\Delta\Psi_m$-sensitive fluorophore TMRE (10 nM) then voltage-clamped in the whole-cell configuration. CDMNB-caged AG10 (62 μM) was introduced to the cytosol *via* the pipette solution. Ai: Brightfield image of a cell with the site of localised photolysis ('flash site') highlighted. TMRE fluorescence (Aii-Ax) is predominantly localised to mitochondria and was reduced only in the region of photolytic release of AG10 **94**. The images (Aii-x) are derived from the time points indicated by arrows to line traces of the data in B & C. The TMRE fluorescence measurements (B & C) are derived from the corresponding coloured areas in Aii; red is the flash site. TMRE fluorescence decreased only in the region of photolysis.

In order to confirm that neither UV light alone nor the caged compound in the absence of UV light cause mitochondrial depolarisation, control experiments

were carried out. In the absence of DMNB-caged AG10 **98**, repetitive exposure to UV flashes produced no reduction of TMRE fluorescence. TMRE fluorescence was also unaffected by DMNB-caged AG10 **98** in the absence of UV light.

Exposure to intense light in the presence of mitochondrially-loaded fluorescent dyes may depolarise mitochondria *via* the production of free radicals or other oxidative species.[77] To determine whether oxidative species contribute to $\Delta\Psi_m$ depolarisation observed after photolytic release, AG10 **94** was released in two separate regions of the same cell. In this experiment, the first photolysis event occurred in the absence, and the second in the presence of a cocktail of antioxidants (ascorbic acid (1 μM), catalase (250 units/mL), (*R*)-Trolox methyl ether (Trolox, 1 mM) and 2,2,6,6-tetramethylpiperidin-1-yloxy (TEMPO, 500 μM)). $\Delta\Psi_m$ depolarisation by localised photolytic release of AG10 **94** was unchanged by the presence of the antioxidants.

2.6. Summary

In summary, the synthesis and characterisation of two novel caged AG10 derivatives has been reported.[78] It has been demonstrated that the photolysis of these compounds leads to the release of AG10 **94**. Localised photorelease of AG10, furthermore, leads to mitochondrial uncoupling only in regions proximal to the photolysis site. Despite the less efficient photolysis observed for CDMNB-caged AG10 **99**, it is better suited for applications in biological systems due to its improved solubility in aqueous solutions, compared with DMNB-caged AG10 **98**. These novel caged AG10 derivatives have allowed, for the first time, mitochondrial uncoupling in a spatially predefined manner. It is envisaged that caged AG10 will be used as a tool to clarify the role of localised mitochondrial activity in Ca^{2+} signalling.

Chapter 3:

Results and Discussion - Design and Development of Tools to Study TRPV1

3. Design and Development of Tools to Study TRPV1

The aim of this project was to design and synthesise caged molecular probes to investigate the TRPV1 receptor, which is involved in processes such as pain mediation, with spatial and temporal control. It was aimed to employ caged TRPV1 agonists and antagonists to selectively control receptor activation and inhibition with light. In the final section of this chapter, caged membrane-impermeant TRPV1 agonists were designed to probe the location of the TRPV1 agonist-binding site, which is currently ambiguous.

3.1. Caged TRPV1 Agonists and Antagonists

3.1.1. Introduction to TRPV1

Capsaicin is the main pungent component of chilli peppers. Application to the skin and tongue results in a burning sensation.[79] However, application to the eyes, nose, mouth and throat produces an intensely painful sensation. Pain is experienced as a result of noxious chemical (such as capsaicin), mechanical or thermal stimuli activating a subgroup of sensory neurons, called nociceptors, which transmit information to pain-processing centres in the brain and spinal cord. Nociceptors are characterised by their sensitivity to capsaicin. However, the reason for capsaicin's cellular specificity and its precise mechanism of action were not known. Caterina *et al.* made a significant break-through by identifying, isolating and cloning the capsaicin

receptor.[80] The complementary DNA (cDNA) encoding this receptor was 'fished-out' using a functional screening strategy. A cDNA library from dorsal root ganglion-derived messenger RNA was used to transfect human embryonic kidney-derived cells, which are not capsaicin responsive. Cells which became responsive to capsaicin, as observed by Ca^{2+} influx, were used to narrow down the cDNA library until an individual clone, which conferred capsaicin sensitivity by itself, was found. This receptor was named vanilloid receptor subtype 1 (VR1) and later renamed as transient receptor potential channel, vanilloid subfamily member 1 (TRPV1). It was demonstrated that this receptor is a non-selective cation channel. It is activated by capsaicin and other TRPV1 agonists, heat above 45 °C and pH below 5.[80] TRPV1 is important in both nociception and the inflammatory response. It has, therefore, become a significant therapeutic target.

TRPV1 consists of six transmembrane domains (TM1–TM6), Figure 3.1.[81] The N- and C-termini are on the cytosolic side of the cell membrane. A short, pore-forming hydrophobic region exists between TM5 and TM6. These characteristics are common to all TRP-like proteins, which consists of six members, TRPV1-TRPV6.[82] The C-terminus domain contains a phosphatidylinositol-4,5-bisphosphate (PIP2) binding site. This site plays a key role in capsaicin receptor sensitivity.[83] Mutations that weaken the TRPV1–PIP2 interaction notably reduce the thresholds for chemical and thermal stimuli.[82,83] Mutation studies demonstrated that Glu 600 and 648, in the pore-forming region, are involved in proton activation of TRPV1.[84] The non-selective cation channel is formed from a TRPV1 tetramer. However, whether

the receptor exists functionally as a homomeric or heteromeric tetramer is not fully understood.[81] TRPV1 does not discriminate among monovalent cations but demonstrates a preference for divalent cations.[80]

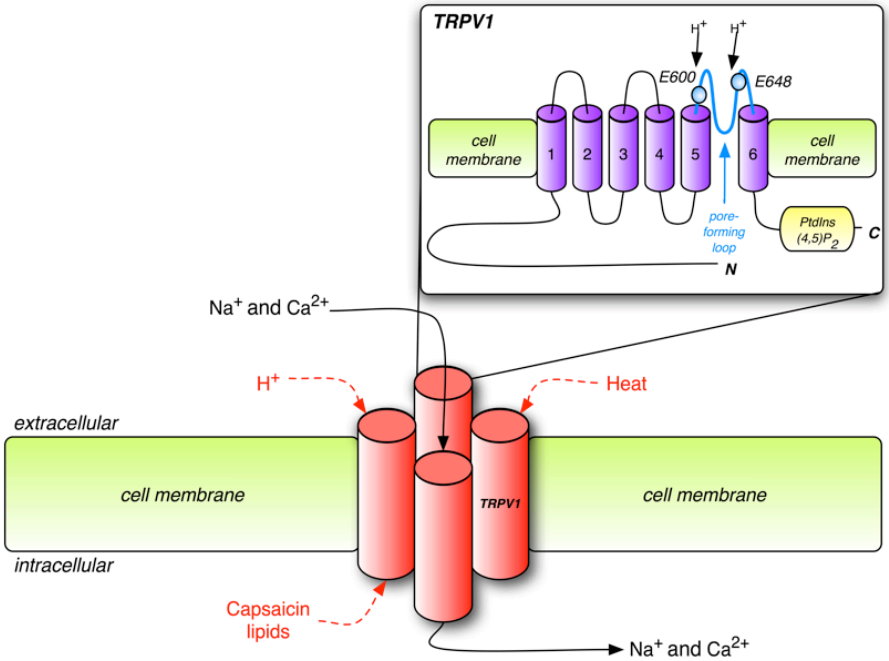

Figure 3.1.[81] A representation of four TRPV1 proteins forming a functional tetrameric ion pore. A single TRPV1 protein is highlighted. It consists of six transmembrane domains. The pore-forming loop between TM5 and TM6, and the PIP2 binding site on the C-terminus are shown. Reproduced by permission of The Royal Society of Chemistry.

TRPV1 is localised to the internal membranes in addition to the plasma membrane. TRPV1 can release Ca^{2+} from endoplasmic stores, upon agonist treatment, as well as permit Ca^{2+} entry from outside the cell,[85] resulting in the generation of an action potential from the nociceptor. This potential is

propagated along the length of the vanilloid-sensitive neuron and may be perceived as an itch or pain in the central nervous system (CNS).

TRPV1 is activated by many exogenous and endogenous ligands. Capsaicin **100**, Figure 3.2, and the ultrapotent daphnane diterpene, resiniferatoxin (RTX) **101**, from the latex of the Moroccan cactus-like plant *Euphorbia resinifera*, are the most well known. Desensitisation of TRPV1 occurs with prolonged exposure to capsaicin and RTX. This is probably due to an agonist-induced conformational change, which ultimately leads to the closing of the channel pore.[86]

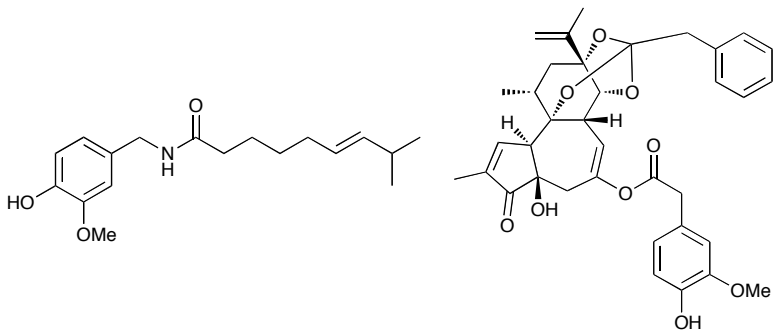

100 **101**

Figure 3.2. Structure of capsaicin **100** and the most potent TRPV1 agonist, RTX, **101**.

Mutation studies undertaken by Julius and Jordt have identified certain residues that are important in ligand binding to TRPV1.[87] Tyrosine 511 is vital for capsaicin activation of TRPV1. Mutation of tyrosine 511 to alanine resulted in a channel that lacked capsaicin sensitivity, but showed the same responses to pH and heat as the wild type receptor. Replacement of the tyrosine residue with phenylalanine had only a moderate effect on capsaicin sensitivity. This

observation suggests that the aromatic nature of residue 511 is essential for ligand binding.[87]

Before TRPV1 was identified as the molecular target of capsaicin, Walpole *et al.* undertook extensive structure-activity studies of capsaicin.[88-90] The compound was divided into three sections, whose structure-activity profiles were investigated systematically. These sections were the aromatic ring, A-region; the amide bond, B-region; and the hydrophobic side chain, C-region, Figure 3.3. In the A-region, it was demonstrated that alkylation of the phenol functional group rendered the molecule biologically inactive.[90] In the B-region, both the amide and reverse amide were tolerated but the bridging atom had to be sp^3 hybridised.[89] The C-region needed to be hydrophobic but the double bond was not necessary. Any hydrophobic alkyl chain between 8 and 12 carbons in length exhibited maximum activity.[88]

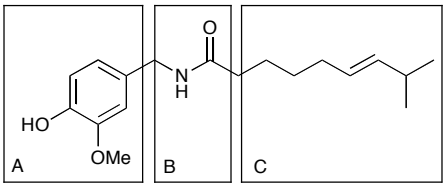

100

Figure 3.3. The division of capsaicin **100** into A, B and C regions in order to investigate its structure-activity relationships.

The identification of TRPV1 as a target for pain-inducing stimuli; and its involvement in urinary urge incontinence, chronic cough and irritable bowel syndrome;[91] has resulted in a massive effort to discover novel TRPV1

antagonists for therapeutic applications.[91,92] The first competitive antagonist of capsaicin activity, capsazepine, was reported in 1994.[93] Since then, a number of small-molecule TRPV1 antagonists are undergoing or have undergone Phase I/II clinical trials for the treatment of chronic inflammatory pain and migraine.[91] However, concerns have been raised about the use of TRPV1 antagonists as drugs.[92,94,95] While TRPV1 is predominantly expressed on nociceptors, it is also present in various brain nuclei[96] and non-neuronal tissues such as the epidermis, urothelium, mast cells, fibroblasts and smooth muscle.[86,96] Therefore, the blockade of TRPV1 by clinical use of TRPV1 antagonists may have serious, complicated effects, especially if they cross the blood-brain barrier. An example of an unexpected effect of a TRPV1 antagonist, considered for therapeutic application, was reported by Gavva *et al*.[94,95] During Phase I clinical trials with the selective TRPV1 antagonist AMG 517, an increase in body temperature (hyperthermia) was observed.[94] Greater understanding into the action of TRPV1 antagonists on different tissue types is required. It remains to be seen if the beneficial actions of TRPV1 antagonists outweigh their adverse effects.[92]

3.1.2. Caged TRPV1 Ligands - Background

Chemical probes that are able to interact selectively with TRPV1 are important for the study of these channels. It would be particularly useful if these probes could be released with temporal and spatial control. Caging technology has, therefore, been employed by a number of research groups.

Zemelman *et al.* were the first to report a 4,5-dimethoxy-2-nitrobenzyl carbonate (CDMNB)-caged capsaicin derivative **102**, Figure 3.4, which was used in their studies of photochemical ion channel gating.[97]

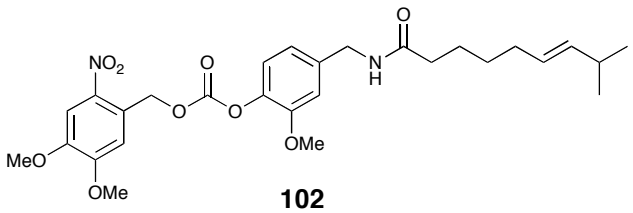

102

Figure 3.4. The first caged capsaicin derivative, a 4,5-dimethoxy-2-nitrobenzyl carbonate (CDMNB)-caged capsaicin derivative **102**, reported by Zemelman *et al.* in 2003.[97]

Katritzky *et al.* synthesised a DMNB-caged biologically inactive capsaicin model compound with only one methyl carbon in the C-region **103**, Figure 3.5. This compound was caged at the phenol position.[76]

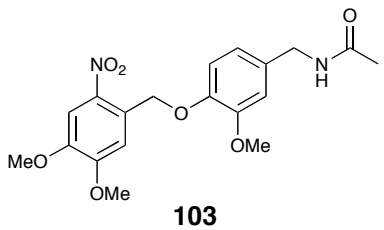

103

Figure 3.5. DMNB-caged inactive capsaicin derivative **103**, reported by Katritzky *et al.* in 2003.[76]

Methoxyphenacyl (MPA)-caged **104** and DMNB-caged **105** TRPV1 agonists, Figure 3.6, were reported by Conway and co-workers.[98] The photorelease of

the TRPV1 agonist nonivamide **116** (Scheme 3.1) was demonstrated in dorsal root ganglion neurons. Nonivamide is a capsaicinoid which is structurally and functionally similar to capsaicin. These caged derivatives were also caged at the phenol position. This is in accordance with the observation by Walpole *et al.* that alkylation of the phenol functional group rendered capsaicin inactive.[90]

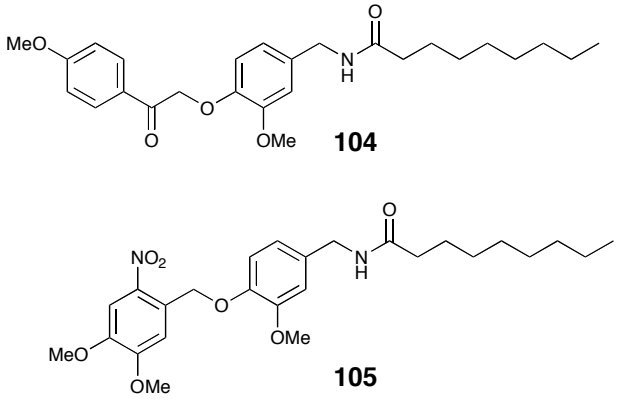

Figure 3.6. Methoxyphenacyl-caged **104** and DMNB-caged **105** TRPV1 agonists, reported by Conway and co-workers.[98]

Zhao *et al.* demonstrated that by attaching the nitrobenzyl or DMNB caging groups to the amide position of the TRPV1 agonist nonivamide, the agonist was rendered biologically inert **106**, Figure 3.7. Photoinduced TRPV1 receptor activation was demonstrated with these compounds.[99]

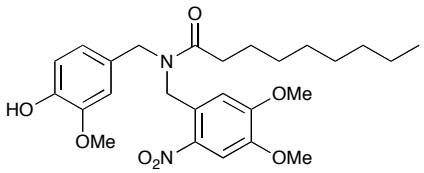

106

Figure 3.7. Attaching the DMNB caging group to the amide position of the TRPV1 agonist nonivamide rendered it biologically inert.[99]

Gilbert *et al.* reported the synthesis of α-carboxy-4,5-dimethoxy-2-nitrobenzyl-caged capsaicin **107**, Figure 3.8. This charged compound had greater solubility in aqueous media but it exhibited residual agonist activity, which limited its use to concentrations below 2 μM.[100] A coumarin-caged derivative, {7-bis(carboxymethyl)amino]coumarin-4-yl}methoxycarbonyl-caged capsaicin **108**, suitable for one- and two-photon photolysis was also synthesised.[100]

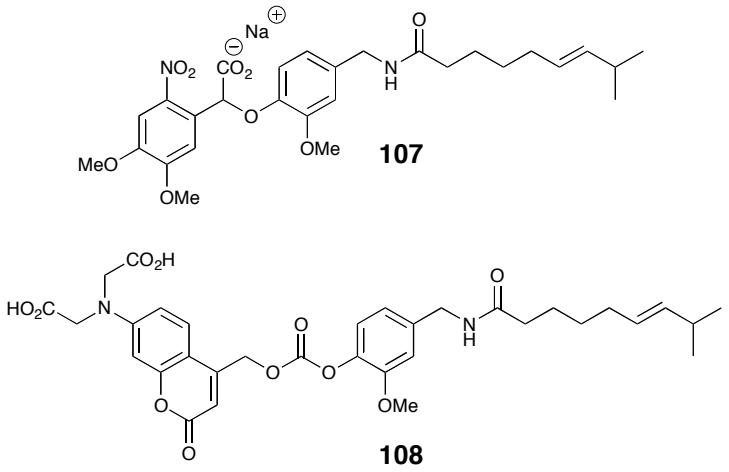

Figure 3.8. Aqueous-soluble α-carboxy-4,5-dimethoxy-2-nitrobenzyl-caged capsaicin **107** and {7-bis(carboxymethyl)amino]coumarin-4-yl}methoxycarbonyl-caged capsaicin **108** reported by Gilbert *et al.*[100]

3.1.3. Aims

The previous caged TRPV1 agonists reported by the Conway group were based on the caging of nonivamide **116** (Scheme 3.1).[98] This compound is synthetically simpler to achieve than capsaicin and has very similar pharmacological activity.[88] As discussed above, alkylation of the phenol functional group renders capsaicin biologically inactive.[90] Therefore, it was proposed to attach the caging group to the phenol functional group of nonivamide in order to terminate its biological activity. In order to extend previous work in the group, it was aimed to cage the TRPV1 agonist with a carbonate-linked DMNB group (CDMNB) in addition to the ether linkage originally employed. Appendino and co-workers have demonstrated that halogenation of nonivamide at the C-6' position yields TRPV1 antagonists.[101] As only caged TRPV1 agonists have been reported, the development of caged TRPV1 antagonists, which would allow inactivation of TRPV1 with spatial and temporal control, was proposed. Therefore, it was aimed to synthesise DMNB- and CDMNB-caged antagonists based on the halogenated nonivamide skeleton. Figure 3.9 illustrates the caged TRPV1 agonist (**105** and **110**) and antagonist (**109** and **111**) synthetic targets.

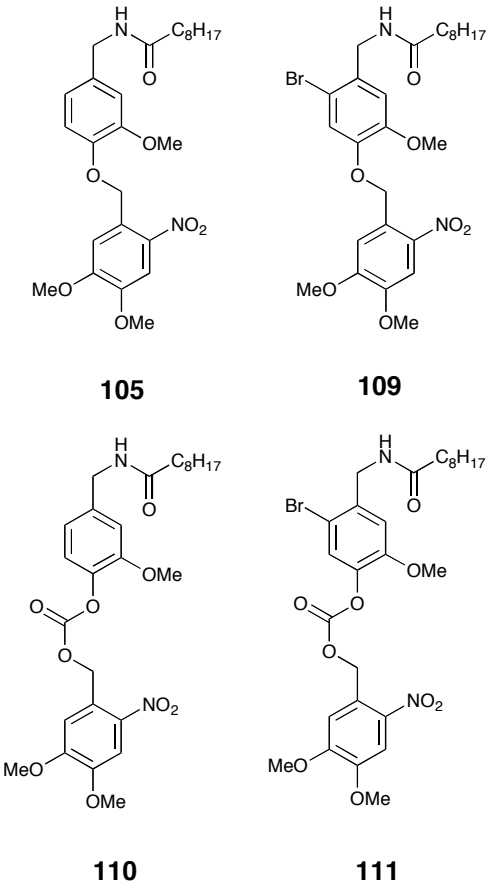

Figure 3.9. The caged TRPV1 synthetic targets: DMNB-caged TRPV1 agonist **105** and antagonist **109**; and CDMNB-caged TRPV1 agonist **110** and antagonist **111**.

3.1.4. Synthesis of Caged TRPV1 Agonists and Antagonists

A synthetic route was developed that afforded both the unhalogenated (agonist) **116** (Scheme 3.1) and halogenated (antagonist) **118** (Scheme 3.2) nonivamide derivatives.[98] The commercially available benzonitrile **112** was protected with a TIPS group using TIPS chloride and imidazole in DMF to obtain **113** in 87% yield, Scheme 3.1. This protection was used to reduce the risk of the phenol reacting with nonanoyl chloride, and also to achieve selectivity in the bromination reaction to synthesise the TRPV1 antagonist **118**, Scheme 3.2. The nitrile group was reduced to the corresponding benzylamine **114** in 80% crude yield by treatment with $LiAlH_4$ in THF. This primary amine was used without further purification and treated with nonanoyl chloride and DMAP in CH_2Cl_2 to obtain the protected TRPV1 agonist **115** in 41% yield. The TIPS group was deprotected with TBAF in THF to afford the TRPV1 agonist, nonivamide **116** in 84% yield.

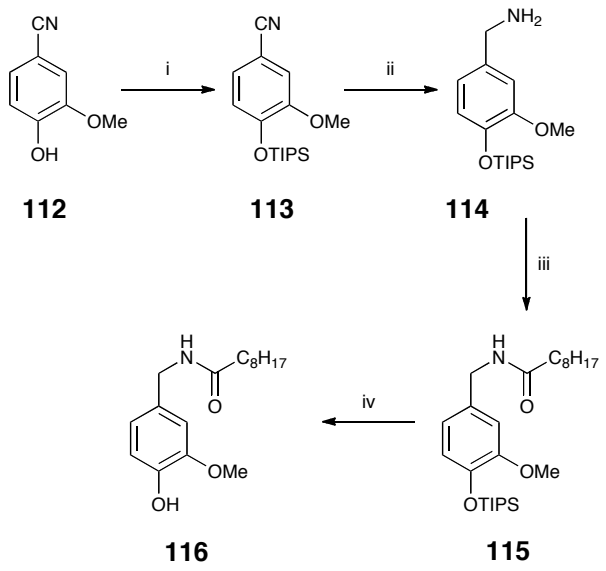

Scheme 3.1. Synthesis of the TRPV1 agonist **116**. *Reagents and conditions:* i. TIPSCl, imidazole, DMF, RT, 87%; ii. $LiAlH_4$, THF, RT, 80% crude yield; iii. Nonanoyl chloride, 4-DMAP, pyridine, CH_2Cl_2, 0 °C → RT, 41%; iv. TBAF, THF, RT, 84%.

In order to synthesise the caged TRPV1 antagonist **118** (Scheme 3.2) it was necessary to brominate the phenyl ring at the 6-positon. Bromination of the TIPS ether **115** was achieved in 71% yield by treatment with bromine in CH_2Cl_2 at -78 °C, Scheme 3.2. The low temperature was required in order to obtain the desired regiochemistry. The TIPS group was deprotected with TBAF in THF to afford the TRPV1 antagonist **118** in 89% yield.

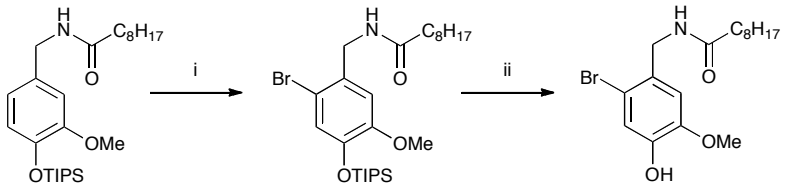

115 **117** **118**

Scheme 3.2. Synthesis of the TRPV1 antagonist **118**. *Reagents and conditions:* i. Br_2, CH_2Cl_2, -78 °C, 71%; ii. TBAF, THF, RT, 89%.

Addition of the DMNB caging group to the unbrominated phenol **116** and the brominated phenol **118** was achieved by treatment with potassium *tert*-butoxide and 4,5-dimethoxy-2-nitrobenzyl bromide, Scheme 3.3. The DMNB-caged agonist **105** (R = H) was obtained in 57% yield while the DMNB-caged antagonist **109** (R = Br) was obtained in 55% yield.

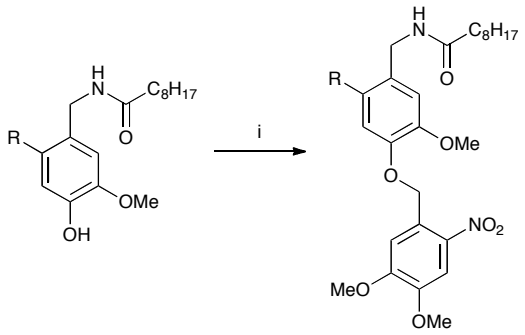

R = H, **116**
R = Br, **118**

R = H, **105**
R = Br, **109**

Scheme 3.3. Protection of the TRPV1 agonist **116** (R = H) and antagonist **118** (R = Br) with the DMNB caging group. *Reagents and conditions:* i. ^{t}BuOK, 4,5-dimethoxy-2-nitrobenzyl bromide, THF, RT. R = H: 57%. R = Br: 55%.

The unbrominated **116** and brominated phenols **118** were also reacted with 4,5-dimethoxy-2-nitrobenzyl chloroformate in the presence of triethylamine to afford the ligands coupled to the DMNB group *via* a carbonate linker, Scheme 3.4. The CDMNB-caged agonist **110** (R = H) was obtained in 96% yield while the CDMNB-caged antagonist **111** (R = Br) was obtained in 92% yield.

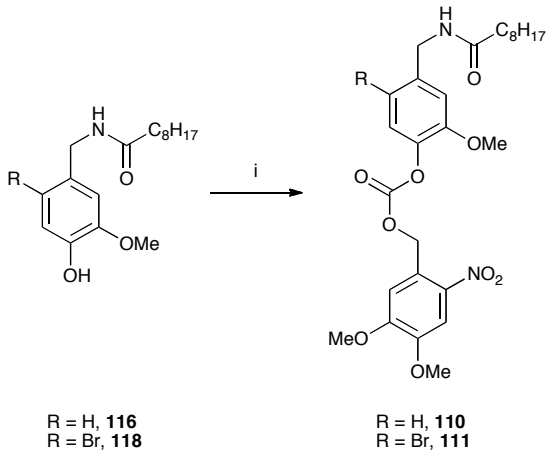

R = H, **116**
R = Br, **118**

R = H, **110**
R = Br, **111**

Scheme 3.4. Protection of the TRPV1 agonist **116** (R = H) and antagonist **118** (R = Br) with the DMNB caging group *via* a carbonate linker. *Reagents and conditions:* i. 4,5-Dimethoxy-2-nitrobenzyl chloroformate, NEt_3, CH_2Cl_2, 0 °C → RT. R = H: 96%. R = Br: 92%.

3.1.5. UV/Vis Spectra of DMNB and CDMNB-Caged TRPV1 Ligands

The UV/Vis absorption spectra of the caged TRPV1 ligands were obtained to provide an indication of which wavelengths were most likely to evoke successful photolysis. The UV/Vis absorption spectra were obtained from 0.1 mM solutions of the caged compounds in THF, Figure 3.10.

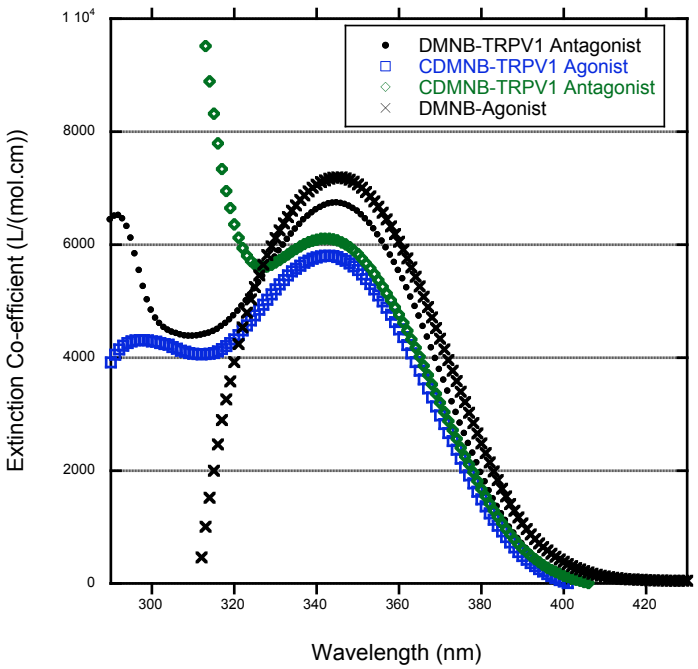

Figure 3.10. UV/Vis absorption spectrum of DMNB- and CDMNB-caged TRPV1 agonists and antagonists (0.1 mM in THF).

DMNB-caged TRPV1 agonist **105** and antagonist **109** were observed to have λ_{max} of 345 nm and extinction co-efficients (ε) of 7191 and 6728 $L.mol^{-1}cm^{-1}$ respectively, Figure 3.10. CDMNB-caged TRPV1 agonist **110** and antagonist **111** were observed to have λ_{max} of 342 nm and extinction co-efficients (ε) of 5804 and 6107 $L.mol^{-1}cm^{-1}$ respectively.

3.1.6. Photolysis of DMNB- and CDMNB-Caged TRPV1 Ligands

Before the caged TRPV1 ligands were employed in *in vitro* studies, their photolysis characteristics were investigated. This work was carried out with the assistance of our collaborators at the School of Physics and Astronomy,

University of St Andrews, Craig McDougall and Dr Tom A. Brown. Please refer to the General Experimental Procedures for details.

Solutions of caged TRPV1 agonists and antagonists in THF (3 mM) were prepared. For photolysis experiments, aliquots (1mL) of the solution were placed into UV transmitting quartz cuvettes and irradiated with a laser source for fixed time durations. After exposure to laser radiation the solution was analysed by ^{1}H NMR. Quantification of the amount of caged and uncaged material present was achieved by the addition of an internal standard, hexamethyldisiloxane, to each irradiated sample before ^{1}H NMR.

3.1.6.1. High Power Photolysis

The first set of experiments involved irradiating the caged compounds at 355 nm and 95 mJ energy for a time period of 1, 2, 3 and 4 minutes. A control sample that was left on the bench for the duration of the experiment but not exposed to laser irradiation was also analysed. Figure 3.11 illustrates the quantified results of the photolysis of DMNB-caged agonist **105** at 355 nm with 96 mJ of energy. The control sample confirmed that no uncaged material was present before irradiation. By ^{1}H NMR (300 MHz) after irradiation, the disappearance of the doublet at 4.40 ppm, corresponding to the caged material **105**, and the appearance of the double at 4.36 ppm, corresponding to the uncaged material (agonist **116**), were observed. After 1 minute of high power photolysis, nearly all of the caged material was consumed (11% remained). After 2 minutes, no caged material was observed. It is interesting

to note, however, that the amount of free agonist **116** did not increase throughout the time course but remained at approximately 50% of the total initial material.

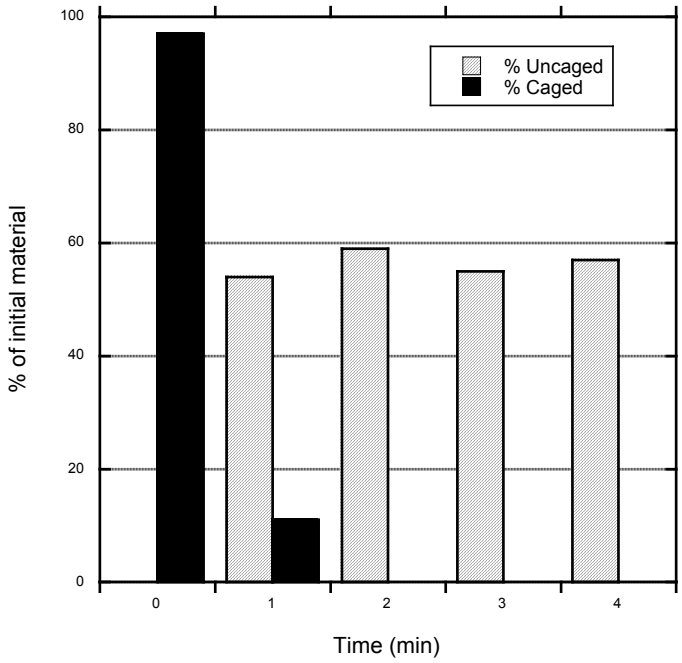

Figure 3.11. The photolysis profile of DMNB-caged agonist **105** when irradiated at 355 nm, 96 mJ and analysed by ^{1}H NMR (300 MHz). The black bars represent the amount of caged material **105** present, at the time shown, expressed as a percentage of the initial amount of caged material. The light bars represent the amount of uncaged material **116** present at the time shown. The data point at time = 0 is taken from the control sample, which was exposed to the same experimental procedure as the other samples, except for laser irradiation.

The ^{1}H NMR spectra of the photolysis samples of DMNB-caged agonist **105** after exposure to irradiation at 95 mJ, 355 nm in THF for zero, 1, 2, 3 and 4 minutes, are overlaid in Figure 3.12. The disappearance of peaks from the caged compound **105** (○), including those at 4.32, 5.49, 7.43 and 7.67 ppm,

and the appearance of peaks from what appears to be free agonist **116** (□), including a doublet at 4.29 ppm, were observed. The top spectrum is that of free agonist **116** in the same solvent system. The ^{1}H NMR of this solution supports the hypothesis that the peaks that appear during photolysis are in fact from free agonist and not other potential photolysis products of DMNB-caged agonist. The caged compound was completely consumed by photolysis after 2 minutes.

Figure 3.12. Partial 300 MHz ^{1}H NMR spectra in $CDCl_3$ of DMNB-caged agonist **105** irradiated at 355 nm, 95 mJ in THF for zero, 1, 2, 3 and 4 minutes. Hexamethyldisiloxane standard in $CDCl_3$ was added to each sample after irradiation. The disappearance of peaks from the caged compound **105** (○), including those at 4.32, 5.49, 7.43 and 7.67 ppm, and the appearance of peaks from what appears to be free agonist **116** (□), including a doublet at 4.29 ppm, were observed. The top spectrum is that of uncaged agonist **116** in the same NMR solvent. The peaks from this spectrum correspond to those which appear due to photolysis. The control sample was not exposed to laser irradiation.

sSimilar results were obtained for DMNB-caged antagonist **109**, irradiated at 355 nm, with 96 mJ of energy. The caged material was completely consumed after 2 minutes, with photorelease of antagonist **118** observed. CDMNB-caged agonist **110** was photolysed less efficiently than DMNB-caged agonist **105** at 355 nm, 96 mJ. The caged material was only completely consumed after 3 minutes and the maximum amount of uncaged agonist **116** observed was 43%, Figure 3.13. This was observed by the disappearance of the doublet at 4.44 ppm, corresponding to the caged material **110**, and the appearance of the double at 4.37 ppm, corresponding to the uncaged material **116** (agonist). Photolysis of CDMNB-caged antagonist **111** at 355 nm, 96 mJ also resulted in complete consumption of caged material after 3 minutes.

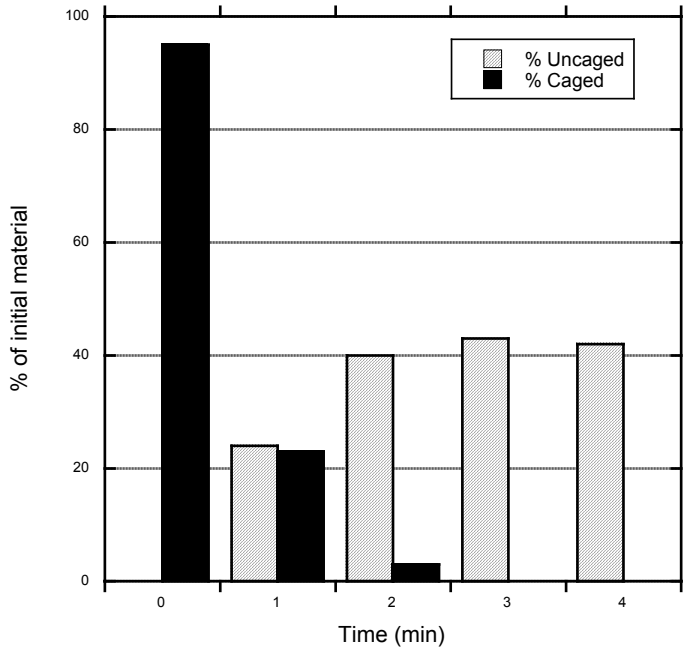

Figure 3.13. The photolysis profile of CDMNB-caged agonist **110** when irradiated at 355 nm, 96 mJ and analysed by ^{1}H NMR. The black bars represent the amount of caged material **110** present, at the time shown, expressed as a percentage of the initial amount of caged material. The light bars represent the amount of uncaged material (agonist **116**) present at the time shown. The data point at time = 0 is taken from the control sample, which was exposed to the same experimental procedure as the other samples, except for laser irradiation.

3.1.6.2. Low Power Photolysis

Having observed rapid and complete photolysis of the caged TRPV1 ligands at 355 nm, 96 mJ, the second set of experiments involved irradiating the caged compounds at 355 nm and 20 mJ energy for a time period of 1, 2, 3 and 4 minutes. A control sample that was left on the bench for the duration of

the experiment but not exposed to laser irradiation was also analysed (t = 0). As expected, at lower power photorelease of the uncaged compounds occurred more slowly than at 96 mJ. DMNB-caged agonist **105** was photolysed by laser irradiation to give the expected TRPV1 agonist **116**. After 4 minutes 61% (of the total initial material) of uncaged agonist **116** was observed. Approximately 4% of the caged material **105** remained. CDMNB-caged agonist **110** was photolysed less efficiently than DMNB-caged agonist **105**. After 4 minutes, 21% of the desired uncaged TRPV1 agonist **116** was observed while 23% of the caged material **110** remained, Figure 3.14.

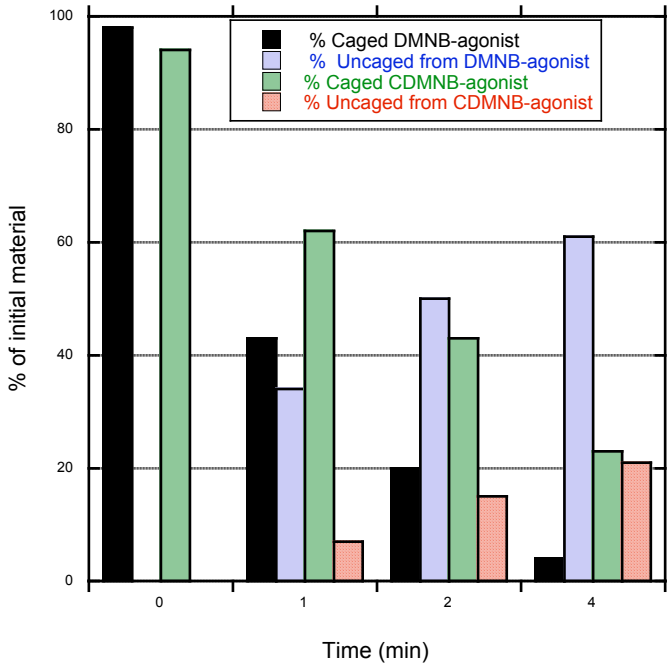

Figure 3.14. The photolysis profiles of DMNB-caged agonist **105** and CDMNB-caged agonist **110** when irradiated at 355 nm, 20 mJ and analysed by ^{1}H NMR. Results are expressed as a percentage of the initial amount of caged material. The black bars represent the amount of DMNB-caged agonist **105** present, while the green bars represent the amount of CDMNB-caged agonist **110** present, at the time shown. The blue bars represent the amount of uncaged agonist **116** photoreleased from DMNB-caged agonist **105**, at the time shown. The red bars represent the amount of uncaged agonist **116** photoreleased from CDMNB-caged agonist **110**, at the time shown. The data point at time = 0 was taken from the control sample, which was exposed to the same experimental procedure as the other samples, except for laser irradiation. No background photolysis was observed in the control sample.

The ^{1}H NMR spectra of the photolysis samples of DMNB-caged agonist **105** after exposure to irradiation at 20 mJ, 355 nm in THF for zero, 1, 2, 3 and 4 minutes, are overlaid in Figure 3.15. The disappearance of peaks from the

caged compound **105** (○), including those at 4.33, 5.50, 7.45 and 7.70 ppm, and the appearance of peaks from what appears to be free agonist **116** (□), including a doublet at 4.28 ppm, were observed. The top spectrum is that of free agonist **116** in the same solvent system. The ^{1}H NMR of this solution supports the hypothesis that the peaks that appear during photolysis are in fact from free agonist and not other potential photolysis products of DMNB-caged agonist **105**.

Figure 3.15. Partial 300 MHz ^{1}H NMR spectra in $CDCl_3$ of DMNB-caged agonist **105** irradiated at 355 nm, 20 mJ in THF for zero, 1, 2, 3 and 4 minutes. Hexamethyldisiloxane standard in $CDCl_3$ was added to each sample after irradiation. The disappearance of peaks from the caged compound **105** (○), including those at 4.33, 5.50, 7.45 and 7.70 ppm, and the appearance of peaks from what appears to be free agonist **116** (□), including a doublet at 4.28 ppm, were observed. The top spectrum is that of uncaged agonist **116** in the same NMR solvent. The peaks from this spectrum correspond to those which appear due to photolysis. The control sample was not exposed to laser irradiation.

Figure 3.16 illustrates that DMNB-caged antagonist **109** released 42% of the desired TRPV1 antagonist **118** upon photolysis, while 5% of the caged material **109** remained after 4 minutes irradiation at 355 nm, 20 mJ. Again, CDMNB-caged antagonist **111** was photolysed less efficiently than DMNB-caged antagonist **109**. After 4 minutes irradiation of CDMNB-caged antagonist **111** at 355 nm, 20 mJ, 28% of the desired TRPV1 antagonist **118** was released and 24% of the caged material **111** remained.

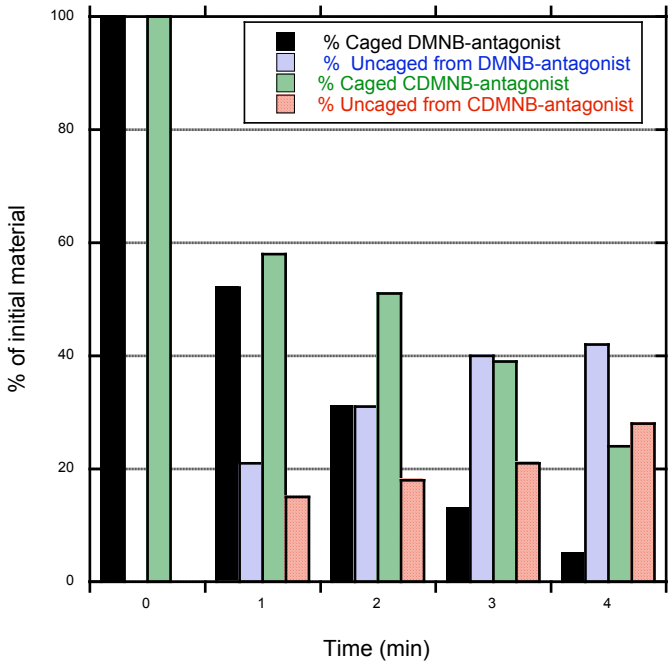

Figure 3.16. The photolysis profiles of DMNB-caged antagonist **109** and CDMNB-caged antagonist **111** when irradiated at 355, 20 mJ and analysed by ^{1}H NMR. Results are expressed as a percentage of the initial amount of caged material. The black bars represent the amount of DMNB-caged antagonist **109** present, while the green bars represent the amount of CDMNB-caged antagonist **111** present, at the time shown. The blue bars represent the amount of uncaged antagonist **118** photoreleased from DMNB-caged antagonist **109**. The red bars represent the amount of uncaged antagonist **118** photoreleased from CDMNB-caged antagonist **111**. The data point at time = 0 was taken from the control sample, which was exposed to the same experimental procedure as the other samples, except for laser irradiation.

The ^{1}H NMR spectra of the photolysis samples of DMNB-caged antagonist **109** after exposure to irradiation at 20 mJ, 355 nm in THF for zero, 1, 2, 3 and 4 minutes, are overlaid in Figure 3.17. The disappearance of peaks from the caged compound **109** (○), including those at 4.38, 7.40 and 7.70 ppm, and

the appearance of peaks from what appears to be free antagonist **118** (□), including a doublet at 4.35 ppm and a singlet at 6.85 ppm, were observed. The top spectrum is that of free antagonist **118** in the same solvent system. The ^{1}H NMR of this solution supports the hypothesis that the peaks that appear during photolysis are in fact from free antagonist **118** and not other potential photolysis products of DMNB-caged antagonist **109**.

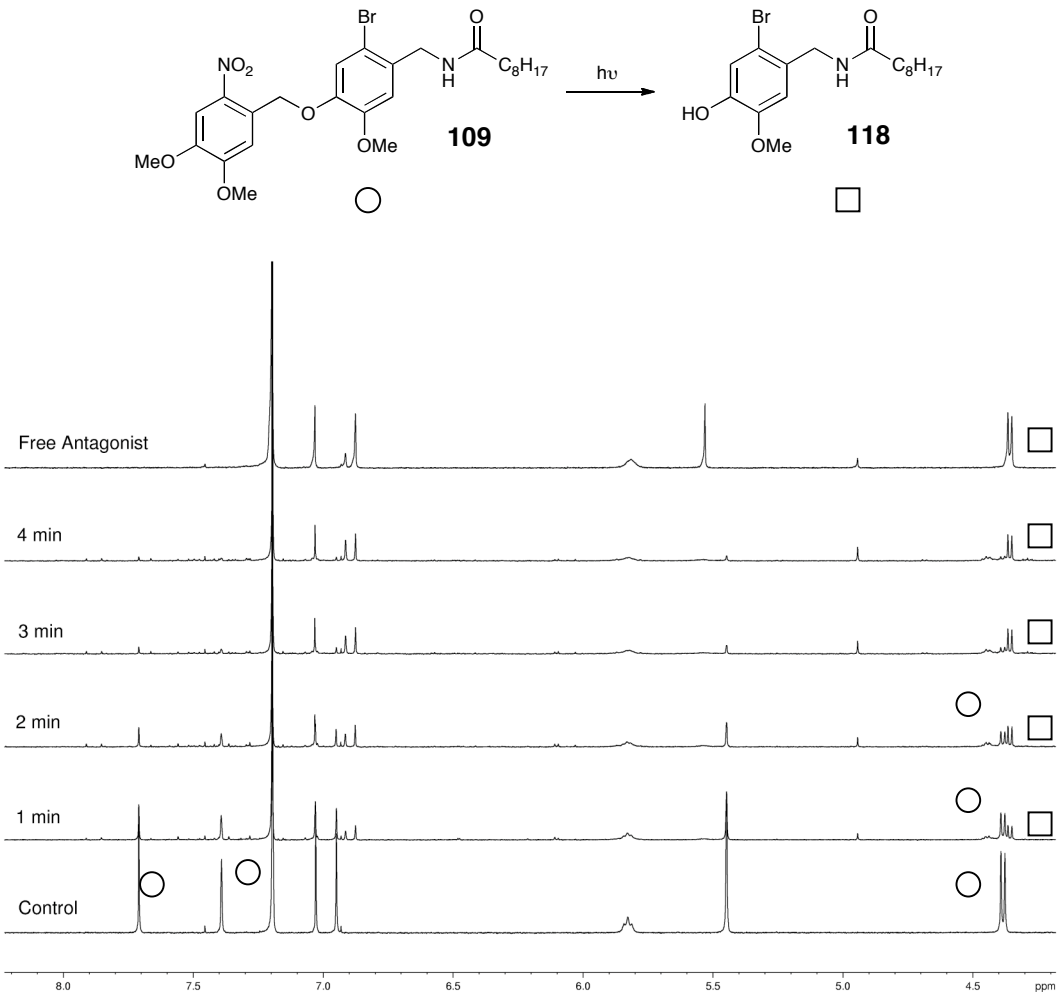

Figure 3.17. Partial 300 MHz ^{1}H NMR spectra in $CDCl_3$ of DMNB-caged antagonist **109** irradiated at 355 nm, 20 mJ in THF for zero, 1, 2, 3 and 4 minutes. Hexamethyldisiloxane standard in $CDCl_3$ was added to each sample after irradiation. The disappearance of peaks from the caged compound **109** (○), including those at 4.38, 7.40 and 7.70 ppm, and the appearance of peaks from what appears to be free antagonist **118** (□), including a doublet at 4.35 ppm and a singlet at 6.85 ppm, were observed. The top spectrum is that of uncaged antagonist **118** in the same NMR solvent. The peaks from this spectrum correspond to those which appear due to photolysis. The control sample was not exposed to laser irradiation.

In conclusion, in the absence of the carbonate linker, 4% caged agonist **105** and 5% caged antagonist **109** were observed after 4 minutes irradiation at 355 nm at 20 mJ. After an equivalent period of 355 nm irradiation of the carbonate linked caged derivatives at 20 mJ, 23% caged agonist **110** and 24% caged antagonist **111** were observed. This seems to indicate that more efficient photolysis was observed when DMNB-caged compounds (**105** and **109**) were employed compared to when CDMNB-caged compounds (**110** and **111**) were photolysed. This is consistent with a comparison made between these caging groups when photoreleasing the mitochondrial uncoupler AG10 **94**.[78] In the case of AG10, however, it emerged that despite the reduced efficiency of the CDMNB-caged compound **99**, it was significantly more soluble in aqueous solutions than the DMNB-caged material **98** and hence a more useful biological tool (Chapter 2).

During photolysis of all four of the caged derivatives, the sum of the caged material and the uncaged material was less than the maximum amount of material that was present at the start of the experiment. Given that the control samples contained approximately all of the material that would be expected, loss of material simply through experimental handling was unlikely. Therefore, it was proposed that unwanted photodegradation of either the caged material or the uncaged product was occurring. To investigate whether the uncaged material was further degrading once the photolabile protecting group was removed, uncaged agonist **116** and antagonist **118** were irradiated for 4 minutes with a 355 nm laser at 95 mJ in THF. Neither irradiation of the TRPV1 agonist **116** (i.e. the material that is produced by photolysis of **105** and

110) nor the TRPV1 antagonist **118** (i.e. the material that is produced by photolysis of **109** and **111**) produced loss of material. This suggests that the desired product is photostable once produced. Therefore, there may be more than one photodegradation pathway for the caged material, one of which leads to the desired material and one of which leads to production of an unidentified and unwanted product. Alternatively, the caging group, once excited, may interact with the photolysis product in some way.

While these photolysis experiments are useful for observing the release of the uncaged agonist **116** and antagonist **118**, as well as general photolysis trends and characteristics of the caging groups, it is difficult to extrapolate the significance of these results to *in vitro* photolysis. In these experiments, a greater quantity of material is used, in order to make detection of the products possible, and irradiation for a greater length of time is required in order to photolyse a significant proportion of the caged material. In contrast, photolysis in cells is carried out on micromolar concentrations for less than a second. It is therefore possible that the observed wasteful photodegradation is an artefact of the conditions employed and may not be significant for *in vitro* experiments.

3.1.7. Application of DMNB-Caged TRPV1 Agonist 105 to a Biological System

Having demonstrated that DMNB-caged TRPV1 agonist **105** is photoreleased efficiently in a cuvette at 355 nm to give the free agonist, nonivamide **116**, this caged compound was employed in *in vitro* photolysis experiments on trigeminal neurons in culture. These experiments were carried out by our collaborators at the Neuroscience Center, University of Helsinki, in Prof. Leonard Khiroug's and Prof. Rashid Giniatullin's laboratories. Please see General Experimental Procedures for details.

A subpopulation of trigeminal neurons known to express native TRPV1 receptor channels that are highly permeable to Ca^{2+} were employed for this study.[102] Upon agonist binding, depolarising membrane currents and transient increases in intracellular concentration of Ca^{2+} ($[Ca^{2+}]_i$) are observed in cultured neurons.[102] In order to detect TRPV1 channel activation induced by the TRPV1 agonist, nonivamide **116**, which is photoreleased from the caged agonist **105**, electrophysiological recordings and Ca^{2+} imaging were performed, Figure 3.18.

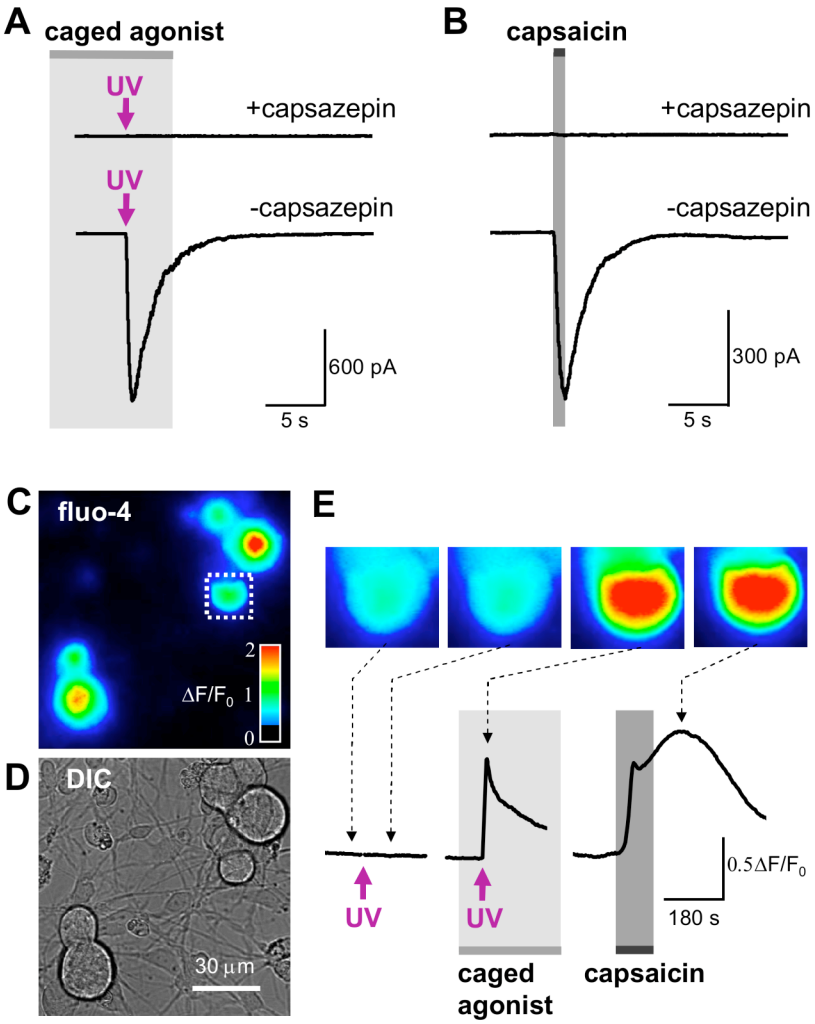

Figure 3.18.[103] Membrane currents and intracellular Ca^{2+} transients induced by TRPV1 receptor agonist in cultured trigeminal neurons. (A), Patch-clamp recordings of transmembrane current from a single cultured neuron stimulated by UV laser photolysis of DMNB-caged TRPV1 agonist **105** (1 μM). The caged agonist **105** was applied through the fast perfusion system (light grey box) 30 s prior to the laser flash. No membrane current activation was observed in response to the caged compound itself. In contrast, immediately after the UV laser flash (500 ms, violet arrow) a large membrane current was observed in the absence of the TRPV1 receptor antagonist capsazepine (lower trace) but not in the presence (10 μM) of this antagonist (upper trace). (B), Transmembrane current recorded from another cultured neuron

stimulated by application of capsaicin **100** (0.2 μM) for 1 s *via* fast perfusion system (dark grey box). The response was fully blocked by capsazepine (10 μM, upper trace). Similarity was observed between membrane currents induced by capsaicin **100** application and by photolysis of the caged agonist **105** (lower traces in A and B). (C), Pseudo-coloured image of cultured neurons loaded with a Ca^{2+}-sensitive indicator fluo-4. Dashed-line box indicates the cell shown in E. (D), Translucent image of the same field as in C obtained using differential interference contrast (DIC) technique. (E), changes in intracellular Ca^{2+} concentration in a single neuron (boxed in C). A lack of change was observed in response to UV flash alone (flat trace in the left panel), as well as in response to application of the caged TRPV1 agonist **105** in the absence of UV irradiation (light grey bar in the middle panel). In contrast, the UV flash in the presence of the caged agonist **105** induced a large and rapid increase in $[Ca^{2+}]_i$ (middle panel), comparable in amplitude to the response to capsaicin **100** (right panel). Four fluorescence images corresponding to four specific time points are shown above the traces.[103]

Using whole-cell patch clamp recordings in voltage clamp mode, application of the caged compound **105** (1 μM) in the absence of UV light did not produce any measurable membrane current, Figure 3.18, A. However, when trigeminal neurons were exposed to a brief flash of UV laser light (500 ms, 375 nm), large inward currents with peak current amplitude of 2036 ± 375 pA were observed (Figure 3.18, A, lower trace). In order to demonstrate that the current was due to activation of TRPV1 and not some other pathway, two experiments were carried out. Firstly, capsaicin **100** was applied to the same cells to compare the currents produced and secondly a selective TRPV1 antagonist, capsazepine, was employed. The blocking of current response by the antagonist would provide evidence for the activation of TRPV1 receptors

upon irradiation of the caged agonist **105**. The shape and time-course of the uncaging-induced currents were similar to those triggered in the same cells by rapid application of capsaicin **100** (1 μM, 1 s; Figure 3.18, B, lower trace). Both the responses to capsaicin, and the responses to uncaging of **105** were fully blocked by the TRPV1 antagonist capsazepine[93] (10 μM, Figure 3.18, A and B, upper traces). It was concluded that the photoreleased agonist **116** activates TRPV1 receptor-mediated currents, as the observed currents are similar to capsaicin-induced currents and highly sensitive to the selective TRPV1 antagonist capsazepine.[93]

In a second series of experiments, cultured trigeminal neurons were loaded with a Ca^{2+}-sensitive dye, fluo-4, to monitor changes in cytoplasmic Ca^{2+} concentration ($[Ca^{2+}]_i$) induced by photolysis of the caged agonist **105**. Images of colour-coded fluo-4 fluorescence and the translucent image of the same cells are illustrated in Figure 3.18 (C, D and E). Prior to bath application of the caged agonist **105**, exposure to UV light alone did not produce measurable changes in $[Ca^{2+}]_i$, Figure 3.18, E. When the caged compound **105** was bath-applied to the same cells, no change in $[Ca^{2+}]_i$ was detected. However, in the presence of the caged compound **105** the 50 ms UV flash induced a rapidly rising $[Ca^{2+}]_i$ transient (Figure 3.18, E, middle trace). Within 10 min of stimulation, the $[Ca^{2+}]_i$ level returned to the pre-stimulus baseline, after which cells were exposed to bath-applied capsaicin **100** (0.2 μM, 100 s). The capsaicin-induced $[Ca^{2+}]_i$ rise had a comparable amplitude but a much slower rise time compared to the uncaging-induced $[Ca^{2+}]_i$ transient, Figure 3.18, E right trace. These results support the conclusions from the electrophysiological data, demonstrating that the caged compound **105** alone,

as well as UV light alone, have no effect on $[Ca^{2+}]_i$; that photolysis of the caged compound **105** produces a $[Ca^{2+}]_i$ transient in capsaicin-sensitive trigeminal neurons; and that the $[Ca^{2+}]_i$ response to uncaging has a more rapid onset than that induced by bath application of capsaicin **100**.

3.1.8. Summary

A robust route for the synthesis of a set of TRPV1 agonists and antagonists, based on the nonivamide skeleton, and their caged derivatives has been reported.[103] The photolysis characteristics of four caged TRPV1 ligands were investigated using a 355 nm laser. It was demonstrated that, in all cases, the desired TRPV1 ligand was released during irradiation. More efficient photolysis was observed when DMNB-caged compounds were employed compared to when CDMNB-caged material was photolysed. This is consistent with a comparison made between these caging groups when photoreleasing the mitochondrial uncoupler AG10.[78] Photolysis of DMNB-caged TRPV1 agonist **105** was investigated in cultured trigeminal neurons. It was demonstrated to be inactive in the absence of UV irradiation. However, upon UV irradiation, fast responses consistent with activation of TRPV1 receptors were observed. In conclusion, DMNB-caged TRPV1 agonist **105**, used in micromolar or submicromolar concentrations enables the activation of TRPV1 receptors *in vitro* with enhanced spatial and temporal control over standard methods of compound application. It is envisaged that this compound will be a useful molecular probe for the study of TRPV1 receptors and Ca^{2+} signalling in general.

3.2. Membrane-Impermeant TRPV1 Agonists - Probing the location of the TRPV1 capsaicin-binding site

3.2.1. Introduction and Aims

There is still much to be discovered about TRPV1 channel function. The precise location of the capsaicin-binding site on TRPV1 has not been conclusively determined. Significantly different conclusions to this question have been reported. Most studies conclude that the capsaicin-binding site on TRPV1 is located intracellularly. Caterina *et al.* reported identical capsaicin responses from either side of a patch excised from a cell expressing TRPV1.[80] It was speculated that either capsaicin permeates the lipid bilayer freely or that there are functionally equivalent capsaicin-binding sites on both sides of the plasma membrane.[80] Jung *et al.* reported that a capsaicin derivative with a protonated primary amine, DA-5018·HCl **119**, Figure 3.19, activated channel currents only when applied to the inner surface of the membrane. When applied extracellularly, DA-5018·HCl **119** did not activate currents in sensory neurons.[104] This was interpreted as evidence for an intracellular capsaicin-binding site. However, the membrane permeability of the charged capsaicin derivative was not measured. Also, the compound employed as a TRPV1 agonist seems to contradict the structure-activity observations of Walpole *et al.*,[90] that alkylation of the phenol renders the molecule inactive.

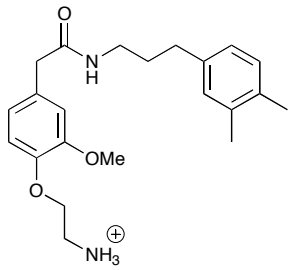

119

Figure 3.19. The charged capsaicin derivative, DA-5018·HCl **119**, employed by Jung *et al*.[104]

The development of urea-based TRPV1 antagonists was reported by Rami *et al*.[105] An active antagonist was methylated to obtain a charged quaternary ammonium salt **120**, Figure 3.20. This charged antagonist did not inhibit capsaicin-mediated responses when applied intracellularly. However, a full blockade of TRPV1 was observed when applied extracellularly. This was interpreted as evidence for an extracellularly accessible binding site on the TRPV1 receptor for capsaicin and for this competitive antagonist.[105] The membrane permeability of this compound was not specifically tested.

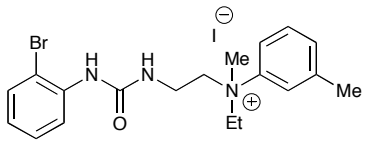

120

Figure 3.20. The charged TRPV1 antagonist **120** employed by Rami *et al*. to demonstrate that TRPV1 was only blocked when the charged antagonist was applied extracellularly.[105]

The coumarin-caged capsaicin derivative, {7-bis(carboxymethyl)amino]coumarin-4-yl}methoxycarbonyl-caged capsaicin **108**, Figure 3.8 and 3.21, was employed by Gilbert *et al.* to demonstrate an extracellular capsaicin-binding site.[100] The charged caged compound was irradiated intra- and extracellularly in HEK293 cells expressing TRPV1. Small currents were recorded in response to intracellular photolysis; while large currents were observed subsequent to extracellular photolysis. However, the photoreleased agonist, capsaicin **100**, is membrane permeant and identical responses have been reported upon extracellular and intracellular application of capsaicin.[80]

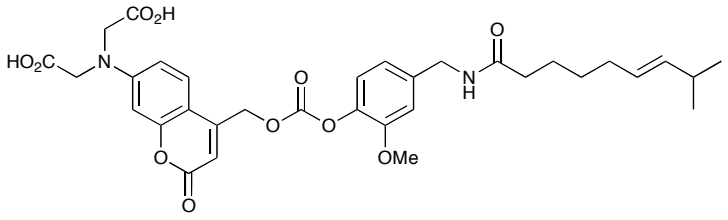

108

Figure 3.21. {7-Bis(carboxymethyl)amino]coumarin-4-yl}methoxycarbonyl-caged capsaicin **108** reported by Gilbert *et al.*[100]

In order to study the location of the TRPV1 capsaicin-binding site, it was aimed to synthesise membrane-impermeant capsaicin derivatives (TRPV1 agonists). It was proposed that including charged or polar moieties would reduce the membrane permeability of such a derivative. It was proposed to include the polar groups at the end of the lipid chain to minimise impact on the vanilloid moiety, Figure 3.22. It was aimed to assess the membrane permeability of these compounds quantitatively and investigate their ability to

activate TRPV1 when applied from both extracellular and intracellular locations.

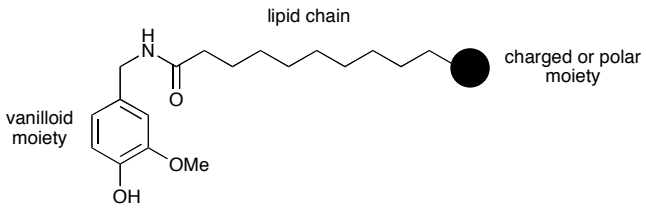

Figure 3.22. Proposed strategy for the synthesis of membrane-impermeant capsaicin derivatives. It was hypothesised that appending a charged or polar moiety at the end of the lipid chain would reduce membrane permeability but not have an impact on the vanilloid moiety.

3.2.2. Design and Synthesis of Potential Membrane-Impermeant TRPV1 Agonists

3.2.2.1. Design of Membrane-Impermeant TRPV1 Agonists

As discussed, structure-activity studies of capsaicin have shown that the vanilloid and amide groups must be maintained for activity.[89,90] The length of the lipid chain in the C-region is less critical but lipophilicity, with carbon chain length 8-12, is important.[88] This requirement makes the design of membrane-impermeant TRPV1 agonists challenging. It was proposed to attach a polar or charged group to the terminal of the lipid chain. It was hypothesised that the compound would have greater polarity but that the TRPV1 binding components would not be affected. This hypothesis was based on the

capsaicin binding model proposed by Gavva *et al.* in which the vanilloid moiety binds to TRPV1 between transmembrane helices TM3 and TM4, making important contacts with threonine 550 and tryptophan 549, Figure 3.23.[106] In this binding model the hydrophobic C-region is less important for binding, making one hydrophobic contact with a tyrosine residue on TM3. This binding model suggests that small structural changes can be made to the C-region without affecting agonist binding.

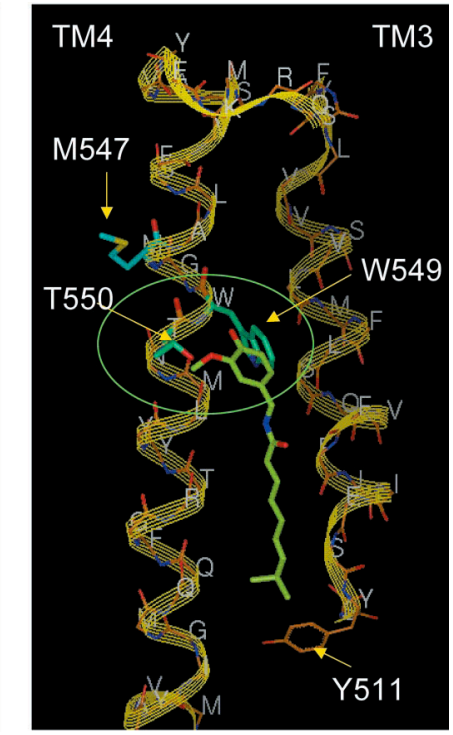

Figure 3.23. Structural model of capsaicin interacting with transmembrane helices TM3 and TM4 of TRPV1. The important interactions of the vanilloid moiety with T550 and W549 are shown. A hydrophobic contact between the C-region of capsaicin and Y511 on TM3 is shown. This research was originally published in the *Journal of Biological Chemistry*. N. R. Gavva *et al.* Molecular Determinants of Vanilloid Sensitivity in TRPV1. 2004; 279:20283-20295. © the American Society for Biochemistry and Molecular Biology.[106]

Considering which polar group to attach to the lipid chain, it was proposed that an amine might be a suitable candidate as it would be protonated at physiological pH and, therefore, reduce membrane permeability of the agonist. However, no activation of TRPV1 was observed by Walpole *et al.* when an analogue of this compound, with five methylene units between the

amide and amine, was applied *in vitro*.[88] Therefore, it was decided to increase the length of the carbon chain to ten methylene units (nonivamide **116** employed in the TRPV1 caging project, Chapter 3.1, has eight methylene units), in order to maximise lipophilicity and the distance between the presumed TRPV1 binding region and the polar group. The terminal amine of **121** (Figure 3.24) was used as a handle to synthesise additional polar capsaicin analogues. Urea was incorporated at the terminal amine to form **122**. Urea functional groups can reduce a compound's membrane permeability due to heavy solvation in aqueous solutions. The final compound included a urea coupled to an ethyl ester to form **123**. This ester may be deprotected *in vitro* by non-selective esterases to reveal a carboxylic acid, which would be deprotonated at physiological pH. Figure 3.24 illustrates the potential membrane-impermeant TRPV1 agonists, **121**, **122** and **123**, whose syntheses were undertaken.

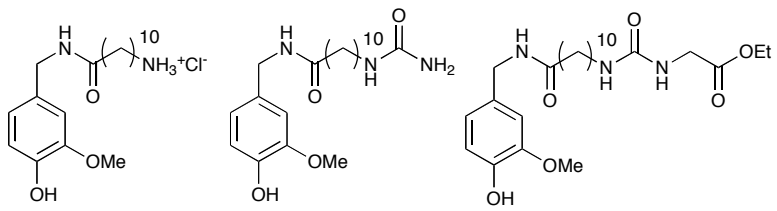

121 **122** **123**

Figure 3.24. The proposed amine **121**, urea **122**, and ester **123** appended membrane-impermeant TRPV1 agonists, to be employed as tools to probe the location of the TRPV1 agonist-binding site.

3.2.2.2. Synthesis of Potential Membrane-Impermeant TRPV1 Agonists

The primary amine **114** was obtained in two steps from benzonitrile **112**, Scheme 3.1. It was used without further purification and coupled with Boc-protected aminoundecanoic acid **124** by treatment with EDC·HCl and HBTU in CH_2Cl_2 to obtain **125** in 51% yield, Scheme 3.5. The Boc-protection of 11-aminoundecanoic acid was achieved in 86% yield by treatment with di-*tert*-butyl dicarbonate in a NaOH/dioxane solution. The TIPS group of **125** was deprotected with TBAF in THF to afford **126** in 85% yield. Attempts to deprotect both the TIPS and Boc group from **125** in one pot by treatment with 1 M HCl in acetic acid; and TFA in THF failed. Therefore, synthesis of the amino-modified TRPV1 agonists, **121**, **122** and **123**, was achieved from the Boc-protected intermediate **126**. Boc-deprotection was achieved in 74% yield by treatment with 1 M HCl in dioxane to obtain the terminal amine **121**. This primary amine was functionalised further: treatment of **121** with a water-urea

solution under reflux formed the carbamide derivative **122** in 62% yield. Treatment of the primary amine **121** with ethyl isocyanatoacetate in dichloroethane under reflux formed the ester-containing derivative **123** in 53% yield.

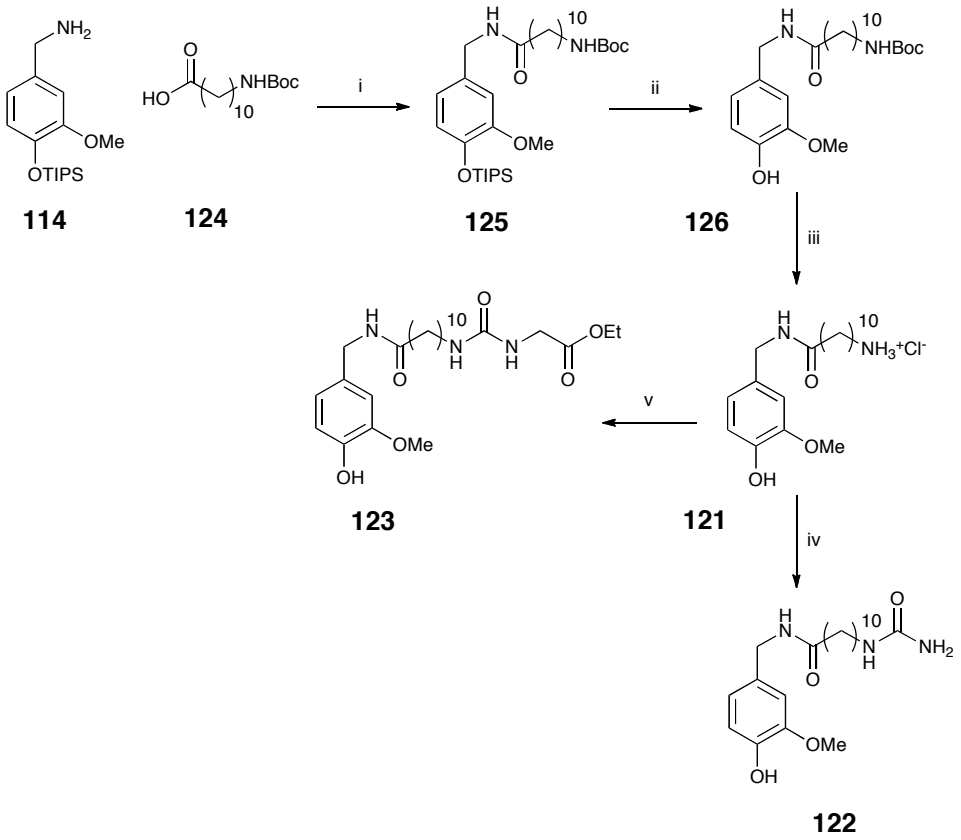

Scheme 3.5. The synthesis of the amino-modified TRPV1 agonists, **121**, **122** and **123**. *Reagents and conditions:* i. EDC·HCl, HBTU, DIPEA, CH_2Cl_2, 51%; ii. TBAF in THF, CH_2Cl_2, 85%; iii. 1 M HCl in dioxane, 74%; iv. urea, H_2O, reflux, 62%; v. Ethyl isocyanatoacetate, dichloroethane, reflux, 53%.

The CDMNB-caged derivative **128** (Scheme 3.6) of the terminal amine-modified membrane-impermeant TRPV1 agonist was synthesised. The caging group was appended to the phenol oxygen. It was proposed that active compound photorelease with spatial and temporal control, in addition to

membrane impermeability, would be a useful tool for investigating the TRPV1 receptor.

The Boc-protected intermediate **126** was reacted with 4,5-dimethoxy-2-nitrobenzyl chloroformate in the presence of triethylamine to attach the caging group to the free phenol position to obtain **127** in 94% yield. Boc-deprotection was achieved in 94% yield by treatment with 1 M HCl in dioxane to obtain the amino-modified caged TRPV1 agonist **128**.

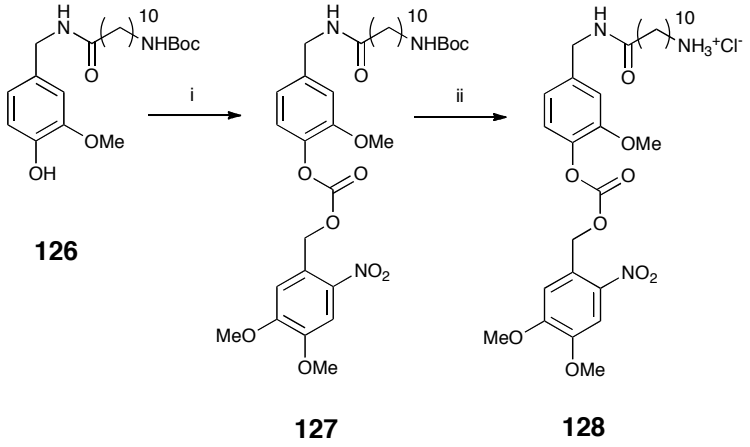

Scheme 3.6. The synthesis of the amine-modified caged TRPV1 agonist **128**. *Reagents and conditions:* i. 4,5-Dimethoxy-2-nitrobenzyl chloroformate, NEt_3, CH_2Cl_2, 0 °C → RT, 94%; ii. 1 M HCl in dioxane, 94%.

3.2.3. Biological Evaluation of the Amino-modified TRPV1 Agonists

In order to probe the location of the TRPV1 capsaicin-binding site, it was first necessary to determine the membrane permeability of the amino-modified TRPV1 agonists **121**, **122**, **123** and **128**. These compounds were then employed in *in vitro experiments* on trigeminal neurons to assess their ability to activate TRPV1 when applied both intra- and extracellularly.

3.2.3.1. Membrane Permeability of the Amino-modified TRPV1 Agonists

The amino-modified TRPV1 agonists, **121**, **122**, **123** and **128**, were analysed for their membrane permeability. This work was carried out by Dr Hitesh Sanganee and Dr Ken Grime, at AstraZeneca UK.

The compounds were analysed for their apparent permeability across a cell monolayer, set up to represent the gut lumen to blood direction of travel for a drug. The unit of permeability, cm/sec, is calculated from the amount of drug transported per unit time (moles/sec); divided by the product of the surface area over which the drug is transported (cm^2) and the starting concentration ($moles/cm^3$). A higher figure indicates higher permeability. The permeability values are shown in Table 3.1.

Compound	Cell monolayer permeability (10^{-6} cm/sec)
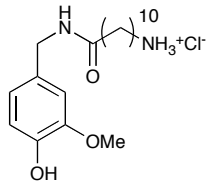 **121** (J14)	5.67
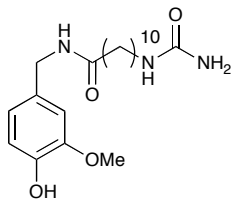 **122** (J17)	5.06
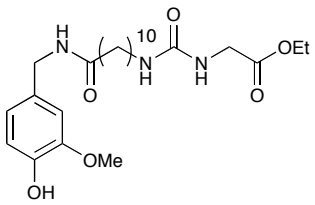 **123**	2.00
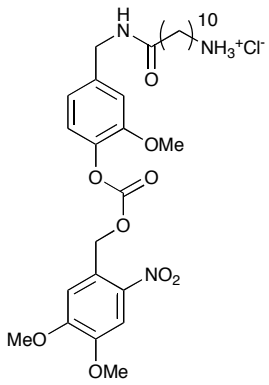 **128** (J29)	18.64

Table 3.1. Permeability data for the amino-modified TRPV1 agonists **121**, **122**, **123** and **128**. The compounds were analysed for their apparent permeability across a cell monolayer set up to represent the gut lumen to blood direction of travel for a drug. A higher figure indicates higher permeability. (Notice that **121**, **122** and **128** have additional codes referred to in the biological results section, Chapter 3.2.3.2.)

The data indicate that the ester-containing derivative **123** has low permeability, the amine-modified TRPV1 agonist **121** and the carbamide-containing derivative **122** have moderate permeability and the caged amine-modified derivative **128** has high permeability.

The data indicate that the addition of a terminal amine or urea functional group to the lipid chain (C-region) did *reduce* membrane permeability. The ester-containing derivative **123** exhibited the lowest permeability.

3.2.3.2. Application of the Amino-modified TRPV1 Agonists to a Biological System

Having synthesised potential TRPV1 agonists with reduced membrane permeability, these compounds were employed in *in vitro* experiments on trigeminal neurons in culture to assess their ability to activate TRPV1 when applied both intra- and extracellularly. These experiments were carried out by our collaborators at the Neuroscience Center, University of Helsinki, in Prof. Leonard Khiroug's and Prof. Rashid Giniatullin's laboratories. Please see General Experimental Procedures for details.

Membrane currents were induced by capsaicin **100** (200 nM) and the amino-modified capsaicin analogues (10 uM), **121**, **122** and **128**, in rat (P10) trigeminal sensory neurons by fast application (exchange time ~30 ms), Figure 3.25. The caged compound **128** was irradiated with UV light for 1 hour before application to the neurons. All of the compounds were applied from the extracellular side. Unlike capsaicin **100**, which induced fast and persistent current flow (Figure 3.25, A), all three modified compounds induced slowly growing currents with minimal early stage (Figure 3.25, B, C and D).

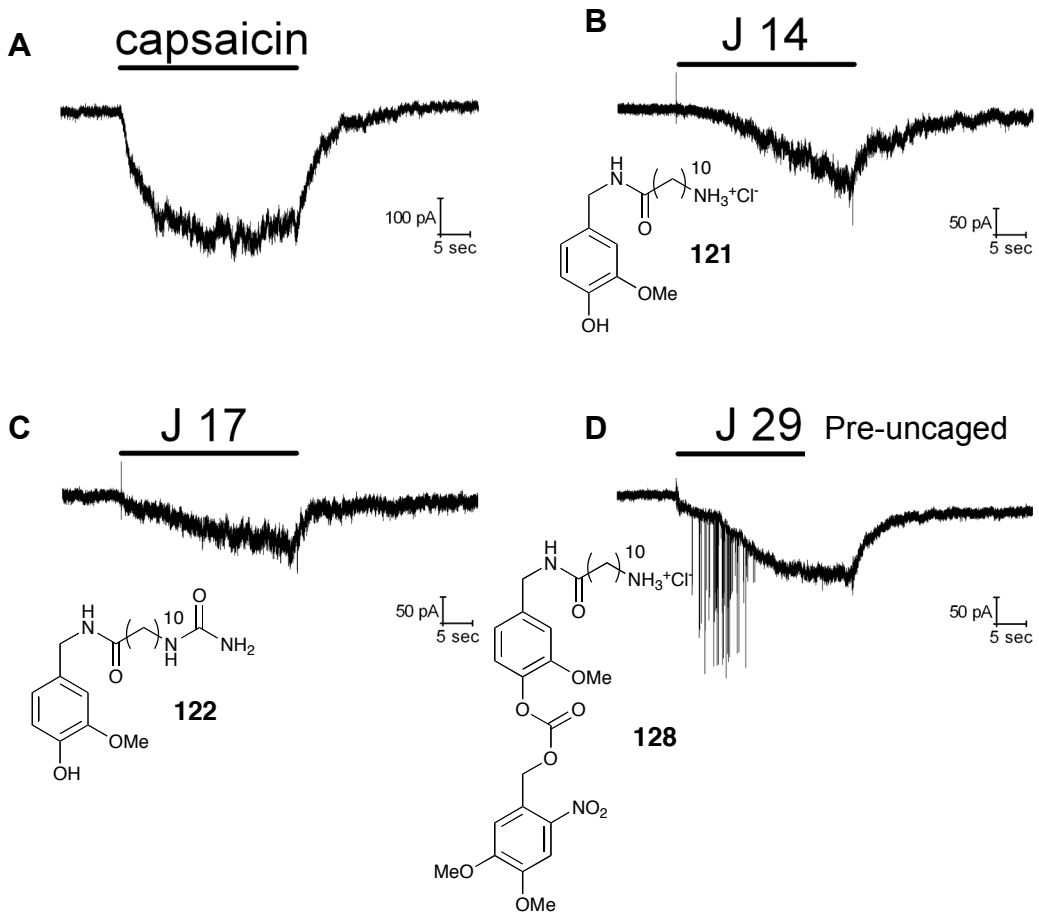

Figure 3.25. Example of membrane currents induced by capsaicin **100** (A) and amino-modified capsaicin analogues (B, C and D) in trigeminal sensory neurons. J14 corresponds to the amine-modified TRPV1 agonist **121**. J17 corresponds to the amino-modified carbamide derivative of the TRPV1 agonist **122**. J29 corresponds to the amine-modified caged TRPV1 agonist **128**. J29 was irradiated with UV light for 1 hour before application to the neuron.

The amine-modified TRPV1 agonist **121** (labelled as J14) and the amino-modified carbamide derivative of the TRPV1 agonist **122** (labelled as J 17) were applied intracellularly *via* patch-pipette, Figure 3.26. This produced a large leak (outward) current. This leak was hypothesised to be due to

activation of TRPV1 channels from *inside* the cell. This hypothesis was supported by the observation that application of the selective TRPV1 antagonist capsazepine[93] (CPZN) reduced this leak, indicating a TRPV1-medited mechanism. After capsazepine (10 uM) was locally applied for 30 sec, reduced leak current was observed.

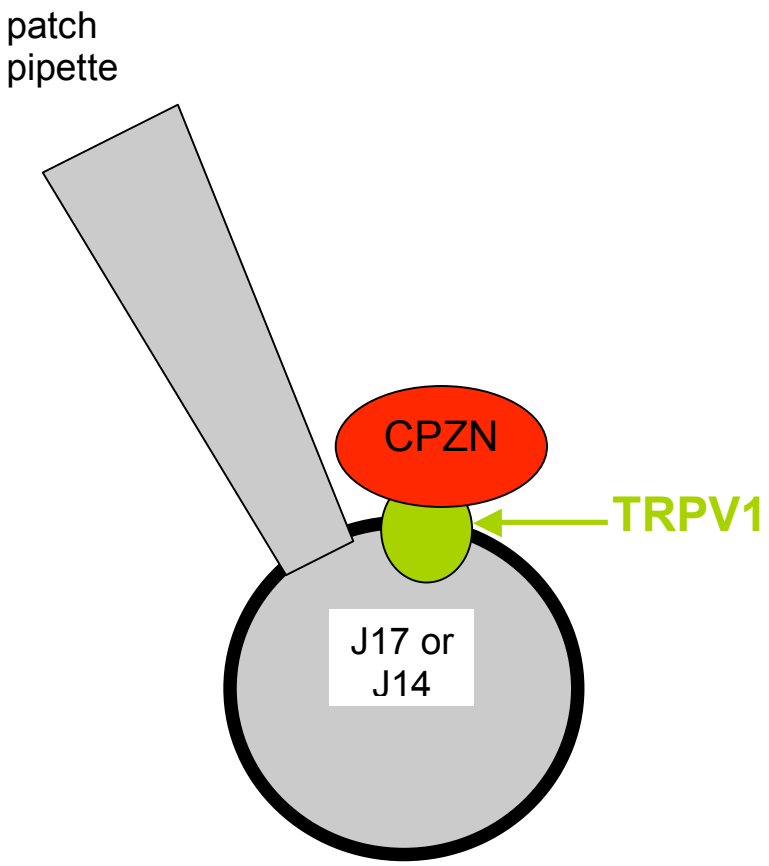

Figure 3.26. Illustration of intracellular delivery, *via* patch pipette, of the modified TRPV1 agonists **121** and **122**. This produced a large leak (outward) current which was reduced by application of the TRPV1 antagonist capsazepine (10 uM), indicating a TRPV1-medited mechanism.

Membrane currents induced by UV uncaging of the amine-modified caged derivative **128** (labelled as J29) in trigeminal sensory neurons were recorded. Unlike capsaicin **100**, intracellular uncaging of **128** (J29) produced immediate

but long lasting responses with a slow recovery of the baseline, Figure 3.27. This observation was hypothesised to be due to low rate of removal of the photoreleased agonist **121** from the cell interior due to its reduced membrane permeability compared to capsaicin. This slow recovery of the baseline was not observed when DMNB-caged TRPV1 agonist **105** was photolysed *in vitro*, Figure 3.18, A. The photoinduced TRPV1-mediated current spike was very similar to capsaicin in that case, Figure 3.18, B. The comparable membrane permeability of the photoreleased TRPV1 agonist **116** and capsaicin **100** may account for the rapid diffusion of both agonists out of the cell, away from TRPV1, resulting in rapid termination of the current spike.

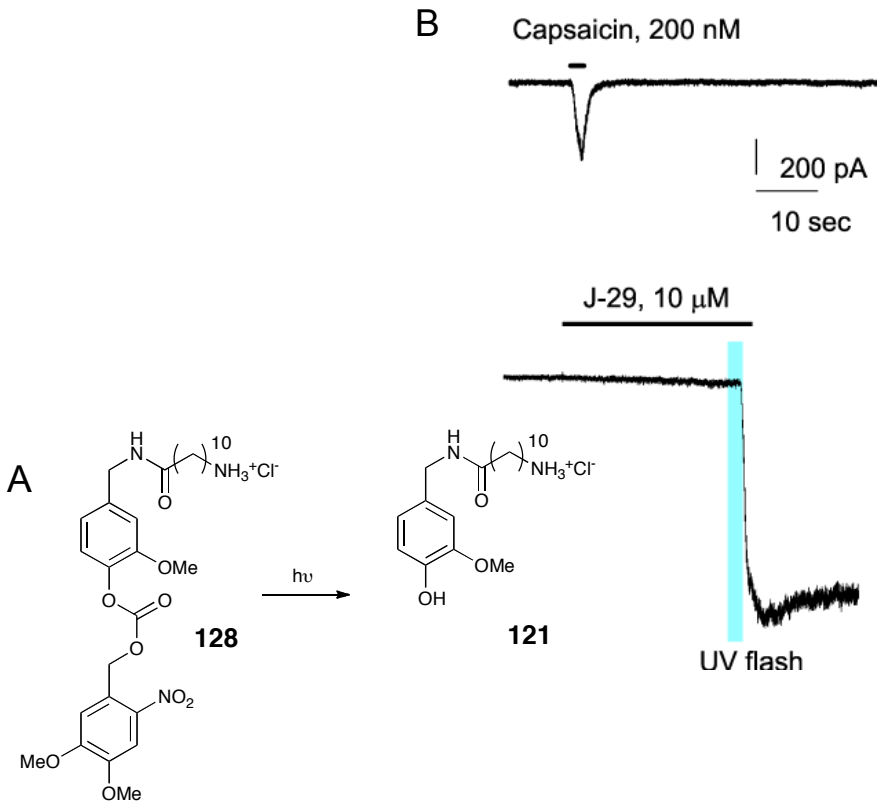

Figure 3.27. A. Photolysis of the amine-modified caged derivative **128** (labelled as J29) yields the uncaged amine-modified derivative **121**. **B.** The membrane current induced by UV uncaging of the amine-modified caged derivative **128** (labelled as J29) in a trigeminal sensory neuron. Unlike capsaicin **100**, intracellular uncaging of **128** (J29) produced long lasting responses with a slow recovery of the baseline. Membrane currents were only observed after a UV flash, not in response to the caged compound **128** (J29) on its own.

In conclusion, these biological results provide evidence that is consistent with an intracellular TRPV1 agonist-binding site. Figure 3.25 (B, C and D), illustrates slowly growing currents with minimal early stage when the modified derivatives, **121**, **122** and **128**, were applied extracellularly. These data suggest that the compounds require a longer time to diffuse across the

membrane and reach the TRPV1 agonist-binding site than capsaicin **100**, with which no lag time was observed, Figure 3.25, A. The intracellular application of the modified TRPV1 agonists **121** and **122** induced large leak currents by a TRPV1-mediated mechanism, Figure 3.26. These data suggest that the TRPV1 agonists activate TRPV1 from the intracellular side. Figure 3.27 B illustrates that, unlike capsaicin **100**, intracellular uncaging of **128** (J29) produced long lasting responses with a slow recovery of the baseline. This observation was hypothesised to be due to low rate of removal of the photoreleased agonist **121** from the cell interior due to its reduced membrane permeability. It continued to activate TRPV1 because it could not diffuse rapidly out of the cell.

A significant observation was that when the caged derivative **128** (J29) was applied extracellularly, after pre-uncaging, Figure 3.25 D, a slow response was observed. However, intracellular uncaging of **128** (J29) resulted in an immediate TRPV1-mediated current response with slow baseline recovery, Figure 3.27 B. These data suggest that the terminal amine modification, and, therefore, potential disruption of protein-ligand binding, is not what caused a slow current response when pre-uncaged **128** was applied extracellularly. It was hypothesised that the *location* of compound delivery and the reduced membrane permeability of the uncaged agonist **121** determined the rate of current response - slow when applied extracellularly and rapid when photoreleased intracellularly.

Despite the lowest membrane permeability being observed for the ester-containing derivate **123**, Table 3.1, this compound has not yet been tested in a biological system. This work is on going.

Figure 3.28 summarises the data obtained from the electrophysiological recordings of capsaicin **100** (a membrane permeant TRPV1 agonist represented by the green triangle), the amino-modified TRPV1 agonists **121** and **122** (TRPV1 agonists with reduced membrane permeability, represented by the red triangle); and the caged amine-modified TRPV1 agonist **128** (represented by the blue circle surrounding a red triangle). The rate and duration of current response measured upon application of these agonists is illustrated. Capsaicin **100**, a membrane permeant TRPV1 agonist, resulted in rapid current flow. The amino-modified TRPV1 agonists with reduced membrane permeability, **121** and **122**, resulted in slowly growing currents. Extracellular photolysis of the caged amine-modified TRPV1 agonist **128** resulted in slow current response. Intracellular photolysis of the injected caged amine-modified TRPV1 agonist **128** resulted in rapid and prolonged current response. This data is consistent with an intracellular TRPV1 capsaicin-binding site.

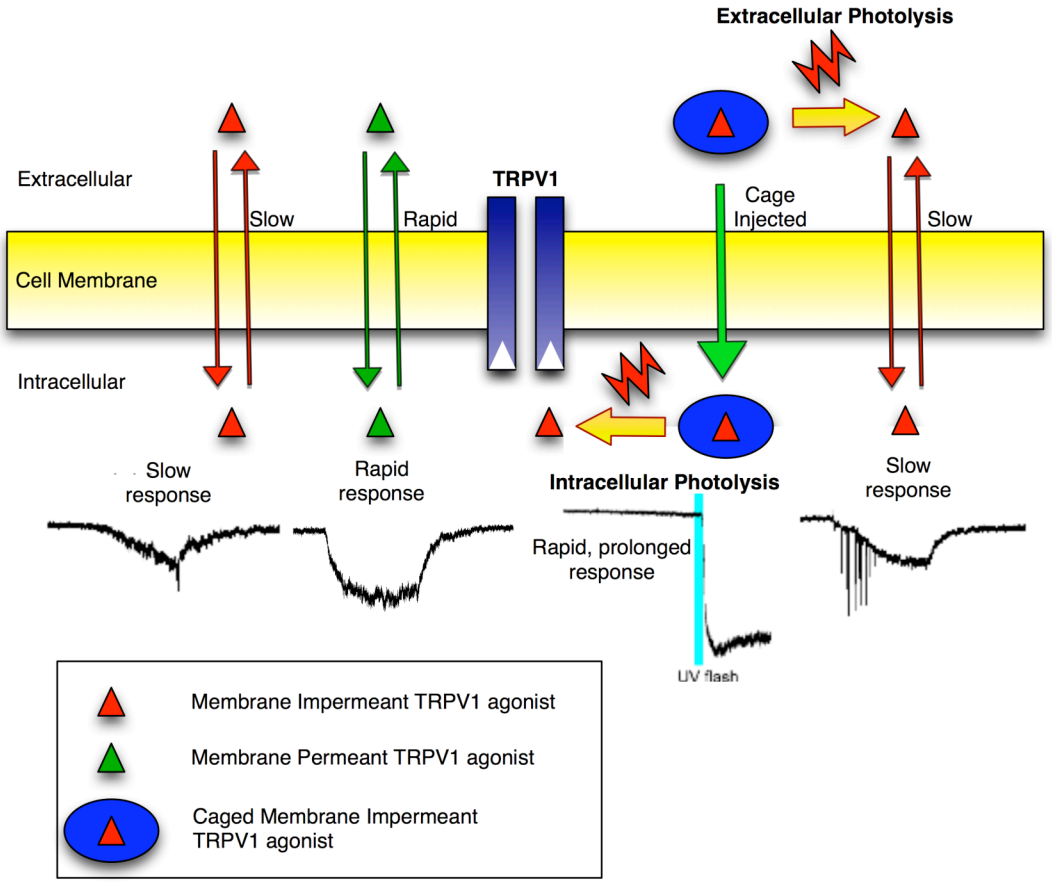

Figure 3.28. Capsaicin **100**, a membrane permeant TRPV1 agonist, resulted in rapid current flow. This is represented by the rapid diffusion of the green triangle across the cell membrane. The amino-modified TRPV1 agonists with reduced membrane permeability, **121** and **122**, resulted in slowly growing currents. This is represented by the slow diffusion of the red triangle across the cell membrane. Extracellular photolysis of the caged amine-modified TRPV1 agonist **128** resulted in slow current response. However, intracellular photolysis of the injected caged amine-modified TRPV1 agonist **128** resulted in rapid and prolonged current response. This observation refutes the hypothesis that the terminal amine modification of **121** disrupts ligand-TRPV1 interaction, resulting in slower current response. Rather, the *location* of application of the amine-modified TRPV1 agonist **121** determines the rate of current response. This data is consistent with an intracellular TRPV1 capsaicin-binding site.

3.2.4. Summary

In order to study the location of the TRPV1 capsaicin-binding site, a range of amino-modified capsaicin derivatives (TRPV1 agonists) were synthesised and analysed for their membrane permeability. Appending a terminal amine or urea functional group to the lipophilic C-region of a capsaicin derivative reduced its membrane permeability. These amino-modified TRPV1 agonists were employed in *in vitro* experiments on trigeminal neurons. Electrophysiological recordings provided evidence for an intracellular TRPV1 capsaicin-binding site.

Chapter 4:

Results and Discussion - Nitroindoline-Caged Glutamate

4. Investigation of Adaptive Immune Response using Nitroindoline-Caged Glutamate

4.1. Introduction and Aims

The aim of this project was to employ caging technology to control T cell activation spatially and temporally. Control over T cell activation would allow for insight to be gained into the initiation of adaptive immune responses and the nature of the resulting immune response.

Adaptive immune responses are initiated by interactions between dendritic cells (DCs) and naïve (inactive) CD4+ T lymphocytes. The surrounding molecules present, such as soluble interleukin (IL)-12 protein,[107] as well as the duration of this initial interaction critically determine the differentiation pathway of the interacting CD4+ T cell. This differentiation pathway defines the nature of the resulting immune response. Therefore, in order to understand how immune responses develop, the cellular interactions between a DC and a T cell need to be investigated.

Greater understanding of the factors regulating the induction of antigen-specific immune responses has been gained using mice expressing transgenic T cell receptors with defined antigenic specificity.[108] These antigen-specific T cells allow for analysis of naïve T cell differentiation. New imaging methods using multiphoton microscopy and fluorescently-labelled cells have

also enabled researchers to directly observe these interactions in living tissues.[109,110] However, it is not currently possible to trigger DC:T cell interactions in specific anatomical locations, or precisely control the time when these interactions begin.

DCs have the unique capacity to migrate to lymph nodes and activate naïve T cells.[111] This activation requires that a molecular complex on the DCs' surface, (containing a DC-encoded major histocompatibility complex (MHC) class II molecule) and an exogenously acquired antigenic peptide are 'presented' to the T cell receptor (TCR) of a naïve T cell of the appropriate specificity. T cells from TCR-transgenic mice are a source of naïve T cells with specificity for defined peptides, such as peptides derived from ovalbumin (OVA). When a DC presents the MHC:OVA peptide complex to a T cell with OVA specificity, the T cell may respond in a number of different ways, depending on the particular characteristics of the presenting DC (DCs are heterogeneous, i.e. have different functional properties)[111] and the responding T cell. For instance, if an activated DC presents OVA to a naïve T cell, the T cell may proliferate, and differentiate into a Th1-type (T helper) cell, able to secrete proteins that enable the killing of intracellular pathogens.[112]

DeMond *et al.* demonstrated control of antigen peptide presentation with a photoreleasable agonist peptide.[113] A 16-mer antigenic peptide was prepared which contained a NVOC-caged lysine residue known to be critical to this particular MHC-TCR interaction. After photolysis, the uncaged antigenic peptide was presented by the MHC to the TCR. This elicited a signalling

cascade response.[113] A year later, in 2007, Huse *et al.* prepared a caged version of a 16-mer antigenic peptide from moth cytochrome c that activates T cells in an MHC-dependent fashion upon irradiation with UV light.[114] It was aimed to apply this strategy to OVA antigenic peptide. It hypothesised that control over the specific anatomical location and time of DC:T cell interaction could be achieved using a photoactivatable (caged) synthetic OVA peptide. The OVA peptide would be rendered biologically inactive by the addition of a photolabile protecting group to glutamate residue 333 that is essential for TCR binding and subsequent T cell activation.[115] It was aimed to synthesise nitroindoline-caged glutamate[42] which would be incorporated into the OVA peptide sequence at this specific site essential for OVA function. It was hypothesised that the inactive peptide would be able to bind to MHC class II molecules on DCs but not activate T cells. Upon photolysis of the caging group, the active antigenic peptide would be revealed. This would enable the active peptide, contained in the MHC/peptide complex on the DC surface, to interact with the TCR on the transgenic T cells and initiate T cell responses. Therefore, the caged OVA peptide would only acquire the ability to activate T cells after irradiation with UV light. An illustration of the process is shown in Figure 4.1.

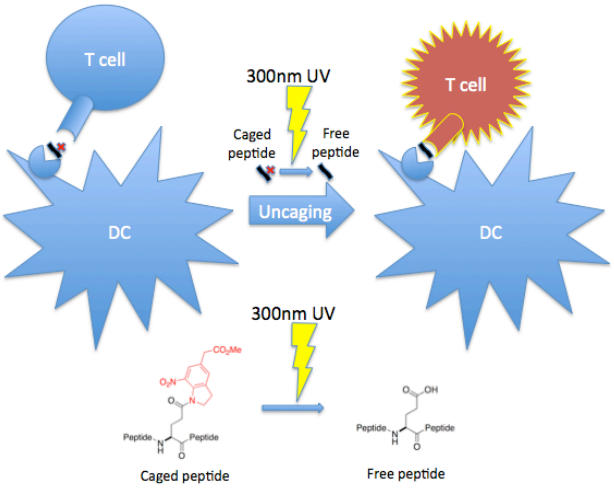

Figure 4.1. OVA-specific transgenic T cell activation by an interaction between a naïve T cell and an OVA peptide 'presented' to the T cell receptor (TCR) by a molecular complex on the DC surface. This activation only occurs after UV irradiation of the caged inactive OVA peptide.

4.2. Synthesis of Nitroindoline-Caged Glutamate

Nitroindoline-caged glutamate **134** was synthesised from 1-acetylindoline **129** in five steps, Scheme 4.1.[42] 1-Acetylindoline **129** was acylated by treatment with acetyl chloride and $AlCl_3$ in CH_2Cl_2 under reflux to obtain 1,5-diacetylindoline **130** in 85% yield.[116] Thallium nitrate (III) trihydrate, in the presence of perchloric acid and MeOH, was used to oxidise 1,5-diacetylindoline **130** to obtain **131** in 60% yield.[117] Acidic methanolysis was used to deprotect the acetyl group from nitrogen to afford **132** in 71% yield. The Boc-protected *tert*-butyl ester of (*S*)-glutamate was coupled to **132** using EDC and DMAP coupling conditions to obtain **133** in 33% yield. Nitration and Boc- and *tert*-butyl-deprotection were achieved in one step by treatment with sodium nitrate in trifluoroacetic acid to obtain the final product, 1-acyl-7-nitroindoline-caged glutamate **134**, in 75% yield. The UV/Vis spectrum of nitroindoline-caged glutamate **134** was recorded. A peak with λ_{max} of 344 nm with an extinction co-efficient of 3200 (L/[mol.cm]) was observed.

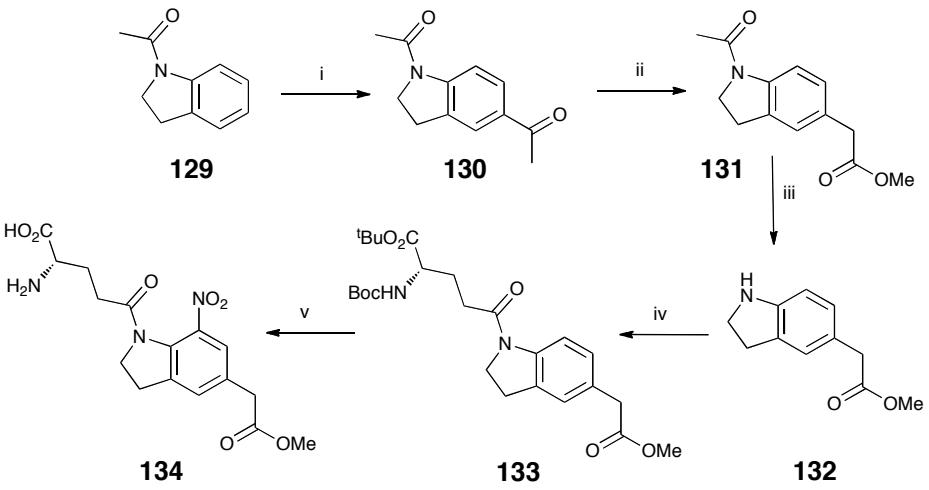

Scheme 4.1. Syntheses of nitroindoline-caged glutamate **134**. *Reagents and conditions:* i. AcCl, $AlCl_3$, CH_2Cl_2, reflux, 85%; ii. $Tl(NO_3)_3$, $HClO_4$, MeOH, 60%; iii. HCl, MeOH, reflux, 71%; iv. (*S*)-5-(*tert*-Butoxy)-4-((*tert*-butoxycarbonyl)amino)-5-oxopentanoic acid, EDC, DMAP, CH_3CN, 33%; v. $NaNO_3$, TFA, 75%.

4.3. Biological Application of Nitroindoline-Caged Glutamate

This work was carried out by our collaborators at the Glasgow Biomedical Research Centre, University of Glasgow, in Dr Simon Milling's laboratory.

Nitroindoline-caged glutamate **134** was incorporated into an $OVA_{323-339}$ polypeptide. This particular peptide ($OVA_{323-339}$) is widely used to generate maximal responses from TCR transgenic ovalbumin-specific T lymphocytes.[115] The purity of the caged peptide was analysed by HPLC and mass spectrometry. The appearance of a new peak in the HPLC trace after exposure to UV light (Figure 4.2) suggested that photolysis of the caging

group had occurred, releasing uncaged OVA peptide. UV light was delivered by a low power, hand-held UV lamp.

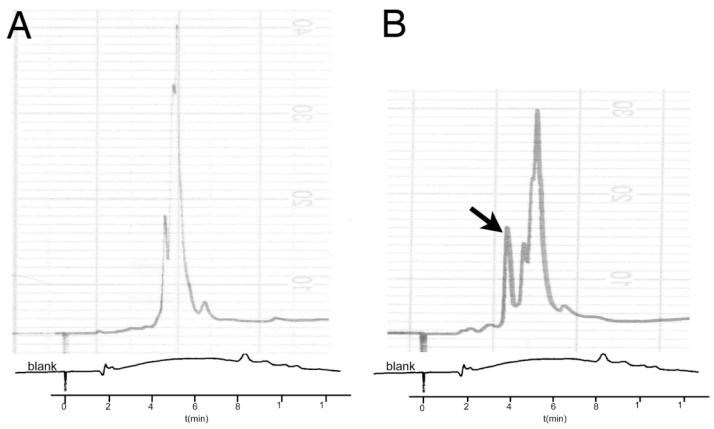

Figure 4.2. A. An HPLC trace of caged OVA peptide. **B.** After irradiation at 365 nm from a low power lamp for 2 hours, a new peak was observed in the HPLC trace due to the photorelease of uncaged OVA peptide. Reversed phase HPLC was carried out using a Vydac C18 column. Two buffers were employed in the elution. Buffer A consisted of 0.05% trifluroacetic acid (TFA) in water; while buffer B consisted of 0.05% TFA in acetonitrile. An elution gradient of 10 - 70% buffer B over 10 min was applied to the column and elution was monitored with UV light at 220nm.

To demonstrate the biological activity of OVA antigenic peptide in T cell activation, the following experiment was performed. DCs were cultured from bone-marrow precursors. On the final day of DC culture, normal OVA peptide was added to the culture well as the positive control. The negative control had no OVA peptide added to the DC culture well. The DCs were then washed and incubated with OVA-specific transgenic T cells for 16 hours. After culture, the T cells were analysed by flow cytometry to determine their activation

status and degree of proliferation. Figure 4.3 represents flow cytometry and immunofluorescence data for the positive control in which normal OVA peptide was added to the DC culture well (top panel), and the negative control in which no OVA peptide was added to the DC culture well (bottom panel).

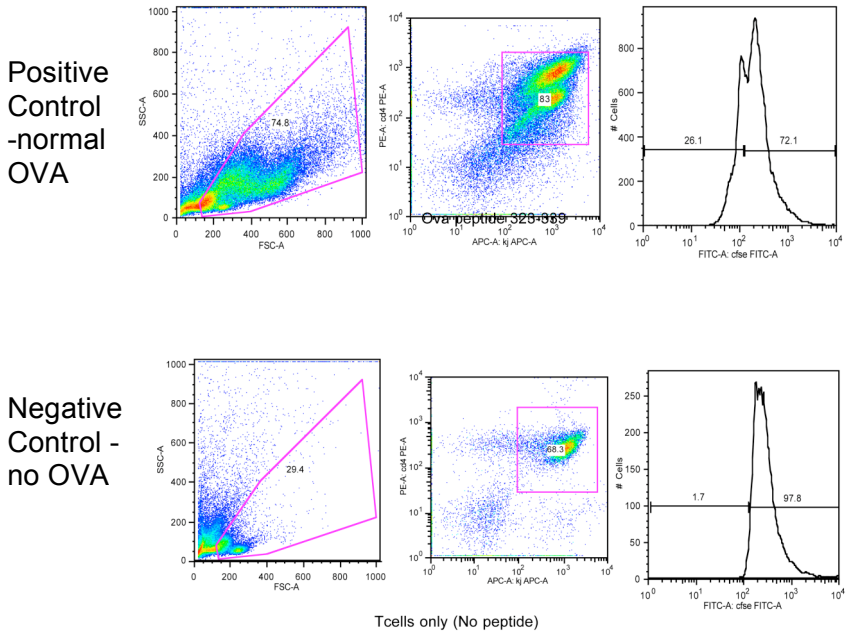

Figure 4.3. Only the DCs cultured with OVA peptide (top panel, positive control) were able to activate T cells, as observed by T cell proliferation. T cell activation was not observed in the negative control (bottom panel), in which no OVA peptide was added to the DC culture well. The proliferating T cells in the positive control are larger than the inactive T cells in the negative control, as observed by a higher forward scatter (x-axis, left-hand graph). The top panel (positive control), right-hand side histogram shows a new cell population (26%) with half the fluorescence of the main cell population (72%). No new cell population was observed in the negative control (bottom panel).

The left-hand graphs in Figure 4.3 represent the side (SSC, y-axis) and forward (FSC, x-axis) scatter measured for every particle. Each particle (which may be a cell) is represented by a dot. These give a representation of the physical characteristics of the particles in the flow cytometer. Where the dots become too dense for individual particles to be observed, colour is used to indicate increasing density. The particles that are within certain parameters can be confidently assigned as cells. Side scatter (y-axis) is a measure of how granular the particle is. Secretory cells, for example, which possess many organelles and secretory vesicles, have high side scatter. T cells tend to have low side scatter. Forward scatter (x-axis) is a measure of the size of the particle. The larger the particle, the higher the forward scatter. The purple boundary in the left-hand graphs (Figure 4.3) denotes which dots are probably cells. The dense region of spots close to the origin of the graph represents cell debris in the flow cytometer. Evidence of T cell activation only in the presence of OVA was observed in the left-hand graphs (Figure 4.3). The proliferating T cells in the positive control are larger than the inactive T cells in the negative control, as observed by a higher forward scatter (x-axis).

The middle graph in each panel of Figure 4.3 represents the fluorescent measurements taken from the cells within the purple boundary in the left-hand graph. The y-axis is the red fluorescence measured from a phycoerythrin-labeled monoclonal antibody which binds to CD4 and, therefore, indicates the presence of CD4 cells. The x-axis indicates the degree of fluorescence at 660 nm, the emission wavelength of antibodies labeled with allophycocyanin (APC), and enables identification of cells bound by the KJ16 monoclonal

antibody. In the transgenic mice from which these cells were derived, the majority of the T cells are from the same clone and have the same specificity, i.e. for OVA, and are KJ16-positive. This antibody recognises the transgenic OVA-specific TCR. Therefore, all the cells within the purple square in this middle graph express CD4 (CD4-PE-positive), and are specific for the OVA peptide (KJ16-APC-positive). Two populations of T cells were observed in the middle graph in the positive control (Figure 4.3, top panel). The population which is lower on the y-axis expresses less CD4. This phenotype is expected when T cells become activated. Only one T cell population (non-activated) was observed in the negative control (Figure 4.3, bottom panel).

The T cells from the purple square in the middle graph (Figure 4.3) were analysed for their proliferation. This is represented in the right-hand box as a histogram, Figure 4.3. The y-axis represents the number of cells. The x-axis is a fluorescence measurement of the carboxyfluorescein succinimidyl ester (CFSE) content of each cell. CFSE is a fluorescent cell-staining dye which is retained within cells because it covalently couples to intracellular protein molecules. The dye can be used to monitor cell proliferation because the CFSE fluorescence is halved within the daughter cells after each cell division.[118] The top panel (Figure 4.3, positive control), right-hand side histogram shows a new cell population (26%) with half the fluorescence of the main cell population (72%). No new cell population was observed in the negative control (Figure 4.3, bottom panel). This confirms that in the presence of $OVA_{323-339}$ antigenic peptide, naïve T cells are activated by the MHC:OVA

peptide complex presented by the DCs and, therefore, proliferate. They are not, however, activated in the absence of the OVA peptide.

The same experiment as described above was used to investigate the biological activity of irradiated caged OVA peptide in T cell activation. DCs were cultured from bone-marrow precursors. On the final day of DC culture, caged OVA peptide, which had been exposed to UV irradiation, was added to the culture well. Caged OVA peptide was irradiated for defined time periods (0, 1, 2, 5 and 10 minutes). The DCs were washed and incubated with OVA-specific transgenic T cells for 16 hours. After culture, the T cells were analysed by flow cytometry to determine their activation status and degree of proliferation (Figure 4.4). It was found that the caged peptide functioned as proposed - only the UV-irradiated, and, therefore, uncaged peptide was able to activate T cells. The longer the irradiation time, the higher the population of daughter T cells, i.e., the greater activation of naïve T cells to active proliferating T cells. Figure 4.4 represents flow cytometry and immunofluorescence data for caged OVA peptide irradiated for zero (top panel) and 10 minutes (bottom panel) and then added to the DC culture well.

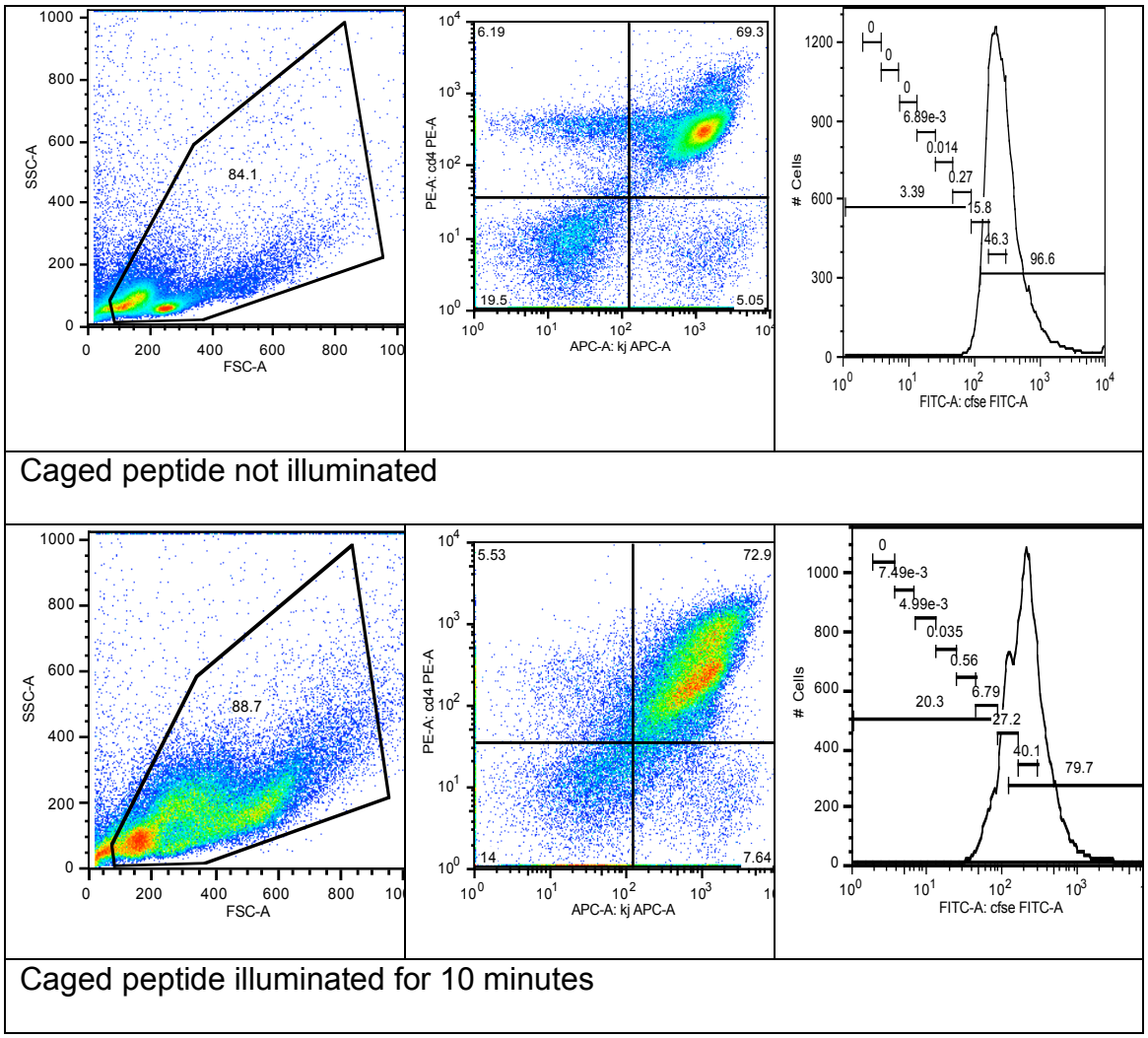

Figure 4.4. Only the DCs cultured with UV-irradiated caged OVA peptide (bottom panel) were able to activate T cells, as observed by T cell proliferation. T cell activation was not observed when the DCs were cultured with caged OVA peptide which had not been irradiated (top panel). The proportion of large cells (which have high forward scatter, x-axis on left-hand graph) and activated cells (low CD4, y-axis on middle graph) was larger due to exposure of the caged peptide to UV light. Using CFSE fluorescence, no new cell population was observed when the caged OVA peptide had not been irradiated (top panel, right-hand histogram). However, a new cell population with half the fluorescence of the parent cell population was observed

when the caged OVA peptide had been irradiated for 10 minutes before addition to the DC culture well (bottom panel, right-hand side histogram).

The proportion of large cells (which have high forward scatter, x-axis on left-hand graph, Figure 4.4) and activated cells (low CD4, y-axis on middle graph, Figure 4.4) appeared to increase with increasing duration of exposure of the caged peptide to UV light. Using CFSE fluorescence, no new cell population was observed when the caged OVA peptide had not been irradiated (top panel, right-hand histogram, Figure 4.4). However, a new cell population with half the fluorescence of the parent cell population was observed when the caged OVA peptide had been irradiated for 10 minutes before addition to the DC culture well (bottom panel, right-hand side histogram, Figure 4.4). This confirms that in the presence of irradiated caged OVA peptide, naïve T cells are activated by the MHC:OVA peptide complex presented by the DCs and, therefore, proliferate. They are not, however, activated by caged OVA peptide in the absence of UV light.

4.4. Summary

These experiments confirm that control over OVA-specific T cell activation can be achieved using OVA antigenic peptide into which nitroindoline-caged glutamate **134** has been incorporated. Using flow cytometry and immunofluorescence measurements, T cell activation and proliferation were not observed in the absence of OVA peptide (Figure 4.3, bottom panel) or in the presence of caged OVA peptide which had not been irradiated with UV

light (Figure 4.4, top panel). However, UV irradiation of caged OVA peptide before addition to the DC culture well did result in T cell activation (Figure 4.4, bottom panel). This is consistent with what was observed when normal OVA peptide was applied to DC cells (Figure 4.3, top panel). It has, therefore, been demonstrated that control over DC:T cell interactions can be achieved using photoactivatable (caged) synthetic OVA peptide. The caged OVA peptide only acquired the ability to activate T cells after irradiation with UV light. However, while the utility of this tool has been demonstrated in this system, it remains to be employed in a study in which the specific anatomical location and time of DC:T cell interactions is controlled in order to gain insight into the role these interactions play in adaptive immune responses.

Chapter 5:

Results and Discussion - Caged Lidocaine

5. Caged Lidocaine: Photoactivatable Na^+ Channel Blocker

5.1. Introduction and Aims

Sodium ion (Na^+) channels are transmembrane proteins which allow for the passage of Na^+ ions across the plasma membrane in response to changes in the cell's membrane potential. In excitable cells, such as neurons, the passage of Na^+ ions into the cell, down its electrochemical gradient, results in further depolarisation. This depolarisation is responsible for the rise phase of an action potential.

The Na^+-conducting α-subunit of the transmembrane Na^+ channel is a single polypeptide chain with a relative molecular mass of approximately 260 000.[119] The channel consists of four domains (D), Figure 5.1. These are referred to as DI, DII, DIII and DIV. Each domain contains six helices, referred to as S1 to S6, which span the membrane.[119] The link between S5 and S6 in each domain forms the outer pore. This link contains the amino acid sequence 'DEKA' in each domain. These four links (one from each domain) together form the selectivity filter, allowing only Na^+ ions to pass through the pore. As a voltage-dependent channel, a voltage sensor is required for its function. The S4 transmembrane helices have been identified as the voltage sensors. These are charged regions containing a number of positively charged lysine

and arginine residues. Substituting uncharged amino acids in this region reduces voltage sensitivity.[120]

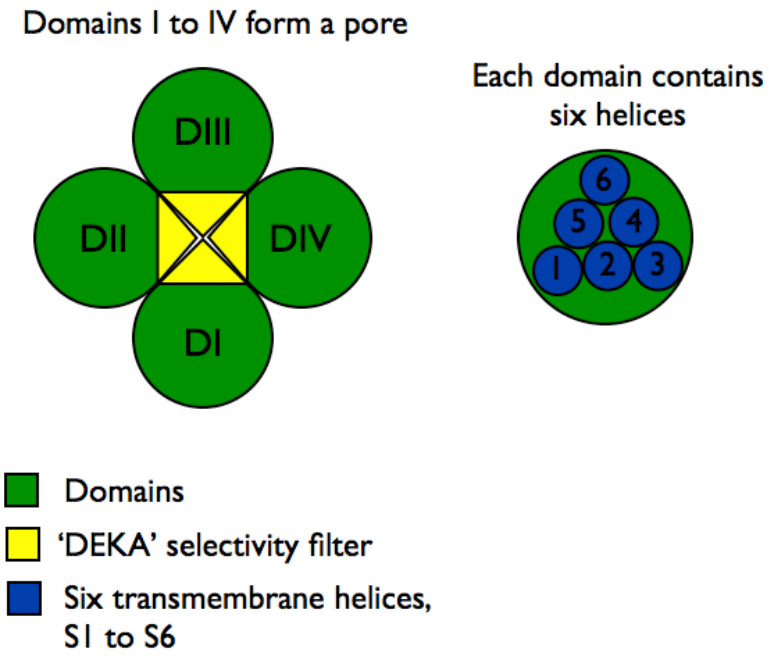

Figure 5.1. A cartoon representation of the Na^+ channel α-subunit. This image represents the top-down view of the four domains (in green) which form the Na^+ conducting pore. Each domain consists of six helices (in blue) which span the membrane. The amino-acid link 'DEKA' between S5 and S6 of each domain acts as a selectivity filter in the outer pore mouth. This selectivity filter, represented by the yellow triangles, allows only Na^+ ions to pass through the pore.[119]

The Na^+ channel is involved in the generation and propagation of action potentials in neurons and muscle cells. The Na^+ channel operates in three states (Figure 5.2). The closed state below -70 mV does not allow passage of ions. The open state is initiated by depolarisation of the transmembrane potential to the threshold potential of -40 mV. Na^+ ions can flow across the membrane through the channel causing further depolarisation and the

generation of an action potential in excitable cells. In this open state, the S4 segments twist back, opening the outer pore mouth.[119] The inactivated third state follows pro-longed depolarisation, caused by an action potential. It allows for re-polarisation of the membrane, by the action of Na^+-K^+ pumps, without the firing of a new action potential.

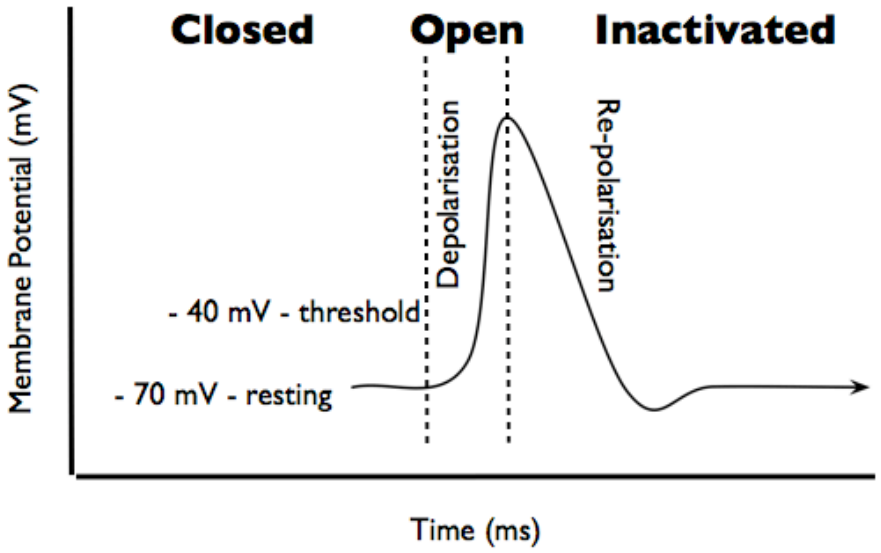

Figure 5.2. The three states of the Na^+ channel are shown in relation to the course of an action potential. The closed state below -70 mV does not allow passage of ions. The open state is initiated by depolarisation of the transmembrane potential to the threshold potential of -40 mV. Na^+ ions can flow across the membrane through the channel causing further depolarisation and the generation of an action potential in excitable cells. The inactivated third state follows pro-longed depolarisation and allows for re-polarisation of the membrane.

Local anaesthetics have been in clinical use for over a century. However, only in the past few decades has the Na^+ channel been identified as the protein target of these compounds.[119] Carl Koller and Sigmund Freud were the first to report the use of cocaine **135**, Figure 5.3, as a local anaesthetic. They noticed a numbing effect on the tongue after swallowing cocaine. They demonstrated

that, within a few minutes of applying cocaine, they could use pins to touch the cornea without any sensation of pain.[119] Many local anaesthetics are now known. Most of those in clinical use consist of a benzene ring linked *via* an amide or ester bond to an amine group.[119] The charged form of the drug, protonated at the amine position, is the active form.[121]

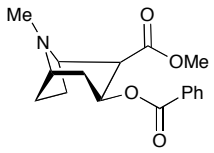

135

Figure 5.3. Structure of cocaine **135**, the crystalline tropane alkaloid obtained from the leaves of the coca plant.

Lidocaine **136**, Figure 5.4, is a local anaesthetic that inhibits voltage-gated Na^+ channels. It has been in clinical use for over 60 years and is one of the most widely used local anaesthetics. Lidocaine binds to voltage-gated Na^+ channels in a 1:1 ratio and prevents the flow of Na^+ ions through the pore. Site-directed mutagenesis studies suggest that multiple S6 segments form a lidocaine binding site within the channel.[122] Lidocaine inhibition is voltage- and use-dependent. The modulated receptor hypothesis has been proposed to account for lidocaine's complex action.[123] This hypothesis proposes that the Na^+ channel can exist in multiple voltage-dependent configurations, and that the affinity and binding rates of local anaesthetics depend on the channel's state.[123] Sheets and Hanck investigated the allosteric consequences of lidocaine binding in the pore on the movement of the voltage sensors (S4

segments).[124] It was demonstrated that lidocaine binding locked movement of the gating charge associated with the S4 segments of domains III and IV but not domains I and II.[124] Therefore, focusing on the S4 segments of domains III and IV, Sheets and Hanck subsequently demonstrated that the depolarised or outward configuration of the voltage sensors of Na^+ channels is the high affinity state in which lidocaine is most tightly bound.[125] This evidence supports the modulated receptor hypothesis for lidocaine block.

136 **137**

Figure 5.4. Lidocaine **136** and its membrane impermeant derivative QX-314 **137**.

QX-314 **137**, Figure 5.4, a quaternary derivative of lidocaine **136**, also blocks Na^+ channels with voltage-dependence.[126,127] However, it only blocks the channels when applied intracellularly. The permanent positive charge of QX-314 **137** renders it membrane impermeant. Most local anaesthetics are sufficiently hydrophobic so as to gain access to their binding site on the Na^+ channel by diffusing into or through the cell membrane.[123] Their ability to diffuse into cells non-selectively and block Na^+ channels causes local anaesthetics to block the excitability of all neurons, not just sensory neurons. In a recent study, it has been demonstrated by Binshtok *et al*.[128] that primary sensory nociceptor (pain-sensing) neurons can be selectively blocked by introducing the charged, membrane-impermeant lidocaine derivative, QX-314

137, into the neurons through TRPV1 channels. Nociceptors are sensory neurons that mediate slowly developing, persistent pain. The TRPV1 receptor is expressed primarily on nociceptors. It forms large ion channels activated by noxious heat and capsaicin **100** (Figure 3.2) the compound responsible for the spiciness of chilli peppers.[80] The ion pore is large enough to allow for the passage of QX-314 into the sensory neuron where it blocks the Na^+ channels. By applying QX-314 **137** and capsaicin **100** together, *in vivo*, only neurons expressing TRPV1 (i.e. sensory nociceptors neurons) were accessible to QX-314 and, therefore, the Na^+ channels of these neurons were selectively blocked. QX-314 could not enter and, therefore, could not block other neurons. Binshtok *et al*.[128] observed long-lasting decreases in mechanical and thermal pain sensitivity but no motor or tactile deficits that are observed with conventional lipid-soluble local anaesthetics, such as lidocaine **136**.

It was proposed that caging technology could be used to study receptors in intact neurons without the contribution of Na^+ channels. Na^+ channels could be 'switched off' with spatial and temporal control by photorelease of the active channel blocker from the inactive precursor. The localised, immediate effect on neighbouring receptors and the neuron as a whole could be observed. In particular, it was planned to apply this tool to the study of *N*-methyl D-aspartate (NMDA) receptors and their role in memory and learning. It was aimed to cage lidocaine **136** and QX-314 **137** with a DMNB caging group and it was proposed that these compounds could be employed to block Na^+ channels, upon photorelease, with spatial and temporal control within neurons. 'Turning off' the Na^+ channels selectively may allow for clarity to be

gained as to the role and function of neural receptors, including the NMDA receptor.

5.2. Synthesis of Caged Lidocaine

Attempts were made to append the 4,5-dimethoxy-2-nitrobenzyl (DMNB) caging group directly onto the amide nitrogen of lidocaine **136** under basic conditions, Scheme 5.1.

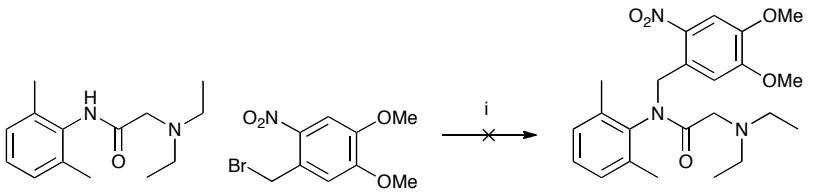

136 **95** **138**

Scheme 5.1. The attempted protection of lidocaine **136** with 4,5-dimethoxy-2-nitrobenzyl bromide **95**. *Reagents and conditions:* i. See Table 5.1.

This reaction proved unsuccessful, possibly because the amide nitrogen's lone pair is delocalised onto the aromatic ring as well as the amide bond, causing it to be a poor nucleophile. Table 5.1 outlines the conditions under which this protection of lidocaine was attempted. In all cases only starting material was isolated.

Base	Equivalents	Solvent	Reaction Conditions
NaH	1.2	THF	RT o/n
NaH	1.1	DMF	RT o/n, then 38 °C 6h
^{t}BuOK	1	THF	RT o/n, TBAI added, heated 50 °C o/n
K_2CO_3	1.1	DMF	40 °C o/n

Table 5.1. Conditions employed to attempt to cage lidocaine **136** with DMNB bromide **95**.

As a result of the failure of this synthetic strategy, a new retrosynthesis for caged lidocaine **138** was devised as shown in Scheme 5.2.

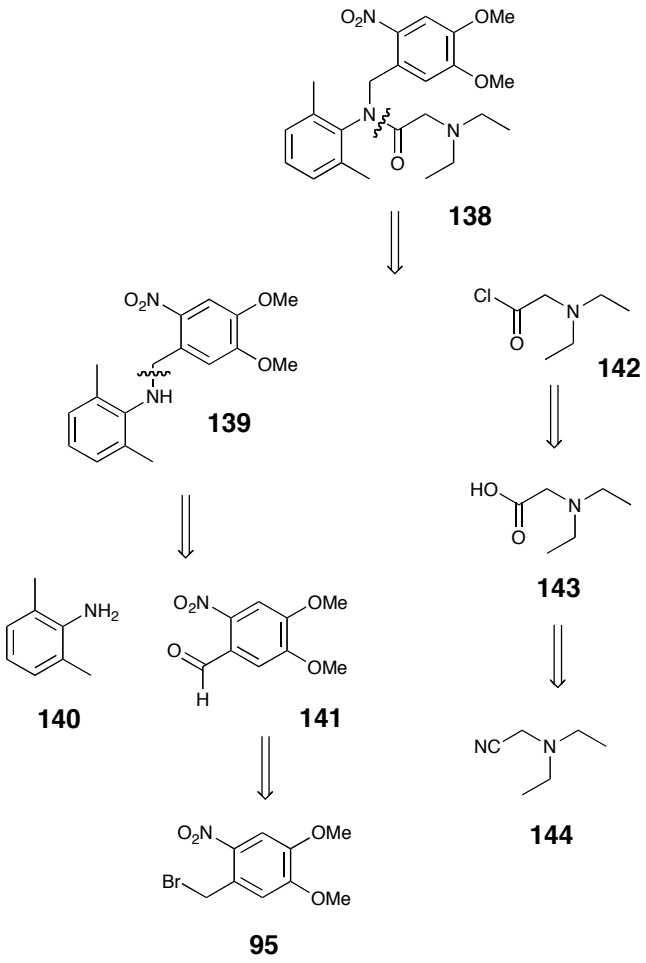

Scheme 5.2. Retrosynthesis for DMNB-caged lidocaine **138**. The proposed synthesis begins with commercially available 2,6-dimethylaniline **140**, 4,5-dimethoxy-2-nitrobenzyl bromide **95** and diethylaminoacetonitrile **144**.

The first disconnection of DMNB-caged lidocaine **138** is at the amide bond to give a secondary amine **139** and an acid chloride **142**. The acid chloride could be obtained from the carboxylic acid, 2-(diethylamino)acetic acid **143**, which in turn could be obtained by hydrolysis of the nitrile group of commercially available diethylaminoacetonitrile **144**. A reductive amination reaction between 2,6-dimethylaniline **140** and 4,5-dimethoxy-2-nitrobenzaldehyde **141** would yield the secondary amine **139**. 4,5-Dimethoxy-2-nitrobenzaldehyde

141 could be obtained *via* oxidation of 4,5-dimethoxy-2-nitrobenzyl bromide **95**.

4,5-Dimethoxy-2-nitrobenzyl bromide **95** was oxidised to the aldehyde **141** using bis(tetrabutylammonium) dichromate in CH_2Cl_2 under reflux. The desired product was obtained in 74% yield, Scheme 5.3.

95 **141**

Scheme 5.3. Oxidation of 4,5-dimethoxy-2-nitrobenzyl bromide **95** to 4,5-dimethoxy-2-nitrobenzaldehyde **141**. *Reagents and conditions:* i. Bis(tetrabutylammonium) dichromate, CH_2Cl_2, reflux, 74%; ii. DMSO, Na_2CO_3, 70 °C, 64%.

An alternative oxidation protocol was investigated using the Kornblum oxidation.[129] The activated benzyl halide undergoes a S_N2 reaction with the nucleophilic oxygen atom of DMSO to form an alkoxysulfonium salt **145** that undergoes deprotonation to form an alkoxysulfonium ylide **146**. A [2,3]-sigmatropic shift of the ylide affords the aldehyde **141**, Scheme 5.4. This reaction yielded 4,5-dimethoxy-2-nitrobenzaldehyde **141** in 64% yield, Scheme 5.3. This method is less toxic than the use of bis(tetrabutylammonium) dichromate as it does not involve the use of chromium ions.

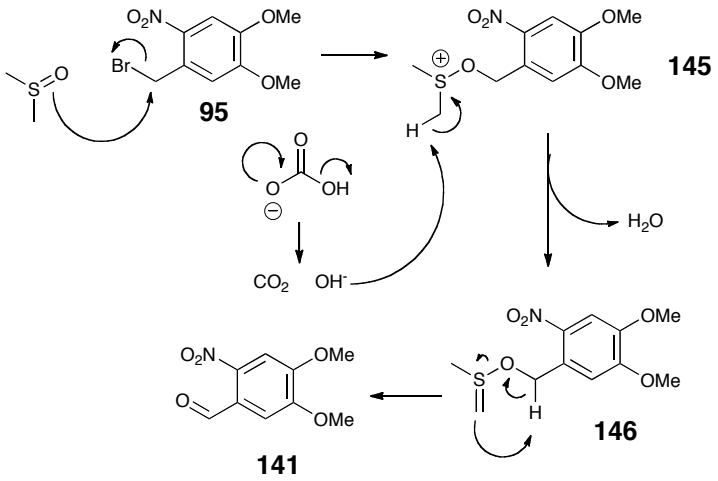

Scheme 5.4. Kornblum oxidation mechanism to obtain 4,5-dimethoxy-2-nitrobenzaldehyde **141** from 4,5-dimethoxy-2-nitrobenzyl bromide **95**.

4,5-Dimethoxy-2-nitrobenzaldehyde **141** was also obtained from 4,5-dimethoxy-2-nitrobenzyl alcohol by treatment with Dess Martin periodinane. This method proved to be the most successful method and yielded the desired aldehyde **141** in 98% yield with little purification required.

The reason for using a reductive amination reaction between dimethylaniline **140** and 4,5-dimethoxy-2-nitrobenzaldehyde **141**, was because attempts to directly couple dimethylaniline **140** and DMNB bromide **95** under basic conditions in DMF under reflux failed, Scheme 5.5. Only starting material was observed.

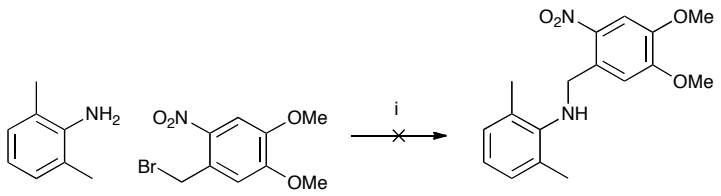

140 **95** **139**

Scheme 5.5. Attempted coupling of dimethylaniline **140** and 4,5-dimethoxy-2-nitrobenzyl bromide **95** to form DMNB-dimethylaniline **139**. *Reagents and conditions:* i. K_2CO_3, TBAI, DMF, reflux.

The first attempt at reductive amination between dimethylaniline **140** and 4,5-dimethoxy-2-nitrobenzaldehyde **141**, using $NaBH_3CN$ as the reducing agent, failed as the imine did not form. The reason that this reaction failed may be due to the poor nucleophilic character of the primary amine of dimethylaniline **140** as its lone pair of electrons is conjugated with the aromatic ring. In addition to this, the two methyl groups cause the amine to be sterically hindered, preventing the amine from forming an imine with the aldehyde under the conditions employed.

It was observed that by heating dimethylaniline **140** and 4,5-dimethoxy-2-nitrobenzaldehyde **141** neat at 100 °C for 3 hours, the imine **147** was obtained, Scheme 5.6. The imine was also obtained using $Ga(OTf)_3$ as a Lewis acid and reacting dimethylaniline **140** and 4,5-dimethoxy-2-nitrobenzaldehyde **141** in CH_2Cl_2 at room temperature. This reaction was successful even when 0.01 equivalents of the catalyst were used. These mild reaction conditions for imine formation were a potential improvement over the

initial conditions, which required high temperatures, however, a lower yield was obtained. The presence of the Lewis acid, even at 0.5 equivalents, did not facilitate imine reduction and so a one-pot reductive amination was not achieved.

Reduction of the imine **147** was surprisingly challenging. The isolated imine **147** was treated with $NaBH_3CN$ in MeOH and left stirring at room temperature overnight. However, only the unreduced imine **147** starting material was obtained from the reaction. Reduction of the isolated imine was attempted using $NaBH_4$ and MeOH under reflux; as well as $NaBH_4$ with $CaCl_2$ and MeOH under reflux. These attempts were unsuccessful as no reduction of the imine was observed. However, treatment of the isolated imine with 6.0 equivalents of $NaBH_4$ in acetic acid at room temperature overnight yielded the secondary amine, DMNB-dimethylaniline **139**, in 97% yield, Scheme 5.6.

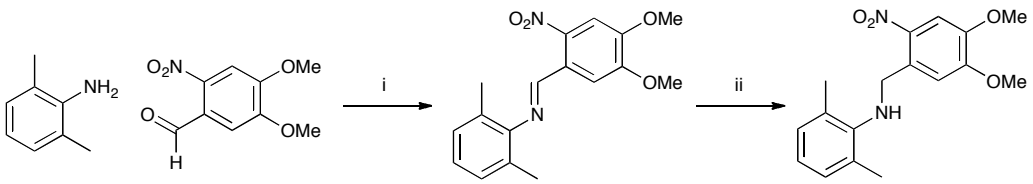

140 **141** **147** **139**

Scheme 5.6. Two-step reductive amination of dimethylaniline **140** and 4,5-dimethoxy-2-nitrobenzaldehyde **141** to form DMNB-dimethylaniline **139**. *Reagents and conditions:* i. 100 °C, 3 h, 100% or $Ga(OTf)_3$, CH_2Cl_2, RT, 75%; ii. $NaBH_4$, acetic acid, RT, 97%.

To form the other half of the desired product, 2-(diethylamino)acetic acid **143** was obtained from diethylaminoacetonitrile **144** by hydrolysis of the nitrile group using excess NaOH in water and THF, Scheme 5.7. 2-(Diethylamino)acetic acid **143** was then acidified using HCl in order to form the protonated carboxylic acid. There were difficulties in purifying this amino acid derivative and removing the large amount of NaCl salt, which formed from the neutralisation of NaOH with HCl. Reverse phase silica gel chromatography and an SCX ion exchange column were unsuccessfully employed. Ultimately the impure product **143** was used in the next reaction with some NaCl present in the product mixture.

In order to couple the secondary amine, DMNB-dimethylaniline **139**, with 2-(diethylamino)acetic acid **143**, synthesis of the acid chloride derivative **142** using oxalyl chloride was attempted. A solution of 2-(diethylamino)acetic acid **143** and distilled oxalyl chloride in DMF was reacted for an hour at room temperature and then added *via* cannula to a solution of the secondary amine **139** in CH_2Cl_2, Scheme 5.7. The resulting reaction mixture was left stirring overnight at room temperature. This coupling reaction was unsuccessful and only amine **139** starting material was obtained from the reaction.

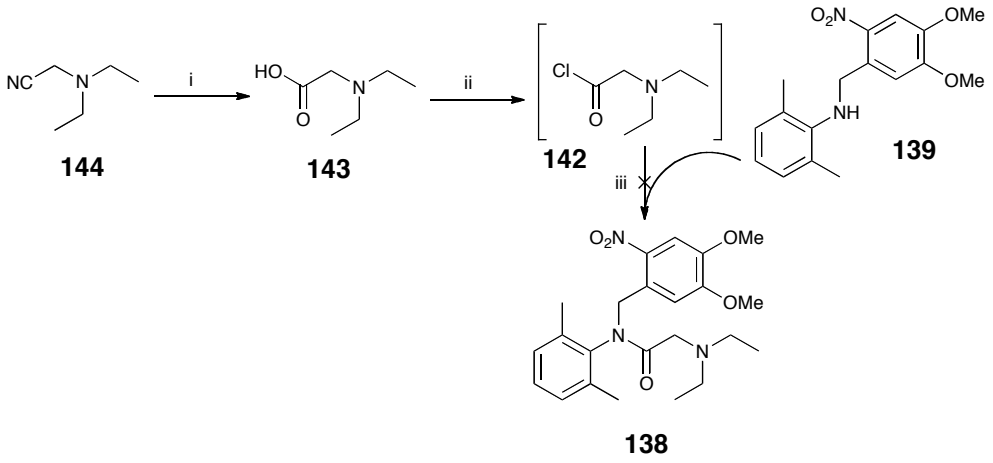

Scheme 5.7. Attempted synthesis of DMNB-caged lidocaine **138** from diethylaminoacetonitrile **144** and DMNB-dimethylaniline **139**. *Reagents and conditions:* i. NaOH, H_2O, THF, reflux; ii. oxalyl chloride, DMF, RT; iii. CH_2Cl_2, RT.

A new synthetic strategy was employed in order to complete the synthesis of DMNB-caged lidocaine **138**, Scheme 5.8. DMNB-dimethylaniline **139** was treated with chloroacetal chloride **148** in toluene under reflux to obtain the amide **149** in 77% yield. The α-chloride of **149** was proposed to be highly susceptible to S_N2 attack by diethylamine due to orbital overlap between the π^* C=O and σ^* C-Cl bonds (Chapter 6).[130] However, an attempt at reacting the α-chloro-containing amide **149** with diethylamine in toluene under reflux was unsuccessful. Only starting material was obtained. However, by reacting the amide **149** with neat diethylamine, using a small volume of DMF to form a homogeneous solution and a catalytic amount of TBAI, DMNB-caged lidocaine **138** was obtained as a yellow solid in 65% yield, Scheme 5.8.

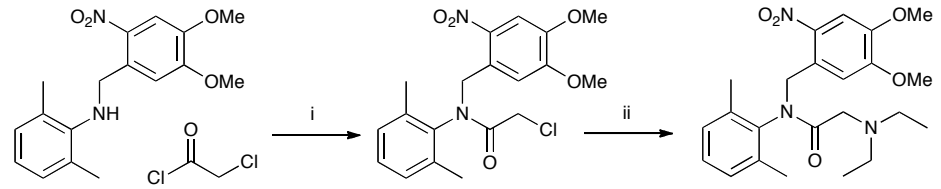

Scheme 5.8. Synthesis of DMNB-caged lidocaine **138** from DMNB-dimethylaniline **139**. *Reagents and conditions:* i. Toluene, reflux, 3 h, 77%; ii. $HNEt_2$, DMF, TBAI, 60 °C, 18 h, 65%.

An additional ethyl group was incorporated at the amine functional group of DMNB-caged lidocaine **138**, using ethyl iodide in CH_3CN, to form DMNB-caged QX-314 **150**, Scheme 5.9.[131]

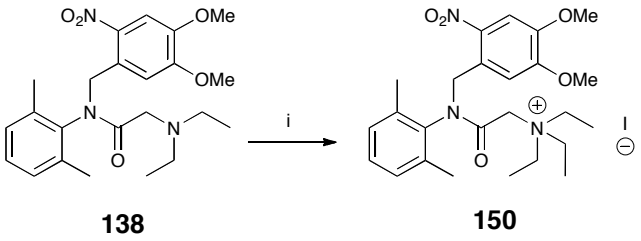

Scheme 5.9. Synthesis of DMNB-caged QX-314 **150** from DMNB-caged lidocaine **138**. *Reagents and conditions:* i. EtI, CH_3CN, RT, 120 h, 83%.

5.3. UV/Vis Spectrum of DMNB-Caged Lidocaine

The UV/Vis absorption spectrum of DMNB-caged lidocaine **138** was obtained to provide an indication of which wavelengths were most likely to evoke successful photolysis.

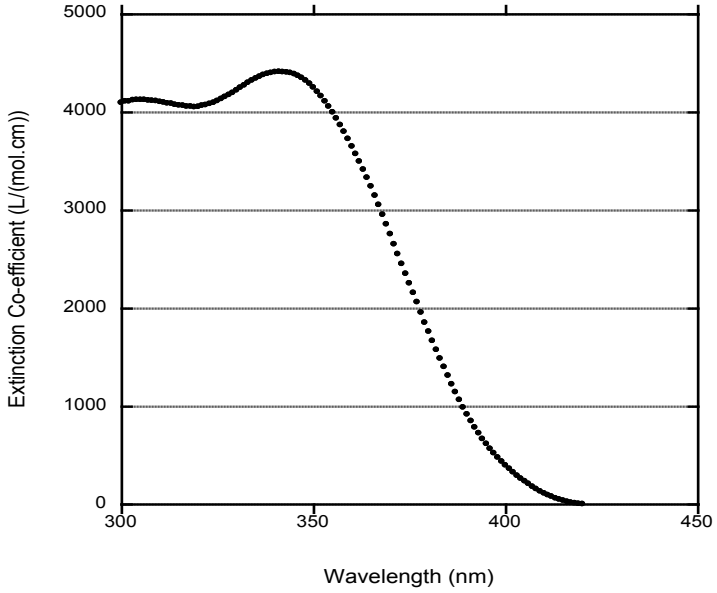

Figure 5.5. UV/Vis absorption spectrum of DMNB-caged lidocaine **138**, 0.1 mM in THF.

DMNB-caged lidocaine **138** (0.1 mM in THF) was observed to have λ_{max} of 340 nm and an extinction co-efficient (ε) of 4410 $M^{-1}cm^{-1}$, Figure 5.5.

5.4. Photolysis of DMNB-Caged Lidocaine

Before DMNB-caged lidocaine **138** was employed in *in vitro* studies, its photolysis characteristics were investigated. It was aimed to observe and quantify the compounds present after irradiation. Photolysis of DMNB-caged lidocaine **138** was proposed to yield free lidocaine **136** and a nitrosoaldehyde photolysis by-product **151**, Scheme 5.10.

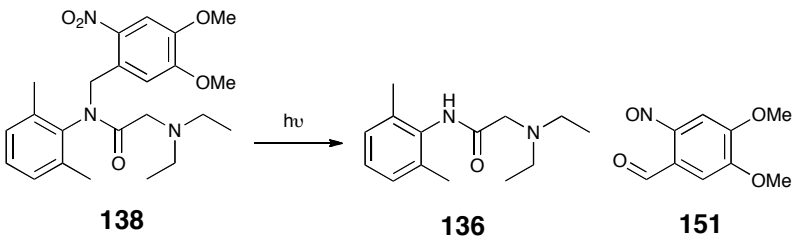

138 **136** **151**

Scheme 5.10. Photolysis of DMNB-caged lidocaine **138** was proposed to yield free lidocaine **136** and a nitrosoaldehyde photolysis by-product **151**.

Photolysis of DMNB-caged lidocaine **138** was carried out on 1 mL samples of a 3 mM solution in THF. During photolysis experiments, aliquots (1 mL) of the solution were placed into UV transmitting quartz cuvettes and exposed to light from the given laser source for fixed time durations. After exposure to laser irrradiation the solutions were analysed using ^{1}H NMR. For quantification by ^{1}H NMR, the THF from each sample was removed and 1 mL $CDCl_3$ added. A standard solution of hexamethyldisiloxane in $CDCl_3$ was added to each sample so that the ratio of sample to standard in each aliquot was 1:1. This ratio was used to determine the amount of caged **138** and uncaged **136** (free

lidocaine) material present in the photolysis samples. Please refer to the General Experimental Section for details about the photolysis experiments.

5.4.1. High Power Photolysis

The first experiment involved exposing the caged compound **138** to laser irradiation at 355 nm and 96 mJ energy for a time period of 1, 2, 3, 4 and 5 minutes. A control sample that was left on the bench for the duration of the experiment but not exposed to laser irradiation was also analysed. It was found that no caged material **138** was observed after 1 minute, it had been consumed *via* photolysis. It is interesting to note, however, that the amount of free lidocaine **136** observed did not increase throughout the time course but remained at approximately 50% of the total initial material, as shown in Figure 5.6.

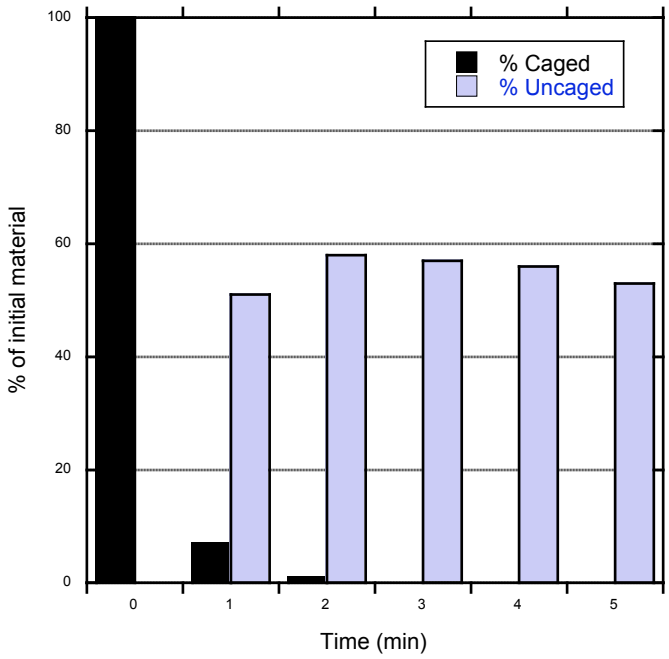

Figure 5.6. Quantification of photolysis of DMNB-caged lidocaine **138** following irradiation at 96 mJ, 355 nm in THF for zero, 1, 2, 3, 4 and 5 minutes, using ^{1}H NMR with hexamethyldisiloxane standard in $CDCl_3$.

The ^{1}H NMR spectra of the photolysis samples of DMNB-caged lidocaine **138** after exposure to irradiation at 96 mJ, 355 nm in THF for zero, 1, 2 and 3 minutes, are overlaid in Figure 5.7. The disappearance of peaks from the caged compound **138** (○), at 0.85, 1.85, 2.50, 3.85 and 5.15 ppm, and the appearance of peaks from what appears to be free lidocaine **136** (□), at 1.10, 2.15, 2.65 and 3.15 ppm, were observed. The 1-minute sample was spiked with commercially available free lidocaine. The ^{1}H NMR of this solution supports the hypothesis that the peaks that appear due to photolysis are in fact from free lidocaine **136** and not other potential photolysis products of DMNB-caged lidocaine **138**.

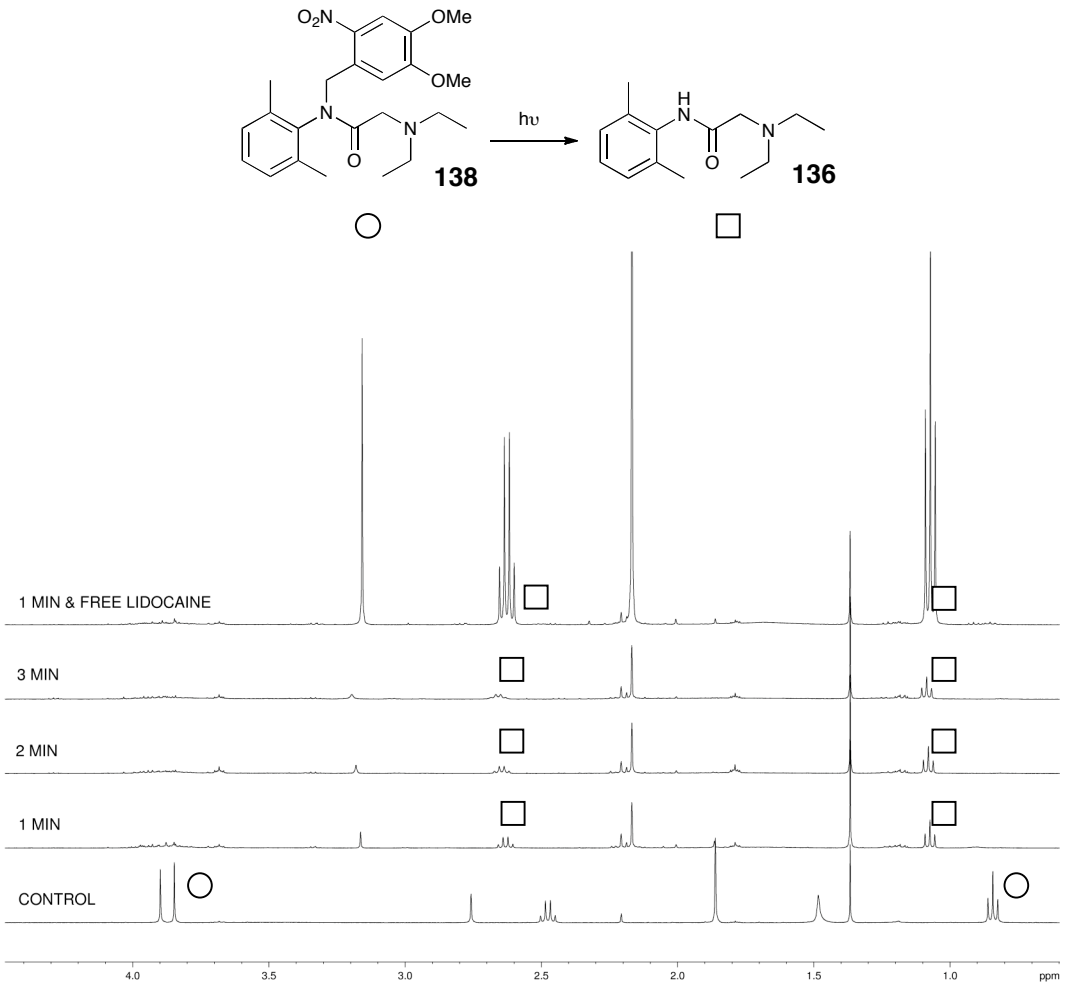

Figure 5.7. Partial 300 MHz ^{1}H NMR spectra in $CDCl_3$ of DMNB-caged lidocaine **138** photolysed at 96 mJ, 355 nm in THF for zero, 1, 2, and 3 minutes. Hexamethyldisiloxane standard in $CDCl_3$ was added to each sample after irradiation. The disappearance of peaks corresponding to the caged compound **138** (○), including those at 0.85, 1.85, 2.50 and 3.85 ppm, and the appearance of peaks from what appears to be free lidocaine **136** (□), at 1.10, 2.15, 2.65 and 3.15 ppm, were observed. The 1-minute sample was spiked with commercially available free lidocaine as shown by the top spectrum.

5.4.2. Lower Power Photolysis

Having observed rapid and complete photolysis of DMNB-caged lidocaine **138** during irradiation at 96 mJ, the caged compound was exposed to laser irradiation at 355 nm and 25 mJ energy for a time period of 1, 2, 3, 4 and 5 minutes. No caged material **138** was observed after 2 minutes. However, once again the amount of free lidocaine **136** did not continue to increase throughout the photolysis run, as one might expect, but levelled off after 1 minute, Figure 5.8.

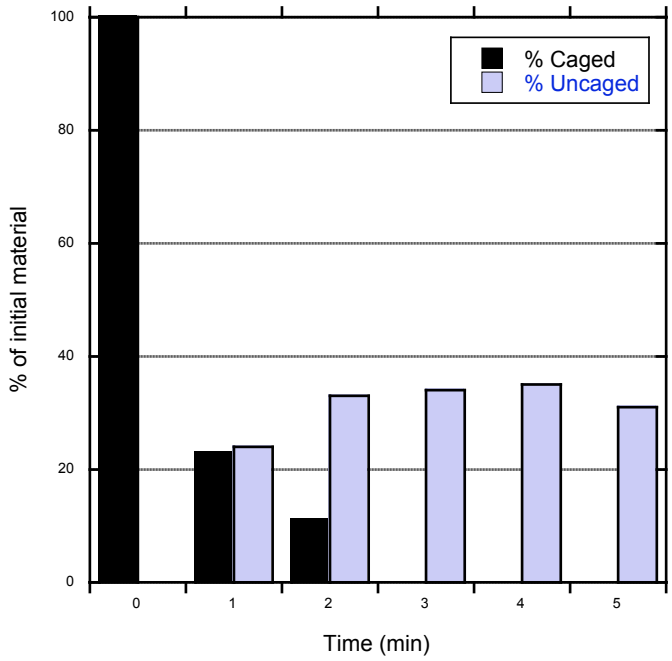

Figure 5.8. Quantification of photolysis of DMNB-caged lidocaine **138**, following irradiation at 25 mJ, 355 nm in THF for zero, 1, 2, 3, 4 and 5 minutes, using ^{1}H NMR with hexamethyldisiloxane standard in $CDCl_3$.

The ^{1}H NMR spectra of the photolysis samples of DMNB-caged lidocaine **138** after exposure to irradiation at 25 mJ, 355 nm in THF for zero, 1, 2, 3, 4 and 5 minutes are overlaid in Figure 5.9. Impurities visible in all of the ^{1}H NMRs are from the standard, hexamethyldisiloxane, as confirmed by a ^{1}H NMR of the standard alone in $CDCl_3$. As with the 96 mJ irradiation, peaks corresponding to the caged compound **138** (○) disappeared while peaks corresponding to free lidocaine **136** (□) appeared during photolysis.

Figure 5.9. Partial 300 MHz ^{1}H NMR spectra in $CDCl_3$ of DMNB-caged lidocaine **138** photolysed at 25 mJ, 355 nm in THF for zero, 1, 2, 3, 4 and 5 minutes. Hexamethyldisiloxane standard in $CDCl_3$ was added to each sample after irradiation. The disappearance of peaks from the caged compound **138** (○), including those at 0.85, 1.85, 2.50 and 3.85 ppm, and the appearance of peaks from what appears to be free lidocaine **136** (□), at 1.10, 2.15, 2.65 and 3.15 ppm, were observed. The top spectrum is that of commercially available free lidocaine in the same NMR solvent. The peaks from this spectrum correspond to those which appear due to photolysis.

Having observed rapid photolysis of **138** at 25 mJ, it was decided to determine whether uncaging would occur at very low power. When DMNB-

caged lidocaine **138** was exposed to laser irradiation at 355 nm and 1 mJ energy for a time period of 1, 2, 3, 4, 5 and 10 minutes, it was found that photolysis did occur. However, caged material **138** was observed even after 10 minutes, Figure 5.10.

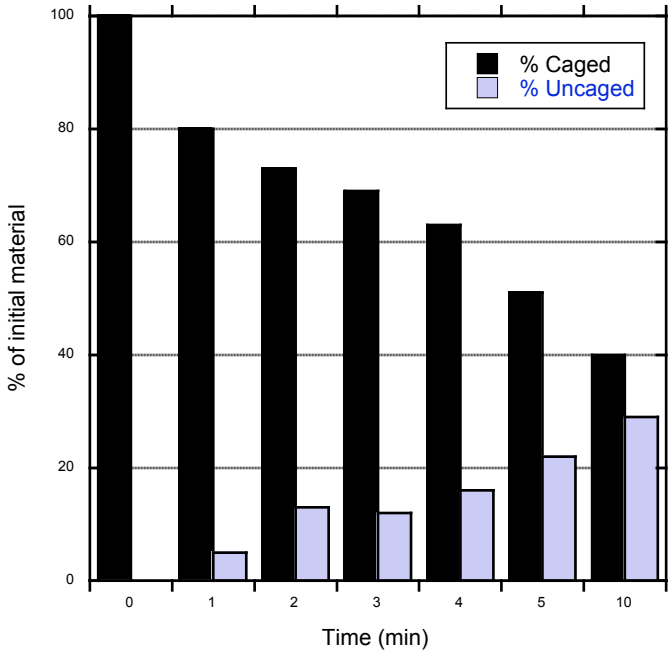

Figure 5.10: Quantification of photolysis of DMNB-caged lidocaine **138**, following irradiation at 1 mJ, 355 nm in THF for zero, 1, 2, 3, 4, 5 and 10 minutes, using ^{1}H NMR with hexamethyldisiloxane standard in $CDCl_3$.

The ^{1}H NMR spectra of the photolysis samples of DMNB-caged lidocaine **138** after exposure to irradiation at 1 mJ, 355 nm in THF for zero, 1, 2, 3, 4, 5 and 10 minutes, are overlaid in Figure 5.11. The triplet at 0.85 ppm, corresponding to the ethyl groups of DMNB-caged lidocaine **138** (○), diminished over the course of irradiation. A triplet at 1.05 ppm, corresponding to free (uncaged) lidocaine **136** (□), appeared and increased with increasing duration of irradiation.

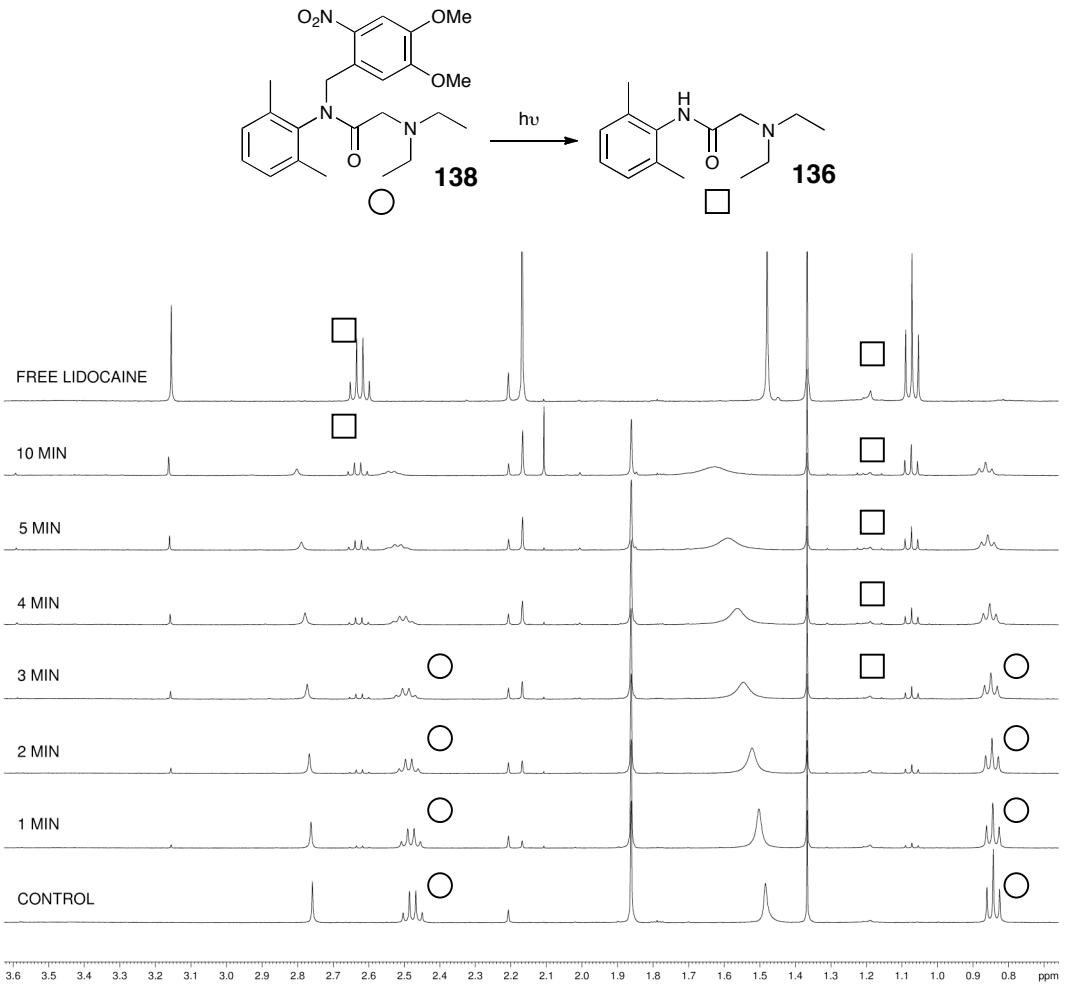

Figure 5.11. Partial 300 MHz ^{1}H NMR spectra in $CDCl_3$ of DMNB-caged lidocaine **138** photolysed at 1 mJ, 355 nm in THF for zero, 1, 2, 3, 4, 5 and 10 minutes. Hexamethyldisiloxane standard in $CDCl_3$ was added to each sample after irradiation. The top spectrum is that of commercially available free lidocaine. Peaks at 0.85, 3.85 and 3.90, corresponding to DMNB-caged lidocaine **138** (○), diminished over the course of irradiation. A triplet at 1.05 ppm, corresponding to free (uncaged) lidocaine **136** (□), appeared and increased with increasing duration of irradiation.

5.4.3. Photolysis Conclusions

These photolysis studies confirmed that photolysis of DMNB-caged lidocaine **138** yields free lidocaine **136**. DMNB-caged lidocaine was, therefore, employed in *in vitro* experiments to assess the effect that this caged anaesthetic has on the generation of action potentials by neurons.

However, in all of the experiments carried out, the total amount of material appeared to decrease as the length of irradiation increased. The percentage of caged **138** and uncaged **136** compound did not add up to 100%. This discrepancy was more pronounced with higher power and longer duration irradiation. It may be that there is another photolysis pathway. If the amide bond of DMNB-caged lidocaine **138** is cleaved, a stable radical **152** is formed, Scheme 5.11. This secondary amine could photolyse further to form a nitrosoaldehyde **151** and 2,6-dimethylaniline **140**, which may have been removed under high vacuum before quantification by ^{1}H NMR was carried out, Scheme 5.11.

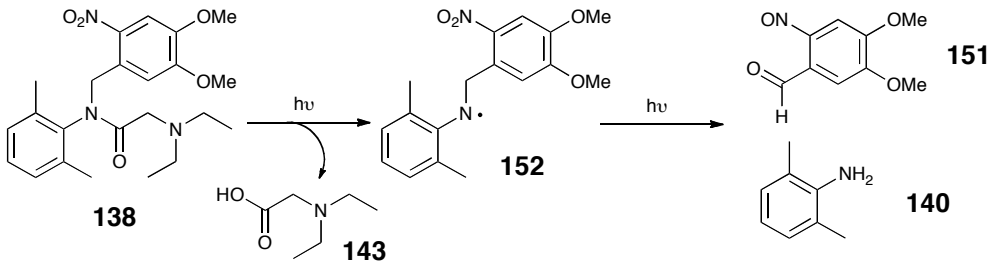

Scheme 5.11. Proposed competing photolysis pathway of DMNB-caged lidocaine **138** to yield 2-(diethylamino)acetic acid **143**, nitrosoaldehyde **151** and 2,6-dimethylaniline **140** as photolysis products.

In order to determine if the uncaged lidocaine **136** itself breaks down when exposed to laser irradiation, 1 mL aliquots of a 3 mM solution of commercially available free lidocaine in THF were exposed to laser irradiation at 355 nm and 96 mJ energy for 1, 2, 3, 4 and 5 minutes. It was found that free lidocaine **136** did not decompose when exposed to this high power laser irradiation. However, this does not rule-out that radicals formed from photolysis of the caging group may cause degradation of lidocaine.

It is difficult to extrapolate the significance of these results to *in vitro* photolysis. In cuvette experiments, a greater quantity of material is used, in order to make detection of the products possible, and irradiation for a greater length of time is required in order to photolyse a significant proportion of the caged material. In contrast, photolysis in cells is carried out on micromolar concentrations for less than a second. It is therefore possible that the

observed wasteful photodegradation is an artefact of the conditions employed and would not have an affect on *in vitro* experiments.

5.5. Application of DMNB-caged Lidocaine to a Biological System

Having demonstrated photorelease of lidocaine **136** from DMNB-caged lidocaine **138** in a cuvette, photolysis in neurons was attempted. The application of the caged anaesthetic to hippocampal pyramidal neurons was carried out by our collaborators at the Department of Pharmacology at the University of Oxford, Dr Nigel Emptage and Dr Chanel Taylor.

It was observed that DMNB-caged lidocaine **138** was not inactive. It still acted as an anaesthetic, blocking Na^+ channels and, therefore, the propagation of action potentials, Figure 5.12.

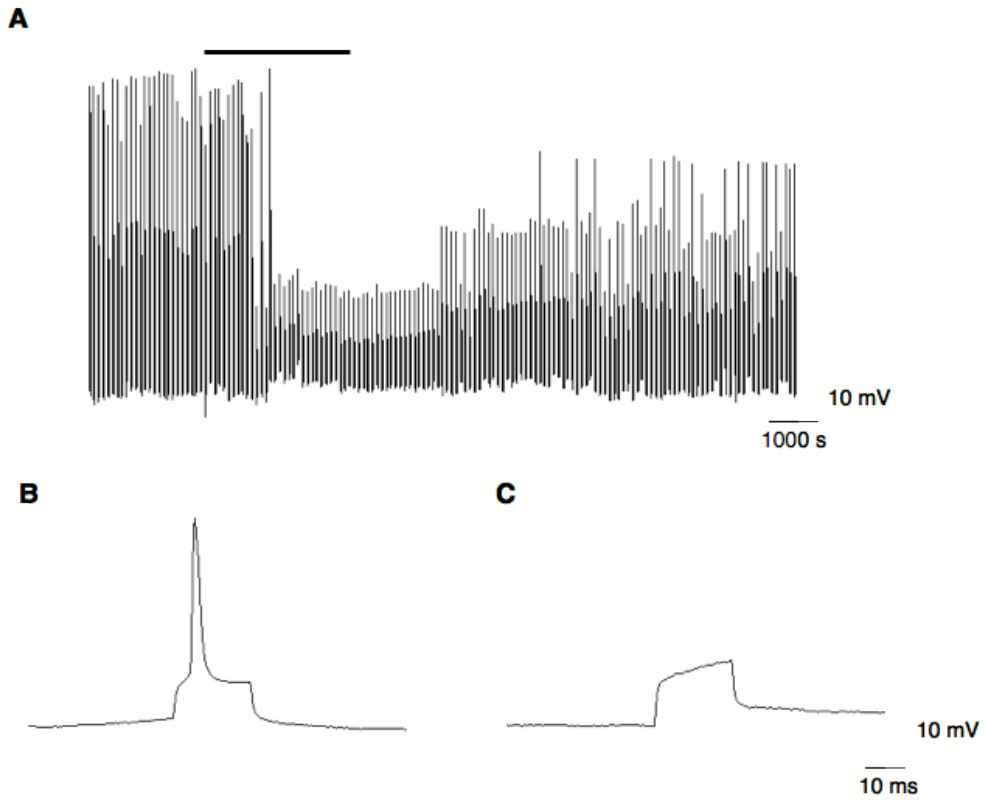

Figure 5.12. Voltage traces obtained from a representative neuron showing the effect of adding 1 mM DMNB-lidocaine **138** to the bathing solution. Panel A: addition of DMNB-lidocaine **138** (represented by the horizontal line) terminated action potential firing. Panel B: somatic current injection elicits action potentials under control conditions. Panel C: under the same conditions, after the addition of DMNB-lidocaine **138** to the bath solution, no further action potentials could be elicited in response to the same current injection.

Panel A, Figure 5.12, is a summary of the experiment recorded using sharp micro-electrodes. DMNB-lidocaine **138** was added for the duration of the horizontal line in A. The concentration of the compound was 1 mM. Panel B shows that current injection resulted in action potential firing under control conditions. Panel C shows that when caged lidocaine **138** had been added,

no further action potentials could be elicited in response to the same current injection. The membrane potential of the cell remained stable at -70mV for the duration of the experiment.

The caged compound **138** was thoroughly assessed for purity to ensure that no free lidocaine **136** was present in the sample. ^{1}H NMR and elemental analysis confirmed that only DMNB-lidocaine **138** was present in the biological sample. Upon repeating the current injection experiment, the same result (Figure 5.12) was obtained.

It has previously been observed that caging a biologically active compound did not result in termination of its activity. A nitrobenzyl-caged ∝-adrenoceptor agonist blocked Ca^{2+} channels in smooth muscle cells at high concentrations.[132] Nitrophenyl(ethyl) (NPE)-caged ATP was observed to block ATP-dependent K^{+} channels.[133]

The DMNB caging group attached to the amide nitrogen was not able to block the activity of lidocaine. The charged, (amine) protonated form of lidocaine is required for its activity as a Na^{+} channel blocker.[121] It seems that charged DMNB-caged lidocaine **138**, protonated at the amine nitrogen, could still block the Na^{+} channel despite the steric bulk of the DMNB caging group. A new caging group and position of attachment of the caging group were considered.

5.6. Caging Lidocaine at the Amine Functional Group

Caging a biologically active compound can change its electronic characteristics, not just its steric bulk, in order to render the compound inactive. It was proposed to cage a lidocaine derivative **154** (Scheme 5.12) at the amine position. This derivative has one ethyl group appended to its amine nitrogen, instead of two ethyl groups which are appended to the tertiary amine of lidocaine **136**. It was hypothesised that caging this lidocaine derivative at the amine group may block its activity by changing the pK_a of the nitrogen lone pair. Preventing protonation of the nitrogen may prevent the caged compound from blocking Na^+ channels. It was aimed to synthesise a caged lidocaine derivative with a DMNB carbamate (CDMNB) group appended at the amine position **153** (Scheme 5.12). The amine would, therefore, exist as a carbamate in the caged compound. The conjugate acid of carbamates has a pK_a below zero. Therefore, protonation of this nitrogen would not occur in the caged compound. Photolysis of this compound would yield a lidocaine-like derivative **154**, in which the secondary amine is appended with only one ethyl group, Scheme 5.12.

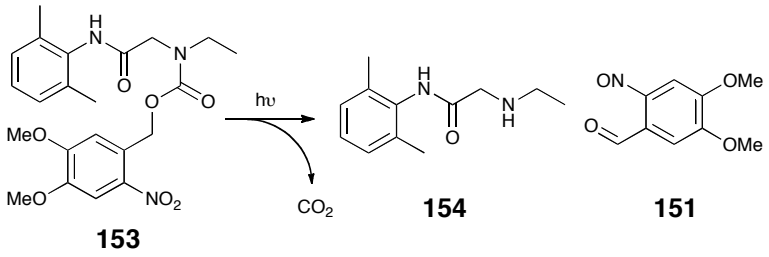

153 **154** **151**

Scheme 5.12. Proposed new DMNB Carbamate (CDMNB)-caged lidocaine derivative **153**. Photolysis would yield a lidocaine-like derivative **154**.

2,6-Dimethylaniline **140** was treated with chloroacetal chloride **148** in CH_2Cl_2 with anhydrous pyridine at room temperature to obtain the amide **155** in quantitative yield, Scheme 5.13. Upon treatment of the α-chloro amide intermediate **155** with ethylamine, the lidocaine derivative **154** was obtained in 52% yield. Coupling of this secondary amine **154** with DMNB chloroformate in CH_2Cl_2 with triethylamine, yielded the CDMNB-caged lidocaine derivative **153** in 35% yield.

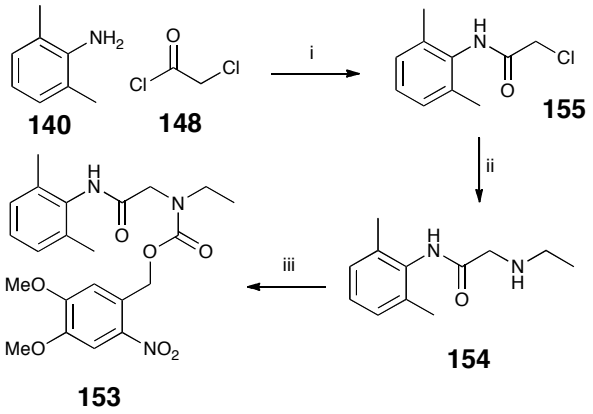

Scheme 5.13. Synthesis of the CDMNB-caged lidocaine derivative **153** from dimethylaniline **140**. *Reagents and conditions:* i. Pyridine, CH_2Cl_2, RT, 100%; ii. H_2NEt, THF, RT, 52%; iii. DMNB chloroformate, NEt_3, CH_2Cl_2, 0 °C → RT, 35%.

A more complex than expected ^{1}H NMR spectrum of the CDMNB-caged lidocaine derivative **153** was obtained, Figure 5.13. A possible explanation could be that two conformations of **153** were observed by ^{1}H NMR. Upon heating the ^{1}H NMR sample to 90 °C (363 K) in DMSO, half the number of peaks were observed. Merging of two peaks into one was observed, Figure 5.13. It was hypothesised that the amide bond of **153** is in *cis* and *trans* conformations at room temperature, with an energy barrier to overcome to switch between the two. This energy barrier can be overcome at high temperatures.

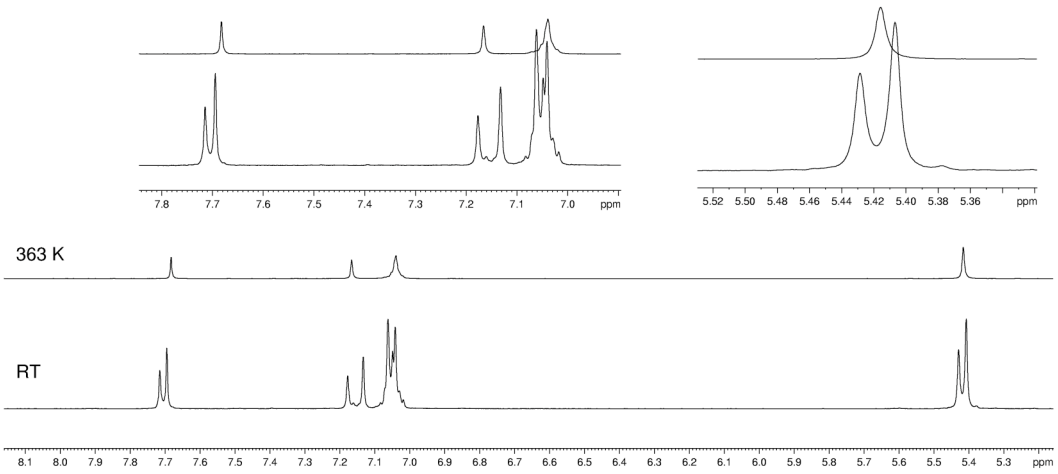

Figure 5.13. Partial 500 MHz ^{1}H NMR spectra of CDMNB-caged lidocaine **153** in DMSO at room temperature and 363 K (90 °C). The multiple peaks observed at RT converged upon heating to 363 K.

Neither the free lidocaine derivative **154**, nor the CDMNB-caged lidocaine derivative **153**, have been tested *in vitro* for their effect on the firing of action potentials in neurons. This work is in progress.

5.7. Caging Lidocaine with a Bulkier Caging Group

It was proposed that caging lidocaine at the original position (amide nitrogen) with a bulkier caging group (than the DMNB group originally employed) might inhibit its ability to block Na^{+} channels. It was aimed to cage lidocaine with the dibenzofuran-acyl group, which was being investigated as a potential new caging group (Chapter 6). Photolysis of dibenzofuran-acyl caged lidocaine **156** would yield free lidocaine **136** and a photolysis by-product **157**, Scheme 5.14.

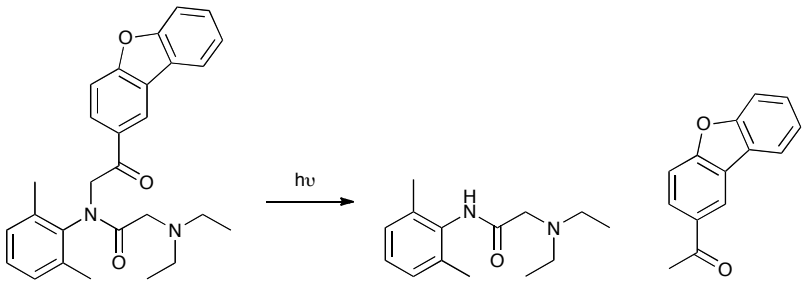

156 **136** **157**

Scheme 5.14. Proposed new dibenzofuran-acyl caged lidocaine **156**. Photolysis of dibenzofuran-acyl-caged lidocaine **156** would yield free lidocaine **136** and a photolysis by-product **157**.

Dimethylaniline **140** was reacted with the α-bromo intermediate **158** in DMPU with Na_2CO_3 to obtain the secondary amine **159** in 53% yield, Scheme 5.15. Treatment of **159** with chloroacetal chloride **148** in CH_2Cl_2 with anhydrous pyridine at room temperature yielded the α-chloro amide intermediate **160** in 22% yield.

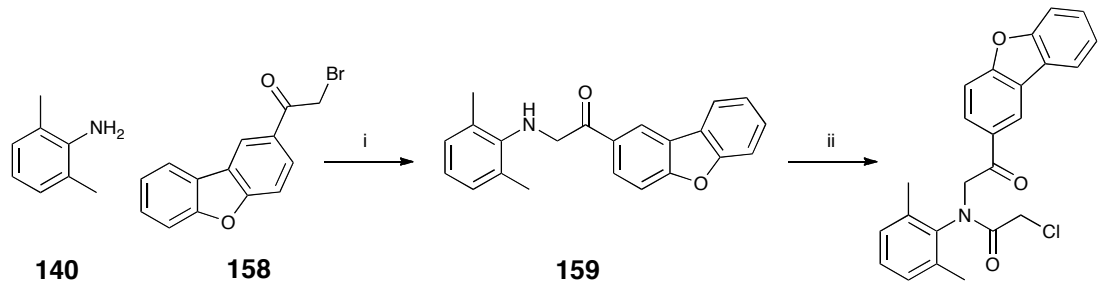

140 **158** **159** **160**

Scheme 5.15. Towards the synthesis of dibenzofuran-acyl caged lidocaine **156** from dimethylaniline **140**. *Reagents and conditions:* i. Na_2CO_3, DMPU, 100 °C, 53%; ii. chloroacetal chloride, pyridine, CH_2Cl_2, 0 °C → RT, 22%.

Based on the synthesis of DMNB-caged lidocaine **138**, it was proposed to treat the α-chloro amide intermediate **160** with diethylamine to obtain the final product, dibenzofuran-acyl caged lidocaine **156**. However, this product was not observed. Rather, a cyclic compound **161** was isolated, Scheme 5.16. Diethylamine had acted as a base, instead of as a nucleophile, and deprotonated the α-carbon of **160**. This enolate reacted intramolecularly with the ketone to form a 5-membered ring **161**, Scheme 5.16.

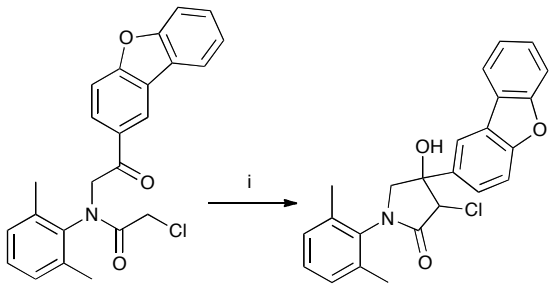

160 **161**

Scheme 5.16. Unsuccessful synthesis of dibenzofuran-acyl caged lidocaine **156** to form a cyclic product **161**. *Reagents and conditions:* i. $HNEt_2$, DMF, TBAI, 60 °C.

To prevent this cyclisation, selective protection of the ketone of the α-chloro amide intermediate **160** with an acetal protecting group was unsuccessfully attempted. The aim of synthesising dibenzofuran-acyl caged lidocaine **156** was not achieved due to time constraints.

5.8. Summary and Future Work

DMNB-caged lidocaine **138** was synthesised and it was demonstrated in a cuvette that photolysis of DMNB-caged lidocaine **138** results in photorelease of lidocaine **136**. However, this caged compound was still biologically active. It acted as an anaesthetic and blocked Na^+ channels. This was observed by the termination of action potential firing upon application of DMNB-caged lidocaine **138** to the bath solution of hippocampal pyramidal neurons. Therefore, it was proposed to cage lidocaine at the amine functional group in order to reduce its pK_a and stop protonation of the nitrogen, which is known to be a mechanism by which Na^+ channel blockers act.[121] CDMNB-caged lidocaine **153** was synthesised, however, neither the caged compound **153** nor the photolysis product, a lidocaine derivative **154**, have been applied *in vitro* to access their effect on neurons and Na^+ channels. An attempt to synthesise dibenzofuran-acyl caged lidocaine **156** at the amide nitrogen was not completed due to the formation of a cyclic product **161** instead of the desired final compound **156**. A new synthesis employing protecting groups could be used to achieve the synthesis of dibenzofuran-acyl caged lidocaine **156**.

Chapter 6:

Results and Discussion -

New Caging Groups

6. Two Potential New Caging Groups

6.1. Introduction and Aims

6.1.1. Nitrodibenzofuran-acyl Caging Group

In order to cage the Ca^{2+} chelator ethylene glycol tetraacetic acid (EGTA), Ellis-Davies and co-workers developed a new highly effective caging group, nitrodibenzofuran (NDBF).[52] Photolysis of NDBF-EGTA **162** allowed for the photorelease of Ca^{2+} in cardiac myocytes, Scheme 6.1.

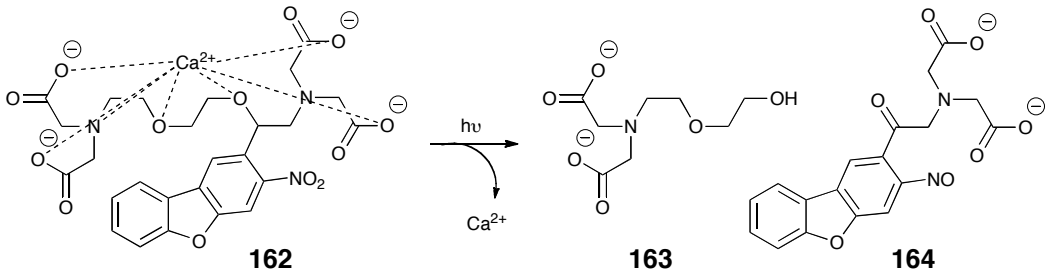

Scheme 6.1. Photorelease of Ca^{2+} upon photolysis of NDBF-EGTA **162**. Caged EGTA **162** has a 140 000-fold higher affinity for Ca^{2+} than the uncaged fragments (**163** and **164**). Therefore, Ca^{2+} is released upon photolysis of the NDBF cage.[52]

The NDBF-EGTA chromophore **162** has an extinction co-efficient ~ 4 fold larger than the DMNB caging group, and was uncaged at 347 nm with a high quantum yield (Φ) of 0.7. Therefore, for single-photon photolysis, NDBF is a more efficient caging group than the traditionally employed nitrobenzyl caging

groups. The two-photon cross-section of NDBF-EGTA **162** is 0.6 GM, compared with 0.01 GM for dimethoxynitrophenyl (DMNPE)-EGTA **165**,[134] Figure 6.1, indicating superior two-photon photolysis of NDBF. DMNPE-EGTA **165** was reported by Ellis-Davies in 1998.[134]

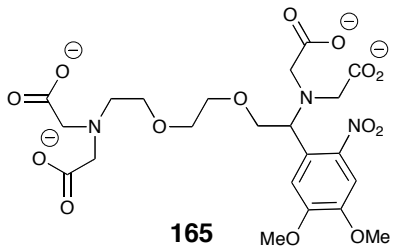

165

Figure 6.1. Structure of DMNPE-EGTA **165**.

This increased two-photon cross-section of **162** can be attributed to NDBF-EGTA's extended π-system and increased conjugation, which results in red-shifted (longer wavelength) absorption and an increase in the molar extinction co-efficient (ε).[51] However, the photolysis by-product of this caging group is a nitrosoketone **164**, which is potentially toxic to biological systems. This electrophile may be attacked by nucleophiles in the cell, for example DNA and proteins, causing cellular damage.

The aim of this research was to combine the conjugated aromatic system of the dibenzofuran group with the acyl group utilised in the phenacyl chromophore, Figure 6.2.[29]

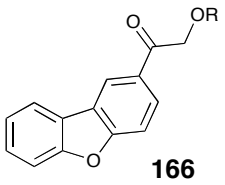

166

Figure 6.2. The proposed new caging group, combines the dibenzofuran skeleton and phenacyl cleavage mechanism.

It was hypothesised that the large aromatic scaffold of **166** could act as a sensitiser, increasing absorbance of light, and result in a red-shift in absorption. Therefore, photolysis could be achieved at longer wavelengths, minimising cellular damage by UV absorption of peptides and nucleotides. Also, the phenacyl cleavage mechanism would yield an inert photolysis by-product (Chapter 1.6),[22] a favourable feature for application of caged compounds to biological systems. If this group exhibits a large two-photon cross-section and is, therefore, suitable for two-photon photolysis, high-resolution photolysis at wavelengths towards the IR region could be achieved. It was aimed to cage GABA and glutamate with the dibenzofuran-acyl caging group **166** in order to test the efficiency of this potential new caging group.

6.1.2. Thiophenacyl Caging Group

A second approach to developing a novel caging group was to introduce a heteroatom into the aromatic ring of a phenacyl-like caging group, which may result in interesting changes to its photolysis characteristics. It was aimed to

investigate whether a thiophenacyl cage **167**, Figure 6.3, would exhibit favourable photolysis characteristics.

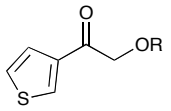

167

Figure 6.3. The proposed new thiophenacyl caging group.

The aromatic thiophene ring is more electron rich than the benzene ring. Thiophene exhibits an increased rate of electrophilic aromatic substitution compared to benzene, due to the electron density of the sulfur lone pair increasing the stability of the cationic intermediate. It was hypothesised that this sulfur lone pair conjugated with the ring may increase UV absorption. This could potentially result in favourable photolysis characteristics. It was aimed to synthesise the thiophenacyl group and use it to cage GABA and a ^{19}F probe, 4-fluorobenzoic acid, to access this hypothesis. The probe would facilitate quantification of photolysis by ^{19}F NMR using a fluorinated standard.

6.2. Synthesis of Dibenzofuran-acyl Caged Glutamate and GABA

The free dibenzofuran-acyl caging group **169** was synthesised from dibenzofuran **168** in 3 steps, Scheme 6.2. Dibenzofuran **168** was acylated using acetic anhydride and $AlCl_3$ in CH_2Cl_2 to obtain the monoacylated product **157** in 44% yield. The diacylated product was isolated in 11% yield. Monoacylated dibenzofuran **157** was brominated at the α-position by treatment with Br_2 and $AlCl_3$ in ether. The dibrominated product was a significant side-product. The desired monobrominated product **158** was isolated in 74% yield. Hydroxylation to obtain the free dibenzofuran-acyl caging group **169** was achieved in 81% yield by heating the brominated intermediate **158** in sodium formate and ethanol under reflux for 5 h.

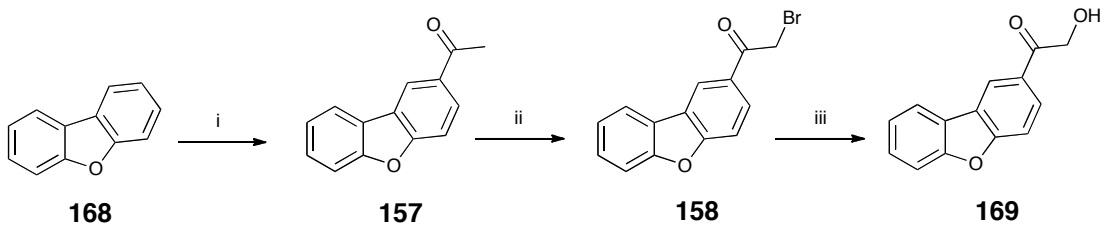

168 **157** **158** **169**

Scheme 6.2. Synthesis of the free dibenzofuran-acyl caging group **169**. *Reagents and conditions*. i. Ac_2O, $AlCl_3$, CH_2Cl_2, 44%; ii. Br_2, $AlCl_3$, Et_2O, 0 °C → RT, 74%; iii. sodium formate, EtOH, reflux, 5 h, 81%.

Boc-protected GABA **170** was coupled to the dibenzofuran-acyl caging group **169**, in 90% yield, using EDC and HBTU coupling conditions, Scheme 6.3. The Boc-protected caged intermediate **171** was deprotected by treatment with

1 M HCl in acetic acid to obtain dibenzofuran-acyl-caged GABA **172** in 76% yield.

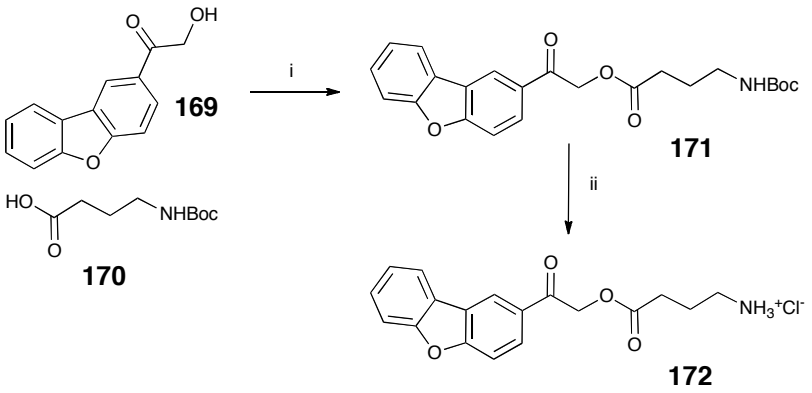

Scheme 6.3. Synthesis of dibenzofuran-acyl-caged GABA **172**. *Reagents and conditions*. i. EDC, HBTU, DIPEA, CH_2Cl_2, 90%; ii. 1 M HCl in acetic acid, 76%.

The Boc-protected *tert*-butyl ester of (*S*)-glutamate **173** was coupled to the dibenzofuran-acyl caging group **169** using EDC and HBTU coupling conditions to obtain the protected caged intermediate **174** in 62% yield, Scheme 6.4. Global deprotection of the Boc and *tert*-butyl groups was achieved by treatment with 1 M HCl in acetic acid at 45 ºC for 4 h to obtain dibenzofuran-acyl-caged glutamate **175** in 72% yield.

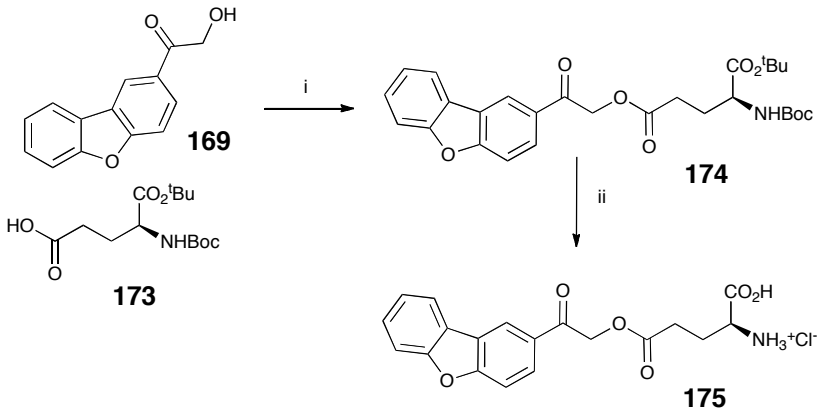

Scheme 6.4. Synthesis of dibenzofuran-acyl-caged glutamate **175**. *Reagents and conditions*. i. EDC, HBTU, DIPEA, CH_2Cl_2, 62%; ii. 1 M HCl in acetic acid, 45 °C, 72%.

6.3. Photolysis Potential of the Dibenzofuran-acyl Caging Group

The UV/Vis absorption spectrum of dibenzofuran-acyl-caged glutamate **175** (0.01 mM in MeOH) was recorded, Figure 6.4. A λ_{max} of 255 nm with an extinction co-efficient of 22 500 $M^{-1}cm^{-1}$ was observed. This is similar to the extinction co-efficient recorded for NDBF-EGTA **162** (18 400 $M^{-1}cm^{-1}$).[52]

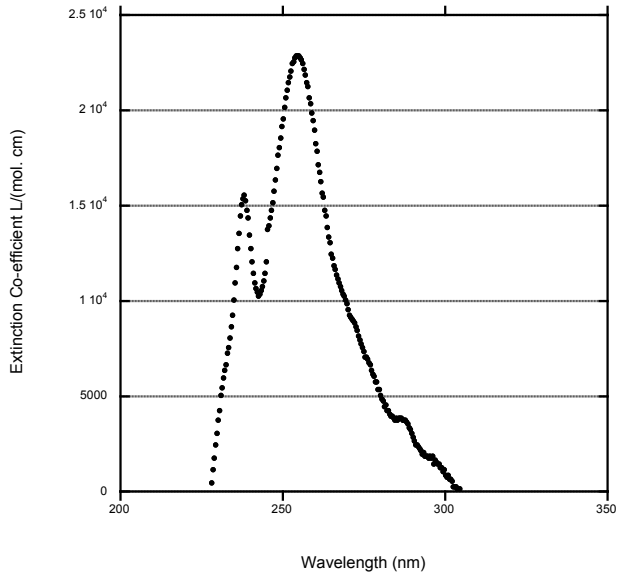

Figure 6.4. Dibenzofuran-acyl-caged glutamate **175** UV/Vis spectrum (0.01 mM in MeOH).

This large extinction co-efficient suggests that this caging group strongly absorbs light and, therefore, has potential as an effective caging group. The strong absorbance at short wavelengths suggests that this caging group may be a suitable orthogonal partner to the DMNB caging group (Chapter 7). It may even be suitable as a two-photon caging group. Photolysis would yield a benign by-product, making this chromophore attractive for use in biological systems. While the data is promising at this stage, this group was not analysed for its photolysis characteristics and parameters due to time and equipment constraints.

6.4. Synthesis of the Thiophenacyl Caging group

3-Acetylthiophene **176** was brominated at the α-position by treatment with Br_2 and $AlCl_3$ in ether, Scheme 6.5. The desired monobrominated product **177** was isolated in 70% yield. This brominated intermediate **177** was coupled to Boc-protected GABA **170**, using DBU in THF, to obtain the Boc-protected caged GABA intermediate **178** in 78% yield. Deprotection was achieved with 1 M HCl in dioxane to obtain thiophenacyl-caged GABA **179** in 51% yield, Scheme 6.5.

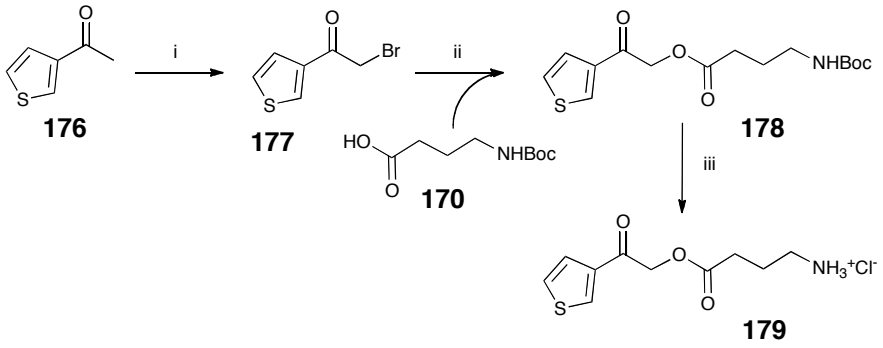

Scheme 6.5. Synthesis of thiophenacyl-caged GABA **179**. *Reagents and conditions*. i. Br_2, $AlCl_3$, Et_2O, 0 °C → RT, 70%; ii. DBU, THF, 78%. iii. 1 M HCl in dioxane, 51%.

The brominated intermediate **177** was also coupled to 4-fluorobenzoic acid **180** in 98% yield using DBU in THF to obtain the thiophenacyl-caged ^{19}F probe **181**, Scheme 6.6.

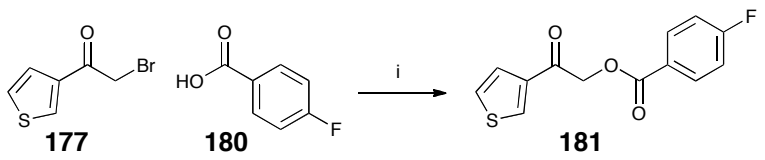

Scheme 6.6. Synthesis of thiophenacyl-caged 4-fluorobenzoic acid **181**. *Reagents and conditions*. i. DBU, THF, 98%.

The S_N2 reaction of the α-bromo carbonyl intermediate **177** with the carboxylic acid nucleophiles, Boc-GABA **170** and 4-fluorobenzoic acid **180**, is facilitated by the carbonyl group. The low energy π^* orbital from C=O and σ^* orbital from C-Br combine to form a molecular LUMO ($\pi^* + \sigma^*$), Figure 6.5.[130] This orbital is lower in energy than either individual orbital. Nucleophilic attack occurs where this new orbital has its largest co-efficients. Attack at the carbonyl is reversible while displacement of the bromide is irreversible, resulting in the S_N2 product. DBU is a hindered base which serves to quench HBr from the reaction.

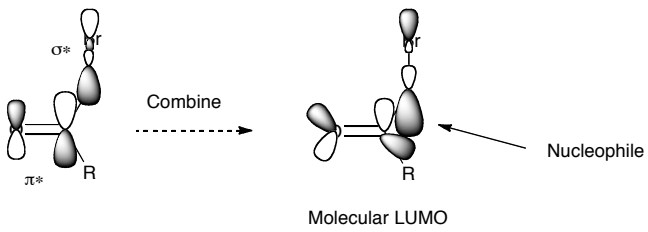

Figure 6.5. Orbitals of $RC(O)CH_2Br$ combine to form a low-energy molecular LUMO ($\pi^* + \sigma^*$) into which a nucleophile can attack. This facilitates S_N2 reactions of α-bromo carbonyl compounds.[130]

6.5. Photolysis Potential of the Thiophene-acyl Caging Group

The UV/Vis absorption spectrum of thiophenacyl-caged 4-fluorobenzoic acid **181** (0.01 mM in MeOH) was recorded, Figure 6.6. A λ_{max} of 250 nm with an extinction co-efficient of 8700 $M^{-1}cm^{-1}$ was observed. This is higher than that observed for the DMNB chromophore used in the orthogonal caging of neurotransmitters (Chapter 7). Extinction co-efficients of 4300 and 6042 $M^{-1}cm^{-1}$ were recorded for DMNB-glycine **209** and DMNB-GABA **205** respectively (Figures 7.3 and 7.8). However, the extinction co-efficient is lower than that recorded for methoxyphenacyl (MPA)-glutamate **234** (13648 $M^{-1}cm^{-1}$, Figure 7.8).

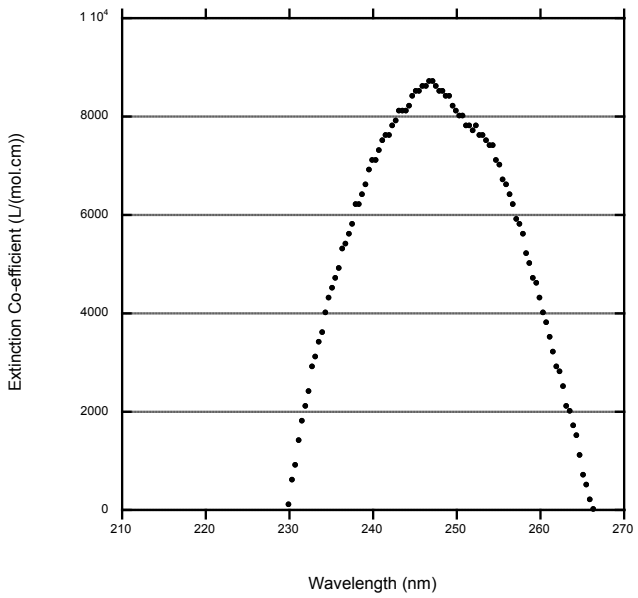

Figure 6.6. Thiophenacyl-caged fluorobenzoic acid **181** UV/Vis spectrum (0.01 mM in MeOH).

In order to investigate its photolytic efficiency, thiophenacyl-caged fluorobenzoic acid **181**, was irradiated at 266 nm. The resulting solutions were analysed by ^{19}F NMR. 1,4-Difluorobenzene **182** was used as an internal standard to quantify photolysis.

Solutions (1 mL, 3 mM) of thiophenacyl-caged fluorobenzoic acid **181** in MeOH were placed in quartz cuvettes and photolysed for 5 h and 17 h using a 266 nm YAG laser. Analysis by ^{19}F NMR indicated that the thiophenacyl caging group remained intact during irradiation. No photolysis by-product or uncaged fluorobenzoic acid were observed. The peak at -107.5 ppm, corresponding to thiophenacyl-caged fluorobenzoic acid **181**, did not diminish during irradiation, Figure 6.7.

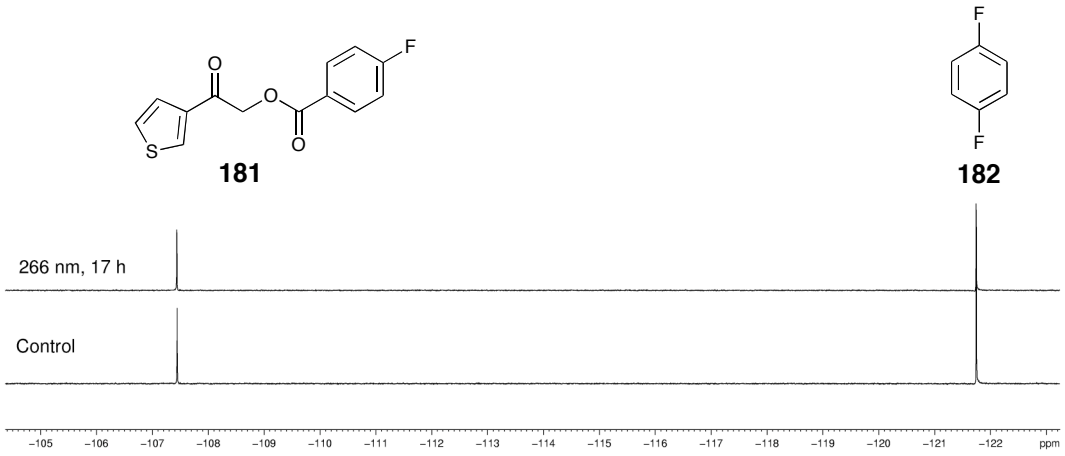

Figure 6.7. Partial ^{19}F NMR spectra (MeOD) of thiophenacyl-caged fluorobenzoic acid **181** photolysed at 266 nm. The peak at -107.5 ppm, corresponding to thiophenacyl-caged fluorobenzoic acid **181** did not diminish during irradiation. The peak at -121.8 ppm corresponds to the internal standard added after photolysis, 1,4-difluorobenzene **182**.

This disappointing result indicates that the thiophenacyl group is a poor caging group in MeOH at 266 nm. However, considering the proposed heterolytic photolysis mechanism for the phenacyl caging group, (Scheme 1.9 Chapter 1.6.1)[34] it may be interesting to perform this experiment in a solution which has some water in it, as water may be more effective at trapping the spiroketone intermediate to yield 2-(thiophen-3-yl)acetic acid photolysis by-product. Alternatively, if the photolysis mechanism involves formal reduction to 3-acetylthiophene by β-homolytic cleavage followed by hydrogen abstraction from the solvent (observed during photolysis of the 4-methoxyphenacyl caging group,[29] Scheme 1.8 Chapter 1.6.1), then a good hydrogen donor such as dioxane may facilitate photolysis. It would also be interesting to investigate whether oxidation of the sulfur atom (from sulfide to sulfone) would have an affect on photolysis. Kitani *et al.* reported a study on 3-arylthiochromone derivatives as new caging groups. Only upon oxidation were these derivatives photo-reactive.[135]

6.6. Summary

The synthesis of dibenzofuran-acyl-caged GABA **172** and glutamate **175** was completed. Dibenzofuran-acyl-caged glutamate **175** has a λ_{max} of 255 nm and a large extinction co-efficient (ε) of 22 500 $M^{-1}cm^{-1}$, which indicates that this caging group may be an efficient single-photon and even two-photon caging group. This hypothesis remains to be confirmed. The synthesis of thiophenacyl-caged GABA **179** and 4-fluorobenzoic acid **181** was completed. Irradiation of thiophenacyl-caged 4-fluorobenzoic acid **181** at 266 nm was

quantified by an internal standard. No photolysis was observed after 5 h and 17 h 266 nm irradiation in MeOH. This result suggests that thiophenacyl is not a useful caging group, however, additional parameters such as the solvent and sulfur oxidation remain to be explored.

Chapter 7:

Results and Discussion - Wavelength-Orthogonal Photolysis of Neurotransmitters

7. Wavelength-Orthogonal Photolysis of Neurotransmitters

7.1. Introduction and Aims

Differentiation between two or more caging groups to allow for selective deprotection of caged compounds would mark a significant step forwards in the application of caging technology. The irradiation wavelength is one of the few properties of light that could be utilised to afford this selectivity. Chromatic orthogonality would allow for the cleavage of one or two photolabile caging groups in the presence of others, in either order, depending on the wavelength of irradiation, Figure 7.1.

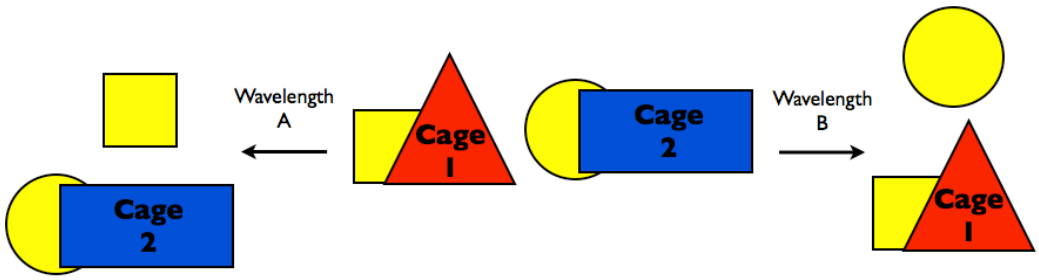

Figure 7.1. A cartoon representation of selective deprotection of caged compounds. At Wavelength A, Cage 2 remains intact while Cage 1 is cleaved, photoreleasing one functional group (represented by a yellow square). However, at Wavelength B, Cage 1 remains intact while Cage 2 is cleaved, photoreleasing the other functional group (represented by a yellow circle). The photolysis by-products of Cage 1 and 2 are not illustrated.

Bochet pioneered the development of one-photon wavelength-orthogonal caging groups. The 2-nitroveratryl photolabile group (see Figure 1.3) was introduced by Patchornik and Woodward.[136] Bochet demonstrated that by changing the substitution pattern around the aromatic ring of 2-nitroveratrole-derived carbamate caging groups, and thereby shifting their UV/Vis absorbance, different photolysis rates were observed according to the irradiation wavelength.[137] At this stage the selectivity factors were modest but the door had been opened for the development and application of orthogonal caging groups. Bochet summarised the requirements for achieving wavelength-orthogonal deprotection of photolabile protecting groups - the stability of the caging groups should be significantly different at various wavelengths; the energy transfer between an excited chromophore and the ground state of the orthogonal partner should be minimal; and cleavage at high energy should be fast to avoid photodegradation of sensitive functional groups.[138] By exploiting differences in wavelength sensitivity between 3',5'-dimethoxybenzoin esters and 4,5-dimethoxy-2-nitrobenzyl (DMNB) esters, and minimising intermolecular energy transfer by shortening the lifetime of the excited state of the benzoin ester, Bochet achieved wavelength-orthogonal photolysis of these two photolabile groups using monochromatic light.[138,139] By attaching these two caging groups to carboxylic acid functional groups at different sites on the *same* molecule, intramolecular wavelength-orthogonal photolysis was also demonstrated, Scheme 7.1.[139]

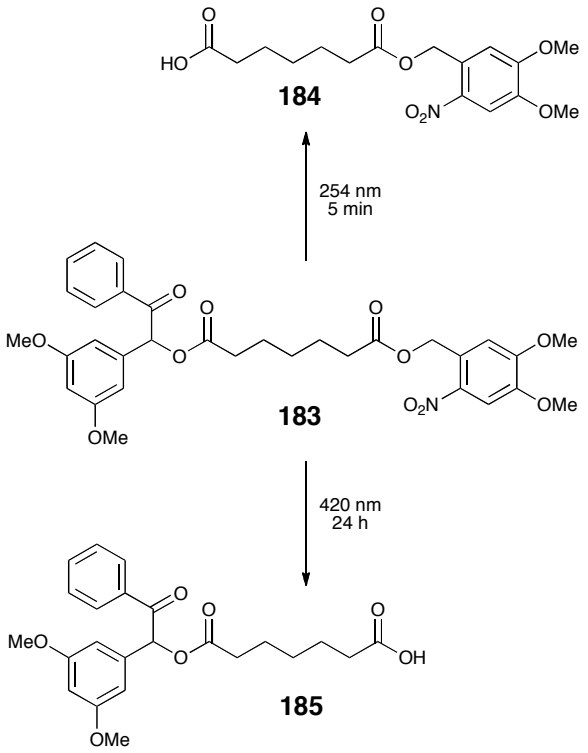

Scheme 7.1. Intramolecular wavelength-orthogonal photolysis achieved by exploiting differences in wavelength sensitivity between the 3',5'-dimethoxybenzoin and 4,5-dimethoxy-2-nitrobenzyl (DMNB) esters. Bochet and co-workers observed that at 254 nm only the benzoin ester was cleaved, while at 420 nm only the DMNB ester was cleaved.[138]

Bochet has also demonstrated chromatic orthogonal photolysis of photolabile protecting groups belonging to the same family of chromophores, the 2-nitrobenzyl family. The kinetic isotope effect (KIE) was used to tune the quantum yield and control the overall reaction rate. The C-D bond is slightly stronger than the C-H bond, therefore, isotopic substitution will affect a reaction in which a C-H(D) bond is broken in the rate-determining step.[140] Benzylic hydrogen abstraction is one of the multiple rate-limiting steps in photolysis of the nitrobenzyl caging group, therefore, it was proposed that substituting the two benzylic hydrogen atoms with deuterium atoms would

result in slower photolysis.[140] One of the nitrobenzyl caging groups employed (the 4-phenyl-6-nitrobenzyl group) was deuterated at the benzylic position, resulting in slower reactivity at 419 nm. Therefore, selective photolysis of the non-deuterated 4,5-dimethoxy-2-nitrobenzyl group was achieved at 419 nm, Scheme 7.2.[141] At 254 nm the kinetic isotope effect is reduced[140] and the 4-phenyl-6-nitrobenzyl group was cleaved in preference to the 4,5-dimethoxy-2-nitrobenzyl group as it has higher absorbance at this wavelength.

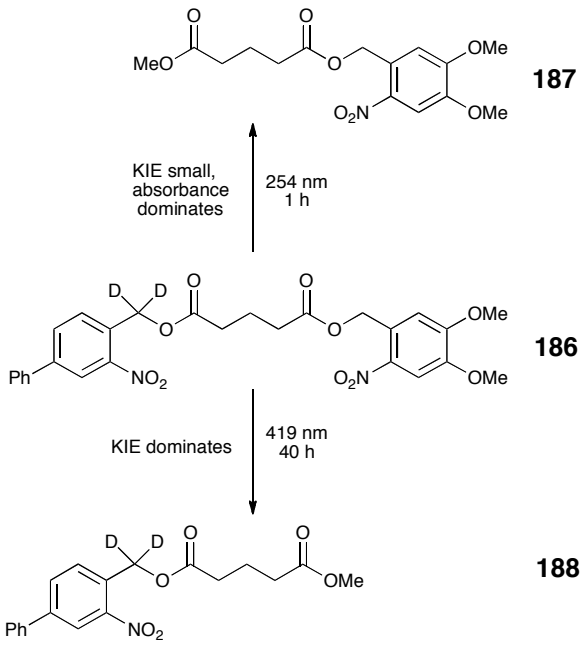

Scheme 7.2. Chromatic orthogonal photolysis of photolabile protecting groups belonging to the same family of chromophores, the 2-nitrobenzyl family. At 419 nm only the 4,5-dimethoxy-2-nitrobenzyl group was cleaved because the deuterated 4-phenyl-6-nitrobenzyl caging group is rate-limited by the kinetic isotope effect. However, at 254 nm (at which the kinetic isotope effect is negligible) only the 4-phenyl-6-nitrobenzyl group was cleaved, as it absorbs light more strongly than the 4,5-dimethoxy-2-nitrobenzyl group at his wavelength. The uncaged products were

isolated as the methyl esters by treatment of the irradiated crude product with $TMSCHN_2$.[141]

The initial application of wavelength selective caging groups was in the area of solid-phase peptide synthesis. Kessler *et al*.[142] utilised nitroveratryloxycarbonyl (NVOC)-caged amino acids and a *tert*-butyl ketone-derived linker to synthesise Leu-Enkephalin. The solid-phase peptide synthesis proceeded *via* cycles of NVOC deprotection of the terminal amino acid followed by peptide coupling of the next NVOC-caged amino acid. NVOC deprotection occurred at wavelengths above 360 nm. The linker remained intact at these wavelengths. Final cleavage of the linker by photolysis was achieved at wavelengths below 305 nm. Successive deprotection with the same reagent using harsher conditions is known as 'modulated lability'[143] and, despite its usefulness, has limited flexibility.[144] It can be referred to as 'wavelength-selective' photolysis, where one cage remains intact under the deprotection conditions of the other cage. However, the order of deprotection could not be reversed, as both cages would be cleaved. True wavelength-orthogonal photolysis requires that each caging group can be removed in the presence of the other in either order.

Using a similar approach, Ladlow *et al*.[145] employed nitroveratryl (NV) and pivaloyl glycol photolinkers in order to achieve wavelength-controlled differential release of a compound array from a solid-phase resin. The NV linker was cleaved at 355 nm, releasing one compound array; while the pivaloyl glycol linker remained intact, Scheme 7.3. Subsequent exposure to

300 nm irradiation resulted in cleavage of the pivaloyl glycol linker and photorelease of the second compound array. This technology has useful applications in high throughput screening of synthetic combinatorial compound libraries, generated using 'split and mix' solid-phase synthesis techniques.

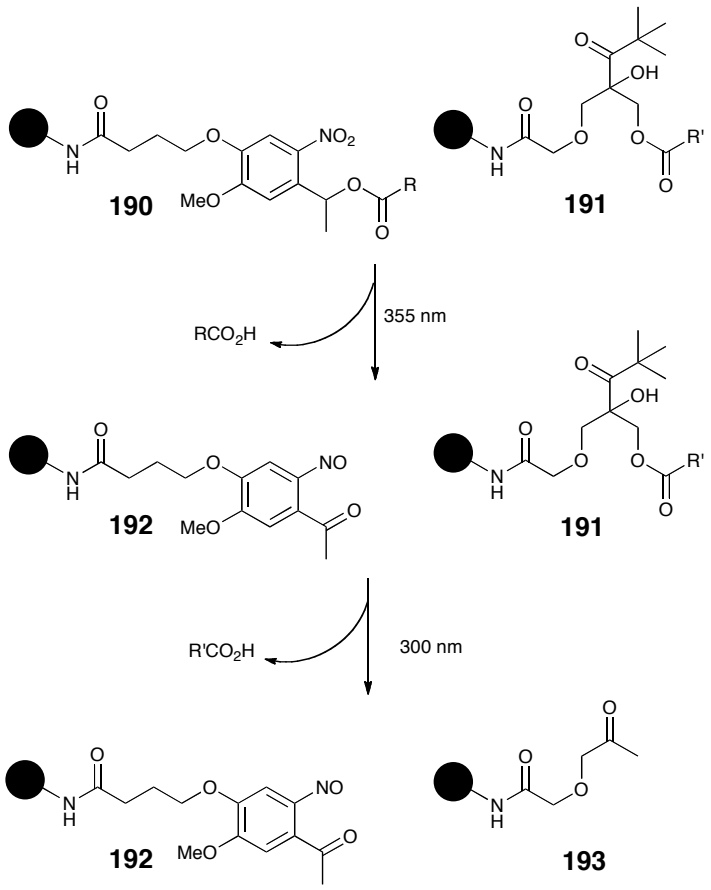

Scheme 7.3. Nitroveratryl (NV) **190** and pivaloyl glycol **191** linkers can be cleaved sequentially to release compounds (RCO_2H and $R'CO_2H$) from the resin selectively. Pivaloyl glycol **191** is stable to irradiation above 330 nm, so that at 355 nm only the NV linker **190** is cleaved, releasing RCO_2H. Subsequent irradiation at 300 nm cleaves the pivaloyl glycol linker to release $R'CO_2H$.

Very recently, Kammari *et al.* reported a monochromophoric photocleavable linker.[146] The 4-acetyl-2-nitrobenzyl moiety **194** (Scheme 7.4) acted as a photocleavable linker and was substituted in both the benzylic and phenacyl positions. The attached groups could be selectively disconnected upon irradiation by changing the chemical components of the reaction solution, not the wavelength of irradiation. Irradiation of the disubstituted linker **194** at 313 nm in acetonitrile resulted in selective cleavage of the nitrobenzyl moiety and release of the alcohol ROH, where R respresents an alkyl or acyl group, Scheme 7.4, A. The monosubstituted linker **195** could be separated from the reaction mixture and irradiated at the same wavelength in the presence of a hydrogen atom donor, 2-propanol (IPA). This resulted in photorelease of the carboxylic acid R'CO_2H, where R' represents an alkyl group. However, the attached groups could not be removed in either order and so true orthogonality was not demonstrated, despite the claim made in the title. Irradiation of the disubstituted linker **194** in IPA at 313 nm resulted in photoreduction of the nitro group to the corresponding amine derivative, as well as photolysis of the phenacyl moiety to release R'CO_2H, Scheme 7.4, B. However, subsequent photorelease of ROH from **197** was not possible as the nitro group, required for the photolysis of the benzylic position, was no longer present.

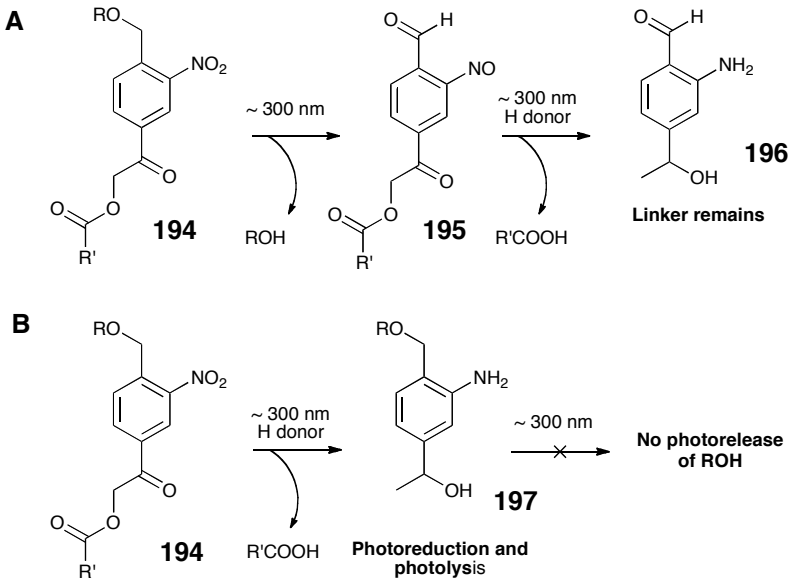

Scheme 7.4. A. Irradiation of the disubstituted linker **194** at 313 nm in acetonitrile resulted in selective cleavage of the nitrobenzyl moiety and release of the alcohol ROH. The monosubstituted linker **195** could be separated from the reaction mixture and irradiated at the same wavelength in the presence of a hydrogen atom donor, 2-propanol (IPA). This resulted in photorelease of the carboxylic acid R'CO_2H. **B**. The order of release from the photocleavable linker could not be reversed. Irradiation of the disubstituted linker **194** in the presence of the hydrogen atom donor IPA resulted in photoreduction of the nitro group to the corresponding amine derivative as well as photolysis of the phenacyl moiety to release R'CO_2H. However, subsequent photorelease of ROH from **197** was not possible because the nitro group, required for the photolysis of the benzylic position, was no longer present.

A second application of wavelength-orthogonal technology is in photolithography. Utilising wavelength orthogonality in chemical photolithography was first demonstrated by Jonas *et al*.[147] Triethoxysilanes with terminal amino, hydroxy and carboxylic acid functionalities were caged with either 3',5'-dimethoxybenzoin or NVOC orthogonal caging groups. These

orthogonal caging groups allowed for wavelength-controlled photoactivation of surfaces in specific patterns. The exposed functional groups in the photolysed regions allowed for the assembly process of specific targets (such as fluorescene dyes) onto the activated areas. This site-selective adsorption of molecules onto solid surfaces is important in the fabrication of novel electronic, mechanical and photonic devices.[147] Subsequent work by this group demonstrated the use of NVOC and diethylaminocoumarin-4-yl (DEACM) caging groups in the synthesis of photoresponsive surfaces for the fabrication of analytical platforms for miniaturised, high throughput chemical and biological analysis systems.[148]

Despite the demonstration of wavelength orthogonality and the widespread use of caged compounds in biological studies,[3] at the start of this work the two areas had not been combined. The lack of wavelength-orthogonally caged biomolecules has been identified as a significant shortcoming in the toolkit of chemical probes available for biological investigations.[1] Wavelength-orthogonally protected probes would have many applications. An example given in a review by Lee and co-workers is that wavelength-orthogonally caged biochemical activators and inhibitors would allow for the initiation and termination of a biochemical pathway in a single experiment.[1] Information could be gained about receptor activation and distribution, signalling pathways, protein folding and function, and many other biological systems. The design and implementation of such investigations is not possible with current pharmacological methods and techniques. Until recently, the photorelease of biologically relevant molecules has been limited to a single

species, because the caging of two biologically important molecules with photophysically distinct (wavelength-orthogonal) caging groups has proved challenging.

The first biological application of wavelength selective caging groups was demonstrated by Kutzur *et al*. who developed water-soluble photolabile protecting groups for thiols based on the 2-nitrobenzyl and (coumarin-4-yl)methyl scaffolds, Scheme 7.5.[149] Cysteine residues play an important role in protein structure *via* formation of disulfide bridges. Therefore, selectively photolysed thiol protecting groups would be a valuable tool for investigations of protein folding in peptides containing several cysteine residues. In order to carry out these studies in aqueous buffer solutions, hydrophilic caging groups are required. Kutzur *et al*. demonstrated the selective, but not orthogonal, photorelease of thiol groups in the 14-mer model peptide 'resact' using the modulated lability or wavelength-selective protecting group strategy. The cysteine residue at position 1 was caged with the α-carboxy-4-methoxy-2-nitrobenzyl (C4MNB) caging group. The cysteine residue at position 8 was caged with the {7-[bis(carboxymethyl)amino]coumarin-4-yl}methoxycarbonyl (BCMACMOC) caging group. At 430 nm the BCMACMOC group was selectively cleaved while the C4MNB group remained intact. The model peptide, which was now protected only at cysteine 1 **199**, was subsequently irradiated at 325 nm to remove the C4MNB group, Scheme 7.5.

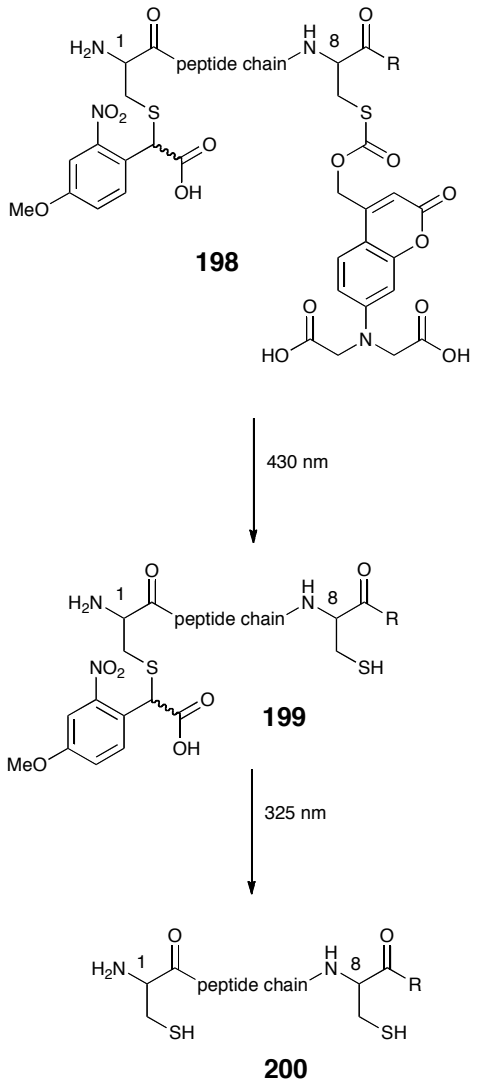

Scheme 7.5. The cysteine residue at position 1 of the model peptide 'resact' was caged with the α-carboxy-4-methoxy-2-nitrobenzyl (C4MNB) caging group. The cysteine residue at position 8 was caged with the {7-[bis(carboxymethyl)amino]coumarin-4-yl}methoxycarbonyl (BCMACMOC) caging group. At 430 nm the BCMACMOC group was selectively cleaved while the C4MNB group remained intact. Subsequently irradiation of **199** at 325 nm removed the C4MNB group. R = resact peptide chain residues 9 to 14.

During the course of these studies, Ellis-Davies and co-workers have published an example of two-photon, two-colour photolysis of the neurotransmitters GABA and glutamate. Wavelength-selective photolysis of 4-carboxymethoxy-5,7-dinitroindolinyl (CDNI)-caged glutamate **201** and 7-(dicarboxymethyl)-aminocoumarin (*N*-DCAC)-caged GABA **202** was observed, Scheme 7.6.[150] The wavelength-selective release of GABA and glutamate was demonstrated *in vitro* using hippocampal CA1 neurons.

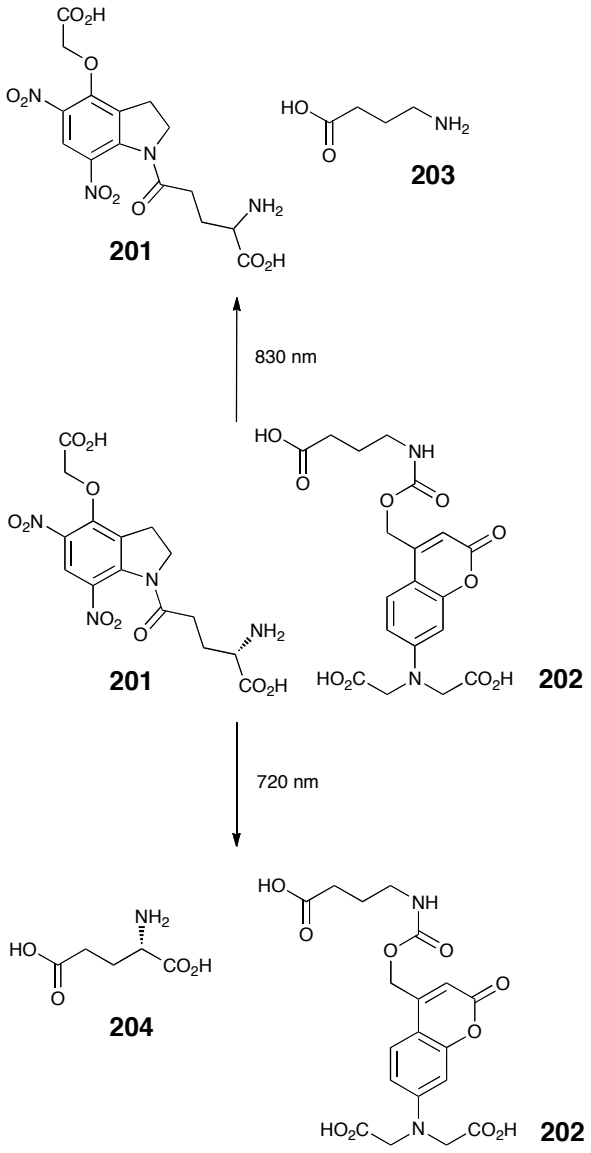

Scheme 7.6. Wavelength-selective photolysis using 4-carboxymethoxy-5,7-dinitroindolinyl (CDNI)-caged glutamate **201** and 7-(dicarboxymethyl)-aminocoumarin (*N*-DCAC)-caged GABA **202**. At 720 nm CDNI-glutamate **201** was photolysed, while at 830 nm *N*-DCAC **202** was photolysed.[150]

Wavelength-orthogonal protection of two different transmitter substances would allow an unprecedented opportunity to study the synaptic integration of excitatory and inhibitory inputs of neurons. Ultimately, important insight into the molecular mechanisms of learning and memory could be gained. It was towards this end that it was aimed to synthesise caged neurotransmitters - glycine, γ-amino butyric acid (GABA) and (*S*)-glutamate (Glu) - and demonstrate the wavelength-orthogonal photolysis of these compounds in neurons. Glutamate and GABA were specifically selected for this study because of their opposing biological actions. It was proposed that a neuron could be turned 'on' or 'off' selectively by putting these neurotransmitters under the control of orthogonal caging groups.

Glycine is the major inhibitory neurotransmitter in the spinal cord.[151] Glycine activates glycine receptors, allowing for an inward flux of Cl^- ions, and hyperpolarisation of the membrane. It is also a co-agonist at NMDA receptors. Glutamate and GABA are the two most significant neurotransmitters in the central nervous system (CNS) and evoke opposing biological responses. Glutamate is an excitatory amino acid that mediates its action *via* activation of a large family of glutamate receptors, which comprise both ligand-gated cation channels and G-protein-coupled receptors (GPCRs). The opening of the ionotropic cation channels depolarises the membrane and an action potential is initiated.[152] GABA is an inhibitory transmitter that exerts its action *via* activation of both ligand-gated Cl^- channels and GPCRs. Action potential firing is inhibited by hyperpolarising inhibition.[152] Consequently, these transmitters have fast biological responses that are easily distinguishable in neurons.

7.2. Synthesis of DMNB- and Benzoin-Caged Neurotransmitters

In order to investigate the potential for orthogonally caged neurotransmitters, it was decided to cage glycine, GABA and glutamate with the 4,5-dimethoxy-2-nitrobenzyl (DMNB) and 3',5'-dimethoxybenzoin (benzoin) caging groups, Figure 7.2. These are the caging groups with which Bochet demonstrated wavelength-orthogonality for the first time.[139]

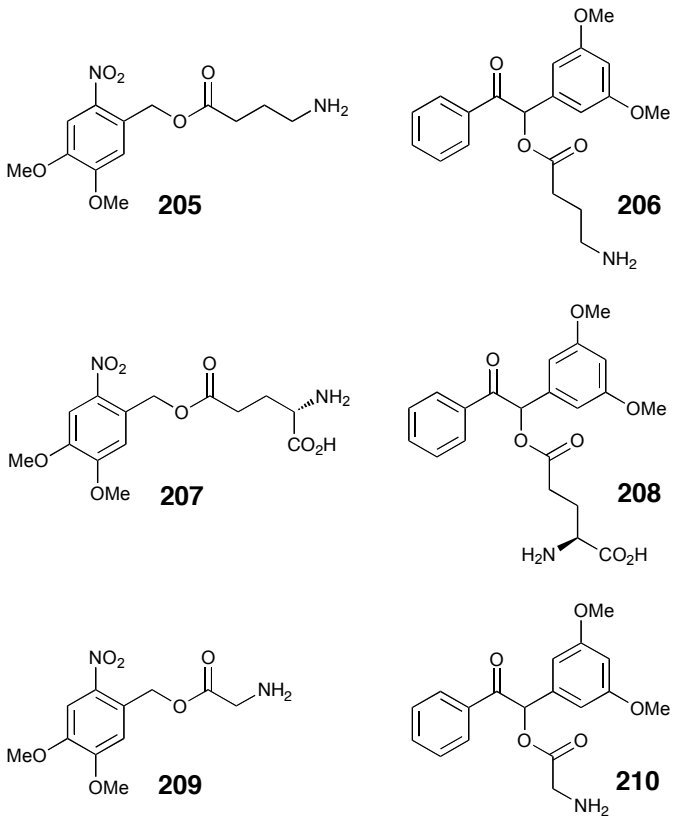

Figure 7.2. 4,5-Dimethoxy-2-nitrobenzyl (DMNB) and 3',5'-dimethoxybenzoin (benzoin) caged GABA, glutamate and glycine. The synthesis of these compounds was undertaken to demonstrate wavelength-orthogonal photolysis of neurotransmitters *in vitro.*

The general synthetic strategy towards these caged neurotransmitters involved coupling of the protected neurotransmitter with the desired caging group. Dicyclohexylcarbodiimide (DCC) and, later in the project, 1-ethyl-3-(3-dimethylaminopropyl)carbodiimide (EDC) and *O*-benzotriazole-*N,N,N',N'*-tetramethyl-uronium-hexafluoro-phosphate (HBTU) coupling conditions were employed. Subsequent deprotection of the Boc and *tert*-butyl groups yielded the desired caged neurotransmitter.

The Boc-protection of glycine **211** was achieved in 75% yield while the protection of GABA **203** was achieved in a yield of 87% upon treatment with di-*tert*-butyl dicarbonate in a NaOH/dioxane solution, Scheme 7.7. DCC coupling of each protected amino acid with 4,5-dimethoxy-2-nitrobenzyl alcohol **213** yielded Boc-protected DMNB-caged glycine **214** and GABA **215** in 63% and 69% respectively. Deprotection of the Boc group under acidic conditions using 1 M HCl in dioxane afforded the desired compounds, DMNB-caged glycine **209** and DMNB-caged GABA **205** in good yield, as shown in Scheme 7.7.

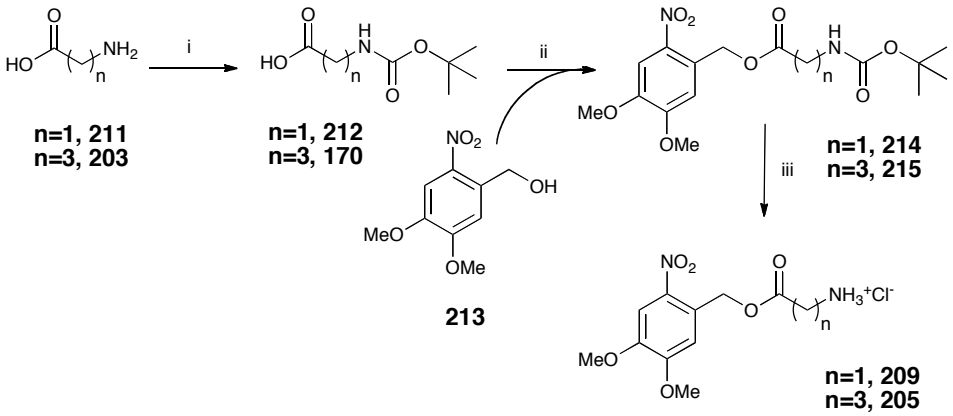

Scheme 7.7. Synthesis of DMNB-caged glycine **209** (n=1) and GABA **205** (n=3). *Reagents and conditions*: Glycine (n=1): i. NaOH, Boc_2O, dioxane, 75%; ii. DCC, DMAP, CH_2Cl_2, 63%; iii. 1 M HCl in dioxane, 100%. GABA (n=3): i. NaOH, Boc_2O, dioxane, 87%; ii. DCC, DMAP, CH_2Cl_2, 69%; iii. 1 M HCl in dioxane, 97%.

The Boc-protected *tert*-butyl ester of (*S*)-glutamate **173** was coupled with 4,5-dimethoxy-2-nitrobenzyl alcohol **213** using a DCC-mediated procedure to obtain the protected DMNB-caged intermediate **216** in 69% yield, Scheme 7.8. Deprotection of both the Boc and *tert*-butyl groups with 1 M HCl in acetic acid was not successful at room temperature. However, heating the acidic reaction solution to 45 °C for 6 h yielded DMNB-caged glutamate **207** in 50% yield.

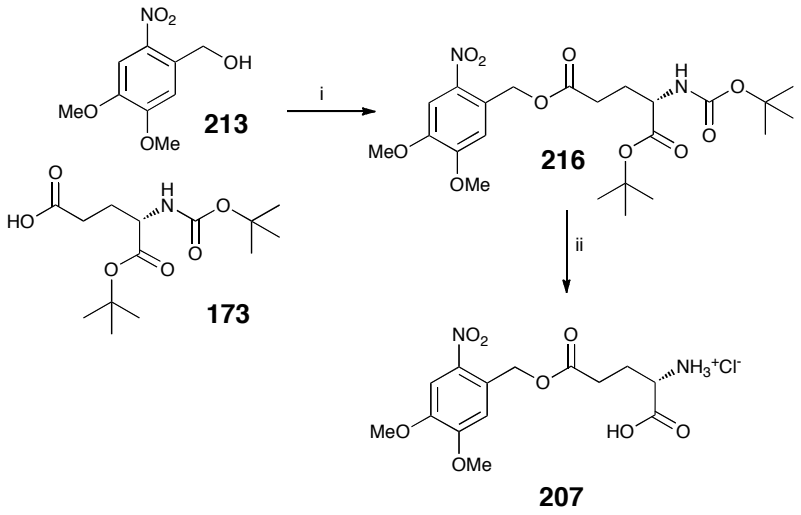

Scheme 7.8. Synthesis of DMNB-caged glutamate **207**. *Reagents and conditions*: i. DCC, DMAP, CH_2Cl_2, 69%; ii. 1 M HCl in acetic acid, 45 °C, 50%.

The 3',5'-dimethoxybenzoin caging group **220** was synthesised from 3,5-dimethoxybenzaldehyde **218** in two steps, as shown in Scheme 7.9.[153] Using Corey-Seebach *umpolung* chemistry, 3,5-dimethoxybenzaldehyde **218** was treated with 2-phenyl-1,3-dithiane **217** and ^{n}BuLi to obtain **219** in modest yield. The dithiane was removed by oxidation with bis(trifluoroacetoxy)iodobenzene. Over-oxidation to the di-ketone was a problem, despite performing the reaction at 0 °C. The 3',5'-dimethoxybenzoin caging group **220** was obtained in moderate yield.

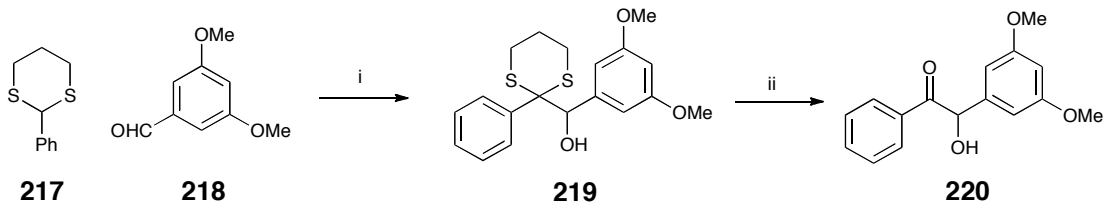

217 **218** **219** **220**

Scheme 7.9. Synthesis of the free 3',5'-dimethoxybenzoin caging group **220**. *Reagents and conditions*: i. ^{n}BuLi, THF, 45%. ii. $PhI(OCOCF_3)_2$, CH_3CN, 0 °C, 43%.

Coupling reactions of 3',5'-dimethoxybenzoin **220** with Boc-protected glycine **212** and GABA **170** using DCC and DMAP yielded a mixture of inseparable compounds, which appeared as one spot by thin layer chromatography (TLC). After many attempts at performing these reactions and analysing the products by ^{1}H NMR and mass spectrometry, it was thought that DMAP may be facilitating a rearrangement resulting in the isolation of isomers in a 1:1 ratio, Scheme 7.10. The products have the same molecular mass and the aromatic and aliphatic ^{1}H NMR signals are very similar. However, the benzylic proton is shifted from 6.79 to 6.83 ppm in the ^{1}H NMRs of the two isomers. This problem was overcome by ensuring that no more than 0.05 eq of DMAP was added to the reaction mixture.

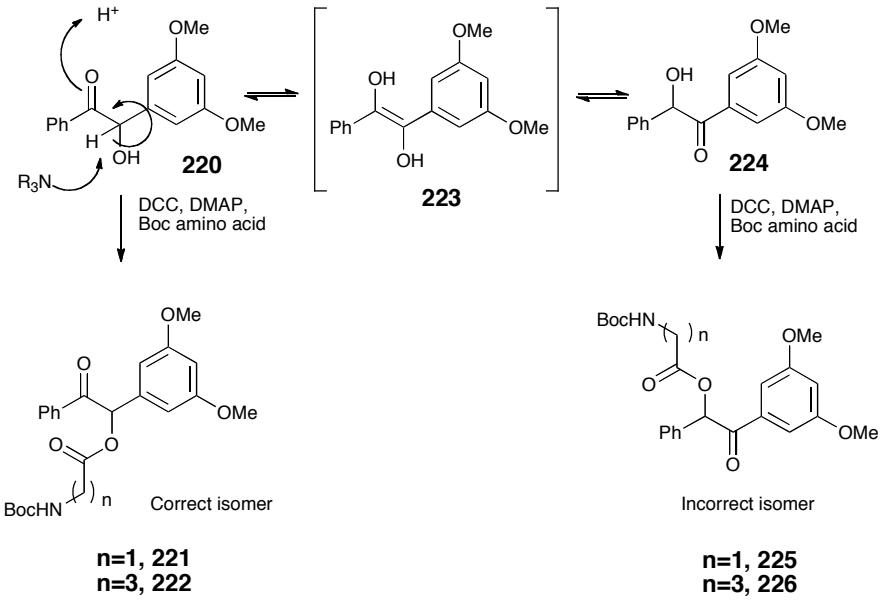

Scheme 7.10. Hypothesised rearrangement of 3',5'-dimethoxybenzoin **220** resulting in isomers from the DCC coupling reaction with Boc-protected amino acids, glycine (n=1) and GABA (n=3).

DCC-mediated coupling of Boc-protected glycine **212** and GABA **170** with 3',5'-dimethoxybenzoin **220** using 0.05 eq. DMAP yielded Boc-protected benzoin-caged glycine **221** and GABA **222** in 95% and 85% respectively, Scheme 7.11. Deprotection of the Boc group under acidic conditions using 1 M HCl in acetic acid afforded the desired compounds, benzoin-caged glycine **210** and benzoin-caged GABA **206** in good yields, as shown in Scheme 7.11.

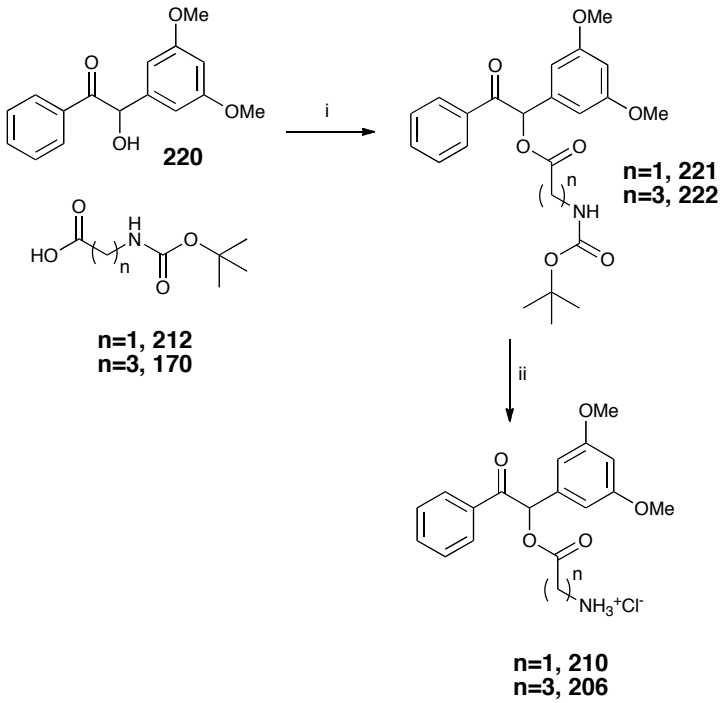

Scheme 7.11. Synthesis of benzoin-caged glycine **210** (n=1) and GABA **206** (n=3). *Reagents and conditions*: Glycine (n=1): i. DCC, DMAP (5 mol %), CH_2Cl_2, 95%; ii. 1 M HCl in acetic acid, 78%. GABA (n=3): i. DCC, DMAP (5 mol %), CH_2Cl_2, 85%; ii. 1 M HCl in acetic acid, 82%.

The Boc-protected *tert*-butyl ester of (*S*)-glutamate **173** was coupled with 3',5'-dimethoxybenzoin **220** using DCC-mediated coupling to obtain the protected benzoin-caged glutamate intermediate **227** in 82% yield, Scheme 7.12. Deprotection of both the Boc and *tert*-butyl groups was achieved by heating the 1 M HCl in acetic acid reaction mixture at 45 °C for 3 h to obtain benzoin-caged glutamate **208** in 62% yield as a mixture of diastereomers.

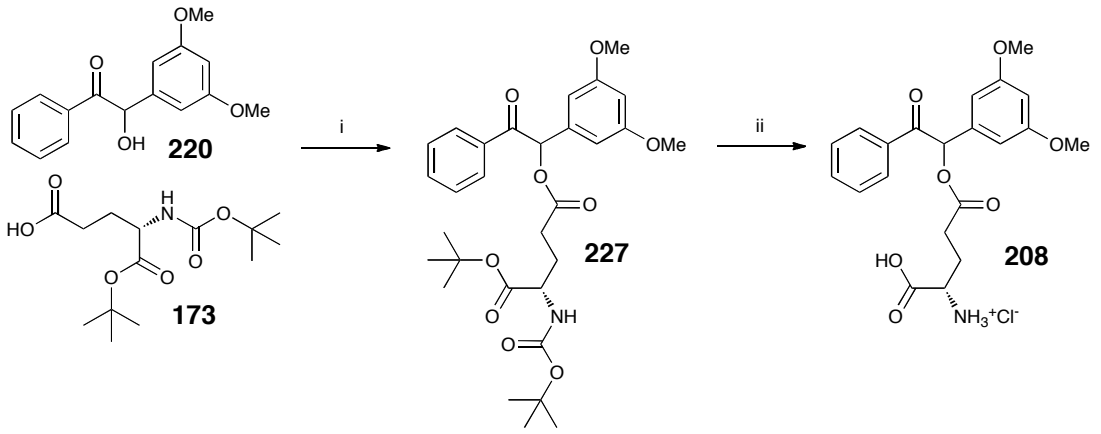

Scheme 7.12. Synthesis of benzoin-caged glutamate **208**. *Reagents and conditions*: i. DCC, DMAP, CH_2Cl_2, 82%; ii. 1 M HCl in acetic acid, 45 °C, 62%.

7.3. UV/Vis Spectra of DMNB- and Benzoin-Caged Neurotransmitters

In order to determine what wavelengths were most likely to evoke successful photolysis and, therefore, whether the compounds were likely to be wavelength-orthogonal, the UV/Vis absorption spectra of the caged neurotransmitters were recorded. Figure 7.3 is an overlay of the UV/Vis spectra of DMNB-glycine **209** and benzoin-GABA **206** (0.01 mM in MeOH). The λ_{max} values of the different caging groups were observed to be significantly different. Benzoin-GABA **206** absorbs strongly at 250-270 nm while DMNB-glycine **209** absorbs strongly at 350 nm. This observation supported the hypothesis that irradiating a mixture of these compounds at 250-270 nm would photolyse only the benzoin-caging group while irradiation above 350 nm would photolyse only the DMNB-caging group. Photolysis experiments were undertaken to test this hypothesis.

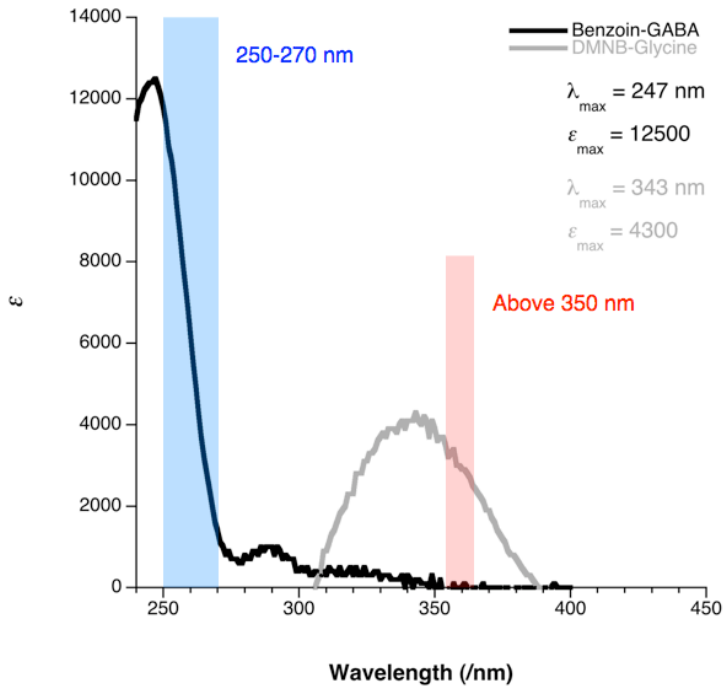

Figure 7.3. Benzoin-caged GABA **206** UV/Vis spectrum (0.01 mM in MeOH) (black); DMNB-caged glycine **209** UV/Vis spectrum (0.01 mM in MeOH) (grey). ε is the extinction co-efficient ($M^{-1}cm^{-1}$).

7.4. Photolysis Investigation of DMNB- and Benzoin-Caged Neurotransmitters

Photolysis of the DMNB- and benzoin-caged neurotransmitters was carried out with the assistance of our collaborators at the School of Physics and Astronomy, University of St Andrews with Craig McDougall and Dr Tom A. Brown. Please refer to the General Experimental Section for details.

During photolysis experiments, 1 mL aliquots of the appropriate solution of caged compound in MeOH (7.5 mM) were placed into UV transmitting cuvettes and exposed to light from the given laser source for fixed time durations. A continuous wave (CW) laser diode provided 405 nm light at a

power of 30 mW. Shorter wavelength radiation was provided by an optical parametric oscillator pumped at 254 nm by a frequency tripled Nd:YAG laser. The photolysis samples were analysed and quantified by ^{1}H NMR using hexamethyldisiloxane as an internal standard in MeOD. Control samples, which had not been exposed to laser radiation, were also analysed.

7.4.1. 250 nm Study

Firstly, photolysis of each individual caged neurotransmitter was investigated. Exposing DMNB-glycine **209** to radiation of 250 nm, 0.7 mJ for 1 h did not result in any observable photolysis. The ^{1}H NMRs of the control and irradiated samples were identical. Exposing DMNB-GABA **205** to radiation of 250 nm, 0.7 mJ for 1 h also did not result in any observable photolysis.

However, exposing benzoin-GABA **206** to radiation of 250 nm, 0.7 mJ for 1 h did result in observable photolysis. As quantified by ^{1}H NMR, the photolysed sample contained 38% intact benzoin-GABA **206** and 56% photolysis by-product, 5,7-dimethoxy-2-phenylbenzofuran **37**, as shown in Figure 7.4.

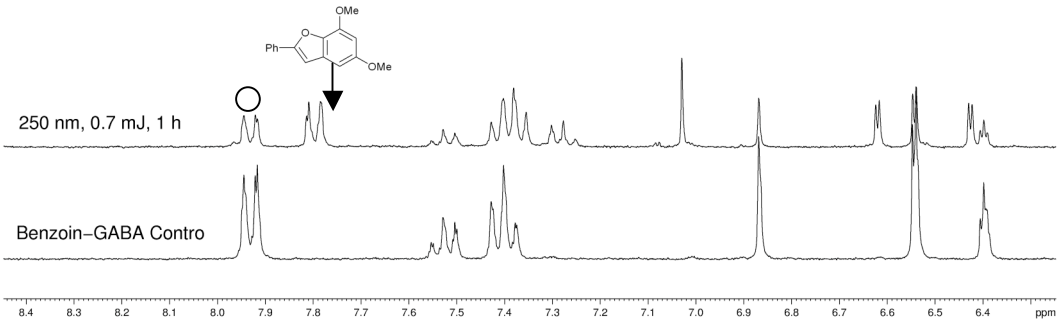

Figure 7.4. Partial 300 MHz ^{1}H NMR spectra of benzoin-caged GABA **206** irradiated at 250 nm, 0.7 mJ in MeOH for 1 h, and an identical control sample, which had not been irradiated. The hexamethyldisiloxane standard in MeOD was added to the samples after irradiation, for quantitative analysis. The aromatic peak at 7.8 ppm (arrow), corresponding to the benzoin photolysis by-product 5,7-dimethoxy-2-phenylbenzofuran **37**, was observed to appear and grow during the photolysis run. The aromatic peak at 7.9 ppm (○), corresponding to the benzoin caging group **206**, was observed to diminish during the photolysis run. The control sample did not possess any uncaged material.

Exposing benzoin-glycine **210** to radiation of 250 nm, 0.7 mJ for 1 h resulted in comparable photolysis to that of benzoin-GABA **206**. As quantified by ^{1}H NMR, the photolysed sample contained 41% intact benzoin-glycine **210** and 35% photolysis by-product, 5,7-dimethoxy-2-phenylbenzofuran **37**.

When a 1:1 mixture of DMNB-glycine **209** and benzoin-GABA **206** was irradiated at 250 nm, 0.7 mJ for 1 h, only photolysis of benzoin-GABA **206** was observed. DMNB-glycine **209** remained intact. 32% caged benzoin material **206** and 50% benzoin photolysis by-product **37** were observed.

Figure 7.5 is an overlay of the partial 300 MHz ^{1}H NMR spectra of benzoin-GABA **206** and DMNB-glycine **209** individual and mixture controls as well as a mixed sample irradiated at 250 nm, 0.7 mJ for 1 h. The singlets at 7.7 and 7.1 ppm (□), corresponding to DMNB-glycine **209**, were observed in both controls containing DMNB-glycine, as well as in the photolysis sample. This peak did not diminish as a result of irradiation. The doublet of doublets at 7.9 ppm (○), corresponding to benzoin-GABA **206**, was observed in both controls containing benzoin-GABA, but was diminished as a result of irradiation. A new peak at 7.8 ppm (arrow) was observed in the photolysis sample, corresponding to the benzoin-GABA photolysis by-product, 5,7-dimethoxy-2-phenylbenzofuran **37**.

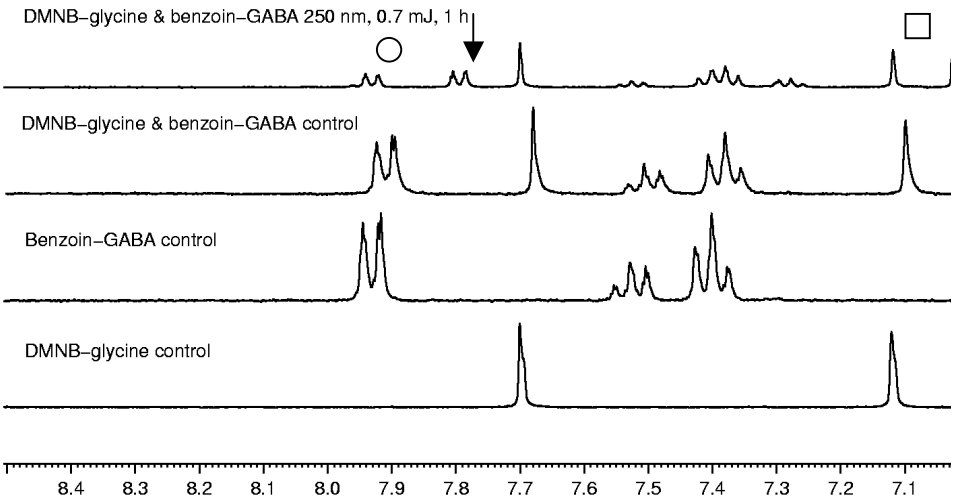

Figure 7.5. Partial 300 MHz ^{1}H NMR spectra of benzoin-GABA **206** and DMNB-glycine **209** individual and mixture controls as well as a mixed sample irradiated at 250 nm, 0.7 mJ for 1 h. The hexamethyldisiloxane standard in MeOD was added to the samples after irradiation, for quantitative analysis. The aromatic peak at 7.8 ppm (arrow), corresponding to the benzoin photolysis by-product 5,7-dimethoxy-2-phenylbenzofuran **37**, was observed to appear and grow during the photolysis run. The aromatic peak at 7.9 ppm (○), corresponding to the benzoin caging group **206**, was observed to diminish during the photolysis run. No photolysis of DMNB-glycine **209** (□) was observed.

When a 1:1 mixture of DMNB-GABA **205** and benzoin-glycine **210** was irradiated at 250 nm, 0.7 mJ for 1 h, only photolysis of benzoin-glycine **210** was observed. DMNB-GABA **205** remained intact. 36% caged benzoin material **210** and 30% benzoin photolysis by-product **37** were observed. Also, when a 1:1 mixture of DMNB-glutamate **207** and benzoin-GABA **206** was irradiated at 250 nm, 0.7 mJ for 1 h, only photolysis of benzoin-GABA **206**

was observed. DMNB-glutamate **207** remained intact. No caged benzoin material **206** was detected while 100% benzoin photolysis by-product **37** was observed.

These results indicate that the DMNB caging group is stable to irradiation at 250 nm. It is not cleaved. However, the benzoin caging group is photolysed at 250 nm, releasing the uncaged neurotransmitter and the benzofuran photolysis by-product. This was observed in solutions containing the individual caged neurotransmitter as well as solutions containing a 1:1 mixture of DMNB- and benzoin-caged neurotransmitter. This exciting result confirmed that wavelength-selectivity had been achieved - the benzoin group can be selectively removed in the presence of the DMNB group at 250 nm. The selective uncaging of the DMNB group in the presence of the benzoin group was attempted at longer wavelengths.

7.4.2. Longer Wavelength Study

In order to achieve selective photolysis of the DMNB caging group in the presence of the benzoin cage, a 1:1 mixture of DMNB-glycine **209** and benzoin-GABA **206** was irradiated at 355 nm, 0.7 mJ for 1 h. No photolysis of DMNB-glycine **209** was observed and only ~ 5% benzoin-GABA **206** photolysis was detected. This indicated that this wavelength at this power was not useful for achieving photolysis in this system. Therefore, photolysis at 355 nm was attempted at a higher power. However, irradiating this mixture at 355 nm, 100 mJ for as little as 5 minutes resulted in photolysis of both caging groups.

It was decided to attempt irradiation at a longer wavelength in order to achieve wavelength orthogonality. However, irradiation at 421 nm, 0.7 mJ for 1 h did not result in observable photolysis of benzoin-GABA **206** alone; DMNB-glycine **209** alone; DMNB-glutamate **207** alone; or a mixture of benzoin-GABA **206** and DMNB-glycine **209**. Therefore, photolysis above 400 nm was attempted at a higher power.

When a 1:1 mixture of DMNB-glycine **209** and benzoin-GABA **206** was irradiated at 405 nm, 30 mW for 16 h using a laser diode, only photolysis of DMNB-glycine **209** was observed. Benzoin-GABA **206** remained intact. 17% caged DMNB-glycine **209** and 11% DMNB-glycine photolysis by-product were observed. The total percentage of caged and uncaged DMNB-glycine was

28%. This indicates that there was a significant loss of DMNB material, possibly due to degradation by other photolysis pathways over the long irradiation duration. In order to overcome this problem, an identical mixture was photolysed at 405 nm, 30 mW for 3 h. However, no photolysis of either caging group was observed.

While both caging groups were cleaved at 355 nm, the results from irradiation at 405 nm indicate that the benzoin caging group is stable to irradiation at sufficiently long wavelengths. However, the DMNB caging group is photolysed at 405 nm, releasing the uncaged neurotransmitter. This was observed in a solution containing a 1:1 mixture of DMNB- and benzoin-caged neurotransmitter. This confirmed that wavelength-orthogonality had been achieved in a cuvette - the benzoin and DMNB caging groups can be selectively removed from their respective neurotransmitter in the presence of the other utilising irradiation at 250 nm and 405 nm.

7.5. Application of DMNB- and Benzoin-Caged Neurotransmitters to a Biological System

Having demonstrated wavelength-orthogonal photorelease of neurotransmitters from the DMNB and benzoin caging groups in a cuvette at 250 nm and 405 nm, wavelength-orthogonal photolysis in neurons was attempted. The application of the caged neurotransmitters to neurons was carried out by our collaborators at the Department of Pharmacology at the

University of Oxford by Dr Nigel Emptage, Dr Ruth Taylor and Dr Mike Hart. Please refer to General Experimental Section for further details.

In this case, DMNB-caged and 3',5'-dimethoxybenzoin-caged glutamate (**207**, **208**) and GABA (**205**, **206**) were employed in hippocampal pyramidal neurons. DMNB-glutamate **207** and GABA **205** were both shown to have minimal activity on neurons until photolysed and both produced the expected responses when photolysed with a 405 nm diode. Figure 7.6 shows the current traces obtained from pyramidal hippocampal neurons bathed with 100 μM DMNB-glutamate **207** and irradiated at either 405 nm or 253 nm. No response was observed following irradiation at 253 nm. This indicated that DMNB-glutamate **207** remained intact. However, following irradiation at 405 nm, a large cation current was observed consistent with the activation of glutamate receptors. This indicated that glutamate was photoreleased. This exciting result confirmed that wavelength-selectivity in one direction had been achieved using the DMNB caging group.

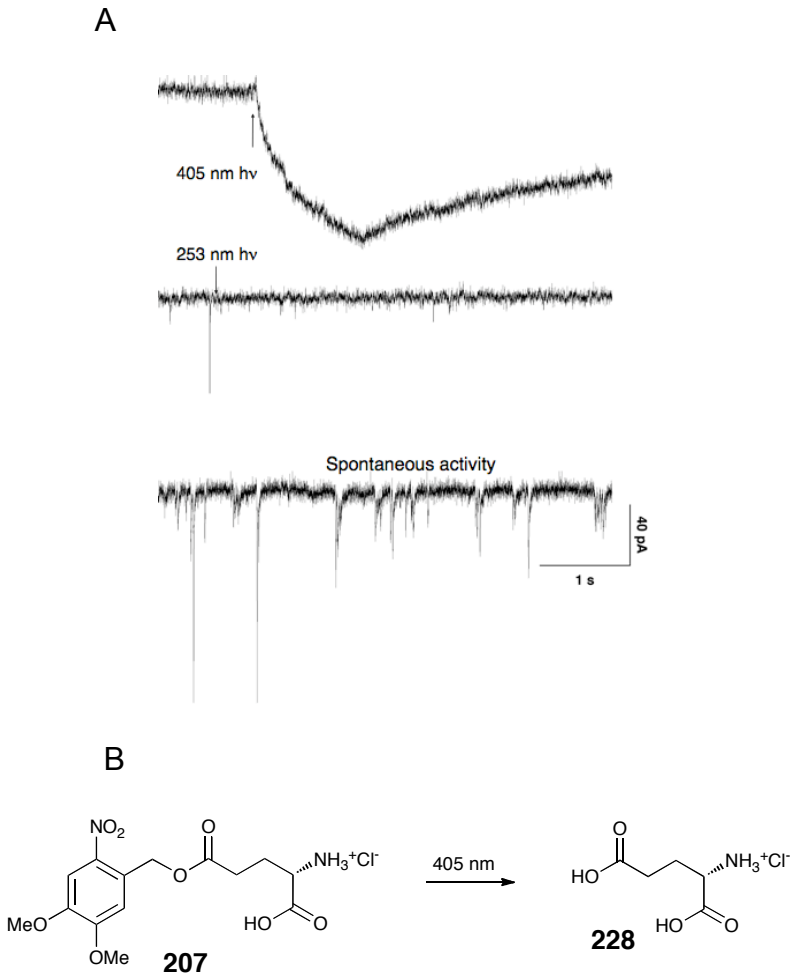

Figure 7.6. A. Current traces obtained from hippocampal pyramidal neurons bathed with 100 μM DMNB-glutamate **207** and irradiated at either 405 nm or 253 nm. Following irradiation at 405 nm, a large cation current was observed consistent with the activation of glutamate receptors. No response was observed following irradiation at 253 nm. The bottom panel is a trace of the spontaneous electrical activity of an isolated cell. mEPSCs in its holding current indicate that the cell was healthy. **B.** The photorelease of glutamate **228** from DMNB-Glu **207** at 405 nm which results in the observed cation current in the current trace in **A**.

However, both 3',5'-dimethoxybenzoin-caged glutamate **208** and GABA **206** produced unexpected toxicity when applied to neurons. Given that both caged

glutamate and GABA produced similar toxicity, it was hypothesised that the effect was non-selective and not mediated by a receptor-ligand interaction. In order to test this hypothesis, 3',5'-dimethoxybenzoin (free caging group) **220** (100 μM) was applied to the neurons and similar toxicity was observed. Figure 7.7 shows a pyramidal cell in voltage clamp, held at a membrane potential of -50 mV. mEPSCs (excitatory postsynaptic potentials), i.e. downward deflections, in its holding current indicate that the cell was healthy before addition of benzoin, highlighted in inset A, Figure 7.7. Upon addition of benzoin **220** to the bathing solution of the cell, the holding current increased, as observed by a downward drift in the trace. This indicated that the membrane potential of the cell was depolarised. Also, a large increase in the number of mEPSCs, highlighted in inset B, Figure 7.7, indicated an increase in presynaptic release of transmitter. The cell did not recover.

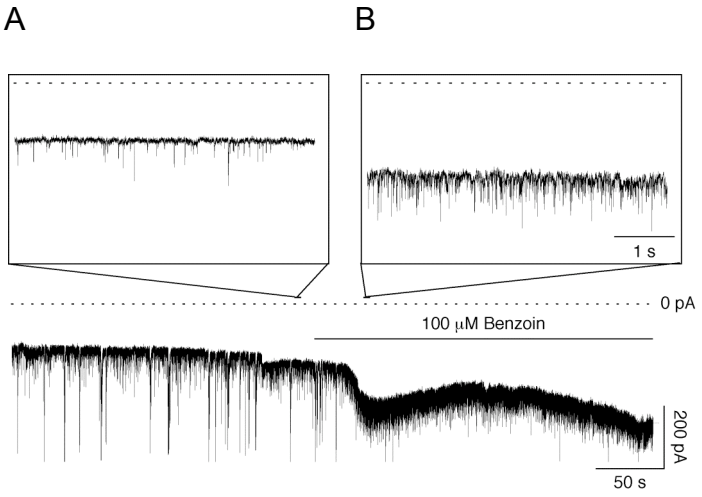

Figure 7.7. Current trace obtained from a hippocampal pyramidal neuron in voltage clamp at -50 mV showing the effect of adding 100 μM benzoin **220** to the bathing solution. Benzoin is toxic to the neurons because it depolarises them as observed by the downward shift in holding current and the significant increase in the number of mEPSCs.

Although 3',5'-dimethoxybenzoin-caged ATP has been used *in vitro* previously without toxicity being reported,[154] given our results, it is clear that 3',5'-dimethoxybenzoin is not a suitable caging group for use in studies on neuronal function. Therefore, a new orthogonal caging group partner to DMNB had to be developed. In previous work on the development of caged TRPV1 agonists and antagonists,[98,103] the use of Sheehan's 4-methoxyphenacyl (MPA) caging group has been investigated.[29] Epstein and Garrossian first demonstrated the application of 4-methoxyphenacyl esters as caging groups for phosphates.[30] This group and its derivatives have since been employed by Givens to cage phosphates,[31,155] neurotransmitters[34,156,157] and protein kinase A.[67] The MPA group typically displays a λ_{max} value of shorter wavelength than the DMNB group and was, therefore, a potential wavelength-orthogonal partner to the DMNB group. In order to assess whether the MPA caging group would cause neuronal toxicity, compounds similar to the photolysis by-products from the MPA group (4-hydroxyacetophenone, 4-methoxyacetophenone and 4-hydroxyphenylacetic acid) were applied to the neurons, but they did not cause neuronal toxicity. Therefore, MPA-glutamate was synthesised

7.6. Synthesis of 4-Methoxyphenacyl (MPA)-Caged Glutamate and GABA

The free MPA caging group **230** was obtained in two steps from 4-methoxyacetophenone **42**, Scheme 7.13. 4-Methoxyacetophenone **42** was brominated at the α-position by treatment with Br_2 and $AlCl_3$ in ether at 0 °C. The dibrominated product was a significant side-product and the desired monobrominated product **229** was isolated in a low yield. Hydroxylation to obtain the free MPA caging group, 2-hydroxy-1-(4-methoxyphenacyl)ethanone **230**, was achieved in 77% yield by heating the brominated intermediate **229** in sodium formate and ethanol under reflux for 4 h.

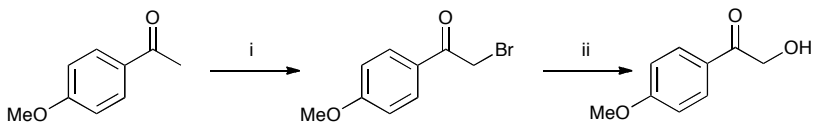

42 **229** **230**

Scheme 7.13. Synthesis of the MPA caging group **230**. *Reagents and conditions*: i. Br_2, $AlCl_3$, Et_2O, 0 °C, 30%; ii. sodium formate, EtOH, reflux, 4 h, 77%.

Boc-protected GABA **170** was coupled to the MPA caging group **230** in 62% yield using EDC and HBTU coupling conditions, Scheme 7.14. These new coupling conditions were employed as purification is easier than when using DCC-mediated coupling, in which the N,N-dicyclohexylurea by-product is difficult to remove completely. The Boc-protected MPA-GABA intermediate **231** was deprotected using 1 M HCl in acetic acid to obtain MPA-GABA **232** in 79% yield, Scheme 7.14.

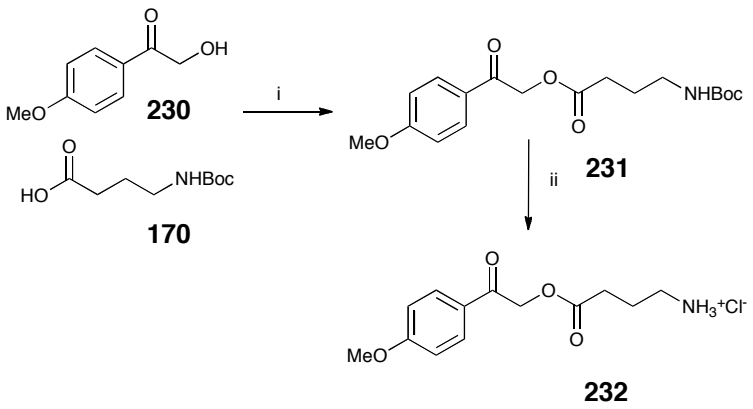

Scheme 7.14. Synthesis of MPA-caged GABA **232**. *Reagents and conditions*. i. EDC, HBTU, DIPEA, CH_2Cl_2, 62%; ii. 1 M HCl in acetic acid, 79%.

The Boc-protected *tert*-butyl ester of (*S*)-glutamate **173** was coupled to the MPA caging group **230** in 67% yield using EDC and HBTU coupling conditions, Scheme 7.15. The protected MPA-glutamate intermediate **233** was globally deprotected by treatment with 1 M HCl in acetic acid at 45 °C for 4 h to obtain MPA-glutamate **234** in 76% yield, Scheme 7.15

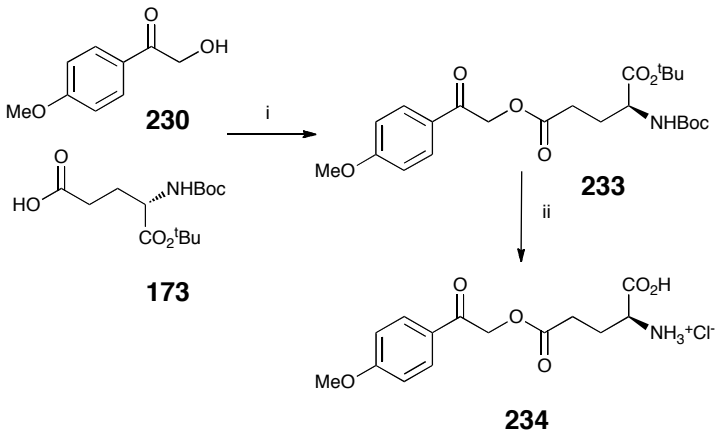

Scheme 7.15. Synthesis of MPA-caged glutamate **234**. *Reagents and conditions*. i. EDC, HBTU, DIPEA, CH_2Cl_2, 67%; ii. 1 M HCl in acetic acid, 45 °C, 76%.

7.7. UV/Vis Spectra of MPA-Caged Neurotransmitters

In order to determine what wavelengths were most likely to evoke successful photolysis of the MPA group and, therefore, whether this caging group was likely to be a suitable wavelength-orthogonal partner to the DMNB group, the UV/Vis absorption spectra of the MPA-caged neurotransmitters were recorded. Figure 7.8 is an overlay of the UV/Vis spectra of MPA-glutamate **234** and DMNB-GABA **205** (0.01 mM in artificial cerebral spinal fluid). The λ_{max} values of the different caging groups were observed to be significantly different. MPA-Glu **234** does not absorb above 310 nm and has greater absorbance than DMNB-GABA **205** at 260-270 nm, whereas DMNB-GABA absorbs strongly above 310 nm. This indicated that wavelength-orthogonal

photolysis of these two compounds may be possible. Therefore, photolysis experiments were undertaken.

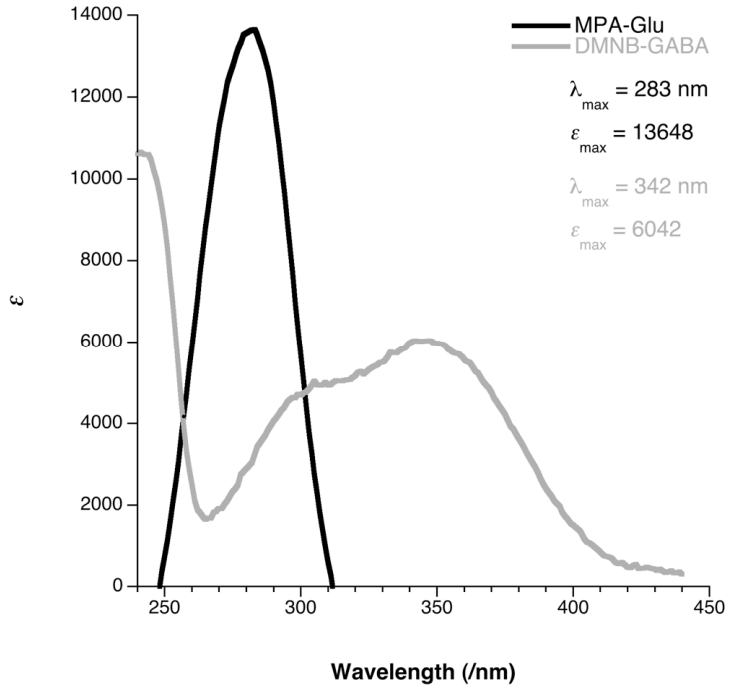

Figure 7.8. MPA-glutamate **234** UV/Vis spectrum (0.01 mM in artificial cerebral spinal fluid) (black); DMNB-GABA **205** UV/Vis spectrum (0.01 mM in artificial cerebral spinal fluid) (grey). ε is the extinction co-efficient ($M^{-1}cm^{-1}$).

7.8. Photolysis Investigation of MPA- and DMNB-Caged Neurotransmitters

In order to confirm that wavelength-orthogonal photolysis of MPA-Glu **234** and DMNB-GABA **205** could be achieved, solutions of these compounds were irradiated at 405 nm, 270-310 nm and 266 nm and the resulting solutions analysed by ^{1}H NMR using hexamethyldisiloxane as an internal standard. Please refer to the General Experimental Section for details.

Solutions containing 1:1 mixtures of DMNB-GABA **205** and MPA-Glu **234** in DMSO were added to a quartz cuvette and irradiated for 2, 7.5 and 15 h using a 405 nm, 30 mW laser diode. This 1:1 DMNB-GABA **205** and MPA-Glu **234** solution was also irradiated for 5 and 14 h using a 270-310 nm transmitting filter box and a 300 W ultraviolet lamp. Figure 7.9 is a collection of partial ^{1}H NMR spectra demonstrating the selective photolysis of DMNB-GABA **205** to give free GABA **203** in the presence of MPA-Glu **234** (Figure 7.9, A and B) following irradiation at 405 nm; and the selective photolysis of MPA-Glu **234** in the presence of DMNB-GABA **205** (Figure 7.9, C and D) following irradiation at 270-310 nm. Figure 7.9A shows that the aromatic peaks corresponding to MPA-Glu **234**, at 7.9 and 7.1 ppm, did not diminish during irradiation at 405 nm. However, the peaks corresponding to DMNB-GABA **205**, at 7.7, 7.2 and 5.4 ppm, did diminish during irradiation. Figure 7.9B confirms that free GABA **203** was released during irradiation of MPA-Glu **234** and DMNB-GABA **205** at 405 nm. The aliphatic peaks which were observed to appear and increase during photolysis, at 2.8, 2.3 and 1.8 ppm, correspond to the peaks observed when the 15 h, 405 nm photolysis sample was spiked with commercially available free GABA.

Figure 7.9C shows that the aromatic peaks corresponding to DMNB-GABA **205**, at 7.7 and 7.2 ppm, did not diminish during irradiation at 270-310 nm. However, the peaks corresponding to MPA-Glu **234**, at 7.9, 7.1 and 5.5 ppm, did diminish during irradiation. Also, peaks from a MPA photolysis by-product were observed. Figure 7.9D confirms that free GABA **203** was not released

during irradiation of MPA-Glu **234** and DMNB-GABA **205** at 270-310 nm. No peaks corresponding to the ones observed when the 5 h photolysis sample was spiked with free GABA were observed after irradiation.

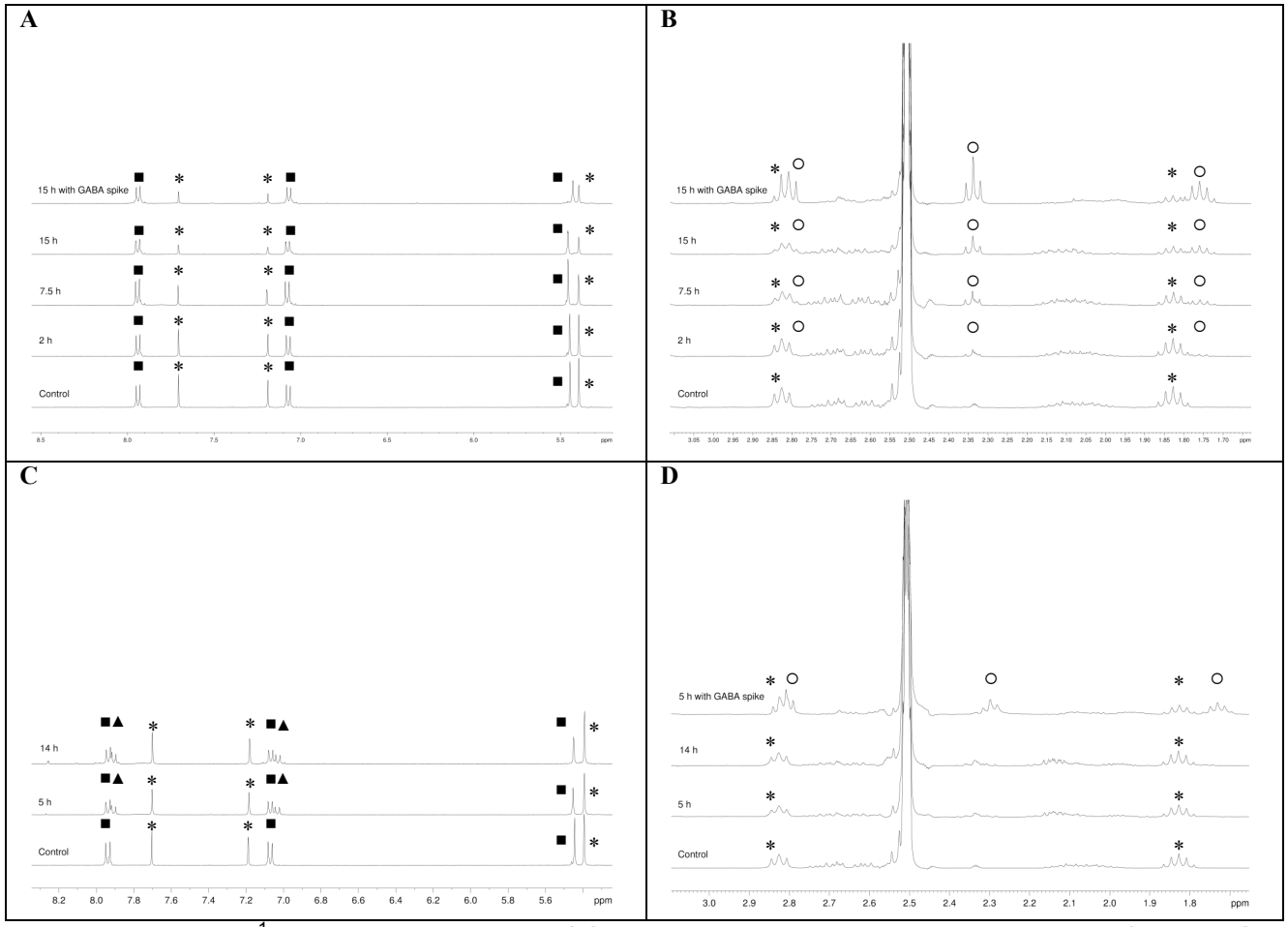

Figure 7.9. Partial ^{1}H NMR spectra (D_6-DMSO) demonstrating the selective photolysis of DMNB-GABA **205** (*) to give free GABA **203** (○) in the presence of MPA-Glu **234** (■) (**A** and **B**) following irradiation at 405 nm; and the selective photolysis of MPA-Glu **234** (■) in the presence of DMNB-GABA **205** (*) (**C** and **D**) following irradiation at 270-310 nm. The appearance of a MPA photolysis by-product (▲) was observed (**C**).

The irradiated samples whose NMRs are represented in Figure 7.9 were quantitatively analysed using hexamethyldisiloxane as an internal standard. Figure 7.10 shows the quantified products observed after irradiation of a 1:1 mixture of DMNB-GABA **205** and MPA-Glu **234** in DMSO for 2, 7.5 and 15 h using a 405 nm, 30 mW laser diode. The black bars represent the percentage of MPA-Glu **234**, which did not change during irradiation. The grey bars represent the percentage of DMNB-GABA **205** - which decreased significantly during irradiation. The longer the radiation exposure, the less DMNB-GABA **205** was detected in the photolysis sample. No free glutamate **228** was observed in the photolysis samples. Free GABA **203** was released during photolysis. This confirms that at sufficiently long wavelengths, the MPA caging group remains intact while the DMNB caging group is cleaved.

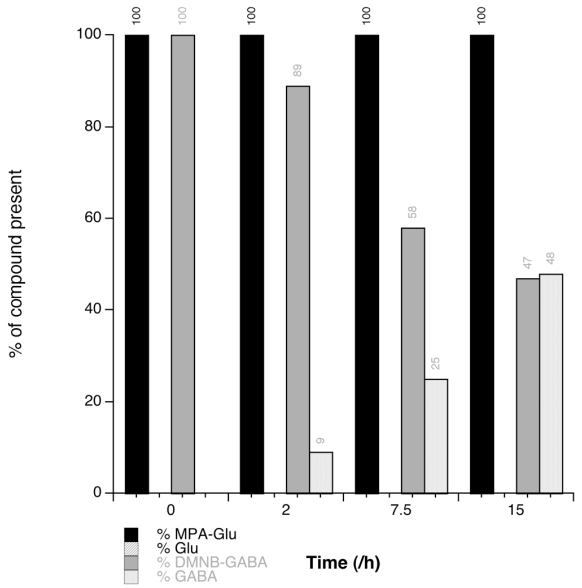

Figure 7.10. Quantification of photolysis of a mixture of MPA-Glu **234** and DMNB-GABA **205**, following irradiation at 405 nm, 30 mW in DMSO for 2, 7.5, and 15 hours. Photolysis samples were analysed by ^{1}H NMR with hexamethyldisiloxane standard in DMSO. The black bars represent the percentage of MPA-Glu **234**. The grey bars represent the percentage of DMNB-GABA **205**.

Figure 7.11 shows the quantified products observed after irradiation of a 1:1 mixture of DMNB-GABA **205** and MPA-Glu **234** in DMSO for 5 and 14 h using a 270-310 nm transmitting filter box and a 300 W ultraviolet lamp. The black bars represent the percentage of MPA-Glu **234** - which decreased significantly during irradiation. The longer the radiation exposure, the less MPA-Glu was detected in the photolysis sample. The grey bars represent the percentage of DMNB-GABA **205** - which did not change during irradiation. This confirms that at sufficiently short wavelengths, the DMNB caging group remains intact while the MPA caging group is cleaved.

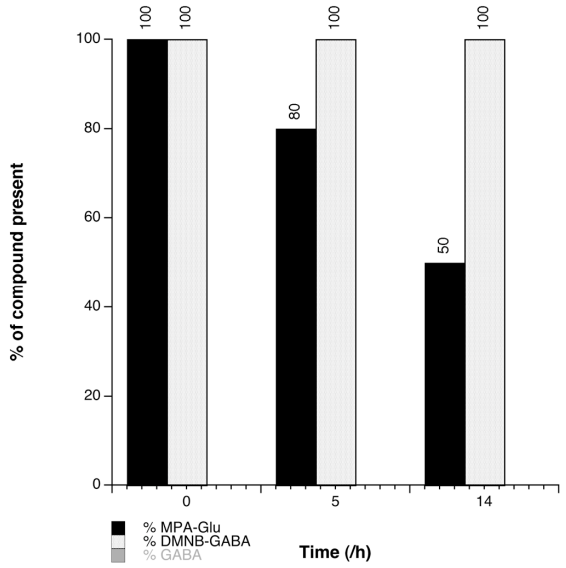

Figure 7.11. Quantification of photolysis of a mixture of MPA-Glu **234** and DMNB-GABA **205**, following irradiation at 270-310 nm in DMSO for 5 and 14 hours. Photolysis samples were analysed by ^{1}H NMR with hexamethyldisiloxane standard in DMSO. The black bars represent the percentage of MPA-Glu **234**. The grey bars represent the percentage of DMNB-GABA **205**.

In an additional short-wavelength experiment, a 1:1 mixture of DMNB-GABA **205** and MPA-Glu **234** in DMSO was added to a quartz cuvette and photolysed for 2, 5, 8 and 20 h using a 266 nm YAG laser. Figure 7.12 represents the quantified products after irradiation. The black bars represent the percentage of MPA-Glu **234** - which decreased to 87 % after 20 h irradiation. The longer the radiation exposure, the less MPA-Glu was detected in the photolysis sample. A MPA photolysis by-product was also observed, represented by the striped bars. The grey bars represent the percentage of DMNB-GABA **205** - which did not change during irradiation. This provides additional evidence that at sufficiently short wavelengths, the DMNB caging group remains intact while the MPA caging group is cleaved.

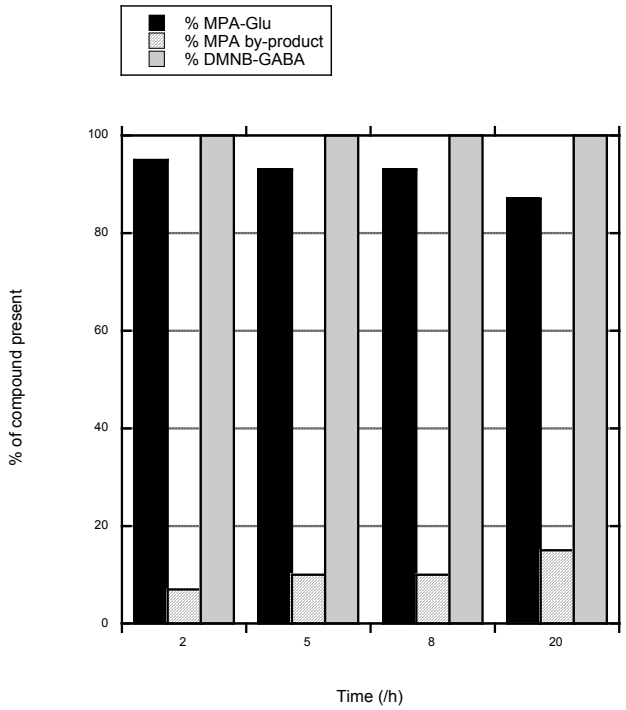

Figure 7.12. Quantification of photolysis of a mixture of MPA-Glu **234** and DMNB-GABA **205**, following irradiation at 266 nm in DMSO for 2, 5, 8 and 20 hours. Photolysis samples were analysed by ^{1}H NMR with hexamethyldisiloxane standard in DMSO. The black bars represent the percentage of MPA-Glu **234**. The grey bars represent the percentage of DMNB-GABA **205**. The striped bars represent the percentage of MPA photolysis by-product.

These results demonstrate that MPA-Glu **234** is a suitable orthogonal partner for DMNB-GABA **205**. Therefore, wavelength-orthogonal photolysis in neurons was attempted using these caged neurotransmitters.

7.9. Application of DMNB- and MPA-Caged Neurotransmitters to a Biological System

In hippocampal pyramidal neurons, MPA-Glu **234** was observed to have no effect when applied to the bath solution, indicated by a lack of discernable increase in neuronal excitability, action potential firing or change in holding potential, Figure 7.13D. Also, when bath-applied MPA-Glu was irradiated at 405 nm, no electrophysiological response was observed, Figure 7.13D. However, Figure 7.13D (left trace) shows that irradiation at 250-270 nm evoked a large cation current, most likely as a result of MPA-Glu **234** photolysis and subsequent glutamate receptor activation (MPA-Glu (62.5-125 μM) was photolysed at 250-270 nm in nine different cells a total of 27 times). DMNB-GABA **205** also showed no activity on cells when applied to the bath solution, Figure 7.13C. Irradiation at 250-270 nm did not produce a response (Figure 7.13C). However, Figure 7.13C (right trace) shows that irradiation at 405 nm evoked a large anion current (DMNB-GABA (25-50 μM) was photolysed at 405 nm in nine different cells a total of 22 times). It is likely that this response is a result of DMNB-GABA **205** photolysis and subsequent activation of GABA receptors.

With the potential for wavelength-orthogonal photolysis *in vitro* established, both MPA-Glu **234** and DMNB-GABA **205** were applied to the bath solution. The compounds showed no significant effect until photolysed (Figure 7.13A). Irradiation of this mixture, using a UV flash lamp equipped with a 250-270 nm

bandpass filter, evoked a cation current consistent with activation of glutamate receptors (Figure 7.13A). A few seconds later, exposure to light of 405 nm caused an anion current, consistent with activation of GABA receptors (Figure 7.13A, n=3). To confirm that wavelength *orthogonality* rather than wavelength *selectivity* was being observed, the order of irradiation was reversed (Figure 7.13B). It was demonstrated that photolysis at 405 nm led to activation of GABA receptors, and subsequent photolysis at 250-270 nm a few seconds later led to activation of glutamate receptors (Figure 7.13B, n=2). Hence, application of both compounds to the bath solution allowed for rapid and interchangeable control of both glutamate and GABA channels, modulated only by the wavelength of irradiating light.

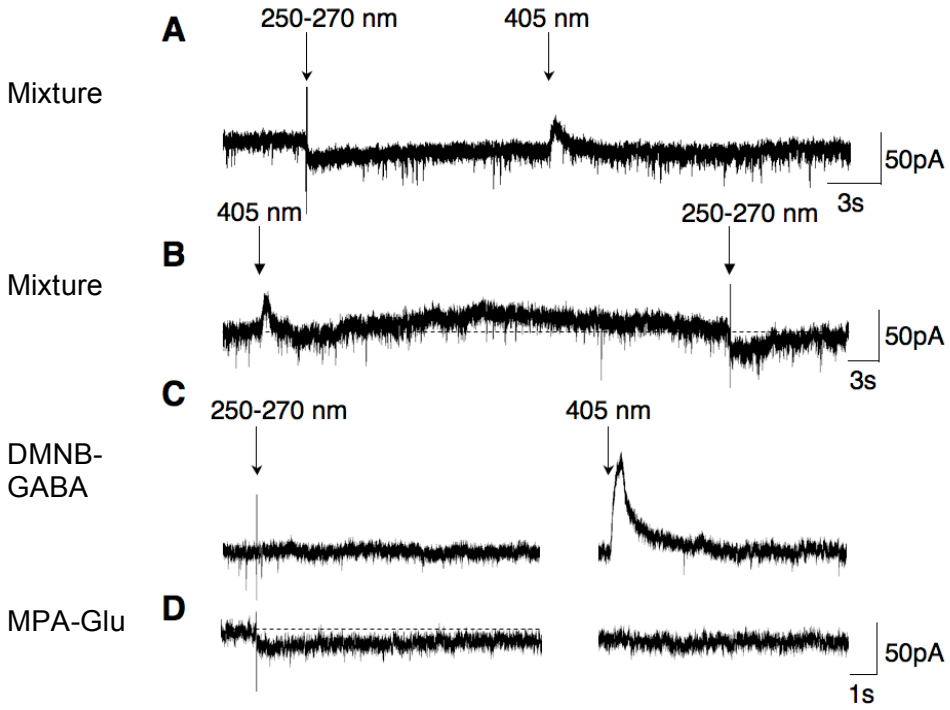

Figure 7.13. Wavelength-orthogonal photolysis of MPA-Glu **234** and DMNB-GABA **205** in neurons. (**A** and **B**) Representative whole-cell patch-clamp recordings of cultured hippocampal pyramidal neurons bathed in a solution containing MPA-Glu (125 mM) and DMNB-GABA (50 mM). (**A**) Illumination at 250-270 nm evoked a rapid inward, cation current, seen as a downward deflection on the record, consistent with photorelease of glutamate **228** from MPA-Glu **234**. Subsequent illumination at 405 nm a few seconds later activated a rapid inward, anion current, seen as an upward deflection on the record, consistent with photorelease of GABA **203** from DMNB-GABA **205**. (**B**) Reversal of the sequence of illumination reversed the sequence in which the currents were evoked. (**C**) A neuron bathed exclusively in DMNB-GABA **205** (50 mM) showed a current when illuminated at 405 nm but no current was evoked at 250-270 nm. (**D**) A neuron bathed exclusively in MPA-Glu **234** (125 mM) responded to illumination at 250-270 nm but not 405 nm. DMNB-GABA and MPA-Glu concentration, illumination power and illumination duration in **C** and **D** were the same as in **A** and **B**.

7.10. Summary

The synthesis of a 4-methoxyphenacyl-caged (*S*)-glutamate derivative (MPA-Glu) **234** and a 4,5-dimethoxy-2-nitrobenzyl-caged γ-amino butyric acid derivative (DMNB-GABA) **205** has been reported. It was demonstrated, in cultured hippocampal pyramidal neurons, that irradiation at 250-270 nm evoked selective photorelease of (*S*)-glutamate and subsequent activation of glutamate receptors, whereas photolysis at 405 nm caused selective photorelease of GABA and activation of GABA receptors. The caged compounds could be released in either order, affording unprecedented control over *in vitro* photorelease of these neurotransmitters. These data represent the first example of single-photon wavelength-orthogonal photolysis *in vitro.* Figure 7.14 is a representation of wavelength-orthogonal photolysis of caged glutamate and GABA within a synaptic cleft. Neural response can be controlled by the irradiating wavelength, which determines which neurotransmitter is photoreleased and, therefore, which receptor is activated.

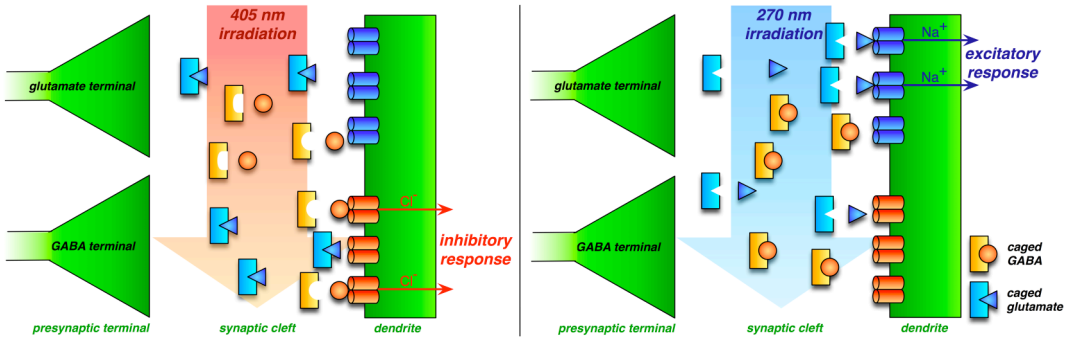

Figure 7.14. A cartoon representation of wavelength-orthogonal photolysis of caged glutamate and GABA within a synaptic cleft. In this example, irradiation at 405 nm exclusively activates GABA receptors, resulting in an inhibitory response, whereas irradiation at 250-270 nm exclusively activates glutamate receptors, resulting in an excitatory response.

This demonstration of wavelength-orthogonal photolysis of biologically relevant compounds also proves the principle that this technology can be applied to a plethora of other signalling molecules. Orthogonally caged biologically significant molecules will improve the current tool-kit for the study of challenging biological problems.

7.11. Extending the Applicability of Wavelength-Orthogonal Caging Groups

In order to increase the biological applicability of the MPA derivative by increasing its solubility in aqueous solutions, glutamate was caged with a 4-hydroxyphenacyl caging group.[22,33,157] This group was developed by Givens.[33] 4-Hydroxyacetophenone **235** was brominated at the α-position by treatment with Br_2 and $AlCl_3$ in ether, Scheme 7.16. The dibrominated product was a significant side-product and the desired monobrominated product **236** was isolated in 51% yield. This brominated intermediate **236** was coupled to the Boc-protected *tert*-butyl ester of (*S*)-glutamate **173** using DBU in THF to obtain the protected HPA-caged glutamate intermediate **237** in 64% yield. Global deprotection of the Boc and *tert*-butyl groups was achieved by treatment with 1 M HCl in acetic acid at 45 ºC to obtain HPA-caged glutamate **238** in 74% yield.

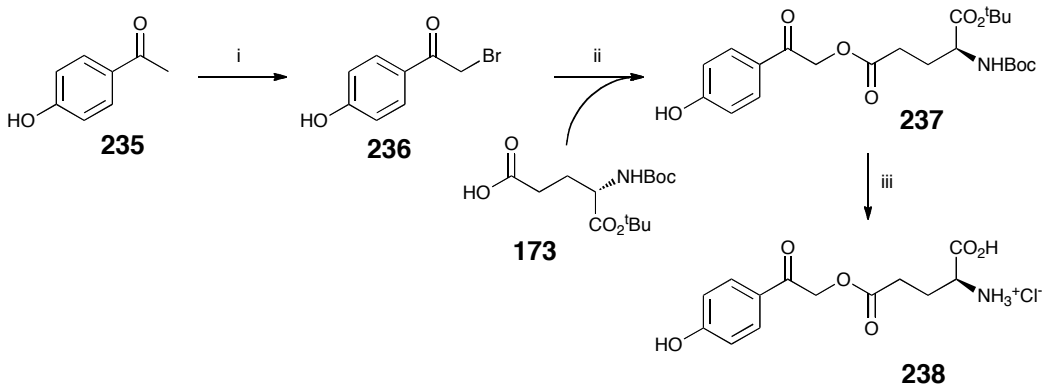

Scheme 7.16. Synthesis of HPA-Glu **238**. *Reagents and conditions*: i. Br_2, $AlCl_3$, Et_2O, 51%; ii. DBU, THF, 64%; iii. 1 M HCl in acetic acid, 45 °C, 74%.

HPA-caged glutamate **238** has not yet been applied to neurons and so no conclusions can be drawn about its applicability as a wavelength-orthogonal partner to the DMNB caging group in biological systems.

7.12. Future Work – Using Wavelength-Orthogonality to Explore the Integrative Code of CNS Neurons

Neurons receive a number of simultaneous excitatory and inhibitory synaptic inputs. Whether or not a neuron fires an action potential, the output signal, is determined by integrating these multiple synaptic inputs. The understanding of neuronal systems at a molecular level remains a significant challenge to science and medicine. The control of multiple synaptic inputs would allow for dendritic integration to be investigated. Using wavelength-orthogonally caged neurotransmitters and multi-point illumination; the number, location, temporal sequence and polarity (excitatory or inhibitory) of synaptic inputs could be controlled. By controlling the input signal and observing the output signal, the way in which neurons receive, integrate, propagate and store information could be studied.

Chapter 8:

Results and Discussion -

pH-Dependent Photolysis

8. Development of a pH-Dependent Caging Group

8.1. Introduction and Aims

The ability to photorelease biologically active compounds from caged precursors with selectivity determined by the surrounding environment would be a powerful extension to existing photolysis technology. One environmental factor that could be employed is the pH of the medium surrounding the caged compound. This additional selectivity would allow for a biologically active compound to be delivered selectively to a certain tissue or cellular area which has a particular pH environment, Figure 8.1. The design of a pH sensing caging group would require incorporation of a functional group which would confer different absorbance characteristics to the caging group in its protonated and deprotonated states.

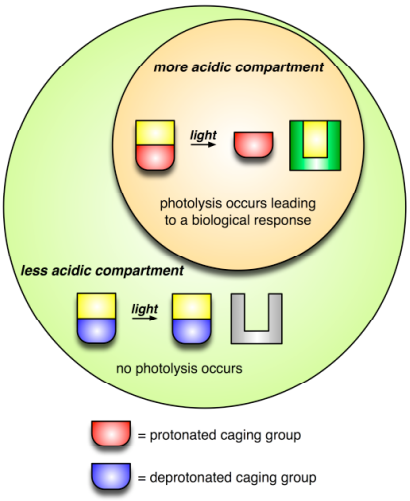

Figure 8.1. A cartoon representation of proposed pH-dependent photolysis, which allows for selective photorelease of a biologically active compound in an acidic organelle or tissue. No photolysis occurs in the less acidic compartment, while photorelease of the biologically active compound does occur in the more acidic compartment.

The long-term goal of targeted drug delivery to defined tissue would be a valuable application of photodynamic therapy in humans. The caged, inactive, drug could be administered intravenously or orally and the affected tissue or organ irradiated so that the active drug is site-selectively delivered. This strategy would minimise drug-induced damage to healthy tissues. In addition to this, differences between healthy and unhealthy tissues could be exploited for refined control over drug delivery. For example, cancer cells have a lower pH environment than healthy cells. A caged drug which is photoreleased only in the lower pH environment would target cancer cells and protect healthy cells from exposure to harmful drug molecules.

This technology would also allow for targeting of organelles and cellular compartments which are smaller than the diffraction limit currently available. The biologically active compound could be released in a volume smaller than that of the light beam, as determined by the pH environment of that cellular compartment.

The effect of pH on photolysis has been previously reported.[11,19,158] The effect of pH on the rate constants of the formation and decay of intermediates in the photolytic pathway can be recorded by time-resolved IR spectra, Fourier transform infrared spectroscopy (FTIR), after flash photolysis. An example of pH affecting a photolysis pathway is that of the photorelease of alcohols from 2-nitrobenzyl ethers. Wirz and co-workers studied the photorelease of alcohols from 2-nitrobenzyl ethers.[158] They concluded that the reaction occurs *via* formation of a hemiacetal intermediate **26**, C (Scheme 8.1), and that decay from this intermediate is the rate-limiting step at pH below 7. Above pH 7, a complex mixture of products of high molecular weight was observed by gas chromatography and mass spectrometry (GC-MS). A similar study by Hutter and co-workers reached different conclusions about the reaction mechanism - no hemiacetal intermediate was observed in the FTIR spectrum recorded during photolysis of a nitrobenzyl-caged glycolic ether.[159] However, this study was conducted at pH 8.5 with high buffer concentrations. Wirz concludes that because of the reaction conditions employed by Hutter, the hemiacetal intermediate did not accumulate and was, therefore, not observed.

In an interesting earlier study by Wirz and co-workers, the dependencies of the reaction rates of three intermediates, A, B and C, (Scheme 8.1), in the photolytic pathway of nitrobenzyl ethers were studied as a function of pH, buffer concentration, and solvent, using laser flash photolysis with UV/Vis and IR detection.[19] The rate of reaction of intermediate A to B (referred to as 'ab' in Scheme 8.1) decreased sharply with increasing pH. This observation is consistent with the fact that the neutral species A is more reactive than its deprotonated form (i.e. cyclisation of the *aci*-anion has a higher activation barrier than for the neutral intermediate A). This observation is mentioned in Chapter 1.4. The rate of reaction of intermediate B to C (referred to as 'bc' in Scheme 8.1) reached a maximum at pH 6 and then decreased with increasing pH.

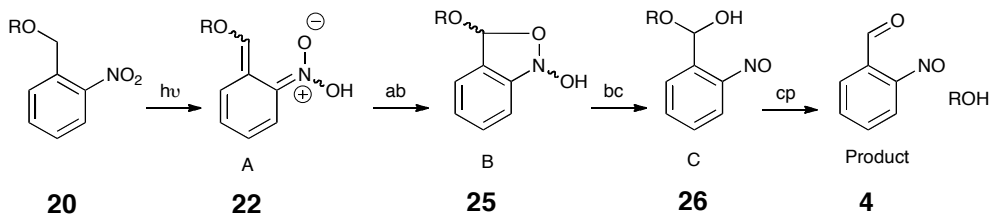

Scheme 8.1. Intermediates observed in the photolysis pathway of 2-nitrobenzyl ethers.[19]

Given the complex role of pH on the photolysis rates, intermediates and products, with an example highlighted above, it is probably not surprising that only one example of the design of a photolabile caging group with different reactivities at different pHs has been reported. Bochet demonstrated a new safety-catch photolabile protecting group[160] to prevent premature unwanted

cleavage. An amino group was incorporated *para* to the nitro group of nitrobenzyl-derived esters **239**, Scheme 8.2. This amino group quenches photoreactivity by electron donation onto the nitro group in the excited state. In the protonated form this electron donation does not occur and photoreactivity is restored. Therefore, both light and a chemical promoter (H^+) are required for cleavage.

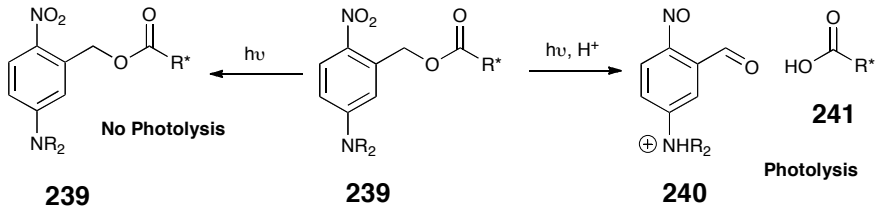

Scheme 8.2. Safety-catch caging group **239** which requires both protonation and light for photorelease.[160] R = alkyl chain, R* = alkyl chain.

8.2. Evaluating the Nitrophenol Skeleton as a Potential pH-Dependent Caging Group

The proposed strategy for the development of a pH-dependent caging group was based on the assumption that photolysis of one protonation state can occur at a given pH at one wavelength, and not at a different wavelength, Scheme 8.3. The nitrophenol skeleton was a proposed candidate for the development of such a pH-dependent caging group because the protonated and deprotonated states have significantly different UV/Vis absorbances.[161]

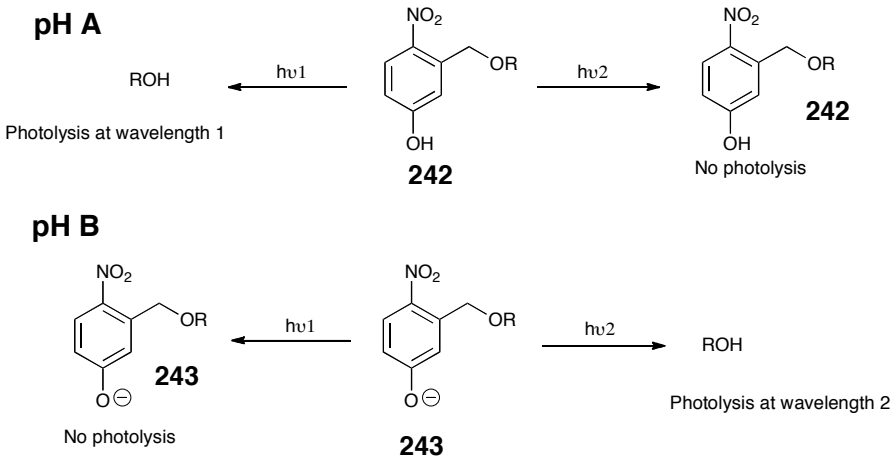

Scheme 8.3. Illustration of proposed pH-dependent photolysis using the 4-nitrophenol skeleton as the caging group. Wavelengths 1 and 2 are the irradiation wavelengths which correspond to the maximum absorbance of the protonated **242** and deprotonated **243** states respectively. The protonated form **242** could be photolysed at wavelength 1 and not wavelength 2, because it does not absorb at wavelength 2. Similarly, the deprotonated form **243** could be photolysed at wavelength 2 and not wavelength 1, because it does not absorb at wavelength 1.

Ando *et al.* observed significant red-shift (i.e. to longer wavelengths) and an increase of the electronic transitions upon deprotonation of 4-nitrophenol.[161] To confirm this observation, UV/Vis absorption spectra of protonated and deprotonated 3-methyl-4-nitrophenol and 4-methyl-3-nitrophenol were recorded, Figures 8.2 and 8.3. Solutions were prepared in methanol at 0.1 mM. The acidic solutions were prepared by adding a few drops of HCl (38%) to obtain an apparent pH of 2. The basic solutions were prepared by adding a few drops of DBU to obtain an apparent pH of 12.

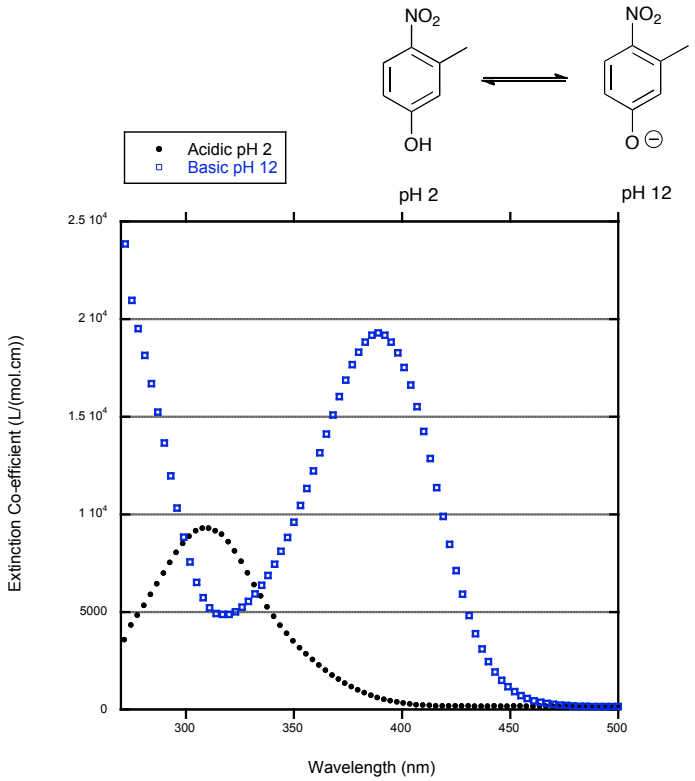

Figure 8.2. The UV/Vis spectra of protonated and deprotonated 3-methyl-4-nitrophenol, 0.1 mM in MeOH.

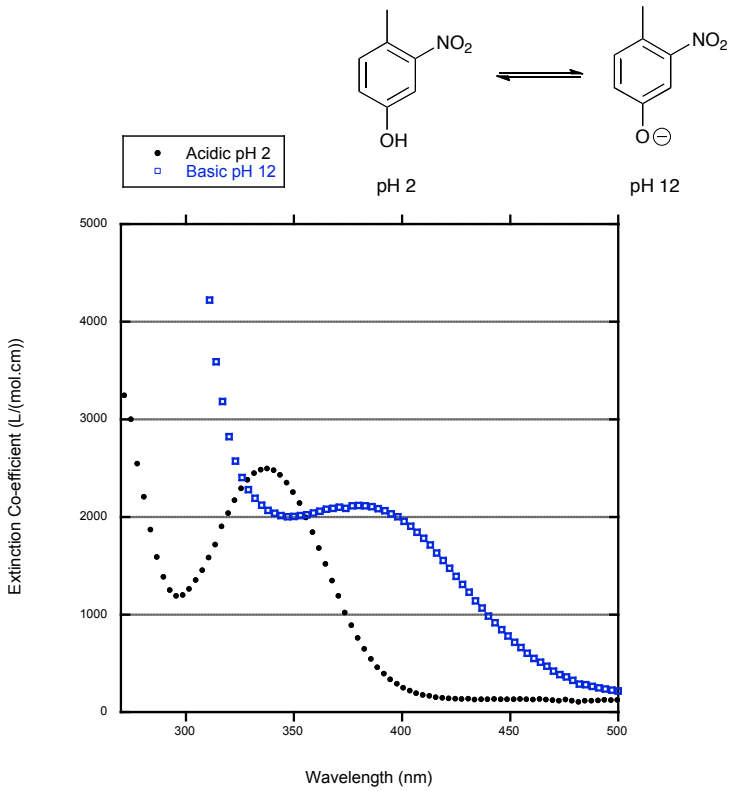

Figure 8.3. The UV/Vis spectra of protonated and deprotonated 4-methyl-3-nitrophenol, 0.1 mM in MeOH.

The resonance electron withdrawing ability of the *para* nitro group in 3-methyl-4-nitrophenol stabilises the negative charge of the conjugate phenolate base and lowers the pKa of the phenol group, Figure 8.4. The removal of the phenol proton leads to two additional electrons delocalised throughout the aromatic ring. This increases conjugation and lowers the HOMO-LUMO energy gap and, therefore, the energy needed for an electronic transition.

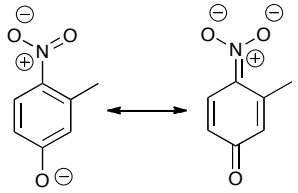

Figure 8.4. The resonance electron withdrawing ability of the *para* nitro group in 3-methyl-4-nitrophenol stabilises the negative charge of the conjugate phenolate base.

Consistent with the observations of Ando *et al*.[161], deprotonation led to a substantial red-shift in the electronic spectra as well as an increase in the intensity of the electronic transitions.[161] The UV/Vis spectra show that λ_{max} of 3-methyl-4-nitrophenol shifts from 330 nm to 400 nm in its different protonation states, while the λ_{max} of 4-methyl-3-nitrophenol shifts from 350 nm to 400 nm (Figures 8.2 and 8.3). These initial results are promising as they confirm that there is a significant shift in the λ_{max} value between the different protonation states of the phenol. It was hypothesised that at 400 nm, only the deprotonated compound will absorb light resulting in selective uncaging as determined by the pH of the solution.

The extinction co-efficient of 4-methyl-3-nitrophenol was significantly lower than 3-methyl-4-nitrophenol, suggesting that this compound may not be suitable as a caging group. It was, therefore, not employed in further investigations.

Having established that the 4-nitrophenol skeleton may be suitable as a pH-dependent caging group, it was proposed to cage the mitochondrial uncoupler AG10 **94** with the nitrophenol-caging group. It was envisaged that this synthesis would be readily achieved and that the caged compound could be tested for its photolysis characteristics in a cuvette as well as *in vitro* in a biological system with which we have experience.[78]

8.3. Synthesis of Nitrophenol-Caged AG10

In order to investigate the proposal of pH-dependent caging groups, it was aimed to protect AG10 with the nitrophenol-caging group. The proposed retrosynthesis is shown in Scheme 8.4.

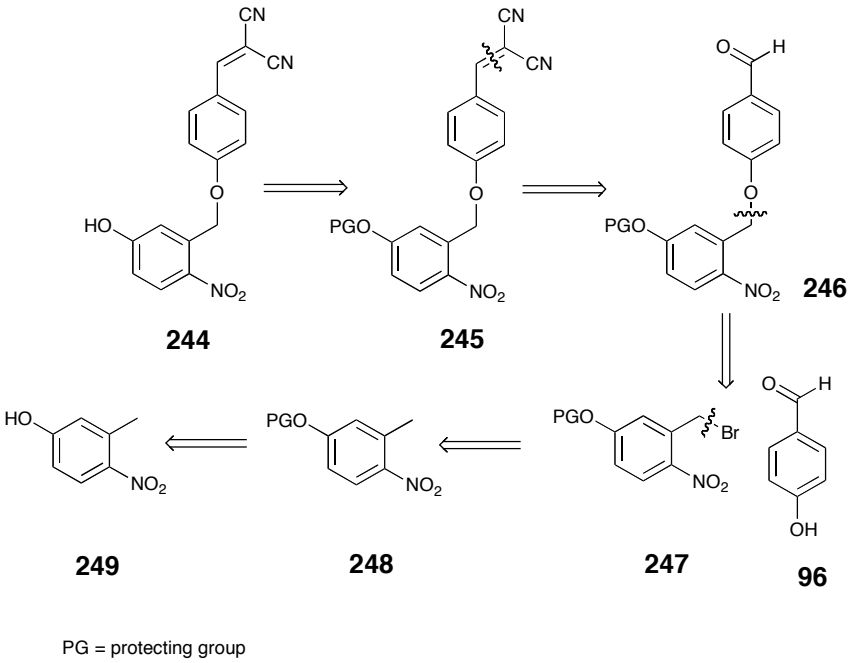

Scheme 8.4. Proposed retrosynthesis of nitrophenol-caged AG10 **244** starting from commercially available 3-methyl-4-nitrophenol **249**.

The first disconnection in the proposed retrosynthesis of nitrophenol-caged AG10 **244** involves a deprotection step followed by a Knoevenagel-like condensation of the benzaldehyde **246**. The next disconnection is at the phenol position to obtain 4-hydroxybenzaldehyde **96** and the protected

nitrophenol **247**. The bromide could be incorporated at the benzylic position of protected 3-methyl-4-nitrophenol **248**.

Before protecting the phenol position of 3-methyl-4-nitrophenol **249**, an attempt was made to selectively brominate the benzylic position to form 3-(bromomethyl)-4-nitrophenol by treatment with *N*-bromosuccinimide (NBS) and benzoyl peroxide in chloroform under reflux conditions. However, 2-bromo-3-methyl-4-nitrophenol **250** was isolated, Scheme 8.5. The ring had been brominated instead of the benzylic position. The phenol group activates the *ortho* position to bromination by delocalisation of its lone pair of electrons onto the aromatic ring. Two aromatic doublets with identical coupling constants, at 7.83 and 6.93 ppm, were observed in the ^{1}H NMR. These peaks correspond to the hydrogen atoms at position 5 and 6 on the aromatic ring. No other aromatic peaks were observed. It is surprising that the more sterically hindered 2-position was brominated instead of the 6-position.

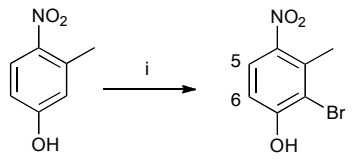

249 **250**

Scheme 8.5. Undesired synthesis of 2-bromo-3-methyl-4-nitrophenol **250**. *Reagents and conditions*: i. NBS, benzoyl peroxide, $CHCl_3$, reflux.

It was decided that the phenol group should be protected with a TIPS group in order to prevent the activation of the ring to bromination. 3-Methyl-4-

nitrophenol **249** was reacted with imidazole and triisopropylchlorosilane (TIPSCl) in DMF at room temperature. Triisopropyl (3-methyl-4-nitrophenoxy)silane **251** was obtained as a light-yellow oil in 99% yield, Scheme 8.6.

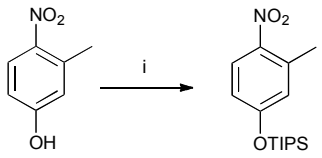

249 **251**

Scheme 8.6. Synthesis of TIPS-protected 3-methyl-4-nitrophenol **251**. *Reagents and conditions*: i. TIPSCl, imidazole, DMF, RT, 99%.

Attempts at benzylic bromination of the TIPS-protected nitrophenol **251** using recrystallized NBS and purified benzoyl peroxide, as well as using molecular bromine and purified benzoyl peroxide, resulted in bromination of the TIPS group at the carbon α to silicon as shown in Scheme 8.7. This result may be because of the stability of the radical at this position.

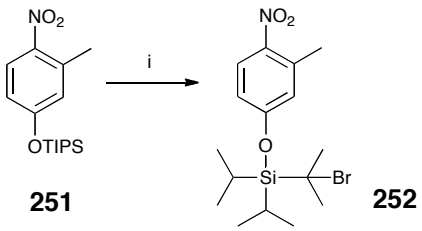

251 **252**

Scheme 8.7. Bromination of the TIPS-protected methyl-nitrophenol **251** at the TIPS group itself, not at the desired benzylic position. *Reagents and conditions*: i. NBS, benzoyl peroxide, CCl_4, reflux, o/n; or Br_2, benzoyl peroxide, CCl_4, reflux, o/n.

To circumvent this problem, another protecting group was employed. The phenol group of 3-methyl-4-nitrophenol **249** was protected with a *tert*-butyldimethylsilyl (TBS) protecting group by treatment with TBSCl in CH_2Cl_2 with NEt_3, Scheme 8.8. The product **253** was obtained in 80% yield. TBS-protected 3-methyl-4-nitrophenol **253** was reacted with recrystallised NBS and dibenzoyl peroxide in dichloroethane, under reflux. The brominated product **254** was obtained in low yield. Mostly starting material **253** was obtained from this reaction.

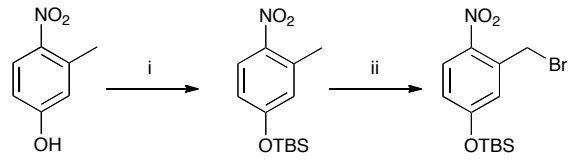

249 **253** **254**

Scheme 8.8. Synthesis of TBS-protected 3-(bromomethyl)-4-nitrophenol **254**. *Reagents and conditions*: i. TBSCl, NEt_3, CH_2Cl_2, RT, 80%; ii. NBS, dibenzoyl peroxide, dichloroethane, reflux, 15%.

In the next step towards the synthesis of nitrophenol-caged AG10 **244,** an attempt was made to react 4-hydroxybenzaldehyde **96** with the benzylic position of the protected, brominated nitrophenol **254**. This reaction was unsuccessfully attempted by treatment with K_2CO_3 and DMF at 50 ºC overnight. Only baseline material was observed by TLC. However, when using NaH in THF at RT an unexpected product **255** was obtained, Scheme 8.9. The oxygen nucleophile of 4-hydroxybenzaldehyde **96** did not attack the

brominated benzylic position but rather the silyl protecting group. The nitrophenol **254** acted as a silyl transfer reagent so that the isolated product was TBS-protected 4-hydroxybenzaldehyde **255**, Scheme 8.9.

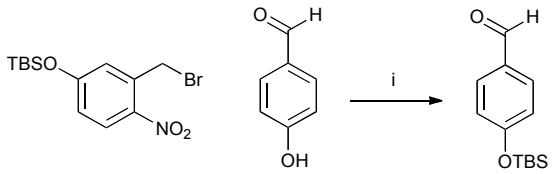

254 **96** **255**

Scheme 8.9. The unexpected outcome of the reaction between 4-hydroxybenzaldehyde **96** and TBS-protected 3-(bromomethyl)-4-nitrophenol **254**. *Reagents and conditions*: i. NaH, THF, -78 °C → RT, 47%.

This synthesis was abandoned in favour of a significantly simpler method to obtain a simple caged model compound which could be investigated for potential pH-dependent photolysis.

8.4. Synthesis of Nitrophenol-caged Fluorobenzoic acid

It was aimed to cage a ^{19}F probe, 4-fluorobenzoic acid **180**, with the nitrophenol caging group. The probe would facilitate quantification of photolysis by ^{19}F NMR using a fluorinated internal standard, 1,4-difuorobenzoic acid **182**.

5-Hydroxy-2-nitrobenzyl alcohol **256** was reacted with 4-fluorobenzoyl chloride with DMAP and anhydrous pyridine in CH_2Cl_2, to obtain nitrophenol-caged fluorobenzoic acid **257** in 50% yield. This product **257** was obtained in 61% yield when 5-hydroxy-2-nitrobenzyl alcohol **256** was coupled to 4-fluorobenzoic acid **180** using EDC and HBTU coupling conditions, Scheme 8.10.

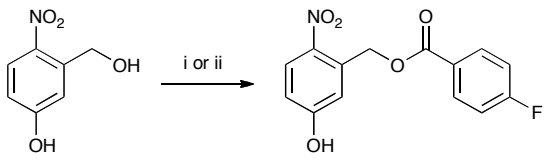

256 **257**

Scheme 8.10. Synthesis of nitrophenol-caged fluorobenzoic acid **257**. *Reagents and conditions*: i. 4-Fluorobenzoyl chloride, pyridine, CH_2Cl_2, 0 °C → RT, 50%; ii. 4-Fluorobenzoic acid, EDC, HBTU, CH_2Cl_2, RT, 61%.

UV/Vis absorption spectra of nitrophenol-caged fluorobenzoic acid **257** in acidic and basic solutions (0.1 mM in THF) were recorded, Figure 8.5. The

acidic solutions were prepared by adding a few drops of HCl (38%) to obtain an apparent pH of 1. The basic solutions were prepared by adding a few drops of DBU to obtain an apparent pH of 12. DBU was used in the blank solution to account for absorption by this organic base.

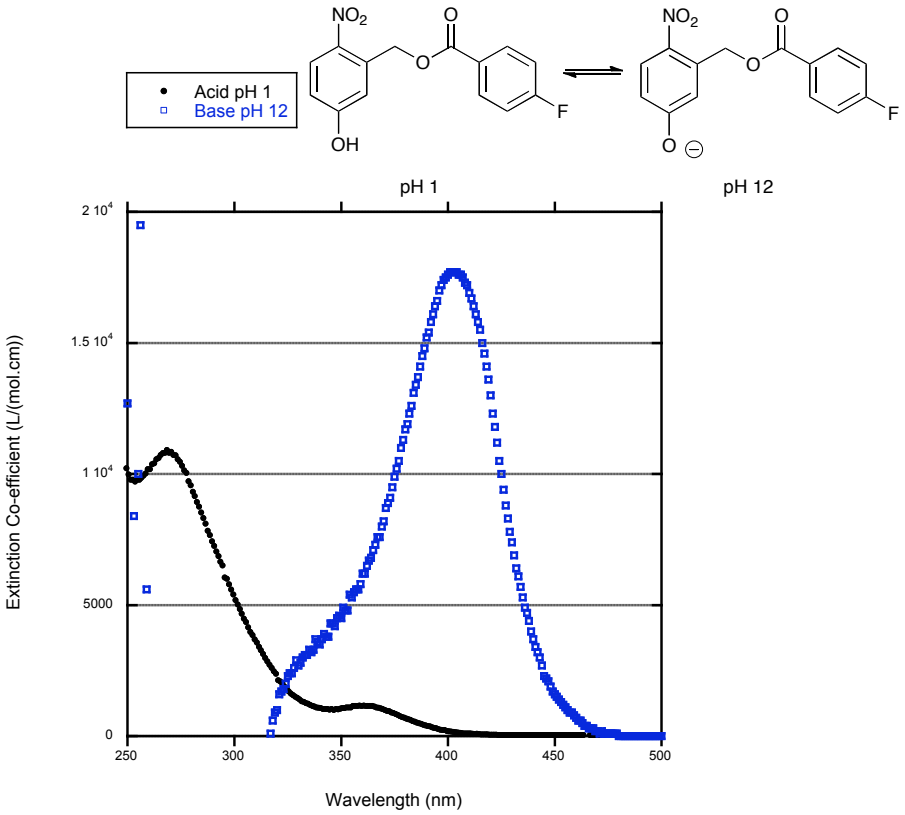

Figure 8.5. The UV/Vis spectra of nitrophenol-caged fluorobenzoic acid **257** in acidic and basic solutions, 0.1 mM in THF.

Nitrophenol-caged fluorobenzoic acid at apparent pH 1 was observed to have λ_{max} of 270 nm and an extinction co-efficient (ε) of 10 800 $L.mol^{-1}cm^{-1}$. At apparent pH 12, λ_{max} of 402 nm and an extinction co-efficient (ε) of 17 700 $L.mol^{-1}cm^{-1}$ were observed. This is consistent with what was observed in the UV/Vis spectra of 3-methyl-4-nitrophenol, Figure 8.2. Deprotonation led to a

substantial red-shift in the UV/Vis spectrum as well as an increase in the intensity of the electronic transitions (extinction co-efficient).

These observations provided incentive to investigate the photolysis characteristics of this caged compound **257** in different pH environments, as there is a significant shift (132 nm) in the λ_{max} value between the protonated and deprotonated states of the phenol. The deprotonated state absorbed light above 400 nm while the protonated state did not. Therefore, it was proposed that at wavelengths above 400 nm, no photolysis would be observed in an acidic solution but photolysis would be observed in a basic solution. However, at wavelengths below 300 nm, the protonated state absorbed light while the deprotonated state did not. Therefore, it was proposed that at wavelengths below 300 nm, no photolysis would be observed in a basic solution but photolysis would be observed in an acidic solution.

8.5. Photolysis Investigation of Nitrophenol-caged Fluorobenzoic acid in Organic Solvent

For photolysis experiments, solutions of nitrophenol-caged fluorobenzoic acid **257** in MeOD at pH 1 and 9 were irradiated with a continuous wave (CW) laser diode at 405 nm at 30 mW for fixed time durations. Please refer to the General Experimental Procedures for details of the photolysis experiments. After irradiation the solutions were analysed by ^{19}F and ^{1}H NMR. Quantification was achieved by the addition of a standard solution of 1,4-difluorobenzene **182** in MeOD to the photolysis samples.

After 15 h irradiation, no photolysis of either the acidic or basic solutions was observed. Only intact caged compound **257** was observed.

8.6. Photolysis Investigation of Nitrophenol-caged Fluorobenzoic acid in Aqueous Buffers

The pH study by Wirz and co-workers, discussed above, demonstrates the effect of pH on reaction rates of intermediates in the photolysis pathway. Very high pHs, above 9, significantly decrease the reaction rates and, therefore, inhibit photolysis.[19] Therefore, it was proposed to attempt irradiation in less extreme pH environments.

In order to confirm that a shift in UV/Vis absorbance could still be observed at less extreme pHs, UV/Vis absorption spectra of nitrophenol-caged fluorobenzoic acid **257** at pH 5 and 10 were recorded, Figure 8.6. The solutions were prepared at 0.01 mM concentration in CH_3CN:buffer, 1:1. Na_2HPO_4 and citric acid buffer at pH 5; and Na_2CO_3 and $NaHCO_3$ buffer at pH 10 were employed.

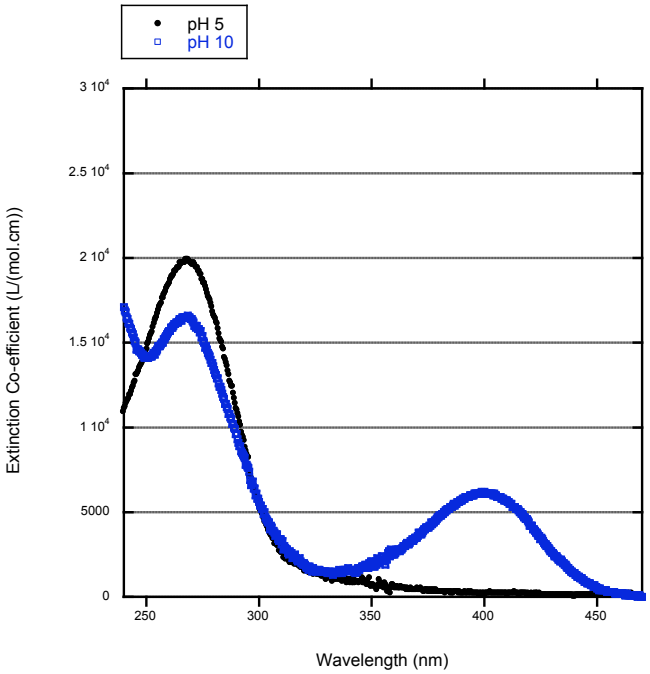

Figure 8.6. The UV/Vis spectra of nitrophenol-caged fluorobenzoic acid **257** at pH 5 and 10, 0.01 mM in CH_3CN:buffer, 1:1.

The peak at λ_{max} 270 nm decreased in intensity with increasing pH while the peak λ_{max} 400 nm increased in intensity with increasing pH. Deprotonation did lead to a substantial red-shift in the electronic spectrum but the expected large increase in the intensity of the electronic transitions was not observed.

Please refer to the General Experimental Procedures for details of the photolysis experiments. Photolysis was carried out at pH 5 and pH 8. Na_2HPO_4 and citric acid buffer at pH 5, and Na_2HPO_4 and NaH_2PO_4 buffer at pH 8 were prepared. Solutions of nitrophenol-caged fluorobenzoic acid **257** were prepared in CH_3CN:buffer, 1:1. After irradiation, the solutions were

analysed by ^{19}F NMR by addition of a standard solution of 1,4-difluorobenzene **182** in MeOD to the photolysis samples.

After irradiation of a pH 5 sample for 15 h at 405 nm, no new peak corresponding to photoreleased product (4-fluorobenzoic acid **180**) was observed. However, no caged material **257** was observed either. In the ^{19}F NMR only the standard **182** was observed. The control sample confirmed that nitrophenol-caged fluorobenzoic acid **257** was observed as a peak at -104.6 ppm in the ^{19}F NMR in the pH 5 CH_3CN:buffer solution before irradiation.

Similarly, after irradiation of a pH 8 sample for 15 h at 405 nm, no new peak corresponding to photoreleased product was observed. No caged material **257** was observed either. Interestingly, two peaks corresponding to nitrophenol-caged fluorobenzoic acid **257** were observed in the pH 8 control, at -104.6 and -106.7 ppm. This may correspond to the protonated and deprotonated states of the caged compound. As pH 8 is a reasonable approximation of the pK_a of the phenol, both protonation states would be present at this pH.

These 15 h irradiation experiments were repeated and the photolysis samples analysed by ^{19}F NMR. The disappearance of the caged compound **257**, with no appearance of uncaged 4-fluorobenzoic acid **180**, was confirmed to be a real phenomenon.

Irradiation of pH 5 and pH 8 samples was repeated at 405 nm for 1 h. At pH 5, no uncaged 4-fluorobenzoic acid **180** was observed in the ^{19}F NMR, and diminished caged compound **257** was observed. Similarly, at pH 8, no uncaged 4-fluorobenzoic acid **180** was observed in the ^{19}F NMR, and diminished caged compound **257** was observed.

8.7. Hydrolytic Stability

The hydrolytic stability of the caged compound **257** was assessed. In addition to the pH 5 and pH 8 buffers, Na_2CO_3 and $NaHCO_3$ buffers at pH 9 and 10 were employed. Solutions of nitrophenol-caged fluorobenzoic acid **257** (0.6 mM) were prepared in CH_3CN:buffer, 1:1. Solutions at pH 5, 8, 9 and 10 were left at RT in the dark for 48 h. After this time the solutions were analysed by ^{19}F NMR by addition of a standard solution of 1,4-difluorobenzene **182** in MeOD.

It was observed that nitrophenol-caged fluorobenzoic acid **257** was stable to hydrolysis in the dark at pH 5. The peak at -104.6 ppm, corresponding to caged material, did not diminish and no new peaks were observed by ^{19}F NMR. However, the caged compound was not stable at pH 8, 9 and 10. 4-Fluorobenzoic acid **180** was observed, confirmed by spiking with an authentic sample of 4-fluorobenzoic acid. Also, at pH 8 the caged compound **257** peak at -104.6 ppm diminished more rapidly than the caged compound peak at -106.7 ppm, Figure 8.7. If the peak at -106.7 ppm corresponds to the deprotonated caged material, it is reasonable to suppose that this compound

is less susceptible to nucleophilic attack. Due to the negative charge already present, an unfavourable dianion would develop upon nucleophilic attack. Therefore, the protonated form, corresponding to the peak at -104.6 ppm, is more susceptible to hydrolysis.

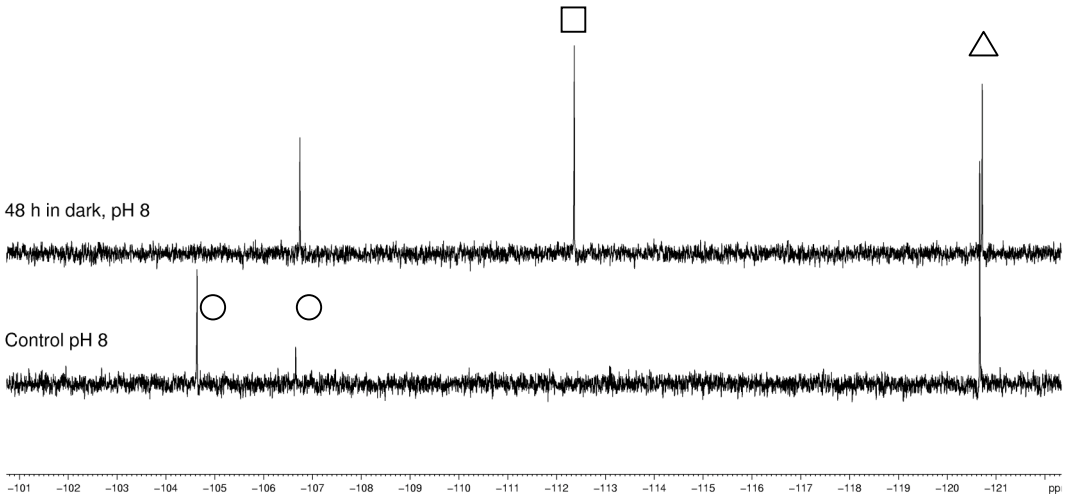

Figure 8.7. Partial 282 MHz ^{19}F NMR of nitrophenol-caged fluorobenzoic acid **257** which was left in the dark at RT for 48 h in CH_3CN:buffer, 1:1, at pH 8 to assess hydrolytic stability. Two caged compound peaks were observed in the control (○), at -104.6 and -106.7 ppm. The peak at -120.7 ppm (△) corresponds to the standard, 1,4-difluorobenzene **182**. After 48 h, the peak at -104.6 ppm had disappeared. A new peak was observed at -112.4 ppm (□). This is 4-fluorobenzoic acid **180**, confirmed by the addition of authentic 4-fluorobenzoic acid to the NMR sample. The top spectrum has been spiked with 4-fluorobenzoic acid.

At pH 9 and 10 only the peak at -106.7 ppm, corresponding to the caged compound **257**, was observed in the ^{19}F NMRs of the controls. This peak was proposed to correspond to the deprotonated caged compound. This peak did diminish over time and 4-fluorobenzoic acid **180** was observed by ^{19}F NMR.

8.8. Conclusions

Having observed the λ_{max} shift of 3-methyl-4-nitrophenol **249** from 330 nm to 400 nm in its different protonation states, it was concluded that the nitrophenol skeleton may be suitable as a pH dependent caging group. It was aimed to synthesise nitrophenol-caged AG10 **244** and investigate its photolysis characteristics in a cuvette as well as *in vitro* in a biological system with which we had experience.[78] This synthesis was not successful and was abandoned in favour of a significantly simpler method to obtain a simple caged model compound which could be investigated for potential pH dependent photolysis.

Therefore, a ^{19}F probe, 4-fluorobenzoic acid **180**, was caged with the nitrophenol caging group. A significant shift (132 nm) in the λ_{max} value between the protonated and deprotonated states of the phenol **257** in THF was observed. The deprotonated state absorbed above 400 nm while the protonated state did not. Therefore, it was proposed that at wavelengths above 400 nm, no photolysis would be observed in an acidic solution but photolysis would be observed in a basic solution. However, 405 nm irradiation in MeOD at pH 1 and 12 did not result in photolysis. Photolysis was attempted at less extreme pHs. However, 405 nm irradiation in CH_3CN:buffer, 1:1, at pH 5 and 8 did not result in photolysis. The caged material was consumed by an unidentified, unwanted pathway. The hydrolytic stability of nitrophenol-caged fluorobenzoic acid **257** was assessed in the absence of light. It was observed

that the caged compound was stable at pH 5 in CH_3CN:buffer, 1:1. However, the caged compound was not stable above pH 8 in CH_3CN:buffer, 1:1.

While interesting results have been obtained from this investigation, the nitrophenol group has not met the criteria of a new pH-dependent caging group. Photolysis in acidic and basic solutions was not observed and the caged compound **257** is not hydrolytically stable.

Referring to the work by Wirz and co-workers, it was noticed that buffers could intercept the primary *aci*-nitro intermediate **22** (A, Scheme 8.1) and inhibit photorelease from 2-nitrobenzyl ethers.[158] The role of the buffers in this pH-dependent photolysis investigation was assumed to be merely maintaining pH. This was perhaps too simplistic an approach. Also, when the proposed reason for Bochet's safety-catch mechanism[160] was carefully considered, it seems that electron donation from the *para* amino group onto the nitro group in the excited state (which prevents photolysis until it is protonated) is similar to the electron donation which could occur from the phenol, and especially the phenolate. It may be that regardless of how these compounds absorb in the UV/Vis region, photolysis is inhibited by charge transfer onto the nitro group in the excited state, Scheme 8.11.

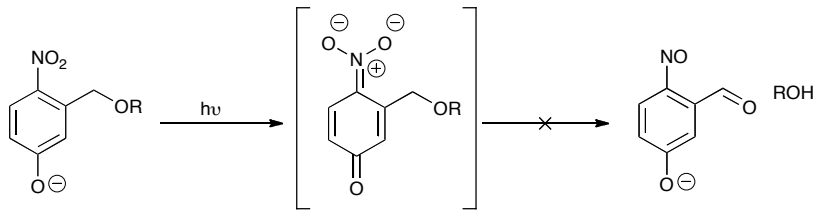

243 **258** **259**

Scheme 8.11. Proposed inhibition of photoreactivity by charge transfer in the excited state from the phenolate to the nitro group, analogous to that observed by Bochet[160] with a *para* amino group.

The pursuit of a pH-dependent caging group is ongoing. However, a different compound or totally different strategy, such as pH-dependent sensitisers, will need to be employed.

Chapter 9:

Experimental Section

9. Experimental Section

9.1 General Experimental Section

9.1.1. Study of Caged AG10

General laser photolysis procedure for ^{1}H NMR and HPLC studies - A solution of the caged AG10 derivative in DMSO (3 mM) was prepared. Care was taken to protect the solution from exposure to background UV irradiation. UV/Vis absorption spectra were obtained using a spectrophotometer (Lambda 950, Perkin Elmer) to provide an indication of which wavelengths were most likely to evoke photolysis.

During photolysis experiments, aliquots (1 mL) of the solution were placed into UV transmitting quartz cuvettes (101-QS, Hellma) and exposed to light from the given laser source for fixed time durations. Continuous wave (CW) laser diodes (iBeam, Toptica photonics) provided light of 375 nm wavelength at powers of up to 8 mW or light of 405 nm wavelength at powers of up to 40 mW. Other wavelengths were obtained using an optical parametric oscillator (Panther EX OPO, Continuum) that was pumped at 355 nm by a frequency tripled Nd:YAG laser (Surelite, Contiuum). The pulses produced by the OPO had a duration of approximately 4 ns at a repetition frequency of 10 Hz. The pulse energy varied depending on the wavelength in use,

however, most photolyses employed a wavelength of 355 nm, which typically had a pulse energy of ~100 mJ. The OPO output energy varies as a function of wavelength, so care was taken to ensure that accurate comparisons could be made between experiments conducted at different wavelengths. Further care was taken to ensure that the laser beam passed through the centre of the solution in the cuvette. After exposure to laser radiation the solution was analysed using ^{1}H NMR and/or HPLC.

Preparation of freshly dissociated cells (Carried out by Prof. John McCarron) - Single smooth muscle cells were enzymatically dissociated from the colon of male guinea-pigs (Cavia porcellus, ~600 g) as described previously.[162] Animals were humanely killed in accordance with the guidelines of the Animal (Scientific Procedures) Act UK 1986. All experiments and loading of cells with fluorescent dyes were carried out at room temperature (22 ± 1 ºC).

Electrophysiology (Carried out by Prof. John McCarron) - Cells were patch-clamped with a conventional tight seal whole-cell patch. The extracellular solution contained (mM): Na glutamate 80, NaCl 40, tetraethylammonium chloride 20, $MgCl_2$ 1.1, $CaCl_2$ 3, Hepes 10, glucose 30 (pH 7.4 with NaOH) and tetramethylrhodamine ethyl ester perchlorate (TMRE, 10 nM). The pipette solution contained (mM): Cs_2SO_4 85, CsCl 20, $MgCl_2$ 1, Hepes 30, MgATP 3, sodium pyruvate 2.5, malic acid 2.5, NaH_2PO_4 1, creatine phosphate 5, NaGTP 0.5, and the caged AG10 derivative 0.025 or 0.062. The high concentration of Hepes was to ensure adequate control of pH during $\Delta\Psi_m$

depolarization; sodium pyruvate and malic acid to maintain mitochondrial activity; and phosphocreatine and ATP to maintain ATP concentration during the experiments. Whole-cell currents were measured using an Axopatch 200B (Molecular Devices, Sunnyvale, CA, USA), low-pass filtered at 500 Hz (8-pole bessel filter; Frequency Devices, Haverhill, MA, USA), digitally sampled at 1.5 kHz using a digidata interface and pClamp (version 8; Molecular Devices) and stored for analysis.

Imaging (Carried out by Prof. John McCarron) - Cells were loaded with the $\Delta\Psi_m$-sensitive dye tetramethylrhodamine ethyl ester perchlorate (TMRE) (10 nM) and wortmannin (10 μM; to prevent contraction) for at least 30 min. TMRE is a lipophilic, cationic, fluorescent dye that accumulates within mitochondria according to their $\Delta\Psi_m$ in a Nernstian fashion.[163,164] $\Delta\Psi_m$ depolarisation decreases mitochondrial TMRE concentration regardless of the concentration of the indicator used, however, TMRE fluorescence of the whole cell may increase or decrease on $\Delta\Psi_m$ depolarization, depending on the concentration of TMRE used.[165] Above a certain concentration (e.g. ~100 nM in the cells used in this study) TMRE self-quenches within mitochondria to reduce the fluorescence emanating from the indicator. In this study a sub-quenching concentration of TMRE (10 nM) was used to monitor $\Delta\Psi_m$ of individual mitochondria.

Two-dimensional images of $\Delta\Psi_m$ were obtained using a wide-field digital imaging system.[166,167] Single cells were excited at 560 nm (Polychrome IV monochromator, TILL Photonics, Martinsried, Germany) and light passed *via* a fiber optic guide through a 553 nm bandpass filter (bandpass 20 nm), a field

stop diaphragm, through a ND4 neutral density filter and reflected off a custom-made long-pass dichroic mirror (transmissive in the range 577-640 nm and reflective from 490 to below 300 nm; Chroma, Rockingham, VT, USA) and then through an oil immersion objective (× 40 U.V. 1.3 NA; Nikon UK, Surrey, UK). Emitted light was guided through a bandpass 594 nm barrier filter (bandpass 18 nm) to an intensified, cooled, frame transfer CCD camera (Pentamax Gen IV; Roper Scientific, Trenton, NJ, USA) controlled by MetaFluor software (Universal Imaging, Downingtown, PA, USA). Full frame images (150 pixels x 150 pixels), with a pixel size of 563 nm at the cell, were acquired sequentially with an exposure period of 50 ms.

Localised flash photolysis (Carried out by Prof. John McCarron) - The output of a xenon flashlamp (Rapp Optoelecktronic, Hamburg, Germany), used to photolyse caged AG10, was focused and merged into the excitation light path *via* the fiber optic bundle and long pass dichroic mirror at the lens part of the microscope's epi-illumination attachment. The diameter of the fiber optic together with the lens magnification determined the area (spot size ~20 μm diameter) of AG10 photolysis.

Data analysis (Carried out by Prof. John McCarron) - Images were analysed using MetaMorph 6.2 (Universal Imaging). TMRE fluorescence was measured over regions of interest drawn around individual mitochondria or the whole cell as described in the text. Each of the fluorescence signals from mitochondria and whole cells were normalised to starting baseline values (taken as 1) and the gradual decline in the signals due to dye photobleaching was corrected for

by subtracting a linear extrapolation of bleaching from each region (thus making the baseline fluorescence values 0). Fluorescence signals were expressed as ratios (F/F_0 or $\Delta F/F_0$) of fluorescence counts (F) relative to baseline values before stimulation (F_0). Results are expressed as means ± s.e.m. for n cells, significance was calculated using an unpaired Student's t-test; $p<0.05$ being considered significant.

9.1.2. Design and Development of Tools to Study TRPV1

General Photolysis Experimental - Solutions of caged TRPV1 agonists and antagonists in THF (3 mM) were prepared. Care was taken to minimise exposure to background UV irradiation. For photolysis experiments, aliquots (1mL) of the solution were placed in UV transmitting quartz cuvettes (101-QS, Hellma) and irradiated with a laser source for fixed time durations. The frequency triple Nd:YAG laser source (Surelite, Continuum) provided approximately 4 ns pulses of up to 100 mJ pulse energy at a repetition rate of 10 Hz and a wavelength of 355 nm. The OPO output energy was determined for each experiment and kept constant throughout a given experiment. Further care was taken to ensure the laser spot (diameter ~4 mm) passed through the centre of the solution and that sufficient mixing of the solution occurred. After exposure to laser radiation the solution was analysed by ^{1}H NMR. For quantification by ^{1}H NMR, the THF from each sample was removed and 1 mL $CDCl_3$ added. A standard solution of hexamethyldisiloxane in $CDCl_3$ was added to each sample so that the ratio of sample to standard in each aliquot

was 1:1. This ratio was used to determine the amount of caged and uncaged material present in the photolysis samples.

Cultivation of primary trigeminal neurons (Carried out by Prof. Rashid Giniatullin) - Primary cultures of trigeminal ganglion sensory neurons were obtained from Wistar rats (P9–12). Animals were anesthetised by slowly raising levels of CO_2 and killed by decapitation. Ganglia were rapidly excised and enzymatically treated and dissociated in F12 medium (Invitrogen, Gibco, Cat. No. 31765), containing 0.25 $mg.mL^{-1}$ trypsin (Sigma), 1 $mg.mL^{-1}$ collagenase (Sigma) and 0.2 $mg.mL^{-1}$ DNAse (Sigma) at 37 °C, 1400 rpm for 20 min using Thermomixer (Eppendorf). Cells were separated from debris by consecutive centrifugation and plated on poly-L-lysine-coated 35 mm Petri dishes, glass-bottomed MatTek dishes or 12 mm coverslips in F12 medium containing 10% foetal calf serum and used within 24-72 h.

Electrophysiology and UV laser photolysis (Carried out by Prof. Rashid Giniatullin) - For electrophysiological experiments, cells plated on either Petri dishes or glass coverslips were used 24 h after plating. Whole-cell patch-clamp recordings (in voltage-clamp mode) were performed using HEKA EPC-10 USB amplifier (HEKA Elektronik) at the holding potential of -70 mV, and currents were recorded using the HEKA Patch Master software (HEKA Elektronik). Patch pipettes (pulled from the Harvard Apparatus GC150F-10 glass, tip resistance of 3-5 MΩ) were filled with a solution containing (mM): 130 CsCl, 5 EGTA, 0.5 $CaCl_2$, 5 $MgCl_2$, 5 K_2ATP, 0.5 NaGTP and 10 HEPES (pH adjusted to 7.2 with CsOH). Cells were superfused (1.5-2 $mL.min^{-1}$ flow

rate) at room temperature (18–22 °C) with standard extracellular solution (SES) containing (in mM): 152 NaCl, 2.5 KCl, 10 glucose, 2 $CaCl_2$, 1 $MgCl_2$ and 10 HEPES (pH adjusted to 7.4 with NaOH). Solutions of the caged TRPV1 agonist were prepared in a dark room with dim red light and kept in light-protected labware. Stock solutions of caged agonist, capsaicin and capsazepine were prepared in DMSO at 1000× concentration, aliquoted and kept at -20 °C. On the day of experiment, the aliquot was thawed and diluted in the SES. Drug application during patch-clamp recordings was performed using rapid solution exchange system (RSC-200; BioLogic Science Instruments) that allows change of perfusion milieu around the studied cell in few milliseconds. For photolysis of caged compounds, 5-500 ms flashes of an Oxxius UV laser (Violet-375, 375 nm, 15 mW) were used. The duration and timing of the UV flashes were controlled with the Patch Master software. Membrane current recordings, drug application with rapid solution exchange system and UV laser flashes were synchronised using TTL trigger signals provided by the Patch Master software.

Calcium imaging and UV lamp photolysis (Carried out by Prof. Rashid Giniatullin) - For $[Ca^{2+}]_i$ imaging experiments, cells were plated on glassbottomed 35 mm Petri dishes (MatTek). One to three days after plating, culture medium was replaced with the SES. $[Ca^{2+}]_i$ was measured using fluorescent Ca^{2+} indicator fluo-4 (Molecular Probes). The indicator was administered as the acetoxymethyl ether (fluo-4 AM; 5 μM, 40-50 min, 23-25 °C), mixed with the nonionic detergent Pluronic F127 (0.02%; Molecular Probes, USA). Upon a 30-60 min post-incubation, cell-bearing dishes were

transferred to the CellR imaging system (Olympus Europe, Hamburg, Germany). The imaging system consisted of the IX-71 inverted microscope (Olympus) equipped with a 175 W xenon burner light source, an automated filter wheel with excitation filters and an automated turret with filter cubes. The microscope frame and all optical elements were maintained at 34 °C using the temperature control incubator (Solent Scientific, Segensworth, UK). Fluorescence of fluo-4 was excited at 500 ± 5 nm and collected at 530 ± 15 nm. Images were collected in a time-lapse mode at a rate of 0.5 Hz with a CCD camera (Orca, Hamamatsu, Japan).

For photolysis of caged TRPV1 agonist, the caged compound was dissolved from the 1000× stock solution in the extracellular solution at the final concentration of 1 μM and applied to cells by bath perfusion (1-1.5 $mL.min^{-1}$ flow rate) using a peristaltic pump. Rate of bath solution exchange was estimated by imaging the dynamics of a perfusion-applied fluorescent dye, and the full exchange time was measured as 20-25 s. Caged TRPV1 agonist was photolysed by a brief (50 ms) flash of the UV light from the 175 W xenon lamp attenuated to 8% and reflected to the cells by a dichroic mirror with the 400 nm cutoff wavelength. Filter cube turret rotation for switching between the fluo-4 imaging and uncaging modes was automatically controlled by the CellR imaging software, with each rotation occurring in 4 s.

Data analysis (Carried out by Prof. Rashid Giniatullin) - Electrophysiological recordings were analysed using the Patch Master (HEKA Elektronik) and Origin (Microcal) software. For analysis of Ca^{2+} imaging data, AnalySIS (Olympus Europe) and Origin software were used. Responses were quantified

as the $\Delta F/F_0$ ratio, where F_0 is the background-subtracted fluo-4 fluorescence prior to stimulation, and ΔF is the difference between the current fluorescence and F_0. Plots and Figures were constructed using Origin and PowerPoint (Microsoft).

9.1.3. Study of Caged Na^+ Channel Blockers

General Photolysis Experimental - Photolysis of DMNB-caged lidocaine was carried out on 1 mL samples of a 3 mM solution in THF. During photolysis experiments, aliquots (1 mL) of the solution were placed into UV transmitting quartz cuvettes (101-QS, Hellma) and exposed to radiation from the given laser source for fixed time durations. Continuous wave (CW) laser diodes (iBeam, Toptica photonics) provided light of 375 nm wavelength at powers of up to 8 mW or light of 405 nm wavelength at powers of up to 40 mW. Another light source was an optical parametric oscillator (Panther EX OPO, Continuum) pumped at 355 nm by a frequency tripled Nd:YAG laser (Surelite, Contiuum). The pulses produced by the OPO had duration of approximately 4 ns at a repetition frequency of 10 Hz. The OPO output energy was determined for each experiment and kept constant throughout a given experiment. Further care was taken to ensure that the laser beam passed through the centre of the solution in the cuvette. After exposure to laser irrradiation the solutions were analysed using ^{1}H NMR. For quantification by ^{1}H NMR, the THF from each sample was removed and 1 mL $CDCl_3$ added. A standard solution of hexamethyldisiloxane in $CDCl_3$ was added to each sample so that the ratio of sample to standard in each aliquot was 1:1. This

ratio was used to determine the amount of caged and uncaged (free lidocaine) material present in the photolysis samples.

9.1.4. Study of Orthogonally Caged Neurotransmitters *in vitro*

General Photolysis Experimental

Photolysis of the Benzoin and DMNB Caging Groups - In order to confirm that wavelength orthogonal photolysis of benzoin- and DMNB-caged GABA, Glu and glycine could be achieved, solutions of these compounds were irradiated at 250 nm, 355 nm, 421 nm and 405 nm and the resulting solutions analysed by ^{1}H NMR using hexamethyldisiloxane as an internal standard. During photolysis experiments, 1 mL aliquots of the appropriate solution of caged compound in MeOH (7.5 mM) were placed into UV transmitting cuvettes (101-QS, Hellma) and exposed to radiation from the given laser source for fixed time durations. A continuous wave (CW) laser diode (iBeam, Toptica photonics) provided 405 nm light at a power of 30 mW. Shorter wavelength radiation was provided by an optical parametric oscillator (Panther EX OPO, Continuum) pumped at 254 nm by a frequency tripled Nd:YAG laser (Surelite, Contiuum). The pulses produced by the OPO had duration of approximately 4 ns at a repetition frequency of 10 Hz. The OPO output energy was determined for each experiment and kept constant throughout a given experiment. The photolysis samples were analysed and quantification achieved by ^{1}H NMR using hexamethyldisiloxane standard in MeOD. Control samples, which had not been exposed to radiation, were also analysed.

Photolysis of the MPA and DMNB Caging Groups - In order to confirm that wavelength orthogonal photolysis of MPA-Glu and DMNB-GABA could be achieved, solutions of these compounds were irradiated at 405 nm, 270-310 nm and 266 nm and the resulting solutions analysed by ^{1}H NMR using hexamethyldisiloxane as an internal standard.

DMNB-GABA (0.5 mL, 7.5 mM solution in D_6-DMSO) and MPA-Glu (0.5 mL, 7.5 mM solution in D_6-DMSO) were added to a quartz cuvette (101-QG Hellma). This sample was photolysed for 2, 7.5 and 15 h using a 405 nm 30 mW laser diode. The sample was placed 15 cm from the irradiation source. The sample was positioned so that the irradiation beam passed through the centre of the solution. A control sample, which had not been exposed to laser irradiation, but was exposed to the same conditions as the photolysis samples, was also analysed.

DMNB-GABA (0.5 mL, 7.5 mM solution in D_6-DMSO) and MPA-Glu (0.5 mL, 7.5 mM solution in D_6-DMSO) were added to a quartz cuvette. This sample was placed inside the filter box with a transmission range of 270-310 nm and photolysed for 5 h and 14 h using a 300 W ultraviolet lamp. The sample was placed 10 cm from the irradiation source. A control sample, which had not been exposed to irradiation, but was exposed to the same conditions as the photolysis samples, was also analysed.

DMNB-GABA (0.5 mL, 7.5 mM solution in D_6-DMSO) and MPA-Glu (0.5 mL,

7.5 mM solution in D_6-DMSO) were added to a quartz cuvette. This sample was photolysed for 2, 5, 8 and 20 h using a 266 nm YAG laser. A control sample, which had not been exposed to irradiation, but was exposed to the same conditions as the photolysis samples, was also analysed.

All photolysis samples were analysed in the same way - a standard solution of hexamethyldisiloxane (125 μL, 30 mM solution in D_4-MeOD) was added to the photolysis sample. This solution was analysed by ^{1}H NMR using the Bruker Avance II 400 (400 MHz) using D_6-DMSO as a reference for internal deuterium lock. Bruker TopSpin software was used to analyse the data.

in vitro Photolysis General Experimental Section

Photolysis rig (Carried out by Craig McDougall in Dr Nigel Emptage's laboratory) -- The *in vitro* orthogonal photolysis of the caged compounds was performed with an inverted microscope (IX71, Olympus) incorporating a high numerical aperture (NA) water immersion objective (UPlanSApo 100x/1.4, Olympus) and a custom-built electrophysiology stage. Biological samples were held in a perfusion chamber which provided the necessary physiological environment to maintain biological viability for the duration of the experiment whilst permitting access for the high NA objective and electrophysiological equipment. Selective orthogonal photolysis of the caged compounds in solution was achieved by means of two independent light sources. Selective photolysis of the MPA-Glu **234** was obtained with a mercury flashlamp (JML-C1, Rapp Optoelectronic) in combination with a 254 nm interference bandpass filter (254FIB25, Knight Optical) mounted externally to the microscope assembly and focussed onto the sample plane by an internal focusing lens. Orthogonal photolysis of the DMNB-GABA **205** was accomplished with a 405 nm UV laser diode (PxLS, Toptica photonics) co-aligned to the optical path of the microscope through the camera port of the microscope utilising a custom built optical cage plate system (Thorlabs) which collimated the output of the diode laser and expanded the beam to match the back aperture of the high NA objective. A dichroic mirror (530 BK 16, Comar) permitted the introduction of the photolysis beam without interrupting image capture with a high quality EMCCD camera (iXon DV887DCS-BV, Andor

technology). A mechanical shutter (Uniblitz VS25, Rochester) provided temporal control of the 405 nm beam. The arrangement provided delivery of both wavelengths at the sample plane of the microscope with exquisite control over exposure duration and intensity.

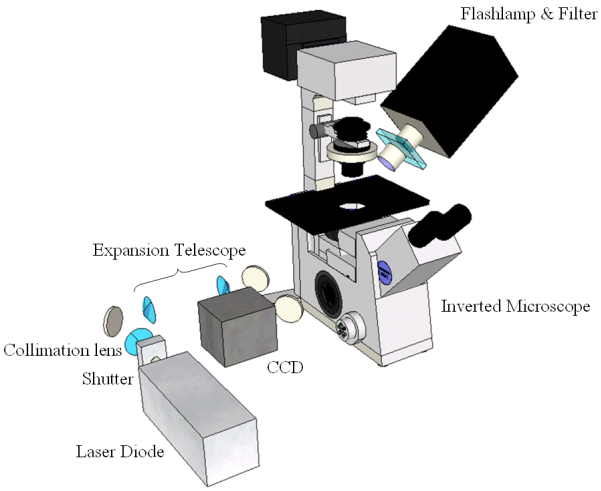

Figure 9.1: 3D schematic of the *in vitro* photolysis apparatus. Orthogonal photolysis was achieved in an inverted microscope. Selective photolysis of the MPA-Glu was accomplished using a flash lamp system (JML-C1, Rapp Optoelectronic, Hamburg, Germany). The flash lamp was focused to cover the entire sample region using the built in focusing lens. The output from the flash lamp was filtered using a bandpass filter (254FIB25, Knight Optical, Harrietsham, UK) which had a central transmission wavelength of 254 nm with a bandwidth of 8 nm. Orthogonal photolysis of DMNB-GABA was achieved using a 405 nm laser diode (Topica Photonics PxLS, Hamburg, Germany) the output of which could be controlled through the use of the mechanical shutter (Uniblitz VS25, Rochester, NY). The laser diode was coupled into the microscope through the use of beam steering mirrors and a dichroic mirror (530 BK 16, Comar, Cambridge, UK) which was placed in the beam path of the electron multiplying charge coupled device (EMCCD) imaging camera. The external optics

were designed to achieve efficient coupling of the laser into the microscope and comprised a x2 telescope for initial beam expansion and collimation and a second x1.3 expansion telescope to ensure that the back aperture of the microscope objective was fully filled.

Tissue Culture (Carried out by Dr Ruth Taylor in Dr Nigel Emptage's laboratory) - Cultured hippocampal neurons were prepared as previously described (Kaech & Banker Nature Protocols 2006). Briefly, rat hippocampal neurons were isolated at E18 and mechanically dissociated in 2.5% trypsin. Hippocampal neurons were then plated (at a density of 20000 cells per coverslip) on coverslips previously coated with poly-D-lysine and fibronectin to aid cell adherence. The coverslips were suspended over astroglia feeder layers and incubated in Neurobasal based conditioned medium at 35 °C and 5% CO_2. Neurons were maintained in culture for up to three weeks.

Conditioned media was a supplemented Neurobasal solution containing: 8% B27 supplement, 0.25 μM GlutaMAX, 0.25 μM Glutamine, 25 μg/mL insulin, 100 μg/mL transferring, 5 ng/mL bFGF, 25 mM 2-mercaptoethanol, 100 μg/mL primocin antibiotic. Antibiotic was removed from the culture media by supplementing with a supplemented Neurobasal solution that was antibiotic free.

Electrophysiology (Carried out by Dr Ruth Taylor in Dr Nigel Emptage's laboratory) - Giga-seal whole-cell patch clamp recordings were obtained from visually identified hippocampal pyramidal neurons. Patch pipettes (4.0-

7.0 MΩ) were pulled from borosilicate glass capillary tubes using a P-97 Flaming/Brown Micropipette Puller (Sutter Instruments). The internal patch pipette solution contained 140 mM KGluconate, 5 mM KCl, 10 mM HEPES, 1 mM $MgCl_2$, 2 mM Na_2ATP and 0.4 mM Na_3GTP; pH 7.2-7.3 with KOH; osmolarity 290-300 mOsM. Recordings were performed at room temperature ~25 °C in a static bath. The bath solution consisted of a Tyrodes solution containing 128 mM NaCl, 5 mM KCl, 1 mM $MgCl_2$, 2 mM $CaCl_2$, 15 mM HEPES, 4 mM $NaHCO_3$; pH 7.25 with NaOH; osmolarity 290-300 mOsM. Caged-neurotransmitters (MPA-glutamate: 62.5-125 μM; DMNB-GABA: 50 μM) were dissolved in DMSO (final concentration 0.1-1%) and added to the bath at the beginning of the experiment. Once a whole-cell recording configuration had been established, the access resistance was monitored throughout the experiment. Cells, in which access varied > 20% over the course of the experiment were discarded. No series resistance compensation and no corrections for liquid junction potentials were made.

Neurons were clamped at a membrane holding potential of –50 mV for the duration of the experiment. Data was generated and acquired using an Axopatch 200 A amplifier (Axon Instruments) and the software WinWCP (Strathclyde). Data was sampled at 7.5 kHz and filtered by a 5 kHz Bessel filter. Data was further filtered offline by a low pass filter with a cut-off at 819.3 Hz.

9.1.5. Development of a pH Dependent Caging Group

General Photolysis Experimental

Photolysis Investigation of Nitrophenol-caged Fluorobenzoic acid in Organic Solvent - A solution of nitrophenol-caged fluorobenzoic acid in MeOD (6 mM) was prepared. A pH 1 solution was prepared by adding 50 μL 36 % HCl to a 1 mL, 6 mM solution of the caged compound in MeOD. Solutions at pH 9 were prepared by adding 50 μL DBU or NEt_3 to a 1 mL, 6 mM solution of the caged compound in MeOD. Care was taken to minimise exposure to background UV irradiation. For photolysis experiments, aliquots (1mL) of the solution were placed in UV transmitting quartz cuvettes (101-QG, Hellma) and irradiated with a continuous wave (CW) laser diode (iBeam, Toptica photonics) at 405 nm at 30 mW for fixed time durations. Further care was taken to ensure the laser spot passed through the centre of the solution. After irradiation the solution was analysed by ^{19}F and ^{1}H NMR. Quantification was achieved by the addition of a standard solution of 1,4-difluorobenzene in MeOD and comparison of the integrals.

Photolysis Investigation of Nitrophenol-caged Fluorobenzoic acid in Aqueous Buffers - Photolysis was carried out at pH 5 and pH 8. Na_2HPO_4 and citric acid buffer at pH 5 and Na_2HPO_4 and NaH_2PO_4 buffer at pH 8 were prepared. Solutions of nitrophenol-caged fluorobenzoic acid (0.6 mM) were

prepared in CH_3CN:buffer, 0.5 mL:0.5 mL (1 mL total photolysis sample). For photolysis experiments, aliquots (1 mL) of the solution were placed in UV transmitting quartz cuvettes (101-QG, Hellma) and irradiated with a continuous wave (CW) laser diode (iBeam, Toptica photonics) at 405 nm at 30 mW for fixed time durations. After irradiation the solutions were analysed by ^{19}F NMR by addition of a standard solution of 1,4-difluorobenzene in MeOD.

9.1.6. General Experimental Protocols

^{1}H NMR spectra were recorded on Bruker DPX250 (250 MHz); Bruker Avance 300 (300 MHz); Bruker Avance 400 (400 MHz); Bruker Avance II 400 (400 MHz); Bruker DRX500 (500 MHz); Bruker Avance 500 (500 MHz); or Bruker Avance III (500 MHz) using deuterochloroform (unless indicated otherwise) as a reference for internal deuterium lock. The chemical shift data for each signal are given as δH in units of parts per million (ppm) relative to tetramethylsilane (TMS) where δH (TMS) = 0.00 ppm. The multiplicity of each signal is indicated by: s (singlet); br s (broad singlet); d (doublet); t (triplet); q (quartet); dd (doublet of doublets); ddd (doublet of doublet of doublets); dddd (doublet of doublet of doublet of doublets); ddt (doublet of doublet of triplets); sp (septet); or m (multiplet). The number of protons (n) for a given resonance signal is indicated by nH. Coupling constants (*J*) are quoted in Hz and are recorded to the nearest 0.1 Hz. Identical proton coupling constants (*J*) are averaged in each spectrum and reported to the nearest 0.1 Hz. The coupling constants are determined by analysis using Bruker TopSpin software.

^{13}C NMR spectra were recorded on Bruker Avance 300 (75 MHz); Bruker Avance II 400 (100 MHz); or Bruker Avance III (125 MHz) spectrometers using the PENDANT or DEPT Q pulse sequences with broadband proton decoupling and internal deuterium lock. The chemical shift data for each signal are given as δC in units of parts per million (ppm) relative to tetramethylsilane (TMS) where δC (TMS) = 0.00 ppm. Where appropriate,

coupling constants (*J*) are quoted in Hz and are recorded to the nearest 0.1 Hz. ^{1}H and ^{13}C spectra were assigned using 2D NMR experiments including COSY, HSQC, HMBC, DEPT-135, HMQC, and DEPT Q.

^{19}F NMR spectra were recorded on a Bruker Avance II 400 (282 MHz) using a broadband proton decoupling pulse sequence and deuterium internal lock. The chemical shift data for each signal are given as δF in units of parts per million (ppm). Where appropriate, coupling constants (*J*) are quoted in Hz and are recorded to the nearest 0.1 Hz.

UV/Vis spectra were recorded using either a PG Instruments Ltd, T60 UV/Vis Spectrophotometer or a Perkin Elmer, Lambda 950 Spectrophotometer.

Mass spectra were acquired on a VG platform spectrometer. For electron impact spectra, the instrument was operating at 70 eV. Chemical ionization spectra were obtained using isobutane as the ionising gas. Electrospray ionisation spectra were obtained on Micromass LCT; Micromass LCT Premier; and Bruker MicroTOF spectrometers, operating in positive or negative mode, from solutions of methanol, acetonitrile or water. *m/z* values are reported in Daltons and followed by their percentage abundance in parentheses.

Melting points were determined using an Electrothermal 9100 melting point apparatus or Kofler hot stage microscope and are uncorrected.

Microanalyses were either obtained on a Carlo Erber EA1110 analyser by the St Andrews University microanalysis service; or submitted to the Elemental Analysis Service, London Metropolitan University, London.

Infrared Specta were obtained either as: **a** thin film on sodium chloride discs; **b** potassium bromide disc; **c** thin film on PTFE cards as indicated. The spectra were recorded on Perkin Elmer GX FT-IR or Bruker Tensor 27 spectrometers. Absorption maxima are reported in wavenumbers (cm^{-1}).

Specific Optical Rotations were measured using Perkin Elmer Model 241 and 341 polarimeters, in cells with a path length of 1 dm. The light source was maintained at 589 nm. The concentration (*c*) is expressed in g/100 mL (equivalent to g/0.1 dm^3). Specific rotations are denoted $[\alpha]_D^T$ and are given in implied units of 10^{-1} deg cm^2 g^{-1} (T = ambient temperature in °C).

Analytical thin layer chromatography (TLC) was carried out on Merck silica gel 60 F_{254} aluminum-supported thin layer chromatography sheets. Visualisation was by absorption of UV light (λ_{max} 254 or 365 nm), or thermal development after dipping in one of: **a** ethanolic solution of phosphomolybdic acid (PMA); **b** aqueous solution of potassium permanganate, potassium carbonate and sodium hydroxide; **c** ethanolic solution of 4-anisaldehyde, sulfuric acid and acetic acid.

Reverse phase analytical thin layer chromatography (TLC) was carried out on Merck silica gel 60 RP-18 $F_{254}S$ aluminum-supported thin layer

chromatography sheets. Visualisation was by absorption of UV light (λ_{max} 254 or 365 nm), or thermal development after dipping in ninhydrin solution.

Flash Column chromatography was carried out on Apollo Scientific Ltd silica gel 40-63 micron or Merck silica gel 60 (240-400 mesh), eluting with solvents as supplied, under a positive pressure of compressed air (unless otherwise stated).

Reverse phase silica gel column chromatography was carried out on C_{18} Fluka silica gel, eluting with the appropriate solvents as supplied, under a positive pressure of compressed air.

Anhydrous solvents were obtained under the following conditions: dry *N*,*N*-DMF and CH_3CN were purchased from SigmaAldrich UK in SureSeal™ bottles and used without further purification; dry DMSO was pre-dried over activated alumina, then distilled from calcium hydride and stored over activated 4 Å molecular sieves under an N_2 atmosphere; anhydrous 1,4-dioxane was distilled from sodium and benzophenone in a recycling still and stored over activated 3 Å molecular sieves under a N_2 atmosphere; anhydrous THF was distilled from sodium and benzophenone in a recycling still and stored over activated 3 Å molecular sieves under a N_2 atmosphere. Anhydrous CH_2Cl_2, Et_2O, toluene, hexane and THF were obtained using a MBRAUN GmbH MB SPS-800 solvent purification system, where solvent was dried by passage through filter columns and dispensed under an atmosphere of N_2 gas. Anhydrous CH_2Cl_2, Et_2O, toluene, hexane and THF were also

obtained using a Dalek drying column, where solvent was dried by passage through filter columns and dispensed under an atmosphere of N_2 gas

Chemicals were purchased from Acros UK, Sigma Aldrich UK, Alfa Aesar UK, Fisher UK, Fluka UK, Fluorochem, Merck or TCI-Europe. All solvents and reagents were purified, when necessary, by standard techniques.[168] Where appropriate and if not stated otherwise, all non aqueous reactions were performed in a flame-dried flask under an inert atmosphere of nitrogen or argon, using a double vacuum manifold with the inert gas passing through a bed of activated 4 Å molecular sieves and self indicating silica gel.

Lyophilisation using a Christ Alpha 2-4-LD lyophiliser was used to remove water from aqueous solutions.

In vacuo refers to the use of a rotary evaporator attached to a diaphragm pump. Brine refers to a saturated aqueous solution of sodium chloride. Hexane refers to a mixture of hexane isomers and petroleum ether to the fraction boiling between 40-60 °C.

9. Experimental Procedures

9.2. Synthesis of Caged AG10 Derivatives

9.2.1. 4-(4',5'-Dimethoxy-2-nitrobenzyloxy)benzaldehyde **97**

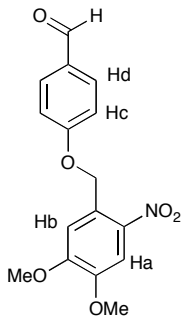

To a stirred solution of 4-hydroxybenzaldehyde (500 mg, 4.09 mmol, 1.0 eq) in dry DMF (10 mL) was added K_2CO_3 (1.70 g, 12.27 mmol, 3.0 eq) and 4,5-dimethoxy-2-nitrobenzyl bromide (1.13 g, 4.09 mmol, 1.0 eq). The reaction mixture was stirred at 40 °C overnight. The RB flask was covered in aluminium foil to ensure that dark conditions were maintained throughout the reaction. After TLC analysis confirmed that the starting materials had been consumed, the reaction mixture was cooled to RT and water (40 mL) was added. After stirring for 20 min the precipitated solid was filtered, washed with water (50 mL) and dissolved in CH_2Cl_2 (100 mL), dried over Na_2SO_4, filtered and the solvent removed *in vacuo*. The crude product was purified by silica gel chromatography, eluting with petroleum ether and EtOAc (8:2 → 3:2), to afford 4-(4',5'-dimethoxy-2-nitrobenzyloxy)benzaldehyde (1.08 g, 83%) as an

orange solid: R_f 0.17 (hexane/EtOAc, 3:7); mp 167-168 °C (from hexane); ν_{max}/cm^{-1} ($CHCl_3$) 3011.2 (w)(Ar-H), 1686.2 (s)(C=O), 1605.4 (s)(C=C), 1520.3 (vs)(NO_2), 1324.8 (s)(NO_2), 1276.4 (vs), 1067.9 (vs)(C-O), 988.5 (m)(Ar-H), 795.9 (s)(two adj. Ar-H); δ_H (300 MHz; $CDCl_3$) 9.90 (1H, s, CHO), 7.87 (2H, d, *J* 8.9, H_d), 7.78 (1H, s, H_a), 7.28 (1H, s, H_b), 7.13 (2H, d, *J* 8.9, H_c), 5.57 (2H, s, CH_2Ar), 3.97 (3H, s, OMe), 3.96 (3H, s, OMe); δ_C (75.5 MHz; $CDCl_3$) 190.7 (C=O), 162.9 (C), 154.0 (C), 148.1 (C), 139.1 (C), 132.1 (C-H_d), 130.6 (C), 128.0 (C), 115.2 (C-H_c), 109.3 (C-H_b), 108.2 (C-H_a), 67.2 ($ArCH_2$), 56.5 (2 × OMe). *m/z* (EI^+) 318 ($[M+H]^+$, 20%), 317 ($[M]^+$, 100%).[78]

9.2.2. 2-(4-(4,5-Dimethoxy-2-nitrobenzyloxy)benzylidene)malononitrile **98**

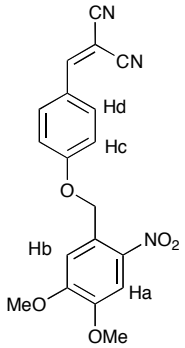

A solution of 4-(4',5'-dimethoxy-2-nitrobenzyloxy)benzaldehyde (735 mg, 2.31 mmol, 1.0 eq) and malononitrile (168 mg, 2.55 mmol, 1.1 eq) in ethanol (20 mL) was prepared. Piperidine (10 drops) was added and the reaction mixture heated under reflux for 2 h. Water (20 mL) was added and the reaction mixture stirred for 10 min. The resulting orange solid was filtered and recrystallised from ethanol to afford 2-(4-(4,5-dimethoxy-2-nitrobenzyloxy)benzylidene)malononitrile (422 mg, 50%) as a yellow solid: R_f

0.54 (hexane/EtOAc, 1:1); mp 227-229 °C (from ethanol); ν_{max}/cm^{-1} (nujol) 2944.4 (m)(C-H), 2250.4 (s)(CN), 2124.6 (s), 1627.8 (m)(C=C), 1583.7 (s)(NO_2), 1030.0 (vs)(C-O); δ_H (400 MHz; D_6-DMSO) 8.42 (1H, s, CH=), 7.99 (2H, d, *J* 8.7, H_d), 7.74 (1H, s, H_a), 7.33 (1H, s, H_b), 7.30 (2H, d, *J* 8.7, H_c), 5.54 (2H, s, $ArCH_2$), 3.88 (3H, s, OMe), 3.87 (3H, s, OMe); δ_C (100 MHz; D_6-DMSO) 163.1 (C-O), 160.5 (CH=), 153.3 (C), 148.3 (C), 139.9 (C), 133.1 (C-H_d), 125.7 (C), 124.3 (C), 115.6 (C-H_c), 114.2 (C), 113.4 (C), 111.7 (C-H_b), 108.3 (C-H_a), 77.2 (*C*-$(CN)_2$), 67.0 ($ArCH_2$), 56.1 (OMe), 56.0 (OMe). *m/z* (Cl^-) [Found: $(M-H)^-$ 364.0938. $C_{19}H_{14}N_3O_5$ requires M^- 364.0939]; *m/z* (Cl^-) 364 ($[M-H]^-$, 10%), 339 ($[M-CN-H]^-$, 25%), 211 ($[M-ArCHC(CN)_2-H]^-$, 55%), 197 (100%).[78]

9.2.3. 2-(4-Hydroxybenzylidene)malononitrile (AG10) **94**

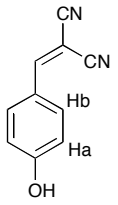

To a solution of 4-hydroxybenzylaldehyde (5.0 g, 40.9 mmol, 1.0 eq) and malononitrile (3.0 g, 45.0 mmol, 1.1 eq) in ethanol (25 mL) was added piperidine (10 drops). The reaction solution was heated under reflux for 1.5 h. After this time, water (50 mL) was added and the resulting orange solid removed by filtration. The solid was recrystallised from ethanol/hexane to afford 2-(4-hydroxybenzylidene)malononitrile (5.71 g, 82%) as a yellow solid: R_f 0.51 (hexane/EtOAc, 1:1); mp 180-182 °C (from ethanol/hexane, Lit.[169] 180

°C); δ_H (300 MHz; D_6-acetone) 9.88 (1H, br s, OH), 8.12 (1H, s, CH=), 7.98 (2H, d, *J* 8.8, H_b), 7.07 (2H, d, *J* 8.8, H_a); δ_C (75.5 MHz; D_6-acetone) 164.3 (C-OH), 160.7 (CH=), 134.8 (C-H_b), 124.5 (C), 117.5 (C-H_a), 115.6 (CN), 114.7 (CN), 77.8 (*C*-$(CN)_2$). *m/z* (EI^+) [Found: $(M)^+$ 170.0474. $C_{10}H_6N_2O$ requires M^+ 170.0475]; *m/z* (EI^+) 170 ($[M]^+$, 90%). These data are in accordance with the literature values.[169]

9.2.4. 4-(2,2-Dicyanovinyl)phenyl 4,5-dimethoxy-2-nitrobenzyl carbonate **99**

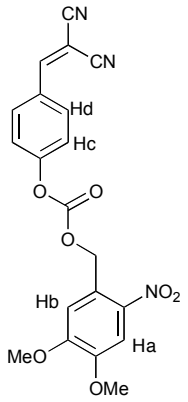

A stirred solution of 2-(4-hydroxybenzylidene)malononitrile (103 mg, 0.61 mmol, 1.0 eq) in THF (5 mL) was cooled to 0 °C. 4,5-Dimethoxy-2-nitrobenzyl chloroformate (500 mg, 1.81 mmol, 3.0 eq) and NEt_3 (183 mg, 252 µL, 1.81 mmol, 3.0 eq) were added and the reaction solution stirred for 4 h at RT. After this time the solvent was removed *in vacuo* and the residue recrystallised from $CHCl_3$ to obtain 4-(2,2-dicyanovinyl)phenyl 4,5-dimethoxy-2-nitrobenzyl carbonate (92 mg, 37%) as a light yellow solid: R_f 0.52 (hexane/EtOAc, 1:1); mp 192-194 °C (from $CHCl_3$); (Found C, 58.32; H, 3.56; N, 10.14. $C_{20}H_{15}N_3O_7$ requires C, 58.68; H, 3.69; N, 10.27); ν_{max}/cm^{-1} (nujol)

2251.3 (s)(CN), 2125.5 (s)(CN), 1663.5 (s)(NO_2), 1055.3 (vs)(C-O); δ_H (400 MHz; D_6-DMSO) 8.57 (1H, s, CH=), 8.04 (2H, d, *J* 8.7, H_d), 7.74 (1H, s, H_a), 7.57 (2H, d, *J* 8.7, H_c), 7.26 (1H, s, H_b), 5.60 (2H, s, $ArCH_2$), 3.92 (3H, s, OMe), 3.89 (3H, s, OMe); δ_C (100 MHz; D_6-DMSO) 160.3 (CH=), 154.4 (C=O), 153.1 (C), 151.7 (C), 148.3 (C), 139.9 (C), 132.3 (C-H_d), 129.3 (C), 124.4 (C), 122.5 (C-H_c), 114.1 (C), 113.1 (C), 111.9 (C-H_b), 108.3 (C-H_a), 81.7 (C), 67.1 ($ArCH_2$), 56.3 (OMe), 56.1 (OMe). *m/z* (ES^+) [Found: $(M+NH_4)^+$ 427.1250. $C_{20}H_{19}N_4O_7$ requires M^+ 427.1248]; *m/z* (EI^+) 427 ($[M+NH_4]^+$, 85%), 196 (100%), 72 (77%).[78]

9.3. Synthesis of Caged TRPV1 Agonists and Antagonists

9.3.1. 3-Methoxy-4-(triisopropylsilyloxy)benzonitrile **113**

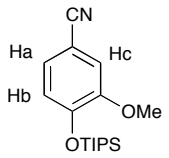

To a solution of 4-hydroxy-3-methoxybenzonitrile (10.0 g, 67.0 mmol, 1.0 eq) and imidazole (14.3 g, 210.0 mmol, 3.1 eq) in dry DMF (100 mL) was added triisopropylsilyl chloride (16.8 g, 18.6 mL, 87.0 mmol, 1.3 eq) at RT. The resulting solution was stirred at RT for 36 h. The solvent was removed *in vacuo*, and the residue purified by silica gel chromatography, eluting with EtOAc and petroleum ether (95:5), to afford 3-methoxy-4-(triisopropylsilyloxy)benzonitrile (17.8 g, 87%) as a colourless solid: R_f 0.38 (EtOAc/petroleum ether, 1:9); mp 47-49 °C (from EtOAc/petroleum ether); δ_H (400 MHz, $CDCl_3$) 7.16 (1H, dd, *J* 8.2, 2.0, H_a), 7.06 (1H, d, *J* 2.0, H_c), 6.90 (1H, d, *J* 8.2, H_b), 3.82 (3H, s, OMe), 1.20-1.34 (3H, m, Si[C*H*$(CH_3)_2]_3$) and 1.08 (18H, d, *J* 7.0, Si[CH(C*H*$_3)_2]_3$); *m/z* (ES^+) 364 ([M+$(CH_3CN{\cdot}NH_4)]^+$, 100%). These data are in accordance with the literature values.[98]

9.3.2 3-Methoxy-4-(triisopropylsilyloxy)benzylamine **114**

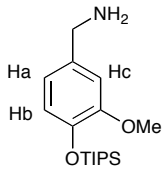

A solution of 3-methoxy-4-(triisopropylsilyloxy)benzonitrile (10.0 g, 32.77 mmol, 1.0 eq) in dry THF (100 mL) was added to a stirred mixture of $LiAlH_4$ (1.87 g, 49.15 mmol, 1.5 eq) in dry THF (400 mL). The reaction mixture was stirred at RT overnight. After this time TLC analysis indicated that the reaction was complete and the $LiAlH_4$ was quenched with EtOAc (200 mL). The reaction mixture was concentrated *in vacuo* and the residue filtered through Celite. The filtrate was evaporated *in vacuo* to afford crude 3-methoxy-4-(triisopropylsilyloxy)benzylamine (8.11 g, crude 80%) as a yellow oil: δ_H (400 MHz, $CDCl_3$) 6.84 (1H, d, *J* 8.0, H_b), 6.82 (1H, br s, H_c), 6.72 (1H, dd, *J* 8.0, 2.1, H_a), 3.81 (3H, s, OMe), 3.79 (2H, s, CH_2-NH_2), 1.20-1.30 (3H, m, Si[CH(CH_3)$_2$]$_3$), 1.09 (18H, d, *J* 6.9, Si[CH(CH_3)$_2$]$_3$). These data are in accordance with the literature values.[98]

9.3.3. 3-Methoxy-4-(triisopropylsilyloxy)-*N*-(nonanoyl)benzylamine **115**

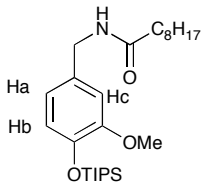

To a solution of 3-methoxy-4-(triisopropylsilyloxy)benzylamine (5.80 g, 18.74 mmol, 1.0 eq) in dry CH_2Cl_2 (100 mL) at 0 °C was added 4-DMAP (114.0 mg, 0.94 mmol, 0.05 eq). Dry pyridine (2.22 g, 2.27 mL, 28.11 mmol, 1.5 eq) was added dropwise. After stirring for 45 min at 0 °C, nonanoyl chloride (3.64 g, 3.71 mL, 20.61 mmol, 1.1 eq) was added dropwise. The reaction solution was allowed to warm to RT during which time it changed from a yellow to a red colour. The reaction was left stirring at RT for 72 h before TLC analysis indicated that the reaction was complete. The reaction was quenched with water (200 mL) and the organic phase collected. The aqueous phase was extracted with Et_2O (2 × 100 mL). The organic fractions were combined, washed with aqueous HCl (1 M, 75 mL), dried over Na_2SO_4, filtered and the solvent removed *in vacuo*. The residue was purified by silica gel chromatography, eluting with EtOAc and petroleum ether (2:8 → 3:7), to afford 3-methoxy-4-(triisopropylsilyloxy)-*N*-(nonanoyl)benzylamine (3.46 g, 41%) a light-brown oil: R_f 0.32 (EtOAc/petroleum ether, 3:7); δ_H (400 MHz, $CDCl_3$) 6.81 (1H, d, *J* 8.0, H_b), 6.76 (1H, d, *J* 2.0, H_c), 6.70 (1H, dd, *J* 8.0, 2.0, H_a), 5.67 (1H, br s, N*H*), 4.36 (2H, d, *J* 5.6, ArCH_2NH), 3.79 (3H, s, OMe), 2.21 (2H, t, *J* 7.6, C(O)CH_2), 1.60-1.70 (2H, m, C(O)CH_2CH_2), 1.18-1.37 (13H,

m, Si[C*H*$(CH_3)_2$]$_3$ and (CH_2)$_5$C*H*$_3$), 1.09 (18H, d, *J* 6.9, Si[CH(C*H*$_3$)$_2$]$_3$), 0.88 (3H, t, *J* 6.7, (CH_2)$_7$C*H*$_3$). ***m/z*** (ES^+) 598 (100%), 508 ([M+($CH_3CN{\cdot}NH_4$)]$^+$, 85%). These data are in accordance with the literature values.[98]

9.3.4. 4-Hydroxy-3-methoxy-*N*-(nonanoyl)benzylamine **116**

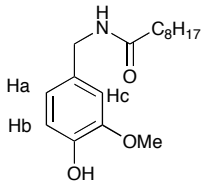

To a solution of 3-methoxy-4-(triisopropylsilyloxy)-*N*-(nonanoyl)benzylamine (2.0 g, 4.45 mmol, 1.0 eq) in dry THF (50 mL) was added tetra-*N*-butylammonium fluoride (1 M solution in THF, 6.67 mL, 6.67 mmol. 1.5 eq). The reaction solution was stirred at RT for 4 h. After this time TLC analysis indicated that the reaction was complete and HCl (1 M aqueous solution, 100 mL) and Et_2O (100 mL) were added to the reaction solution. The aqueous layer was extracted with Et_2O (3 × 75 mL) and the combined organic layers were washed with brine (100 mL), dried over Na_2SO_4, filtered and the solvent removed *in vacuo*. The crude product was purified by silica gel column chromatography, eluting with EtOAc and petroleum ether (4:6), to afford 4-hydroxy-3-methoxy-*N*-(nonanoyl)benzylamine (1.1 g, 84%) as a colourless solid: R_f 0.23 (EtOAc/petroleum ether, 1:1); mp 58-60 °C (from EtOAc/petroleum ether) [lit.[170] mp 52 °C]; δ_H (400 MHz, $CDCl_3$) 6.87 (1H, d, *J* 8.0, H_b), 6.81 (1H, d, *J* 1.9, H_c), 6.77 (1H, dd, *J* 8.0, 1.9, H_a), 5.60-5.71 (2H, m, OH and NH), 4.36 (2H, d, *J* 5.7, C*H*$_2$NH), 3.88 (3H, s, OMe), 2.20 (2H, t, *J* 7.6,

C(O)CH_2), 1.61-1.70 (2H, m, C(O)CH$_2$CH_2), 1.22-1.34 (10H, m, (CH_2)$_5$CH$_3$), 0.88 (3H, t, *J* 6.8, (CH$_2$)$_7$CH_3). *m/z* (ES$^+$) 352 ([M+(CH$_3$CN·NH$_4$)]$^+$, 77%). These data are in accordance with the literature values. [170]

9.3.5. 6-Bromo-3-methoxy-4-(triisopropylsilyloxy)-*N*-(nonanoyl)benzylamine **117**

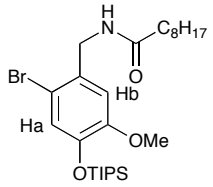

To a solution of 3-methoxy-4-(triisopropylsilyloxy)-*N*-nonanoylbenzylamine (0.85 g, 1.89 mmol, 1.0 eq) in CH_2Cl_2 (80 mL) was added dropwise a solution of bromine (0.63 g, 205 μL, 3.97 mmol, 2.1 eq) in CH_2Cl_2 (30 mL) over a period of 2.5 h at -78 °C. After stirring for a further 1 h, TLC analysis indicated that all of the starting material had been consumed. An aqueous solution of $NaSO_3$ (50 mL, 10% w/v) was added. The aqueous material was removed and the resulting mixture filtered through Celite and the solvent removed *in vacuo*. Purification by silica gel column chromatography, eluting with EtOAc and petroleum ether (1:9) yielded 6-bromo-3-methoxy-4-(triisopropylsilyloxy)-*N*-(nonanoyl)benzylamine (709 mg, 71%) as a colourless solid: R_f 0.42 (EtOAc/petroleum ether, 3:7); mp 50-53 °C (from EtOAc/petroleum ether); ν_{max}/cm^{-1} ($CHCl_3$) 3283.7 (m)(N-H), 2927.4 (s)(C-H), 2866.9 (s)(C-H), 1645.1 (s)(C=O), 1207.6 (s)(C-O); δ_H (400 MHz, $CDCl_3$) 7.03 (1H, s, H_a), 6.90 (1H, s, H_b), 5.86 (1H, t, *J* 5.7, NH), 4.43 (2H, d, *J* 5.7, CH_2NH), 3.78 (3H, s, OMe),

2.20 (2H, t, *J* 7.5, C(O)C*H*$_2$), 1.59-1.68 (2H, m, C(O)CH$_2$C*H*$_2$), 1.20-1.34 (13H, m, Si[C*H*(CH$_3$)$_2$]$_3$ and (C*H*$_2$)$_5$CH$_3$), 1.09 (18H, d, *J* 6.9, Si[CH(C*H*$_3$)$_2$]$_3$), 0.88 (3H, t, *J* 6.7, (CH$_2$)$_7$C*H*$_3$); δ_C (125 MHz, $CDCl_3$) 173.3 (C=O), 150.8 (C), 146.1 (C), 130.5 (C), 124.4 (C-H$_a$), 114.4 (C-H$_b$), 113.7 (C), 56.0 (OMe), 43.9 (C*H*$_2$NH), 37.2 (CH$_2$), 32.2 (CH$_2$), 29.71 (CH$_2$), 29.65 (CH$_2$), 29.6 (CH$_2$), 26.2 (CH$_2$), 23.0 (CH$_2$), 18.3 (CH$_3$), 14.5 (CH), 13.2 (CH$_3$). *m/z* (ES$^+$) 588 ([^{81}M+(CH$_3$CN·NH$_4$)]$^+$, 97%), 586 ([^{79}M+(CH$_3$CN·NH$_4$)]$^+$, 100%).

9.3.6. 6-Bromo-4-hydroxy-3-methoxy-*N*-(nonanoyl)benzylamine **118**

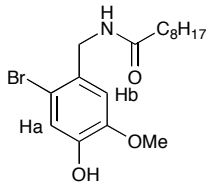

To a solution of 6-bromo-3-methoxy-4-(triisopropylsilyloxy)-*N*-(nonanoyl)benzylamine (390 mg, 0.74 mmol, 1.0 eq) in THF (15 mL) was added tetra-*N*-butylammonium fluoride in THF (1 M, 270 mg, 1.03 mL, 1.03 mmol, 1.4 eq) at RT and the resulting solution stirred for 3 h. After this time TLC analysis indicated that the reaction was complete and HCl (1 M aqueous solution, 30 mL) and Et_2O (100 mL) were added to the reaction solution. The aqueous layer was extracted with Et_2O (3 × 50 mL) and the combined organic layers were washed with brine (100 mL), dried over Na_2SO_4, filtered and the solvent removed *in vacuo*. The crude product was purified by silica gel column chromatography, eluting with EtOAc and petroleum ether (4:6), to afford 6-bromo-4-hydroxy-3-methoxy-*N*-(nonanoyl)benzylamine (245 mg, 89%) as a

colourless solid: R_f 0.51 (EtOAc/petroleum ether, 7:3); mp 90-91 °C (from EtOAc/petroleum ether) [lit.[101] mp 88 °C]; δ_H (400 MHz, $CDCl_3$) 7.09 (1H, s, H_a), 6.93 (1H, s, H_b), 5.92 (1H, t, *J* 5.8, NH), 5.74 (1H, br s, OH), 4.42 (2H, d, *J* 5.8, C*H*$_2$NH), 3.86 (3H, s, OMe), 2.19 (2H, t, *J* 7.6, C(O)C*H*$_2$), 1.59-1.69 (2H, m, C(O)CH$_2$C*H*$_2$), 1.20-1.33 (10H, m, (C*H*$_2$)$_5$CH$_3$), 0.87 (3H, t, *J* 6.7, (CH$_2$)$_7$C*H*$_3$). *m/z* (ES$^+$) 432 ([^{81}M+(CH$_3$CN·NH$_4$)]$^+$, 95%), 430 ([^{79}M+(CH$_3$CN·NH$_4$)]$^+$, 100%). These data are in accordance with the literature values.[101]

9.3.7. 3-Methoxy-4-(4,5-dimethoxy-2-nitrobenzyl)-*N*-(nonanoyl)benzylamine **105**

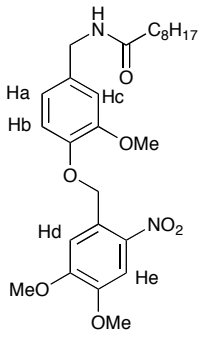

To a solution of 4-hydroxy-3-methoxy-*N*-(nonanoyl)benzylamine (130 mg, 0.44 mmol, 1.0 eq) in dry THF (20 mL) was added potassion *tert*-butoxide (50 mg, 0.44 mmol, 1.0 eq) and the mixture stirred at RT for 30 min. After this time, 4,5-dimethoxy-2-nitrobenzyl bromide (122 mg, 0.44 mmol, 1.0 eq) was added and the resulting mixture stirred at RT overnight. TLC analysis indicated full consumption of the starting material, therefore the solvent was removed *in vacuo*. The residue was partitioned between water (100 mL) and

CH_2Cl_2 (100 mL). The organic fractions were dried over $MgSO_4$, filtered and concentrated *in vacuo*. The resulting solid was purified by silica gel column chromatography, eluting with EtOAc and petroleum ether (4:6) and then recrystallised from CH_2Cl_2 and Et_2O affording 3-methoxy-4-(4,5-dimethoxy-2-nitrobenzyl)-*N*-(nonanoyl)benzylamine (123 mg, 57%) as a yellow solid: R_f 0.20 (EtOAc/petroleum ether, 1:1); mp 135-137 °C (from CH_2Cl_2/Et_2O); ν_{max}/cm^{-1} ($CHCl_3$) 2923.8 (s)(C-H), 2852.2 (s)(C-H), 1636.0 (s)(C=O), 1519.6 (vs)(NO_2), 1327.7 (s)(NO_2); δ_H (400 MHz, $CDCl_3$) 7.76 (1H, s, H_e), 7.49 (1H, s, H_d), 6.89 (1H, br s, H_c) 6.87 (1H, d, *J* 8.2, H_b), 6.78 (1H, dd, *J* 8.2, 1.9, H_a), 5.70 (1H, br s, NH), 5.54 (2H, s, CH_2-O), 4.39 (2H, d, *J* 5.7, C*H*$_2$-NH), 3.97 (6H, s, 2 × OMe), 3.90 (3H, s, OMe), 2.21 (2H, t, *J* 7.6, C(O)C*H*$_2$), 1.60-1.71 (2H, m, C(O)CH_2C*H*$_2$), 1.21-1.36 (10H, m, (C*H*$_2$)$_5CH_3$), 0.88 (3H, t, *J* 6.8, $(CH_2)_7$C*H*$_3$); δ_C (125 MHz, $CDCl_3$) 173.0 (C=O), 154.0 (C), 150.0 (C), 147.8 (C), 147.0 (C), 138.9 (C), 132.6 (C), 129.9 (C), 120.2 (C-H_a), 114.5 (C-H_b), 111.8 (C-H_c), 109.3 (C-H_d), 107.9 (C-H_e), 68.5 (CH_2-O), 56.3 (2 × OMe), 56.0 (OMe), 43.3 (CH_2-NH), 36.9 (CH_2), 31.8 (CH_2), 29.30 (CH_2), 29.29 (CH_2), 29.1 (CH_2), 25.8 (CH_2), 22.6 (CH_2), 14.1 (CH_3). *m/z* (ES^+) 547 ([M+($CH_3CN{\cdot}NH_4$)]$^+$, 100%).[103]

9.3.8. 6-Bromo-3-methoxy-4-(4,5-dimethoxy-2-nitrobenzyl)-*N*-(nonanoyl)benzylamine **109**

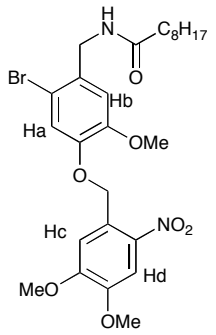

To a solution of 6-bromo-4-hydroxy-3-methoxy-*N*-(nonanoyl)benzylamine (100 mg, 0.27 mmol, 1.0 eq) in THF (15 mL) was added potassium *tert*-butoxide (33 mg, 0.30 mmol, 1.1 eq) and the resulting solution stirred at RT for 30 min. After this time, 4,5-dimethoxy-2-nitrobenzyl bromide (82 mg, 0.30 mmol, 1.1 eq) was added and the resulting mixture stirred at RT overnight. TLC analysis indicated full consumption of the starting material and therefore the solvent was removed *in vacuo*. The resulting solid was crystallised from CH_2Cl_2 and Et_2O affording 6-bromo-3-methoxy-4-(4,5-dimethoxy-2-nitrobenzyl)-*N*-(nonanoyl)benzylamine (83 mg, 55%) as a light-yellow solid: R_f 0.56 (MeOH/CH_2Cl_2, 5:95); mp 183-185 °C (from CH_2Cl_2/Et_2O); ν_{max}/cm^{-1} ($CHCl_3$) 2925.7 (s)(C-H), 2851.2 (s)(C-H), 1645.5 (s)(C=O), 1547.2 (m), 1526.8 (s)(NO_2), 1322.8 (s)(NO_2); δ_H (400 MHz, $CDCl_3$) 7.78 (1H, s, H_d), 7.46 (1H, s, H_c), 7.09 (1H, s, H_a), 7.02 (1H, br s, H_b), 5.92 (1H, t, *J* 5.7, NH), 5.52 (2H, s, O-CH_2), 4.45 (2H, d, *J* 5.7, C*H*$_2$-NH), 3.98 (3H, s, OMe), 3.97 (3H, s, OMe), 3.89 (3H, s, OMe), 2.20 (2H, t, *J* 7.6, C(O)-C*H*$_2$-CH_2), 1.60-1.69 (2H,

m, C(O)-CH_2-CH_2), 1.19-1.35 (10H, m, CH_2(CH_2)$_5$$CH_3$), 0.87 (3H, t, *J* 6.7, CH_2CH_3); δ_C (125 MHz, $CDCl_3$) 173.1 (C=O), 154.1 (C), 149.3 (C), 147.9 (C), 147.6 (C), 138.9 (C), 131.2 (C), 129.1 (C), 118.4 (C-H_a), 114.2 (C-H_b), 113.8 (C), 109.4 (C-H_c), 108.0 (C-H_d), 68.6 (O-CH_2), 56.4 (2 × OMe), 56.2 (OMe), 43.6 (CH_2-NH), 36.8 (CH_2), 31.8 (CH_2), 29.27 (CH_2), 29.25 (CH_2), 29.1 (CH_2), 25.7 (CH_2), 22.6 (CH_2), 14.1 (CH_3). *m/z* (ES^+) 627 ([^{81}M+(CH_3CN·NH_4)]$^+$, 30%), 625 ([^{79}M+(CH_3CN·NH_4)]$^+$, 33%), 465 (100%).[103]

9.3.9. 4,5-Dimethoxy-2-nitrobenzyl-2'-methoxy-4'-(nonanamidomethyl)phenyl carbonate **110**

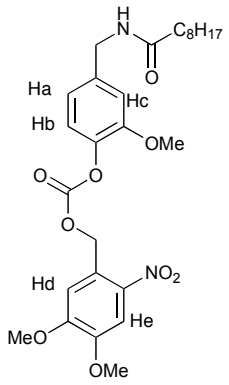

A stirred solution of 4-hydroxy-3-methoxy-*N*-(nonanoyl)benzylamine (100 mg, 0.341 mmol, 1.0 eq) in CH_2Cl_2 (10 mL) was cooled to 0 °C before 4,5-dimethoxy-2-nitrobenzyl chloroformate (235 mg, 0.853 mmol, 2.5 eq) and NEt_3 (0.14 mL 1.023 mmol, 3.0 eq) were added. The resulting solution was stirred at RT overnight. After this time, TLC analysis indicated full consumption of the starting material. Therefore, the solvents were removed *in vacuo* and the crude product purified by silica gel column chromatography

eluting with EtOAc and petroleum ether (1:1) to afford 4,5-dimethoxy-2-nitrobenzyl-2'-methoxy-4'-(nonanamidomethyl)phenyl carbonate (173 mg, 96%) as yellow solid: R_f 0.27 (EtOAc/petroleum ether, 1:1); mp 128-131 °C (from EtOAc/petroleum ether); ν_{max}/cm^{-1} ($CHCl_3$) 2927.6 (m)(C-H), 1769.5 (s)(C=O), 1648.1 (s)(C=O), 1524.5 (s)(NO_2), 1280.4 (s)(NO_2), 1221.3 (m), 1073.4 (m)(C-O); δ_H (500 MHz, $CDCl_3$) 7.77 (1H, s, H_e), 7.19 (1H, s, H_d), 7.10 (1H, d, *J* 7.9, H_b), 6.93 (1H, d, *J* 1.8, H_c), 6.86 (1H, dd, *J* 7.9, 1.8, H_a), 5.74 (1H, t, *J* 5.6, NH), 5.71 (2H, s, $ArCH_2$), 4.43 (2H, d, *J* 5.6, C*H*$_2$-NH), 4.03 (3H, s, OMe), 3.98 (3H, s, OMe), 3.82 (3H, s, OMe), 2.23 (2H, t, *J* 7.6, C(O)-C*H*$_2$-CH_2), 1.61-1.70 (2H, m, C(O)-CH_2-C*H*$_2$), 1.23-1.36 (10H, m, CH_2(C*H*$_2$)$_5$$CH_3$), 0.88 (3H, t, *J* 6.7, CH_2C*H*$_3$); δ_C (125 MHz, $CDCl_3$) 173.0 (C=O), 153.8 (OC=O), 152.8 (C), 151.2 (C), 148.4 (C), 139.6 (C), 139.3 (C), 138.1 (C), 126.7 (C), 122.3 (C-H_b), 120.0 (C-H_a), 112.4 (C-H_c), 109.7 (C-H_d), 108.2 (C-H_e), 67.1 ($ArCH_2$), 56.6 (OMe), 56.5 (OMe), 56.0 (OMe), 43.4 (CH_2-NH), 36.8 (CH_2), 31.8 (CH_2), 29.7 (CH_2), 29.3 (CH_2), 29.2 (CH_2), 25.8 (CH_2), 22.6 (CH_2), 14.1 (CH_3). *m/z* (ES^+) 591 ([M+(CH_3CN·NH_4)]$^+$, 100%).

9.3.10. 4,5-Dimethoxy-2-nitrobenzyl-5'-bromo-2'-methoxy-4'-(nonanamidomethyl)phenyl carbonate **111**

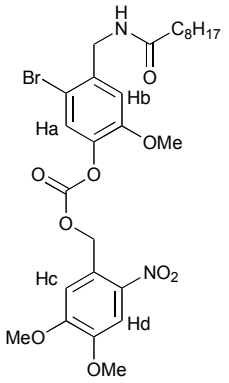

To a stirred solution of 6-bromo-4-hydroxy-3-methoxy-*N*-(nonanoyl)benzylamine (75 mg, 0.202 mmol, 1.0 eq) in CH_2Cl_2 (15 mL) was added NEt_3 (0.11 mL, 0.81 mmol, 4.0 eq) at 0 °C. The resulting solution was stirred for 30 min at 0 °C. After this time, 4,5-dimethoxy-2-nitrobenzyl chloroformate (111 mg, 0.403 mmol, 2.0 eq) was added and the resulting solution was stirred at RT overnight. The solvent was removed *in vacuo* and the crude product was purified by silica gel column chromatography, eluting with EtOAc and petroleum ether (1:1), to yield 4,5-dimethoxy-2-nitrobenzyl-5'-bromo-2'-methoxy-4'-(nonanamidomethyl)phenyl carbonate (113 mg, 92%) as a colourless solid: R_f 0.31 (EtOAc/petroleum ether, 1:1); mp 127-129 °C (from petroleum ether); ν_{max}/cm^{-1} ($CHCl_3$) 2933.8 (s)(C-H), 2849.1 (s)(C-H), 1754.6 (s)(C=O), 1641.5 (s)(C=O), 1519.6 (s)(NO_2), 1339.7 (s)(NO_2); δ_H (500 MHz, $CDCl_3$) 7.78 (1H, s, H_d), 7.35 (1H, s, H_a), 7.15 (1H, s, H_c), 7.09 (1H, s, H_b) 5.92 (1H, t, *J* 6.0, NH), 5.71 (2H, s, O-CH_2), 4.49 (2H, d, *J* 6.0, CH_2-NH), 4.03

(3H, s, OMe), 3.99 (3H, s, OMe), 3.82 (3H, s, OMe), 2.21 (2H, t, *J* 7.6, C(O)-C*H*$_2$-CH$_2$), 1.68-1.62 (2H, m, C(O)-CH$_2$-C*H*$_2$), 1.26-1.31 (10H, m, CH$_2$(C*H*$_2$)$_5$CH$_3$), 0.88 (3H, t, *J* 6.8, CH$_2$C*H*$_3$); δ_C (125 MHz, $CDCl_3$) 173.1 (C=O), 153.8 (OC=O), 152.4 (C), 150.6 (C), 148.4 (C), 139.6 (C), 139.5 (C), 136.7 (C), 126.30 (C), 126.27 (C-H$_a$), 114.9 (C-H$_b$), 113.1 (C), 109.8 (C-H$_c$), 108.2 (C-H$_d$), 67.3 (O-CH$_2$), 56.6 (OMe), 56.5 (OMe), 56.3 (OMe), 43.6 (CH$_2$-NH), 36.7 (CH$_2$), 31.8 (CH$_2$), 29.3 (2 × CH$_2$), 29.1 (CH$_2$), 25.7 (CH$_2$), 22.6 (CH$_2$), 14.1 (CH$_3$). *m/z* (ES$^+$) 671 ([^{81}M+(CH$_3$CN·NH$_4$)]$^+$, 98%), 669 ([^{79}M+(CH$_3$CN·NH$_4$)]$^+$, 100%).

9.4. Synthesis of Amino-modified TRPV1 Agonists

9.4.1. 11-(*tert*-Butoxycarbonylamino)undecanoic acid **124**

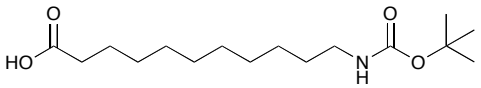

A solution of 11-aminoundecanoic acid (3.0 g, 14.90 mmol, 1.0 eq) and NaOH (0.9 g, 22.35 mmol, 1.5 eq) in water/THF (1:1, 100 mL) was prepared. A solution of Boc_2O (4.9 g, 22.35 mmol, 1.5 eq) in THF (100 mL) was added dropwise to the above solution over 1 h. The solution was stirred at RT overnight. The THF was removed *in vacuo* and the remaining aqueous solution acidified to pH 1 using conc. HCl. This aqueous solution was extracted with CH_2Cl_2 (2 × 100 mL). The organic phases were combined, dried over $MgSO_4$, filtered and the solvent removed *in vacuo*. The residue was purified by silica gel column chromatography, eluting with EtOAc and petroleum ether (2.5:7.5) to afford 11-(*tert*-butoxycarbonylamino)undecanoic acid (3.88 g, 86%) as a colourless solid: R_f 0.43 (EtOAc/petroleum ether, 1:1); mp 58-60 °C (from EtOAc/petroleum ether); δ_H (400 MHz; $CDCl_3$) 4.54 (1H, br s, NH), 3.07-3.13 (2H, m, CH_2), 2.34 (2H, t, *J* 7.5, CH_2), 1.63 (2H, tt, *J* 7.5, 7.5, CH_2), 1.44-1.47 (11H, m, $(CH_3)_3$, CH_2), 1.27-1.31 (12H, m, $(CH_2)_6$). *m/z* (ES^+) 625 (100%), 302 ($[M+H]^+$, 55%). These data are in accordance with the literature values.[171]

9.4.2. *tert*-Butyl 11-(3-methoxy-4-(triisopropylsilyloxy)benzylamino)-11-oxoundecylcarbamate **125**

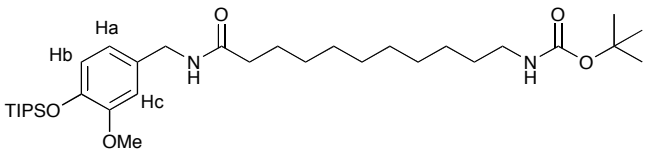

11-(*tert*-Butoxycarbonylamino)undecanoic acid (1.30 g, 4.31 mmol, 1.1 eq), EDC·HCl (0.90 g, 4.70 mmol, 1.2 eq) and HBTU (1.49 g, 3.92 mmol, 1.0 eq) were dissolved in dry CH_2Cl_2 (25 mL) and stirred at RT for 10 min. 3-Methoxy-4-(triisopropylsilyloxy)benzylamine (0.60 g, 1.94 mmol, 0.5 eq) in dry CH_2Cl_2 (10 mL) and Hunig's base (1.01 g, 1.37 mL, 7.84 mmol, 2.0 eq) were added to the above solution. The reaction mixture was stirred at RT under N_2 overnight. After this time the reaction was adjudged complete by TLC. The residue was partitioned between water (100 mL) and CH_2Cl_2 (2 × 100 mL). The organic extract was washed with 1M aqueous HCl (100 mL), a saturated aqueous solution of Na_2CO_3 (100 mL) and water (100 mL). The organic extracts were combined, dried over $MgSO_4$, filtered and the solvent removed *in vacuo*. This residue was purified by silica gel column chromatography, eluting with EtOAc and petroleum ether (2:8) to afford *tert*-butyl 11-(3-methoxy-4-(triisopropylsilyloxy)benzylamino)-11-oxoundecylcarbamate (585 mg, 51%) as a colourless solid: R_f 0.48 (EtOAc/petroleum ether, 1:1); (Found C, 66.83; H, 10.13; N, 4.79. $C_{33}H_{60}N_2O_5Si$ requires C, 66.85; H, 10.20; N, 4.72); mp 76-78 °C (from EtOAc/petroleum ether); ν_{max}/cm^{-1} ($CHCl_3$) 3311.2 (m)(N-H), 2928.6 (s)(C-H), 2865.6 (s)(C-H), 1692.8 (s)(C=O), 1650.8 (s)(C=O), 1282.8

(s)(C-O), 1173.1 (vs)(C-O); δ_H (500 MHz; $CDCl_3$) 6.79 (1H, d, *J* 8.1, H_b), 6.75 (1H, d, *J* 1.6, H_c), 6.68 (1H, dd, *J* 8.1, 1.6, H_a), 5.82 (1H, br s, NH), 4.56 (1H, br s, NH), 4.34 (2H, d, *J* 5.5, $ArCH_2$), 3.77 (3H, s, OMe), 3.06-3.10 (2H, m, CH_2), 2.19 (2H, t, *J* 7.7, CH_2), 1.64 (2H, tt, *J* 7.5, 7.5, CH_2), 1.42-1.44 (11H, m, $(CH_3)_3$, CH_2), 1.24-1.30 (15H, m, $Si[CH(CH_3)_2]_3$, $(CH_2)_6$), 1.08 (18H, d, *J* 7.5, $Si[CH(CH_3)_2]_3$); δ_C (125 MHz; $CDCl_3$) 172.9 (C=O), 156.0 (C=O), 150.9 (C), 144.9 (C), 131.4 (C), 120.2 (C-H_b), 120.0 (C-H_a), 111.9 (C-H_c), 79.1 (C), 55.4 (OMe), 43.5 ($ArCH_2$), 40.8 (CH_2), 36.8 (CH_2), 25.8 (CH_2), 30.0 (CH_2), 29.4 (CH_2), 29.3 (CH_2), 29.24 (2 × CH_2), 29.18 (CH_2), 28.4 ($(CH_3)_3$), 26.7 (CH_2), 17.9 ($Si[CH(CH_3)_2]_3$), 12.9 ($Si[CH(CH_3)_2]_3$). *m/z* (ESI^+) [Found: $(M+Na)^+$ 615.4162. $C_{33}H_{60}N_2O_5SiNa$ requires M^+ 615.4164]; *m/z* (ES^+) 615 ($[M+Na)]^+$, 100%).

9.4.3. *tert*-Butyl 11-(4-hydroxy-3-methoxybenzylamino)-11-oxoundecylcarbamate **126**

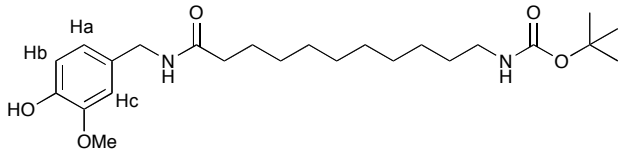

To a solution of *tert*-butyl 11-(3-methoxy-4-(triisopropylsilyloxy)benzylamino)-11-oxoundecylcarbamate (300 mg, 0.506 mmol, 1.0 eq) in CH_2Cl_2 (10 mL) was added tetra-*N*-butylammonium fluoride (1 M solution in THF, 1.51 mL, 1.52 mmol, 3.0 eq) at RT and the resulting solution stirred for 3 h. After this time TLC analysis indicated that the reaction was complete. The reaction mixture was partitioned between water (100 mL) and CH_2Cl_2 (3 × 25 mL). The

organic fractions were combined, dried over $MgSO_4$, filtered and concentrated *in vacuo.* The residue was purified by silica gel column chromatography, eluting with EtOAc and petroleum ether (1:1 → 7:3) to afford *tert*-butyl 11-(4-hydroxy-3-methoxybenzylamino)-11-oxoundecylcarbamate (188 mg, 85%) as a colourless oil: R_f 0.14 (EtOAc/petroleum ether, 1:1); (Found: C, 61.86; H, 10.24; N, 7.16. $C_{20}H_{40}N_2O_5$ requires C, 61.82; H, 10.38; N, 7.21); ν_{max}/cm^{-1} ($CHCl_3$) 3318.3 (m)(N-H), 2927.7 (s)(C-H), 2854.6 (s)(C-H), 1680.9 (s)(C=O), 1642.9 (s)(C=O), 1276.2 (s)(C-O), 1170.9 (s)(C-O); δ_H (400 MHz; $CDCl_3$) 6.85 (1H, d, *J* 8.1, H_b), 6.80 (1H, d, *J* 1.8, H_c), 6.75 (1H, dd, *J* 8.1, 1.8, H_a), 5.83 (1H, br s, NH), 4.56 (1H, br s, NH), 4.34 (2H, d, *J* 5.7, $ArCH_2$), 3.86 (3H, s, OMe), 3.06-3.11 (2H, m, CH_2), 2.19 (2H, t, *J* 7.4, CH_2), 1.64 (2H, tt, *J* 7.5, 7.5, CH_2), 1.41-1.43 (11 H, m, $(CH_3)_3$, CH_2), 1.23-1.29 (12H, m, $(CH_2)_6$); δ_C (125 MHz; $CDCl_3$) 173.0 (C=O), 156.2 (C=O), 146.8 (C), 145.2 (C), 130.4 (C), 120.7 (C-H_a), 114.2 (C-H_b), 110.7 (C-H_c), 79.1 (C), 55.9 (OMe), 43.5 ($ArCH_2$), 40.6 (CH_2), 36.8 (CH_2), 30.0 (CH_2), 29.36 (CH_2), 29.30 (CH_2), 29.22 (CH_2), 29.19 (CH_2), 29.17 (CH_2), 28.4 (($CH_3)_3$), 26.7 (CH_2), 25.7 (CH_2). *m/z* (ESI^+) [Found: $(M+Na)^+$ 459.2833. $C_{24}H_{40}N_2O_5Na$ requires M^+ 459.2829]; *m/z* (ES^-) 471 ($[M+Cl)]^-$, 100%).

9.4.4. *tert*-Butyl (11-((4-[{((4,5-dimethoxy-2-nitrobenzyl)oxy)carbonyl}oxy]-3-methoxybenzyl)amino)-11-oxoundecyl)carbamate **127**

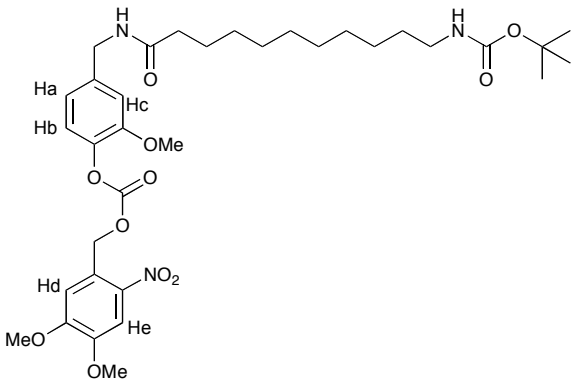

A stirred solution of *tert*-butyl 11-(4-hydroxy-3-methoxybenzylamino)-11-oxoundecylcarbamate (80 mg, 0.183 mmol, 1.0 eq) in dry CH_2Cl_2 (10 mL) was cooled to 0 °C. 4,5-Dimethoxy-2-nitrobenzyl chloroformate (101 mg, 0.367 mmol, 2.0 eq) and NEt_3 (56 mg, 77 µL, 0.549 mmol, 3.0 eq) were added and the reaction solution stirred at RT overnight. After this time TLC analysis indicated that the reaction was complete. The solvent was removed *in vacuo* and the residue purified by silica gel column chromatography, eluting with EtOAc and petroleum ether (1:1 → 7:3) to afford *tert*-butyl (11-((4-[{((4,5-dimethoxy-2-nitrobenzyl)oxy)carbonyl}oxy]-3-methoxybenzyl)amino)-11-oxoundecyl)carbamate (117 mg, 94%) as a yellow solid: R_f 0.10 (EtOAc/petroleum ether, 1:1); (Found: C, 60.57; H, 7.42; N, 6.16. $C_{34}H_{49}N_3O_{11}$ requires C, 60.43; H, 7.31; N, 6.22); mp 61-63 °C (from $CHCl_3$); ν_{max}/cm^{-1} ($CHCl_3$) 2927.7 (m)(C-H), 1769.8 (m)(C=O), 1695.7 (m)(C=O), 1654.0 (s)(C=O), 1524.1 (s)(NO_2), 1279.3 (s)(NO_2), 1220.9 (s)(C-O), 1072.7 (s)(C-O);

δ_H (500 MHz; $CDCl_3$) 7.77 (1H, s, H_e), 7.17 (1H, s, H_d), 7.10 (1H, d, *J* 8.1, H_b), 6.93 (1H, d, *J* 1.8, H_c), 6.86 (1H, dd, *J* 8.1, 1.8, H_a), 5.82 (1H, t, *J* 5.8, NH), 5.70 (2H, s, $OC(O)OCH_2$), 4.49-4.54 (1H, m, NH), 4.42 (2H, d, *J* 5.8, $ArCH_2N$), 4.02 (3H, s, OMe), 3.98 (3H, s, OMe), 3.81 (3H, s, OMe), 3.07-3.11 (2H, m, CH_2), 2.22 (2H, t, *J* 7.7, CH_2), 1.62-1.68 (2H, m, CH_2), 1.43-1.45 (11H, m, $(CH_3)_3$, CH_2), 1.25-1.32 (12H, m, $(CH_2)_6$); δ_C (125 MHz; $CDCl_3$) 173.0 (C=O), 156.0 (C=O), 153.8 (C=O), 152.8 (C), 151.1 (C), 148.3 (C), 139.5 (C), 139.2 (C), 138.1 (C), 126.7 (C), 122.3 (C-H_b), 120.0 (C-H_a), 112.3 (C-H_c), 109.6 (C-H_d), 108.2 (C-H_e), 79.0 ($C(CH_3)_3$), 67.0 ($OC(O)OCH_2$), 56.5 (OMe), 56.4 (OMe), 56.0 (OMe), 43.3 ($ArCH_2N$), 40.6 (CH_2), 36.7 (CH_2), 30.0 (CH_2), 29.4 (CH_2), 29.3 (CH_2), 29.23 (CH_2), 29.21 (CH_2), 29.15 (CH_2), 28.4 ($(CH_3)_3$), 26.7 (CH_2), 25.7 (CH_2). *m/z* (ESI^+) [Found: $(M+Na)^+$ 698.3260. $C_{34}H_{49}N_3O_{11}Na$ requires M^+ 698.3260]; *m/z* (ES^-) 674 ($[M-H]^-$, 100%).

9.4.5. 4-((11-Aminoundecanamido)methyl)-2-methoxyphenyl 4,5-dimethoxy-2-nitrobenzyl carbonate hydrochloride **128**

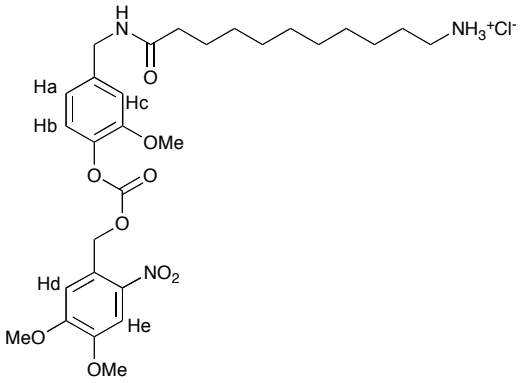

A solution of *tert*-butyl (11-((4-[{((4,5-dimethoxy-2-nitrobenzyl)oxy)carbonyl}oxy]-3-methoxybenzyl)amino)-11-oxoundecyl)carbamate (100 mg, 0.148 mmol, 1.0 eq) in 1 M HCl in dioxane (5 mL) was stirred at RT for 3 h. The dioxane was removed *in vacuo* and the crude mixture precipitated in Et_2O to afford 4-((11-aminoundecanamido)methyl)-2-methoxyphenyl 4,5-dimethoxy-2-nitrobenzyl carbonate hydrochloride (80 mg, 94%) as a yellow solid: Mp 120-121 °C (from Et_2O); ν_{max}/cm^{-1} (MeOH) 3424.9 (m)(N-H), 2925.3 (m)(C-H), 1765.4 (m)(C=O), 1643.0 (s)(C=O), 1523.8 (s)(NO_2), 1279.3 (s)(NO_2), 1220.2 (s)(C-O), 1072.5 (s)(C-O); δ_H (500 MHz; MeOD) 7.81 (1H, s, H_e), 7.21 (1H, s, H_d), 7.12 (1H, d, *J* 8.1, H_b), 7.07 (1H, d, *J* 1.7, H_c), 6.91 (1H, dd, *J* 8.1, 1.7, H_a), 5.63 (2H, s, $OC(O)OCH_2$), 4.38 (2H, s, $ArCH_2N$), 3.98 (3H, s, OMe), 3.95 (3H, s, OMe), 3.82 (3H, s, OMe), 2.93 (2H, t, *J* 7.7, CH_2), 2.27 (2H, t, *J* 7.5, CH_2), 1.63-1.69 (4H, m, $(CH_2)_2$), 1.32-1.42 (12H, m, $(CH_2)_6$); δ_C (125 MHz; MeOD)

176.3 (NC=O), 155.3 (OC=O), 154.4 (C), 152.6 (C), 150.1 (C), 141.3 (C), 140.6 (C), 139.9 (C), 127.3 (C), 123.2 (C-H_b), 120.8 (C-H_a), 113.3 (C-H_c), 111.8 (C-H_d), 109.5 (C-H_e), 68.3 (OC(O)O*C*H_2), 57.0 (OMe), 56.9 (OMe), 56.5 (OMe), 43.8 (Ar*C*H_2N), 40.8 (CH_2), 37.0 (CH_2), 30.44 (CH_2), 30.39 ((CH_2)$_2$), 30.24 (CH_2), 30.19 (CH_2), 28.6 (CH_2), 27.4 (CH_2), 27.0 (CH_2). *m/z* (ESI^+) [Found: $(M+H)^+$ 576.2915. $C_{29}H_{42}N_3O_9$ requires M^+ 576.2916]; *m/z* (ES^+) 576 ($[M+H)]^+$, 100%).

9.4.6. 11-Amino-*N*-(4-hydroxy-3-methoxybenzyl)undecanamide hydrochloride **121**

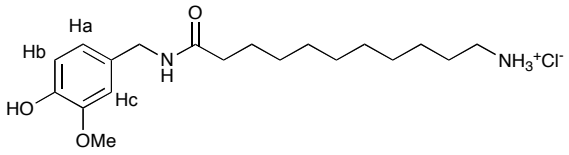

A solution of *tert*-butyl 11-(4-hydroxy-3-methoxybenzylamino)-11-oxoundecylcarbamate (100 mg, 0.23 mmol, 1.0 eq) in 1 M HCl in dioxane (5 mL) was stirred at RT for 5 h. The dioxane was evaporated *in vacuo* and the residue purified by ion exchange chromatography using an SCX 2 column. The column was prepared by eluting with MeOH. The residue was loaded onto the column in a minimal amount of MeOH and impurities washed off by eluting with MeOH. The column was then eluted with a 2 M solution of NH_3 in MeOH to afford 11-amino-*N*-(4-hydroxy-3-methoxybenzyl)undecanamide (57 mg, 74%) as a colourless solid: Mp 98-100 °C (from MeOH/Et_2O); ν_{max}/cm^{-1} (MeOH) 3283.4 (m)(N-H), 2925.7 (s)(C-H), 2853.4 (s)(C-H), 1639.8 (s)(C=O), 1277.6 (s)(C-O); δ_H (500 MHz; MeOD) 6.88 (1H, d, *J* 1.5, H_c), 6.73-6.74 (2H,

m, H_a and H_b), 4.27 (2H, s, $ArCH_2$), 3.85 (3H, s, OMe), 2.66 (2H, t, *J* 7.4, CH_2), 2.23 (2H, t, *J* 7.4, CH_2), 1.61-1.67 (2H, m, CH_2), 1.46-1.52 (2H, m, CH_2), 1.31-1.34 (12H, m, $(CH_2)_6$); δ_C (125 MHz; MeOD) 176.2 (C=O), 149.2 (C), 147.3 (C), 131.4 (C), 121.5 (C-H_a), 116.3 (C-H_b), 112.5 (C-H_c), 56.4 (OMe), 44.1 ($ArCH_2$), 42.4 (CH_2), 37.2 (CH_2), 33.4 (CH_2), 30.6 (($CH_2)_3$), 30.4 (CH_2), 30.2 (CH_2), 28.0 (CH_2), 27.1 (CH_2). *m/z* (ESI^+) [Found: $(M+H)^+$ 337.2486. $C_{19}H_{33}N_2O_3$ requires M^+ 337.2486]; *m/z* (ES^+) 337 ($[M+H]^+$, 100%).

9.4.7. Ethyl 2-(3-(11-((4-hydroxy-3-methoxybenzyl)amino)-11-oxoundecyl)ureido)acetate **123**

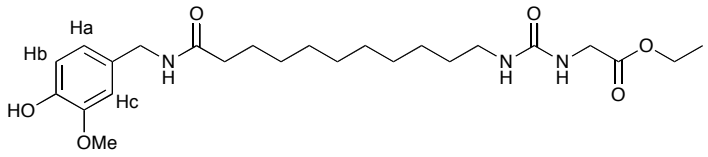

Ethyl isocyanatoacetate (32 mg, 29 μL, 0.250 mmol, 2.0 eq) was added to a solution of 11-amino-*N*-(4-hydroxy-3-methoxybenzyl)undecanamide (42 mg, 0.125 mmol, 1.0 eq) in dichloroethane (5 mL). The reaction mixture was heated under reflux overnight. After this time the reaction mixture was cooled to RT and the solvent removed *in vacuo*. The residue was purified by ion exchange chromatography using an SCX 2 column eluting with MeOH and then a 2 M solution of NH_3 in MeOH. The residue obtained from the column was crystallised from CH_2Cl_2 and Et_2O to obtain ethyl 2-(3-(11-((4-hydroxy-3-methoxybenzyl)amino)-11-oxoundecyl)ureido)acetate (31 mg, 53%) as a colourless gum: R_f 0.27 (EtOAc); ν_{max}/cm^{-1} ($CHCl_3$) 3297.5 (m)(N-H), 2923.2 (s)(C-H), 1740.6 (s)(C=O), 1630.7 (s)(C=O), 1278.8 (s)(C-O), 1207.2 (s)(C-

O); δ_H (400 MHz; MeOD) 6.86 (1H, d, *J* 1.2, H_c), 6.69-6.74 (2H, m, H_a and H_b), 4.26 (2H, s, $ArCH_2$), 4.17 (2H, q, *J* 7.1, OCH_2), 3.85 (2H, s, NCH_2CO), 3.83 (3H, s, OMe), 3.10 (2H, t, *J* 7.0, CH_2N), 2.21 (2H, t, *J* 7.4, $COCH_2$), 1.59-1.65 (2H, m, CH_2), 1.43-1.50 (2H, m, CH_2), 1.28-1.33 (12H, m, $(CH_2)_6$), 1.26 (3H, t, *J* 7.1, CH_3); δ_C (125 MHz; $CDCl_3$) 173.2 (C=O), 171.5 (C=O), 158.1 (NC=ON), 146.8 (C), 145.2 (C), 130.4 (C), 120.7 (C-H_a), 114.5 (C-H_b), 110.9 (C-H_c), 61.3 ($ArCH_2$), 56.0 (OMe), 43.6 (OCH_2), 42.3 (CH_2), 40.6 (CH_2), 36.8 (CH_2), 30.1 (CH_2), 29.21 (CH_2), 29.13 (CH_2), 29.12 (CH_2), 29.09 (CH_2), 29.07 (CH_2), 26.7 (CH_2), 25.7 (CH_2), 14.2 (CH_3). *m/z* (ESI^+) [Found: $(M+Na)^+$ 488.2733. $C_{24}H_{39}N_3O_6Na$ requires M^+ 488.2731]; *m/z* (ES^+) 617 (100%), 488 ($[M+H]^+$, 50%).

9.4.8. *N*-(4-Hydroxy-3-methoxybenzyl)-11-ureidoundecanamide **122**

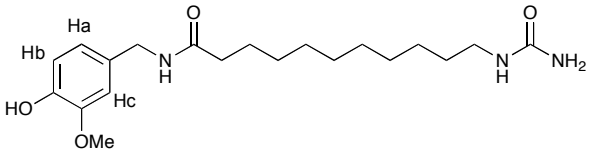

A solution of 11-amino-*N*-(4-hydroxy-3-methoxybenzyl)undecanamide (57 mg, 0.171 mmol, 1.0 eq) and urea (35 mg, 0.583 mmol, 3.4 eq) in H_2O (7 mL) was heated underreflux for 8 h. A brown solid was filtered off and redissolved in MeOH. This residue was adsorbed onto Celite and purified by silica gel column chromatography, eluting with EtOAc, MeOH and NEt_3 (90:5:5) to afford *N*-(4-hydroxy-3-methoxybenzyl)-11-ureidoundecanamide (40 mg, 62%) as a yellow gum: R_f 0.09 (EtOAc); ν_{max}/cm^{-1} (MeOH) 3293.3 (m)(N-H), 2921.9 (s)(C-H), 2848.0 (s)(C-H), 1639.9 (s)(C=O), 1599.9 (s)(C=O), 1277.3 (s)(C-O);

δ_H (500 MHz; MeOD) 6.89 (1H, d, *J* 1.3, H_c), 6.74-6.75 (2H, m, H_a and H_b), 4.28 (2H, s, $ArCH_2$), 3.86 (3H, s, OMe), 3.10 (1H, t, *J* 7.1, $(CH_2)_{10}NH$), 2.23 (2H, t, *J* 7.3, CH_2), 1.61-1.67 (2H, m, CH_2), 1.46-1.51 (2H, m, CH_2N), 1.29-1.36 (14H, m, $(CH_2)_7$); δ_C (125 MHz; MeOD) 176.0 (C=O), 162.4 (C=O), 149.0 (C), 146.9 (C), 131.6 (C), 121.5 (C-H_a), 116.1 (C-H_b), 112.6 (C-H_c), 56.4 (OMe), 43.9 ($ArCH_2$), 41.0 (CH_2), 37.1 (CH_2), 31.2 (CH_2), 30.63 (CH_2), 30.57 (CH_2), 30.46 (CH_2), 30.42 (CH_2), 30.2 (CH_2), 27.9 (CH_2), 27.1 (CH_2). *m/z* (ESI^+) [Found: $(M+Na)^+$ 402.2366. $C_{20}H_{33}N_3NaO_4$ requires M^+ 402.2363]; *m/z* (ES^-) 378 ($[M-H]^-$, 100%).

9.5. Synthesis of Nitroindoline-caged Glutamate

9.5.1. 1,5-Diacetylindoline **130**

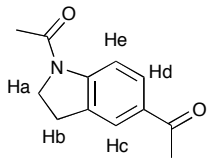

To a solution of 1-acetylindoline (16.0 g, 0.10 mol, 1.0 eq) in dry CH_2Cl_2 (70 mL) was added acetyl chloride (11.1 g, 10 mL, 0.14 mol, 1.4 eq). Anhydrous $AlCl_3$ (40 g, 0.30 mol, 3.1 eq) was added in portions with stirring leading to evolution of heat and HCl. The reaction mixture became a thick, white suspension and then became a red solution. The reaction mixture was heated at 50 °C for 4 h. The resulting dark viscous mass was poured over ice (800 mL). The organic material was extracted with CH_2Cl_2 (4 × 100 mL). The organic fractions were combined, dried over Na_2SO_4, filtered, and the solvent removed *in vacuo*. The resulting residue was crystallised from CH_2Cl_2 and hexane to afford 1,5-diacetylindoline (17.3 g, 85%) as a yellow crystalline solid: R_f 0.32 (EtOAc); mp 144-145 °C (from CH_2Cl_2/hexane) (Lit.[116] mp 146-147 °C); δ_H (300 MHz; $CDCl_3$) 8.24 (1H, d, *J* 8.3, H_e), 7.83 (1H, d, *J* 8.3, H_d), 7.81 (1H, s, H_c), 4.13 (2H, t, *J* 8.5, H_a), 3.24 (2H, t, *J* 8.5, H_b), 2.57 (3H, s, CH_3COAr), 2.26 (3H, s, CH_3CON). These data are in accordance with the literature values.[116]

9.5.2. Methyl 1-acetylindoline-5-acetate **131**

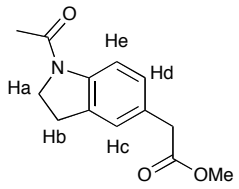

To a solution of 1,5-diacetylindoline (7.7 g, 0.04 mol, 1.0 eq) in MeOH (400 mL) containing perchloric acid (60% w/w) (12 mL) was added thallium nitrate (III) trihydrate (98%) (16.8 g, 0.04 mol, 1.0 eq). The mixture was stirred at RT for 4 h. The precipitated black solid was removed by filtration. The filtrate was concentrated *in vacuo* to 50 mL, diluted with EtOAc (400 mL) and washed with water (500 mL). The aqueous phase was extracted with EtOAc (200 mL) and the organic fractions combined, dried over Na_2SO_4, filtered and the solvent removed *in vacuo*. The resulting black residue was purified by crystallization from EtOAc and hexane to yield methyl 1-acetylindoline-5-acetate (5.3 g, 60%) as a light-brown crystalline solid: R_f 0.33 (EtOAc); mp 102-104 °C (from EtOAc/hexane) (Lit.[42] mp 104-105 °C); δ_H (300 MHz; $CDCl_3$) 8.14 (1H, d, *J* 8.1, H_e), 7.11 (1H, s, H_c), 7.08 (1H, d, *J* 8.1, H_d), 4.06 (2H, t, *J* 8.5, H_a), 3.69 (3H, s, CH_3O), 3.58 (2H, s, CH_2Ar), 3.19 (2H, t, *J* 8.5, H_b), 2.22 (3H, s, CH_3CON). These data are in accordance with the literature values.[42]

9.5.3. Methyl 1-glutarylindoline-5-acetate **132**

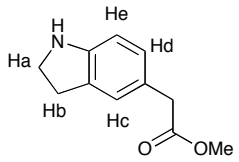

A solution of methyl 1-acetylindoline-5-acetate (534 mg, 2.291 mmol, 1.0 eq) in a mixture of MeOH (100 mL), water (20 mL) and conc. Aqueous HCl (10 mL) was heated under reflux for 4 h. The solution was diluted with water (30 mL) and concentrated *in vacuo* to 50 mL. This solution was basified to pH 8 with K_2CO_3 and extracted with EtOAc (3 × 50 mL). The organic fractions were combined, dried over Na_2SO_4, filtered and the solvent removed *in vacuo* to yield methyl 1-glutarylindoline-5-acetate (311 mg, 71%) as a brown oil: R_f 0.54 (EtOAc/hexane, 3:2); δ_H (300 MHz; $CDCl_3$) 7.04 (1H, s, H_c), 6.91 (1H, d, *J* 7.8, H_d), 6.59 (1H, d, *J* 7.8, H_e), 3.68 (3H, s, OMe), 3.55 (2H, t, *J* 8.4, H_a), 3.52 (2H, s, CH_2Ar), 3.02 (2H, t, *J* 8.4, H_b). These data are in accordance with the literature values.[42]

9.5.4. (*S*)-*tert*-Butyl 2-((*tert*-butoxycarbonyl)amino)-5-(5-(2-methoxyacetyl)indolin-1-yl)-5-oxopentanoate **133**

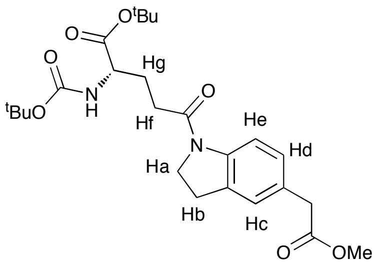

Crude 1-glutarylindoline-5-acetate (130 mg, 0.680 mmol, 1.0 eq) was dissolved in dry CH_3CN (15 mL). DMAP (216 mg, 1.769 mmol, 2.6 eq), *N*-*tert*-BOC-L-glutamic acid α-*tert*-butyl ester (217 mg, 0.714 mmol, 1.1 eq) and EDC·HCl (151 mg, 0.789 mmol, 1.2 eq) were added to this solution. The mixture was stirred at RT for 24 h and then concentrated *in vacuo*. The residue was dissolved in EtOAc (30 mL) and washed successively with 0.5 M aqueous HCl, saturated $NaHCO_3$ and brine. The organic fractions were combined, dried over Na_2SO_4, filtered and the solvent removed *in vacuo* to yield a viscous brown oil. This oil was purified by silica gel column chromatography, eluting with EtOAc and hexane (1:1), to obtain an orange oil. Trituration with Et_2O and crystallisation from EtOAc and hexane afforded *tert*-butyl 2-((*tert*-butoxycarbonyl)amino)-5-(5-(2-methoxyacetyl)indolin-1-yl)-5-oxopentanoate (107 mg, 33%) as an off-white crystalline solid: R_f 0.50 (EtOAc/hexane, 1:1); mp 78-79 °C (from EtOAc/hexane) (Lit.[42] mp 80-81 °C); δ_H (300 MHz; $CDCl_3$) 8.16 (1H, d, *J* 8.3, H_e), 7.12 (1H, s, H_c), 7.09 (1H, d, *J* 8.3, H_d), 5.23 (1H, d, *J* 7.7, NH), 4.20-4.25 (1H, m, CH^*), 4.04 (2H, 2 × t, *J* 8.5,

H_a, rotamers), 3.69 (3H, s, OMe), 3.58 (2H, s, $CH_2C{=}O$), 3.19 (2H, t, *J* 8.5, H_b), 2.43-2.58 (2H, m, H_f), 2.23-2.32 (1H, m, H_g), 1.99-2.08 (1H, m, H_g), 1.48 (9H, s, $(CH_3)_3$), 1.43 (9H, s, $(CH_3)_3$). These data are in accordance with the literature values.[42]

9.5.5. (*S*)-2-Amino-5-(5-(2-methoxyacetyl)indolin-1-yl)-5-oxopentanoic acid **134**

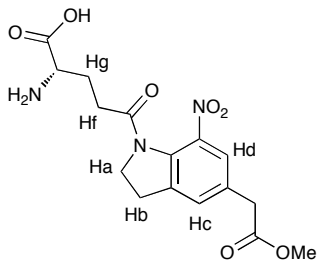

tert-Butyl 2-((*tert*-butoxycarbonyl)amino)-5-(5-(2-methoxyacetyl)indolin-1-yl)-5-oxopentanoate (103 mg, 0.216 mmol, 1.0 eq) was added to a stirred solution of sodium nitrate (20 mg, 0.238 mmol, 1.1 eq) in trifluoroacetic acid (5 mL). The mixture was stirred at RT for 4 h after which time the solution was concentrated *in vacuo*. The resulting brown residue was dissolved in water (50 mL) and adjusted to pH 6.5-7 with aqueous 1 M NaOH. The solution was washed with Et_2O and purified by reverse phase chromatography eluting with water and CH_3CN (2:1) to afford 2-amino-5-(5-(2-methoxyacetyl)indolin-1-yl)-5-oxopentanoic acid (63 mg, 75%) as a yellow solid: R_f 0.61 (reverse phase, CH_3CN/water, 1:1); $[\alpha]_D^{25}$ +144 (*c* 0.013 in DMSO); mp 123-126 °C (from MeOH/Et_2O); δ_H (300 MHz; D_2O) 7.60 (1H, s, H_d), 7.52 (1H, s, H_c), 4.29 (2H, t, *J* 8.0, H_a), 3.79 (2H, s, $CH_2C{=}O$), 3.76 (1H, t, *J* 6.2, CH^*), 3.70 (3H, s, OMe),

3.22 (2H, t, *J* 8.0, H_b), 2.77 (2H, t, *J* 7.5, H_f), 2.12-2.18 (2H, m, H_g). *m/z* (ES^-) [Found: $(M-H)^-$ 364.1155. $C_{16}H_{18}N_3O_7$ requires M^+ 364.1150]; *m/z* (ES^-) 364 ($[M-H]^-$, 100%). These data are in accordance with the literature values.[42]

9.6. Synthesis of Caged Lidocaine Derivatives

9.6.1. 4,5-Dimethoxy-2-nitrobenzaldehyde **141**

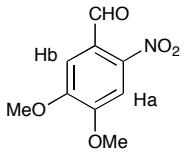

Method A:

A solution of 4,5-dimethoxy-2-nitrobenzyl bromide (2.00 g, 7.24 mmol, 1.1 eq) and bis(tetrabutylammonium) dichromate (4.62 g, 6.59 mmol, 1.0 eq) in CH_2Cl_2 (15 mL) was heated under reflux overnight. The reaction mixture was cooled in an ice bath and filtered through a pad of silica gel to eliminate the inorganic and tetrabutylammonium salts. The silica gel was then washed with Et_2O (100 mL) and the solvent removed *in vacuo*. The residue was purified by silica gel column chromatography, eluting with EtOAc and petroleum ether (7:3), to afford 4,5-dimethoxy-2-nitrobenzaldehyde (1.13 g, 74%) as a yellow solid.

Method B:

To a solution of 4,5-dimethoxy-2-nitrobenzyl bromide (2.28 g, 8.29 mmol, 1.0 eq) in anhydrous DMSO (20 mL) was added anhydrous Na_2CO_3 (2.19 g, 20.65 mmol, 2.5 eq). The reaction mixture was left sirring at 70 °C overnight.

The reaction mixture was partitioned between CH_2Cl_2 (3 × 100 mL) and water (200 mL). The organic fractions were combined, dried over anhydrous Na_2SO_4, filtered and the solvent removed *in vacuo***.** The residue was purified by crystallization from EtOAc and hexane to afford 4,5-dimethoxy-2-nitrobenzaldehyde (1.74 g, 64%) as a yellow solid.

Method C:

To a solution of 4,5-dimethoxy-2-nitrobenzyl alcohol (500 mg, 2.35 mmol, 1.0 eq) in CH_2Cl_2 (10 mL) was added Dess Martin Periodinane (1.49 g, 3.52 mmol, 1.5 eq). The reaction mixture was left stirring at RT for 20 min after which time TLC analysis indicated that the reaction was complete. Et_2O (10 mL), saturated $NaHCO_3$ (10 mL) and sodium thiosulfate (8.95 g, six times the mass of Dess Martin Periodinane) were added to the reaction and the resulting solution stirred for 30 min. After this time the organic layer was collected and the aqueous layer extracted with Et_2O (3 × 80 mL). The organic fractions were combined, washed with a saturated aqueous solution of $NaHCO_3$ (50 mL) followed by water (50 mL). The organic material was dried over anhydrous Na_2SO_4, filtered and the solvent removed *in vacuo* to afford 4,5-dimethoxy-2-nitrobenzaldehyde (211 mg, 98%) as a yellow solid: R_f 0.38 (EtOAc/petroleum ether, 3:7); mp 130-131 °C (from MeOH/water) (Lit.[172] mp 129-131°C); δ_H (300 MHz; $CDCl_3$) 10.45 (1H, s, CHO), 7.62 (1H, s, H_a), 7.43 (1H, s, H_b), 4.04 (3H, s, OMe), 4.03 (3H, s, OMe). *m/z* (ES^+) [Found: $(M+NH_4)^+$ 229.0821. $C_9H_{13}N_2O_5$ requires M^+ 229.0819]; *m/z* (CI^+) 229

([M+NH_4]$^+$, 63%), 199 ([M-OMe+NH_4]$^+$, 100%). These data are in accordance with the literature values.[172,173]

9.6.2. (4,5-Dimethoxy-2-nitrobenzylidene)-2,6-dimethylaniline **147**

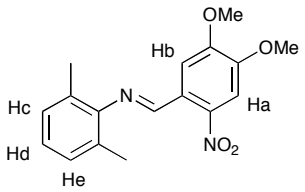

Method A:

4,5-Dimethoxy-2-nitrobenzaldehyde (100 mg, 0.47 mmol, 1.0 eq) and 2,6-dimethylaniline (128 mg, 130 µL, 1.06 mmol, 2.3 eq) were heated together at 100 ºC for 3 h. The yellow benzaldehyde turned orange-red upon addition of dimethylaniline. After 3 h at 100 ºC, the orange-red liquid reaction mixture had solidified to form a grey-orange solid. This solid was allowed to cool to RT. A solution of $NaCNBH_3$ (30 mg, 0.47 mmol, 1.0 eq) in MeOH (0.5 mL) was added to the solid. THF (1.5 mL) was added to improve the solubility of the solid. The solid dissolved to form an orange solution, which was left stirring at RT under N_2 overnight. TLC analysis confirmed that the aldehyde starting material had been consumed. The reaction was taken up in aqueous NaOH solution (10 mL, 0.1 M). The volatile solvents were removed *in vacuo*. The organic material was extracted with CH_2Cl_2 (3 × 80 mL). The organic fractions were combined, dried over anhydrous Na_2SO_4, filtered and the solvent removed *in vacuo* to yield a yellow solid. ^{1}H NMR indicated that the product

obtained was the imine, (4,5-dimethoxy-2-nitrobenzylidene)-2,6-dimethylaniline. Reduction to the amine had not occured. (4,5-Dimethoxy-2-nitrobenzylidene)-2,6-dimethylaniline (148 mg, 100%) was obtained as an orange solid.

Method B:

To a solution of 4,5-dimethoxy-2-nitrobenzaldehyde (280 mg, 1.33 mmol, 1.0 eq) in dry CH_2Cl_2 (5 mL) with 4 Å molecular sieves was added 2,6-dimethylaniline (241 mg, 245 µL, 1.99 mmol, 1.5 eq) and $Ga(OTf)_3$ (69 mg, 0.13 mmol, 0.1 eq). The reaction was left stirring at RT under N_2 overnight. After this time, the aldehyde starting material had been consumed as confirmed by TLC analysis. The reaction mixture was partitioned between CH_2Cl_2 (2 × 50 mL) and water (100 mL). The organic fractions were combined, dried over anhydrous Na_2SO_4, filtered and the solvent removed *in vacuo***.** The resulting residue was purified by silica gel column chromatography eluting with EtOAc and hexane (2:98 → 5:95), to afford (4,5-dimethoxy-2-nitrobenzylidene)-2,6-dimethylaniline (313 mg, 75%) as a yellow solid: R_f 0.29 (EtOAc/hexane, 2:8); mp 137-139 ºC (from EtOAc/hexane); (Found: C, 64.94; H, 5.83; N, 8.91. $C_{17}H_{18}N_2O_4$ requires C, 64.96; H, 5.77; N, 8.91); ν_{max}/cm^{-1} ($CHCl_3$) 2918.4 (m)(C-H), 1685.2 (m)(C=N), 1573.4 (m), 1517.9 (s)(NO_2), 1332.7 (m), 1281.7 (s) (NO_2), 1223.3 (m), 1063.3 (m)(C-O); δ_H (300 MHz; $CDCl_3$) 8.73 (1H, s, N=CH), 7.82 (1H, s, H_a), 7.65 (1H, s, H_b), 7.08 (2H, d, *J* 6.6, H_c, H_e), 6.99 (1H, dd, *J* 6.6, *J* 6.6, H_d), 4.07 (3H, s, OMe), 4.03 (3H, s, OMe), 2.20 (6H, s, 2 × Ar-Me); δ_C (75.5 MHz; $CDCl_3$) 159.0

(N=C), 153.3 (C), 150.7 (COMe), 150.4 (COMe), 142.5 (C), 128.2 (C-H_c, H_e), 127.1 (C), 125.9 (C), 124.2 (C-H_d), 109.7 (C-H_a), 107.3 (C-H_b), 56.6 (2 × OMe), 18.3 (Me). *m/z* (ES^+) [Found: $(M+H)^+$ 315.1339. $C_{17}H_{19}N_2O_4$ requires M^+ 315.1339]; *m/z* (CI^+) 315 ($[M+H]^+$, 10%), 122 (100%).

9.6.3. *N*-(4,5-Dimethoxy-2-nitrobenzyl)-2,6-dimethylaniline **139**

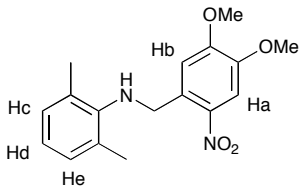

(4,5-Dimethoxy-2-nitrobenzylidene)-2,6-dimethylaniline (600 mg, 1.91 mmol, 1.0 eq) was added to a solution of $NaBH_4$ (434 mg, 11.46 mmol, 6.0 eq) in acetic acid (5 mL). The orange reaction mixture was left stirring at RT overnight. ^1H NMR of an aliquot confirmed that reduction of the imine had occurred. The reaction mixture was taken up in aqueous NaOH solution (30 mL, 0.1 M). The organic material was extracted with CH_2Cl_2 (3 × 80 mL). The organic fractions were combined, dried over anhydrous Na_2SO_4, filtered and the solvent removed *in vacuo*. The orange residue was purified by silica gel column chromatography, eluting with EtOAc and hexane (1:9), to afford *N*-(4,5-dimethoxy-2-nitrobenzyl)-2,6-dimethylaniline (589 mg, 97%) as a yellow solid: R_f 0.19 (EtOAc/hexane, 2:8); mp 105-106 ºC (from EtOAc/hexane); ν_{max}/cm^{-1} ($CHCl_3$) 3381.4 (m)(N-H), 3007.1 (m)(Ar-H), 2938.4 (s)(C-H), 2851.5 (m)(C-H), 1614.0 (m), 1580.3 (s), 1521.4 (s)(NO_2), 1474.0 (s), 1396.1 (m), 1363.0 (s), 1329.5 (s)(NO_2), 1236.4 (s), 1200.6 (s), 1097.2 (m)(C-O), 1061.9

(s)(C-O), 753.4 (s)(three adj. Ar-H); δ_H (300 MHz; $CDCl_3$) 7.63 (1H, s, H_a), 6.99 (2H, d, *J* 7.5, H_c, H_e), 6.84 (1H, dd, *J* 7.5, *J* 7.5, H_d), 6.80 (1H, s, H_b), 4.36 (2H, s, $NHCH_2$), 3.94 (3H, s, OMe), 3.86 (1H, s, NH), 3.78 (3H, s, OMe), 2.21 (6H, s, 2 × Me); δ_C (75.5 MHz; $CDCl_3$) 153.0 (C), 147.8 (C), 145.0 (C), 140.7 (C), 130.8 (C), 130.3 (C), 128.9 (C-H_c, C-H_e), 122.6 (C-H_d), 112.4 (C-H_b), 108.0 (C-H_a), 56.4 (OMe), 56.3 (OMe), 49.6 ($NHCH_2$), 18.4 (Me). *m/z* (ES^+) [Found: $(M+H)^+$ 317.1491. $C_{17}H_{21}N_2O_4$ requires M^+ 317.1496]; *m/z* (Cl^+) 122 ($[M\text{-}CHAr(OMe)_2(NO_2)+H]^+$, 100%).

9.6.4. 2-(Diethylamino)acetic acid **143**

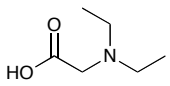

Diethylaminoacetonitrile (5.00 g, 44.58 mmol, 1.0 eq) was added to 25% w/v aqueous NaOH solution (10 mL). THF (5 mL) was added to improve the miscibility of the reaction mixture. The reaction mixture was heated to 90°C for 48 h. After TLC analysis confirmed that the starting material had been consumed, the reaction mixture was cooled to RT. Aqueous HCl (37%) was added to the reaction mixture until a pH of 5 had been reached. The product was freeze-dried to obtain 2-(diethylamino)acetic acid and sodium chloride. δ_H (300 MHz; D_2O) 3.75 (1H, s, CH_2), 3.23 (4H, q, *J* 7.3, $N(CH_2)_2$), 1.24 (6H, t, *J* 7.3, 2 × CH_3); δ_C (75 MHz; MeOD) 56.3 (CH_2), 50.3 (2 × CH_2), 9.75 (2 × CH_3). *m/z* (ES^-) 130 ($[M-H]^-$, 100%).

9.6.5. 2-Chloro-*N*-(4,5-dimethoxy-2-nitrobenzyl)-*N*-(2,6-dimethylphenyl) acetamide **149**

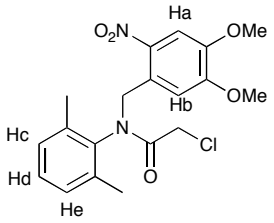

A solution of *N*-(4,5-dimethoxy-2-nitrobenzyl)-2,6-dimethylaniline (220 mg, 0.70 mmol, 1.0 eq) and chloroacetal chloride (166 µL, 236 mg, 2.09 mmol, 3.0 eq) in toluene (10 mL) was heated to 100 °C for 3 h. After TLC analysis confirmed that the starting material had been consumed, the toluene and excess chloroacetal chloride were removed *in vacuo*. The residue was partitioned between CH_2Cl_2 (2 × 50 mL) and water (100 mL). The organic fractions were combined, dried over anhydrous Na_2SO_4, filtered and the solvent removed *in vacuo***.** The residue was purified by crystallisation from EtOAc and hexane to yield 2-chloro-*N*-(4,5-dimethoxy-2-nitrobenzyl)-*N*-(2,6-dimethylphenyl)acetamide (210 mg, 77%) as a yellow solid: R_f 0.48 (EtOAc/hexane, 1:1); mp 144-146 ºC (from EtOAc/hexane); (Found: C, 58.18; H, 5.37; N, 7.10. $C_{19}H_{21}ClN_2O_5$ requires C, 58.09; H, 5.39; N, 7.13); ν_{max}/cm^{-1} ($CHCl_3$) 3013.3 (w)(Ar-H), 2939.8 (m)(C-H), 1671.0 (vs)(C=O), 1522.6 (vs)(NO_2), 1333.0 (s)(NO_2), 1064.5 (s)(C-O), 914.3 (m)(Ar-H), 731.0 (s)(three adj. Ar-H); δ_H (400 MHz; $CDCl_3$) 7.41 (1H, s, H_a), 7.37 (1H, s, H_b), 7.19 (1H, dd, *J* 7.5, 7.5, H_d), 7.07 (2H, d, *J* 7.5, H_c, H_e), 5.28 (2H, s, CH_2Ar), 3.98 (3H, s, OMe), 3.92 (3H, s, OMe), 3.71 (2H, s, CH_2Cl), 1.96 (6H, s, 2 × Me); δ_C (100 MHz; $CDCl_3$) 167.4 (C=O), 153.0 (C), 148.4 (C), 142.0 (C), 137.9 (C),

136.0 (C), 129.6 (C-H_c, C-H_e), 129.1 (C-H_d), 125.7 (C), 114.8 (C-H_b), 107.6 (C-H_a), 56.7 (OMe), 56.4 (OMe), 47.1 (CH_2Ar), 41.9 (CH_2Cl), 17.9 (Me). *m/z* (ES^+) [Found: ($^{35}M+H)^+$ 393.1214. $C_{19}H_{22}N_2O_5{}^{35}Cl$ requires M^+ 393.1212]; *m/z* (ES^+) 395 ($^{37}[M+H]^+$, 35%), 393 ($^{35}[M+H]^+$, 100%).

9.6.6. 2-(Diethylamino)-*N*-(4,5-dimethoxy-2-nitrobenzyl)-*N*-(2,6-dimethylphenyl)acetamide **138**

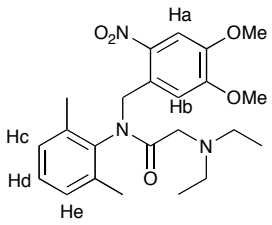

2-Chloro-*N*-(4,5-dimethoxy-2-nitrobenzyl)-*N*-(2,6-dimethylphenyl)acetamide (210 mg, 0.54 mmol, 1.0 eq) was suspended in $HNEt_2$ (8.35 mL, 5.88 g, 80.33 mmol, 150 eq). Dry DMF (1 mL) was added to form a homogenous solution. TBAI (5 mg) was added to this solution and the reaction stirred at 60 °C for 18 h. After this time TLC analysis indicated that the reaction was complete. The $HNEt_2$ and DMF were removed *in vacuo*. The residue was partitioned between CH_2Cl_2 (2 × 50 mL) and water (100 mL). The organic fractions were combined, dried over anhydrous Na_2SO_4, filtered and the solvent removed *in vacuo*. The resulting brown residue was purified by silica gel column chromatography, eluting with EtOAc and hexane (4:6), followed by crystallisation from EtOAc and hexane to afford 2-(diethylamino)-*N*-(4,5-dimethoxy-nitrobenzyl)-*N*-(2,6-dimethylphenyl)acetamide (191 mg, 83%) as a yellow solid: R_f 0.31 (EtOAc); mp 138-139 ºC (from EtOAc/hexane); (Found:

C, 64.33; H, 7.04; N, 9.66. $C_{23}H_{31}N_3O_5$ requires C, 64.32; H, 7.27; N, 9.78); ν_{max}/cm^{-1} ($CHCl_3$) 2966.2 (m)(Ar-H), 2926.0 (m)(C-H), 1652.3 (s)(C=O), 1521.8 (s)(NO_2), 1273.6 (s)(NO_2), 1229.7 (s), 1064.0 (m)(C-O), 797.0 (m)(three adj. Ar-H); δ_H (400 MHz; $CDCl_3$) 7.40 (1H, s, H_a), 7.35 (1H, s, H_b), 7.13 (1H, dd, *J* 7.5, 7.5, H_d), 7.03 (2H, d, *J* 7.5, H_c, H_e), 5.21 (2H, s, CH_2Ar), 3.94 (3H, s, OMe), 3.89 (3H, s, OMe), 2.81 (2H, s, $CH_2C{=}O$), 2.52 (4H, q, *J* 7.2, 2 × CH_2N), 1.91 (6H, s, 2 × CH_3Ar), 0.89 (6H, t, *J* 7.2, 2 × CH_3); δ_C (100 MHz; $CDCl_3$) 171.6 (C=O), 152.8 (C), 148.1 (C), 142.1 (C), 138.6 (C), 135.9 (C), 129.2 (C-H_c, C-H_e), 128.4 (C-H_d), 126.6 (C), 114.9 (C-H_a), 107.4 (C-H_b), 56.6 (OMe), 56.3 (OMe), 54.7 ($CH_2C{=}O$), 47.5 ($N(CH_2CH_3)_3$), 46.1 (CH_2Ar), 17.9 (CH_3Ar), 11.9 ($N(CH_2CH_3)_3$). *m/z* (ES^+) [Found: $(M+H)^+$ 430.2340. $C_{23}H_{32}N_3O_5$ requires M^+ 430.2336]; *m/z* (EI^+) 429 ($[M]^+$, 55%), 399 ($[M\text{-}OMe]^+$, 65%), 284 (100%).

9.6.7. 2-((4,5-Dimethoxy-2-nitrobenzyl)(2,6-dimethylphenyl)amino)-*N*,*N*,*N*-triethyl-2-oxoethanaminium **150**

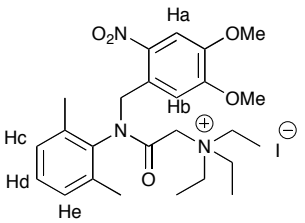

Iodoethane (272 mg, 141 μL, 1.75 mmol, 15.0 eq) was added to a solution of 2-(diethylamino)-*N*-(4,5-dimethoxy-nitrobenzyl)-*N*-(2,6-dimethylphenyl)acetamide (50 mg, 0.17 mmol, 1.0 eq) in CH_3CN (5 mL). The reaction mixture was stirred at RT for 120 h. The CH_3CN and iodoethane were removed *in vacuo*. The residue was partitioned between cyclohexane (50 mL) and water (100 mL). The aqueous layer was collected and lyophilised. The resulting solid was purified by reverse phase silica gel chromatography, eluting with MeOH and water (1:3), to afford 2-((4,5-dimethoxy-2-nitrobenzyl)(2,6-dimethylphenyl)amino)-*N*,*N*,*N*-triethyl-2-oxoethanaminium (48 mg, 62%) as a yellow solid: R_f 0.36 (MeOH/CH_2Cl_2, 1:9); mp 113-116 ºC (from MeOH/Et_2O); ν_{max}/cm^{-1} ($CHCl_3$) 2923.8 (s)(Ar-H), 2853.6 (m)(C-H), 1652.9 (s)(C=O), 1520.7 (s)(NO_2), 1276.5 (s)(NO_2), 1063.7 (m)(C-O), 798.2 (m)(three adj. Ar-H); δ_H (400 MHz; D_2O) 7.60 (1H, s, H_a), 7.29 (1H, dd, *J* 7.5, 7.5, H_d), 7.17 (2H, d, *J* 7.5, H_c, H_e), 6.52 (1H, s, H_b), 5.18 (2H, s, CH_2Ar), 3.88 (3H, s, OMe), 3.63 (3H, s, OMe), 3.56 (6H, q, *J* 7.3, 3 × CH_2N), 3.54 (2H, s, CH_2C=O), 1.91 (6H, s, 2 × CH_3Ar), 1.19 (9H, t, *J* 7.2, 3 × CH_3); δ_C (125 MHz; MeOD) 164.7 (C=O), 154.1 (C), 150.6 (C), 144.2 (C),

137.9 (C), 136.6 (C), 131.1 (C-H_c, C-H_e), 130.9 (C-H_d), 124.6 (C), 116.7 (C-H_b), 109.1 (C-H_a), 56.9 (OMe), 56.8 (OMe), 55.43 (CH_2C=O), 55.41 (N(CH_2CH_3)$_3$), 47.6 (CH_2Ar), 17.9 (CH_3Ar), 8.2 (N(CH_2CH_3)$_3$). *m/z* (ES^+) [Found: $(M-I)^+$ 458.2656. $C_{25}H_{36}N_3O_5$ requires M^+ 458.2649]; *m/z* (ES^+) 458 ($[M-I]^+$, 100%).

9.6.8. 2-Chloro-*N*-(2,6-dimethylphenyl)acetamide **155**

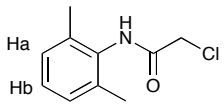

To a solution of 2,6-dimethylaniline (0.49 g, 0.5 mL, 4.06 mmol, 1.0 eq) and dry pyridine (0.64 g, 0.66 mL, 8.12 mmol, 2.0 eq) in dry CH_2Cl_2 (15 mL) was added chloroacetyl chloride (0.92 g, 0.65 mL, 8.12 mmol, 2.0 eq) at 0 °C. The resulting solution was stirred at RT overnight. After this time TLC analysis indicated that the reaction was complete and so the solvent was removed *in vacuo*. The residue was partitioned between water (100 mL) and CH_2Cl_2 (100 mL). The organic fractions were combined, dried over Na_2SO_4, filtered and concentrated *in vacuo*. The residue was purified by silica gel column chromatography, eluting with EtOAc and petroleum ether (2.5:7.5), to afford 2-chloro-*N*-(2,6-dimethylphenyl)acetamide (0.8 g, quantitative) as colourless solid: R_f 0.53 (EtOAc/petroleum ether, 1:1); (Found C, 60.83; H, 6.17; N, 7.03. $C_{10}H_{12}ClNO$ requires C, 60.76; H, 6.12; N, 7.09); mp 120-122 °C (from EtOAc/hexane); ν_{max}/cm^{-1} ($CHCl_3$) 3212.4 (m)(N-H), 2921.3 (m)(C-H), 1680.8 (s)(C=O); δ_H (400 MHz; $CDCl_3$) 7.15 (1H, dd, *J* 8.9, 8.9, H_b), 7.10 (2H, d,

J 8.9, H_a), 4.24 (2H, s, CH_2), 2.24 (6H, s, 2 × CH_3Ar); δ_C (100 MHz; $CDCl_3$) 164.4 (C=O), 135.3 (C), 132.7 (C), 128.4 (C-H), 127.9 (C-H), 42.8 (CH_2), 18.3 (CH_3Ar). *m/z* (ESI^+) [Found: $(M+Na)^+$ 220.0496. $C_{10}H_{12}ClNONa$ requires M^+ 220.0500]; *m/z* (ES^-) 196 ($[M-H]^-$, 100%).

9.6.9. *N*-(2,6-Dimethylphenyl)-2-(ethylamino)acetamide **154**

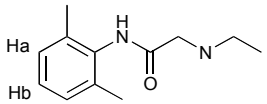

To a solution of H_2NEt in THF (20 mL, 2 M solution) was added 2-chloro-*N*-(2,6-dimethylphenyl)acetamide (300 mg, 1.518 mmol, 1.0 eq). The reaction mixture was stirred at RT for 48 h. After this time TLC analysis indicated that the reaction was complete. The solvent was removed *in vacuo* and the residue partitioned between water (100 mL) and CH_2Cl_2 (2 × 100 mL). The organic fractions were combined, dried over Na_2SO_4, filtered and concentrated *in vacuo*. However, ^1H NMR analysis revealed that the product was not observed in the organic layer. The aqueous fraction was lyophilised and the residue purified by reverse phase silica gel chromatography, eluting with CH_3CN and water (1:4), to afford *N*-(2,6-dimethylphenyl)-2-(ethylamino)acetamide (160 mg, 52%) as a colourless solid: Mp 155 ºC dec. (from MeOH/Et_2O); ν_{max}/cm^{-1} (KBr) 3268.2 (m)(N-H), 2962.3 (s)(Ar-H), 2838.4 (m)(C-H), 1671.3 (s)(C=O); δ_H (400 MHz; D_2O) 7.25 (1H, dd, *J* 7.4, 7.4, H_b), 7.20 (2H, d, *J* 7.4, H_a), 4.19 (2H, s, $C(O)CH_2$), 3.22 (2H, q, *J* 7.3, NCH_2), 2.19 (6H, s, 2 × $ArCH_3$), 1.35 (3H, t, *J* 7.3, CH_3); δ_C (100 MHz; D_2O) 165.4 (C=O),

135.9 (C), 132.1 (C), 128.4 (C-H_b), 128.2 (C-H_a), 47.2 ($C(O)CH_2$), 43.0 ($N(\mathit{C}H_2CH_3)_3$), 17.1 ($ArCH_3$), 10.4 ($N(CH_2\mathit{C}H_3)_3$). *m/z* (ESI^+) [Found: $(M+H)^+$ 207.1495. $C_{12}H_{19}N_2O$ requires M^+ 207.1492]; *m/z* (ES^+) 265 ($[M+(CH_3CN{\cdot}NH_4)]^+$, 100%).

9.6.10. 4,5-Dimethoxy-2-nitrobenzyl 2-(2,6-dimethylphenylamino)-2-oxoethyl(ethyl)carbamate **153**

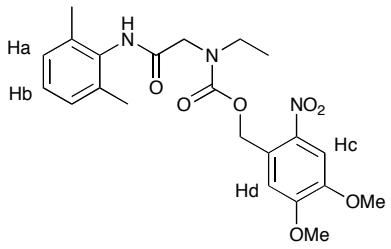

A stirred solution of *N*-(2,6-dimethylphenyl)-2-(ethylamino)acetamide (50 mg, 0.243 mmol, 1.0 eq) in CH_2Cl_2 (5 mL) was cooled to 0 °C. NEt_3 (74 mg, 102 µL, 0.729 mmol, 3.0 eq) was added and the solution stirred at 0 °C for 30 min. 4,5-Dimethoxy-2-nitrobenzyl chloroformate (74 mg, 0.267 mmol, 1.1 eq) was added and the reaction solution stirred at RT overnight. The reaction mixture was partitioned between water (100 mL) and CH_2Cl_2 (2 × 100 mL). The organic fractions were combined, dried over $MgSO_4$, filtered and concentrated *in vacuo*. Purification of the residue by silica gel column chromatography, eluting with EtOAc and petroleum ether (4.5:5.5) afforded 4,5-dimethoxy-2-nitrobenzyl 2-(2,6-dimethylphenylamino)-2-oxoethyl(ethyl)carbamate (38 mg, 35%) as a yellow solid: R_f 0.25 (EtOAc/petroleum ether, 1:1); (Found C, 59.39; H, 5.97; N, 9.36. $C_{22}H_{27}N_3O_7$ requires C, 59.32; H, 6.11; N, 9.43);

mp 75-77 °C (from $CHCl_3$); ν_{max}/cm^{-1} ($CHCl_3$) 2980.2 (m)(Ar-H), 2935.6 (m)(C-H), 1691.4 (s)(C=O), 1585.4 (s)(NO_2), 1368.9 (s)(NO_2), 1163.6 (s)(C-O); δ_H (500 MHz; D_6-DMSO, 363 K) 9.09 (1H, s, NH), 7.70 (1H, s, H_c), 7.18 (1H, s, H_d), 7.04-7.07 (3H, m, H_a and H_b), 5.43 (2H, s, $ArCH_2$), 4.14 (2H, s, $C(O)CH_2N$), 3.89 (3H, s, OMe), 3.83 (3H, s, OMe), 3.43 (2H, q, *J* 6.9, NCH_2), 2.10 (6H, s, 2 × $ArCH_3$), 1.17 (3H, t, *J* 6.9, CH_3); δ_C (125 MHz; D_6-DMSO, 298 K, two conformers observed) 167.4 & 167.0 (C=O), 155.2 & 154.9 (N(C=O)O), 153.5 & 153.3 (C), 147.7 & 147.6 (C), 139.3 & 138.9 (C), 135.2 & 135.1 (C), 134.8 & 134.7 (C), 128.1 (C-H), 127.6 (2 × C-H), 127.4 (C-H), 126.5 & 126.4 (C), 110.4 & 110.1 (C-H_d), 108.2 & 108.0 (C-H_c), 63.5 & 63.3 (OCH_2), 56.2 & 56.1 & 56.0 (OMe), 49.7 & 49.2 ($C(O)CH_2$), 43.5 & 42.9 ($N(CH_2CH_3)_3$), 18.1 & 17.9 ($ArCH_3$), 13.5 & 13.0 ($N(CH_2CH_3)_3$). *m/z* (ESI^+) [Found: $(M+Na)^+$ 468.1742. $C_{22}H_{27}N_3O_7Na$ requires M^+ 468.1741]; *m/z* (ES^+) 913 (100%), 468 ($[M+Na]^+$, 70%).

9.6.11. 1-(Dibenzo[*b*,*d*]furan-2-yl)-2-((2,6-dimethylphenyl)amino)ethanone **159**

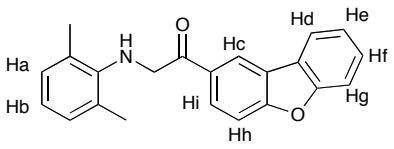

2-Bromo-1-(dibenzo[*b*,*d*]furan-2-yl)ethanone (200 mg, 0.692 mmol, 1.0 eq), 2,6-dimethylaniline (101 mg, 102 μL, 0.830 mmol, 1.2 eq) and Na_2CO_3 (147 mg, 1.384 mmol, 2.0 eq) were dissolved in 1,3-dimethyltetrahydro-2(1H)-pyrimidinone (DMPU) (5mL). The reaction mixture was heated to 100 ° C for 3.5 h. After this time the reaction was adjudged complete by TLC. The reaction solution was partitioned between water (200 mL) and EtOAc (2 × 150 mL). The organic extracts were combined, dried over Na_2SO_4, filtered, and the solvent removed *in vacuo*. The resulting residue was purified by silica gel column chromatography, eluting with EtOAc and petroleum ether (2:8), to afford 1-(dibenzo[*b*,*d*]furan-2-yl)-2-((2,6-dimethylphenyl)amino)ethanone (121 mg, 53%) as a yellow solid: R_f 0.74 (EtOAc/petroleum ether, 1:1); (Found C, 80.29; H, 5.80; N, 4.16. $C_{22}H_{19}NO_2$ requires C, 80.22; H, 5.81; N, 4.25); mp 205-208 °C (from $CHCl_3$); ν_{max}/cm^{-1} ($CHCl_3$) 1681.9 (s)(C=O), 1197.9 (s)(C-O); δ_H (500 MHz; $CDCl_3$) 8.59 (1H, d, *J* 1.8, H_c), 8.09 (1H, dd, *J* 8.8, 1.8, H_i), 8.02 (1H, dd, *J* 7.3, 1.3, H_d), 7.61-7.65 (2H, m, H_h, H_g), 7.51-7.56 (1H, m, H_f), 7.40-7.44 (1H, m, H_e), 7.05 (2H, d, *J* 7.5, H_a), 6.86 (1H, dd, *J* 7.5, 7.5, H_b), 4.68 (2H, s, CH_2), 2.44 (6H, s, 2 × $ArCH_3$); δ_C (125 MHz; $CDCl_3$) 195.9 (C=O), 159.2 (C), 156.9 (C), 146.5 (C), 130.2 (C), 128.9 (C-H_a), 128.7 (C), 128.2 (C-H_f), 127.1 (C-H_i), 124.8 (C), 123.5 (C & C-H_e), 121.7 (C-H_b), 121.00 (C-H_d),

120.97 (C-H_c), 111.99 & 111.95 (C-H_h, C-H_g), 55.3 (OCH_2), 19.0 ($ArCH_3$). *m/z* (ESI^+) [Found: $(M+Na)^+$ 352.1307. $C_{22}H_{19}NO_2Na$ requires M^+ 352.1308]; *m/z* (ES^+) 681 (100%), 352 ($[M+Na]^+$, 70%), 330 ($[M+H]^+$, 50%),

9.6.12. 2-Chloro-*N*-(2-(dibenzo[*b*,*d*]furan-2-yl)-2-oxoethyl)-*N*-(2,6-dimethylphenyl)acetamide **160**

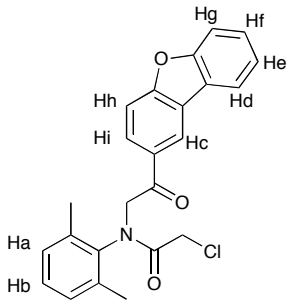

A solution of 1-(dibenzo[*b*,*d*]furan-2-yl)-2-((2,6-dimethylphenyl)amino)ethanone (100 mg, 0.304 mmol, 1.0 eq) and dry pyridine (48 mg, 49 μL, 0.608 mmol, 2.0 eq) in dry CH_2Cl_2 (5 mL) was cooled to 0 °C. Chloroacetal chloride (69 mg, 48 μL, 0.608 mmol, 2.0 eq) was added to the reaction mixture dropwise. The reaction was left stirring at RT overnight, covered in foil. After this time the reaction was adjudged complete by TLC. The solvent was removed *in vacuo* and the residue partitioned between water (100 mL) and CH_2Cl_2 (2 × 100 mL). The organic fractions were combined, dried over Na_2SO_4, filtered and concentrated *in vacuo*. This residue was purified by silica gel column chromatography, eluting with EtOAc and petroleum ether (2:8), to afford 2-chloro-*N*-(2-(dibenzo[*b*,*d*]furan-2-yl)-2-oxoethyl)-*N*-(2,6-dimethylphenyl)acetamide (30 mg, 22%) as a yellow oil: R_f

0.66 (EtOAc/petroleum ether, 1:1); ν_{max}/cm^{-1} ($CHCl_3$) 2960.2 (m)(C-H), 1701.9 (s)(C=O), 1671.5 (s)(C=O), 1196.8 (s)(C-O); δ_H (500 MHz; $CDCl_3$) 8.63 (1H, d, *J* 1.8, H_c), 8.12 (1H, dd, *J* 8.7, 1.8, H_i), 7.99-8.01 (1H, m, H_d), 7.59-7.62 (2H, m, H_h, H_g), 7.50-7.53 (1H, m, H_f), 7.38-7.42 (1H, m, H_e), 7.23 (1H, dd, *J* 7.5, 7.5, H_b), 7.18 (2H, d, *J* 7.5, H_a), 5.01 (2H, s, NCH_2), 3.87 (2H, s, CH_2Cl), 2.44 (6H, s, 2 × $ArCH_3$); δ_C (125 MHz; $CDCl_3$) 191.3 (C=O), 167.1 (NC=O), 159.1 (C), 156.9 (C), 139.7 (C), 136.7 (C), 130.7 (C), 129.6 (C-H_a), 129.1 (C-H_b), 128.1 (C-H_f), 127.6 (C-H_i), 124.7 (C), 123.6 (C), 123.5 (C-H_e), 121.5 (C-H_c), 121.0 (C-H_d), 112.0 & 111.8 (C-H_h, C-H_g), 55.7 (NCH_2), 41.2 (CH_2Cl), 18.5 ($ArCH_3$). *m/z* (ESI^+) [Found: $(M+Na)^+$ 428.1027. $C_{24}H_{20}NClO_3Na$ requires M^+ 428.1024]; *m/z* (ES^+) 833 (100%), 428 ($[M+Na]^+$, 65%).

9.7. Synthesis of Potential New Caging Groups

9.7.1. 1-(Dibenzo[*b*,*d*]furan-2-yl)ethanone **157**

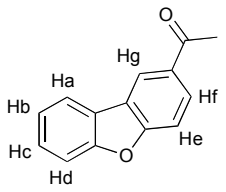

To a solution of dibenzofuran (1.8 g, 10.70 mmol, 1.0 eq) in dry CH_2Cl_2 (20 mL) at 0 °C was added anhydrous $AlCl_3$ (3.1 g, 23.54 mmol, 2.2 eq). Acetic anhydride (1.2 g, 1.11 mL, 11.77 mmol, 1.1 eq) was added slowly with stirring. The reaction mixture was stirred at RT overnight. After this time TLC analysis indicated that the reaction was complete. The dark viscous mass was poured over ice (50 mL) and extracted with CH_2Cl_2 (2 × 50 mL). The organic fractions were combined, dried over Na_2SO_4, filtered, and the solvent removed *in vacuo*. The residue was purified by silica gel column chromatography, eluting with EtOAc and petroleum ether (1.5:8.5), to afford 1-(dibenzo[*b*,*d*]furan-2-yl)ethanone (0.99 g, 44%) as a colourless solid: R_f 0.64 (EtOAc/petroleum ether, 1:1); mp 70-72 °C (from EtOAc/petroleum ether); δ_H (400 MHz; $CDCl_3$) 8.54 (1H, d, *J* 1.8, H_g), 8.07 (1H, dd, *J* 8.6, 1.8, H_f), 7.94-7.98 (1H, m, H_a), 7.54-7.58 (2H, m, H_e, H_d), 7.49 (1H, ddd, *J* 8.4, 7.8, 1.3, H_c), 7.35-7.39 (1H, m, H_b), 2.70 (3H, s, CH_3); δ_C (100 MHz; $CDCl_3$) 197.4 (C=O), 158.9 (C), 156.9 (C), 132.5 (C), 124.6 (C), 123.7 (C), 127.99 (C-H_c), 127.96 (C-H_f), 123.4 (C-H_b), 121.6 (C-H_g), 120.9 (C-H_a), 111.9 and 111.6 (C-H_e, C-

H_d), 27.2 (CH_3). *m/z* (ES^-) 255 (100%), 209 ($[M-H]^-$, 20%). These data are in accordance with the literature values.[174]

9.7.2. 2-Bromo-1-(dibenzo[*b*,*d*]furan-2-yl)ethanone **158**

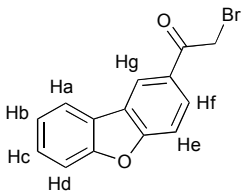

To a solution of 1-(dibenzo[*b*,*d*]furan-2-yl)ethanone (3.20 g, 15.22 mmol, 1.0 eq) and $AlCl_3$ (1.01 g, 7.61 mmol, 0.5 eq) in dry Et_2O (50 mL) at 0 ºC was added bromine (2.68 g, 0.86 mL, 16.742 mmol, 1.1 eq) dropwise. The reaction was left stirring at RT for 1.5 h. After this time TLC analysis indicated that the reaction was complete. An aqueous saturated solution of $Na_2S_2O_3$ (100 mL) was added and the resulting mixture filtered through Celite. The filtrate was partitioned between water (200 mL) and Et_2O (3 × 100 mL). The organic fractions were combined, dried over Na_2SO_4, filtered and concentrated *in vacuo*. Purification by silica gel column chromatography, eluting with toluene and petroleum ether (9:1) yielded 2-bromo-1-(dibenzo[*b*,*d*]furan-2-yl)ethanone (3.24 g, 74%) as a colourless solid: R_f 0.43 (toluene/petroleum ether, 9:1); (Found C, 58.18; H, 3.16. $C_{14}H_9BrO_2$ requires C, 58.16; H, 3.14); mp 88-90 °C (from EtOAc/petroleum ether); ν_{max}/cm^{-1} ($CHCl_3$) 1676.4 (s)(C=O), 1191.6 (s)(C-O); δ_H (500 MHz; $CDCl_3$) 8.59 (1H, d, *J* 1.7, H_g), 8.11 (1H, dd, *J* 8.7, 1.7, H_f), 7.98-8.00 (1H, m, H_a), 7.58-7.62 (2H, m, H_e, H_d), 7.51 (1H, ddd, *J* 8.4, 7.2, 1.3, H_c), 7.37-7.41 (1H, m, H_b), 4.54 (2H,

s, CH_2); δ_C (125 MHz; $CDCl_3$) 190.8 (C=O), 159.3 (C), 156.9 (C), 129.2 (C), 128.5 (C-H_f), 128.3 (C-H_c), 125.0 (C), 123.6 (C-H_b), 123.4 (C), 122.4 (C-H_g), 121.1 (C-H_a), 112.0 and 111.9 (C-H_e, C-H_d), 31.2 (CH_2). *m/z* (ESI^+) [Found: $(M+Na)^+$ 310.9673. $C_{14}H_9{}^{79}BrO_2$ requires M^+ 310.9678; Found: $(M+Na)^+$ 312.9653. $C_{14}H_9{}^{81}BrO_2Na$ requires M^+ 312.9658]; *m/z* (ES^-) 289 ($[^{81}M-H]^-$, 68%), 287 ($[^{79}M-H]^-$, 70%), 187 (100%).

9.7.3. 1-(Dibenzo[*b*,*d*]furan-2-yl)-2-hydroxyethanone **169**

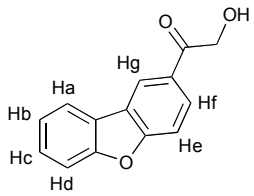

A solution of 2-bromo-1-(dibenzo[*b*,*d*]furan-2-yl)ethanone (0.52 g, 1.798 mmol, 1.0 eq) and sodium formate (0.73 g, 10.788 mmol, 6.0 eq) in ethanol (85%, 30 mL) was heated under reflux for 5 h. The ethanol was removed *in vacuo* and the residue partitioned between water (100 mL) and CH_2Cl_2 (2 × 100 mL). The organic fractions were combined, dried over Na_2SO_4, filtered and concentrated *in vacuo*. Purification of the residue by silica gel column chromatography, eluting with EtOAc and petroleum ether (1:9 → 2:8) yielded 1-(dibenzo[*b*,*d*]furan-2-yl)-2-hydroxyethanone (0.33 g, 81%) as a colourless solid: R_f 0.40 (EtOAc/petroleum ether, 1:1); (Found C, 74.28; H, 4.45. $C_{14}H_{10}O_3$ requires C, 74.33; H, 4.46); mp 133-134°C (from EtOAc/petroleum ether); ν_{max}/cm^{-1} ($CHCl_3$) 3376.6 (m)(O-H), 1677.2 (s)(C=O), 1244.2 (s)(C-O), 1101.2 (s)(C-O); δ_H (500 MHz; $CDCl_3$) 8.57 (1H, d, *J* 1.8,

H_g), 8.06 (1H, dd, *J* 8.8, 1.8, H_f), 8.02 (1H, dd, *J* 7.3, 1.3, H_a), 7.60-7.66 (2H, m, H_e, H_d), 7.53 (1H, ddd, *J* 8.1, 7.5, 1.3, H_c), 7.42 (1H, ddd, *J* 7.5, 7.3, 1.0, H_b), 4.99 (2H, d, *J* 4.5, CH_2), 3.59 (2H, t, *J* 4.5, OH); δ_C (125 MHz; $CDCl_3$) 197.5 (C=O), 159.5 (C), 156.9 (C), 128.6 (C), 128.4 (C-H_c), 127.2 (C-H_f), 125.0 (C), 123.7 (C-H_b), 123.4 (C), 121.09 (C-H_g), 121.05 (C-H_a), 112.2 and112.1 (C-H_e, C-H_d), 65.6 (CH_2). *m/z* (ESI^+) [Found: $(M+Na)^+$ 249.0533. $C_{14}H_{10}O_3Na$ requires M^+ 249.0546]; *m/z* (ES^+) 249 ($[M+Na]^+$, 100%).

9.7.4. 2-(Dibenzo[*b*,*d*]furan-2-yl)-2-oxoethyl 4-(*tert*-butoxycarbonylamino)butanoate **171**

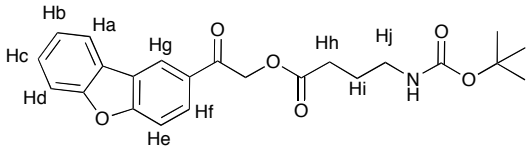

4-(*tert*-Butoxycarbonylamino)butanoic acid (540 mg, 2.655 mmol, 1.5 eq), EDC·HCl (407 mg, 2.124 mmol, 1.2 eq) and HBTU (671 mg, 1.770 mmol, 1.0 eq) were dissolved in dry CH_2Cl_2 (10 mL) and stirred at RT for 10 min. 1-(Dibenzo[*b*,*d*]furan-2-yl)-2-hydroxyethanone (400 mg, 1.770 mmol, 1.0 eq) and Hunig's base (458 mg, 617 μL, 3.540 mmol, 2.0 eq) were added to the above solution. The reaction mixture was covered with foil and stirred at RT under N_2 overnight. After this time the reaction was adjudged complete by TLC. The residue was partitioned between water (100 mL) and CH_2Cl_2 (2 × 100 mL). The organic extract was washed with aqueous 1 M HCl (100 mL), saturated aqueous Na_2CO_3 (100 mL) and water (100 mL). The organic extracts were combined, dried over Na_2SO_4, filtered and the solvent removed

in vacuo. The resulting residue was purified by silica gel column chromatography, eluting with EtOAc and petroleum ether (3:7), to afford 2-(dibenzo[*b*,*d*]furan-2-yl)-2-oxoethyl 4-(*tert*-butoxycarbonylamino)butanoate (652 mg, 90%) as a colourless solid: R_f 0.68 (EtOAc/petroleum ether, 1:1); (Found C, 67.09; H, 6.09; N, 3.45. $C_{23}H_{25}NO_6$ requires C, 67.14; H, 6.12; N, 3.40); mp 116-118 °C (from EtOAc/petroleum ether); ν_{max}/cm^{-1} ($CHCl_3$) 3373.2 (m)(N-H), 2976.8 (s)(C-H), 2934.1 (s)(C-H), 1743.8 (s)(C=O), 1698.4 (vs)(C=O), 1198.7 (s)(C-O), 1165.3 (s)(C-O); δ_H (400 MHz; $CDCl_3$) 8.51 (1H, d, *J* 1.5, H_g), 8.02 (1H, dd, *J* 8.4, 1.5, H_f), 7.98 (1H, dd, *J* 7.8, 1.1, H_a), 7.58-7.61 (2H, m, H_e, H_d), 7.51 (1H, ddd, *J* 7.5, 7.4, 1.1, H_c), 7.39 (1H, ddd, *J* 7.8, 7.5, 0.7, H_b), 5.46 (2H, s, CH_2), 4.85 (1H, br s, NH), 3.26 (2H, dt, *J* 7.2, 5.8, H_j), 2.58 (2H, t, *J* 7.2, H_h), 1.94 (2H, tt, *J* 7.2, 7.2, H_i), 1.45 (9H, s, $(CH_3)_3$); δ_C (100 MHz; $CDCl_3$) 191.5 (C=O), 173.1 (OC=O), 159.2 (NC=O), 156.8 (C), 156.0 (C), 129.4 (C), 128.3 (C-H_c), 127.2 (C-H_f), 124.8 (C), 123.6 (C-H_b), 123.4 (C), 121.1 (C-H_g), 121.0 (C-H_a), 112.0 and 111.9 (C-H_e, C-H_d), 79.2 ($C(CH_3)_3$), 66.3 (CH_2), 40.0 (C-H_j), 31.4 (C-H_h), 28.7 (($CH_3)_3$), 25.6 (C-H_i). *m/z* (ESI^+) [Found: $(M+Na)^+$ 434.1575. $C_{23}H_{25}NO_6Na$ requires M^+ 434.1574]; *m/z* (ES^-) 446 ($[M+Cl]^-$, 100%).

9.7.5. 2-(Dibenzo[*b*,*d*]furan-2-yl)-2-oxoethyl 4-aminobutanoate hydrochloride **172**

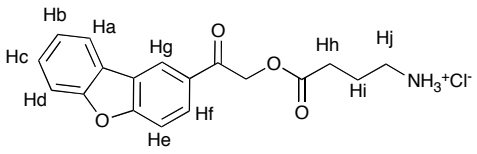

2-(Dibenzo[*b*,*d*]furan-2-yl)-2-oxoethyl 4-(*tert*-butoxycarbonylamino)butanoate (200 mg, 0.486 mmol, 1.0 eq) was dissolved in a solution of 1 M HCl in acetic acid (10 mL) and stirred at RT for 2.5 h. After this time the reaction was adjudged complete by TLC. The reaction mixture was filtered and the solid washed with CH_2Cl_2 (50 mL) to afford 2-(dibenzo[*b*,*d*]furan-2-yl)-2-oxoethyl 4-aminobutanoate hydrochloride (128 mg, 76%) as a yellow solid: mp 185-187 °C (from MeOH/Et_2O); ν_{max}/cm^{-1} (KBr) 3446.4 (m)(N-H), 2995.5 (s)(C-H), 1740.7 (vs)(C=O), 1689.1 (vs)(C=O), 1195.4 (s)(C-O); δ_H (500 MHz; DMSO) 8.89 (1H, d, *J* 1.5, H_g), 8.29 (1H, dd, *J* 7.7, 1.3, H_a), 8.14 (1H, dd, *J* 8.8, 1.5, H_f), 7.87 (1H, d, *J* 8.8, H_e), 7.78 (1H, dd, *J* 8.3, 0.8, H_d), 7.60 (1H, ddd, *J* 8.3, 8.2, 1.3, H_c), 7.49 (1H, ddd, *J* 8.2, 7.7, 0.8, H_b), 5.65 (2H, s, CH_2), 2.87-2.92 (2H, m, H_j), 2.64 (2H, t, *J* 7.7, H_h), 1.92 (2H, tt, *J* 7.7, 7.5, H_i); δ_C (125 MHz; DMSO) 192.2 (C=O), 172.0 (OC=O), 158.4 (C), 156.1 (C), 129.4 (C), 128.6 (C-H_c), 127.6 (C-H_f), 124.0 (C), 123.8 (C-H_b), 123.0 (C), 122.0 (C-H_g), 121.7 (C-H_a), 112.2 (C-H_e), 111.9 (C-H_d), 66.6 (CH_2), 38.0 (C-H_j), 30.3 (C-H_h), 22.6 (C-H_i). *m/z* (ESI$^+$) [Found: $(M+H)^+$ 312.1230. $C_{18}H_{18}NO_4$ requires M^+ 312.1230]; *m/z* (ES$^+$) 312 ($[M+H]^+$, 100%).

9.7.6. (*S*)-1-*tert*-Butyl 5-(2-(dibenzo[*b*,*d*]furan-2-yl)-2-oxoethyl) 2-((*tert*-butoxycarbonyl)amino)pentanedioate **174**

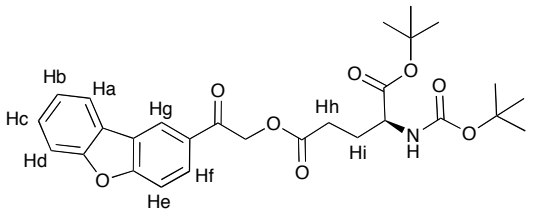

5-*tert*-Butoxy-4-(*tert*-butoxycarbonylamino)-5-oxopentanoic acid (148 mg, 0.487 mmol, 1.1 eq), EDC·HCl (102 mg, 0.530 mmol, 1.2 eq) and HBTU (168 mg, 0.442 mmol, 1.0 eq) were dissolved in dry CH_2Cl_2 (10 mL) and stirred at RT for 10 min. 1-(Dibenzo[*b*,*d*]furan-2-yl)-2-hydroxyethanone (100 mg, 0.442 mmol, 1.0 eq) and Hunig's base (114 mg, 154 μL, 0.884 mmol, 2.0 eq) were added to the above solution. The reaction mixture was covered with foil and stirred at RT under N_2 overnight. After this time the reaction was adjudged complete by TLC. The residue was partitioned between water (100 mL) and CH_2Cl_2 (2 × 100 mL). The organic extract was washed with aqueous 1 M HCl (100 mL), saturated aqueous Na_2CO_3 (100 mL) and water (100 mL). The organic extracts were combined, dried over Na_2SO_4, filtered and the solvent removed *in vacuo*. This residue was purified by silica gel column chromatography, eluting with EtOAc and petroleum ether (3:7), to afford 1-*tert*-butyl 5-(2-(dibenzo[*b*,*d*]furan-2-yl)-2-oxoethyl) 2-((*tert*-butoxycarbonyl)amino)pentanedioate (139 mg, 62%) as a light-yellow solid: R_f 0.77 (EtOAc/petroleum ether, 1:1); $[\alpha]_D^{25}$ +9.14 (*c* 0.35 in $CHCl_3$); (Found C, 65.83; H, 6.67; N, 2.58. $C_{28}H_{33}NO_8$ requires C, 65.74; H, 6.50; N, 2.74);

mp 115-116 °C (from EtOAc/Et_2O); ν_{max}/cm^{-1} ($CHCl_3$) 3378.4 (m)(N-H), 2979.0 (s)(C-H), 2934.0 (s)(C-H), 1732.1 (vs)(C=O), 1702.2 (vs)(C=O), 1368.0 (s)(C-O), 1156.7 (vs)(C-O); δ_H (500 MHz; $CDCl_3$) 8.57 (1H, d, *J* 1.5, H_g), 8.06 (1H, dd, *J* 8.6, 1.5, H_f), 8.02 (1H, d, *J* 7.7, H_a), 7.65 (1H, d, *J* 8.6, H_e), 7.62 (1H, d, *J* 8.3, H_d), 7.54 (1H, dd, *J* 8.3, 7.7, H_c), 7.42 (1H, dd, *J* 7.7, 7.7, H_b), 5.48 (2H, s, CH_2), 5.19 (1H, d, *J* 7.7, NH), 4.26-4.30 (1H, m, CH^*), 2.57-2.70 (2H, m, H_h), 2.25-2.32 (1H, m, H_i), 1.99-2.07 (1H, m, H_i), 1.49 (9H, s, $(CH_3)_3$), 1.46 (9H, s, $(CH_3)_3$); δ_C (125 MHz; $CDCl_3$) 191.3 (C=O), 172.5 (OC=O), 171.4 (OC=O), 159.3 (NC=O), 156.9 (C), 155.5 (C), 129.5 (C), 128.3 (C-H_c), 127.3 (C-H_f), 125.0 (C), 123.6 (C-H_b), 123.5 (C), 121.2 (C-H_g), 121.1 (C-H_a), 112.12 (C-H_d), 112.07 (C-H_e), 82.3 ($C(CH_3)_3$), 79.8 ($C(CH_3)_3$), 66.1 (CH_2), 53.4 (CH^*), 30.2 (C-H_h), 28.4 ($(CH_3)_3$), 28.2 (C-H_i), 28.1 ($(CH_3)_3$). *m/z* (ESI^+) [Found: $(M+Na)^+$ 534.2098. $C_{28}H_{33}NO_8Na$ requires M^+ 534.2098]; *m/z* (ES^+) 534 ($[M+Na]^+$, 100%).

9.7.7. (*S*)-2-Amino-5-(2-(dibenzo[*b*,*d*]furan-2-yl)-2-oxoethoxy)-5-oxopentanoic acid hydrochloride **175**

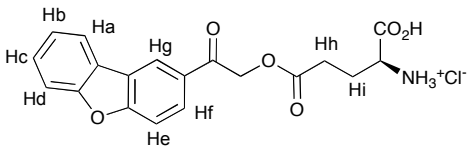

1-*tert*-Butyl 5-(2-(dibenzo[*b*,*d*]furan-2-yl)-2-oxoethyl) 2-((*tert*-butoxycarbonyl)amino)pentanedioate (80 mg, 0.156 mmol, 1.0 eq) was dissolved in a solution of 1 M HCl in acetic acid (5 mL) and stirred at 45 °C for 4 h. Upon cooling to RT, a solid precipitated out of solution. This solid was

filtered and washed with Et_2O to afford 2-amino-5-(2-(dibenzo[*b*,*d*]furan-2-yl)-2-oxoethoxy)-5-oxopentanoic acid hydrochloride (40 mg, 72%) as a light-yellow solid: $[\alpha]_D^{25}$ +11.25 (*c* 0.16 in DMSO); mp 204-206 °C (from MeOH/Et_2O); ν_{max}/cm^{-1} (MeOH) 1752.6 (s)(C=O), 1725.5 (s)(C=O), 1694.3 (s)(C=O), 1227.8 (s)(C-O), 1185.5 (s)(C-O); δ_H (500 MHz; MeOD) 8.75 (1H, d, *J* 1.6, H_g), 8.15-8.18 (2H, m, H_a and H_f), 7.74 (1H, d, *J* 8.5, H_e), 7.66 (1H, d, *J* 8.5, H_d), 7.58 (1H, dd, *J* 8.5, 7.5, H_c), 7.45 (1H, dd, *J* 7.5, 7.5, H_b), 5.65 (2H, 2 × d, *J* 16.5, 16.5, OCH_2), 4.17 (1H, t, *J* 6.6, CH^*), 2.80-2.84 (2H, m, H_h), 2.33-2.40 (1H, m, H_i), 2.22-2.29 (1H, m, H_i); δ_C (125 MHz; MeOD) 193.8 (C=O), 173.2 (OC=O), 171.4 (OC=O), 160.7 (C), 158.4 (C), 130.8 (C), 129.6 (C), 128.6 (C-H_c), 126.1 (C-H_f), 124.9 (C), 124.7 (C-H_b), 122.3 (C-H_a), 122.6 (C-H_g), 113.2 (C-H_e), 112.9 (C-H_d), 68.1 (OCH_2), 53.1 (CH^*), 30.5 (C-H_h), 26.9 (C-H_i). *m/z* (ESI^+) [Found: $(M+Na)^+$ 378.0943. $C_{19}H_{17}NO_6Na$ requires M^+ 378.0948]; *m/z* (ES^+) 378 ($[M+Na]^+$, 100%).

9.7.8. 2-Bromo-1-(thiophen-3-yl)ethanone **177**

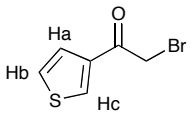

To a solution of 3-acetylthiophene (1.00 g, 7.925 mmol, 1.0 eq) and $AlCl_3$ (0.53 g, 3.963 mmol, 0.5 eq) in dry Et_2O (50 mL) at 0 ºC was added bromine (1.34 g, 0.45 mL, 8.718 mmol, 1.1 eq) dropwise. The reaction was left stirring at RT for 1 h. After this time TLC analysis indicated that the reaction was complete. A saturated aqueous solution of $Na_2S_2O_3$ (100 mL) was added and the resulting mixture filtered through Celite. The filtrate was partitioned between water (200 mL) and Et_2O (3 × 100 mL). The organic fractions were combined, dried over Na_2SO_4, filtered and concentrated *in vacuo*. Purification by silica gel column chromatography, eluting with toluene and petroleum ether (9:1) yielded 2-bromo-1-(thiophen-3-yl)ethanone (1.14 g, 70%) as a colourless solid: R_f 0.27 (toluene/petroleum ether, 8:2); mp 59-60 °C (from EtOAc/petroleum ether) (Lit.[175] mp 61-62 ° C); δ_H (400 MHz; $CDCl_3$) 8.18 (1H, dd, *J* 2.9, 1.3, H_c), 7.59 (1H, dd, *J* 5.1, 1.3, H_b), 7.37 (1H, dd, *J* 5.1, 2.9, H_a), 4.35 (2H, s, CH_2); *m/z* (ES^+) 413 (100%), 229 ($[^{81}M+Na]^+$, 20%), 227 ($[^{79}M+Na]^+$, 20%). These data are in accordance with the literature values.[175]

9.7.9. 2-Oxo-2-(thiophen-3-yl)ethyl 4-fluorobenzoate **181**

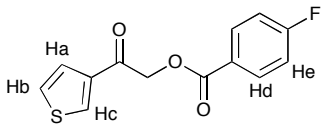

A solution of 2-bromo-1-(thiophen-3-yl)ethanone (100 mg, 0.488 mmol, 1.0 eq) in dry THF (10 mL) was cooled to 0 °C. 4-Fluorobenzoic acid (100 mg, 0.714 mmol, 1.5 eq) was added to this solution and then DBU (82 mg, 80 μL, 0.537 mmol, 1.1 eq) was added dropwise. The reaction mixture was covered with foil and stirred at RT under N_2 overnight. After this time the reaction was adjudged complete by TLC analysis. The reaction mixture was filtered to remove the DBU·HBr salts and the filtrate concentrated *in vacuo*. The residue was partitioned between water (100 mL) and CH_2Cl_2 (2 × 100 mL). The organic extracts were combined, dried over Na_2SO_4, filtered and the solvent removed *in vacuo*. This residue was purified by silica gel column chromatography, eluting with EtOAc and petroleum ether (2:8), to afford 2-oxo-2-(thiophen-3-yl)ethyl 4-fluorobenzoate (126 mg, 98%) as a colourless solid: R_f 0.44 (EtOAc/petroleum ether, 1:1); (Found C, 59.10; H, 3.36. $C_{13}H_9FO_3S$ requires C, 59.08; H, 3.43); mp 75-78 °C (from $CHCl_3$); ν_{max}/cm^{-1} ($CHCl_3$) 1720.2 (s)(C=O), 1685.9 (s)(C=O), 1279.5 (s)(C-O); δ_H (500 MHz; $CDCl_3$) 8.12-8.15 (3H, m, H_c and H_e), 7.57 (1H, d, *J* 5.1, H_b), 7.36 (1H, dd, *J* 5.1, 2.9, H_a), 7.12 (2H, dd, ^3J H_e-H_d 8.7, ^4J H-F 8.5, H_d), 5.42 (2H, s, OCH_2); δ_F (282 MHz; $CDCl_3$) -104.8 (F); δ_C (125 MHz; $CDCl_3$) 186.5 (C=O), 166.0 (d, ^1J 255.4, C-F), 138.7 (OC=O), 132.5 (d, ^3J 9.4, C-H_d), 132.3 (C-H_c), 126.9 (C-

H_a), 126.4 (C-H_b), 125.5 (d, ^4J 2.9, C), 115.6 (d, ^2J 22.3, C-H_e), 66.7 (CH_2). *m/z* (ESI^+) [Found: $(M+Na)^+$ 287.0149. $C_{13}H_9FSO_3Na$ requires M^+ 287.0149]; *m/z* (ES^+) 287 ($[M+H]^+$, 100%).

9.7.10. 2-Oxo-2-(thiophen-3-yl)ethyl 4-((*tert*-butoxycarbonyl)amino)butanoate **178**

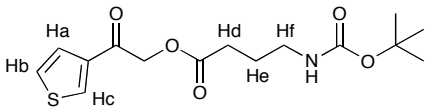

A solution of 2-bromo-1-(thiophen-3-yl)ethanone (130 mg, 0.630 mmol, 1.0 eq) in dry THF (15 mL) was cooled to 0 °C. 4-(*tert*-Butoxycarbonylamino)butanoic acid (140 mg, 0.690 mmol, 1.1 eq) was added to this solution. DBU (123 mg, 120 μL, 0.805 mmol, 1.3 eq) was added dropwise. The reaction mixture was covered with foil and stirred at RT under N_2 overnight. After this time the reaction was adjudged complete by TLC analysis. The reaction mixture was filtered to remove the DBU·HBr salts and the filtrate concentrated *in vacuo*. The residue was partitioned between water (100 mL) and CH_2Cl_2 (2 × 100 mL). The organic extracts were combined, dried over Na_2SO_4, filtered and the solvent removed *in vacuo*. This residue was purified by silica gel column chromatography, eluting with EtOAc and petroleum ether (3:7), to afford 2-oxo-2-(thiophen-3-yl)ethyl 4-((*tert*-butoxycarbonyl)amino)butanoate (160 mg, 78%) as a colourless solid: R_f 0.19 (EtOAc/petroleum ether, 2:8); (Found C, 55.16; H, 6.49; N, 4.17. $C_{15}H_{21}NO_5S$ requires C, 55.03; H, 6.47; N, 4.28); mp 60-61 °C (from $CHCl_3$); ν_{max}/cm^{-1}

($CHCl_3$) 3378.7 (s)(N-H), 2976.8 (s)(C-H), 1743.9 (s)(C=O), 1695.3 (s)(C=O), 1165.9 (s)(C-O); δ_H (500 MHz; $CDCl_3$) 8.09 (1H, dd, *J* 2.8, 1.1, H_c), 7.52 (1H, dd, *J* 5.1, 1.1, H_b), 7.35 (1H, dd, *J* 5.1, 2.8, H_a), 5.20 (2H, s, OCH_2), 4.83 (1H, s, NH), 3.18-3.22 (2H, m, H_f), 2.51 (2H, t, *J* 7.2, H_d), 1.88 (2H, tt, *J* 7.2, 7.1, H_e), 1.41 (9H, s, $(CH_3)_3$); δ_C (125 MHz; $CDCl_3$) 186.6 (C=O), 172.7 (OC=O), 156.1 (OC=O), 138.6 (C), 132.3 (C-H_c), 126.9 (C-H_a), 126.4 (C-H_b), 79.4 ($C(CH_3)_3$), 66.3 (OCH_2), 39.7 (C-H_f), 31.1 (C-H_d), 28.4 ($(CH_3)_3$), 25.3 (C-H_e). *m/z* (ESI^+) [Found: $(M+Na)^+$ 350.1032. $C_{15}H_{21}NSO_5Na$ requires M^+ 350.1032]; *m/z* (ES^-) 326 ($[M-H]^-$, 100%).

9.7.11. 2-Oxo-2-(thiophen-3-yl)ethyl 4-aminobutanoate hydrochloride **179**

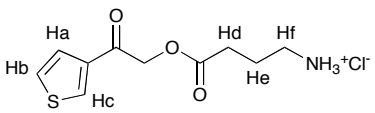

2-Oxo-2-(thiophen-3-yl)ethyl 4-((*tert*-butoxycarbonyl)amino)butanoate (120 mg, 0.367 mmol, 1.0 eq) was dissolved in a solution of 1 M HCl in dioxane (10 mL) and stirred for 5 h at RT. The dioxane was removed *in vacuo* and the crude mixture precipitated in Et_2O. The solid obtained was removed by filtration and washed with Et_2O to afford 2-oxo-2-(thiophen-3-yl)ethyl 4-aminobutanoate hydrochloride (42 mg, 51%) as a colourless solid: Mp 120-123 °C (from MeOH/Et_2O); ν_{max}/cm^{-1} (KBr) 3471.5 (s)(N-H), 2942.5 (s)(C-H), 1739.2 (s)(C=O), 1693.6 (s)(C=O), 1201.2 (s)(C-O); δ_H (500 MHz; MeOD) 8.45 (1H, dd, *J* 2.6, 1.3, H_c), 7.56-7.59 (2H, m, H_a and H_b), 5.40 (2H, s, OCH_2), 3.09 (2H, t, *J* 7.8, H_f), 2.67 (2H, t, *J* 7.0, H_d), 2.05 (2H, tt, *J* 7.8, 7.0,

H_e); δ_C (125 MHz; MeOD) 189.5 (C=O), 173.6 (OC=O), 139.8 (C), 134.5 (C-H_c), 128.4 (C-H_a), 127.3 (C-H_b), 67.6 (OCH_2), 40.0 (C-H_f), 31.4 (C-H_d), 23.9 (C-H_e). *m/z* (ESI^+) [Found: $(M+H)^+$ 228.0690. $C_{10}H_{14}NSO_3$ requires M^+ 228.0689]; *m/z* (ES^+) 228 ($[M+H]^+$, 100%).

9.8. Synthesis of Wavelength-Orthogonally Caged Neurotransmitters

9.8.1. 2-(*tert*-Butoxycarbonylamino)acetic acid **212**

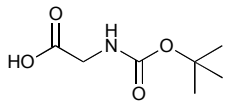

A solution of glycine (5.0 g, 0.067 mol, 1.0 eq) and NaOH (4.0 g, 0.100 mol, 1.5 eq) in water/dioxane (1:1, 300 mL) was prepared. To this a solution of Boc_2O (43.7 g, 0.201 mol, 3.0 eq) in dioxane (100 mL) was added dropwise to the above solution over 1 h. The solution was stirred at RT for 24 h. The dioxane was removed *in vacuo* and the remaining aqueous solution washed with EtOAc (2 × 50 mL). The organic phase was washed with a saturated aqueous solution of $NaHCO_3$ (2 × 50 mL). The aqueous phases were combined and acidified with solid $NaHSO_4$ and extracted with EtOAc (3 × 100 mL). The organic extracts were combined, dried over Na_2SO_4, filtered and the solvent removed *in vacuo* to yield a clear oil. This oil was purified by silica gel column chromatography, eluting with EtOAc and hexane (1:9 → 3:7). Crystallisation (EtOAC/hexane) afforded 2-(*tert*-butoxycarbonylamino)acetic acid (8.75 g, 75%) as a colourless solid: R_f 0.31 (EtOAC/hexane, 1:1); mp 77-78 °C (from EtOAC/hexane); δ_H (300 MHz; $CDCl_3$) 5.09 (1H, br s, NH), 3.90-3.98 (2H, m, CH_2N), 1.46 (9H, s, $(CH_3)_3$). These data are in accordance with the literature values.[176]

9.8.2. 4-(*tert*-Butoxycarbonylamino)butanoic acid **170**

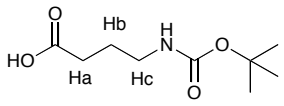

A solution of 4-aminobutyric acid (3.0 g, 0.029 mol, 1.0 eq) and NaOH (1.75 g, 0.044 mol, 1.5 eq) in water/dioxane (1:1, 200 mL) was prepared. To this a solution of Boc_2O (9.52 g, 0.044 mol, 1.5 eq) in dioxane (80 mL) was added dropwise over 1 h. The solution was stirred at RT for 40 h after which time TLC analysis indicated that the reaction was complete. The dioxane was removed *in vacuo* and the remaining aqueous solution extracted with Et_2O (2 × 100 mL). The organic phase was washed with a saturated aqueous solution of $NaHCO_3$ (2 × 50 mL). The aqueous phases were combined and acidified with solid $NaHSO_4$ and extracted with EtOAc (3 × 100 mL). The organic extracts were combined, dried over Na_2SO_4, filtered and the solvent removed *in vacuo* to yield a clear oil. This oil was purified by silica gel column chromatography, eluting with EtOAc and hexane (1:9 → 3:7). Crystallisation from EtOAC/hexane afforded 4-(*tert*-butoxycarbonylamino)butanoic acid (5.16 g, 87%) as a colourless solid: R_f 0.40 (EtOAc/hexane, 1:1); mp 48-50 °C (from EtOAc/hexane) (Lit.[177] mp 52-54 °C); δ_H (400 MHz; $CDCl_3$) 4.78 (1H, br s, NH), 3.09-3.18 (2H, m, H_c), 2.36 (2H, t, *J* 7.4, H_a), 1.79 (2H, tt, *J* 7.4, 7.1, H_b), 1.40 (9H, s, $(CH_3)_3$). These data are in accordance with the literature values.[177]

9.8.3. 4,5-Dimethoxy-2-nitrobenzyl 2-(*tert*-butoxycarbonylamino)acetate **214**

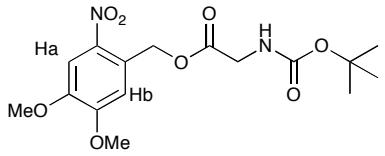

4,5-Dimethoxy-2-nitrobenzyl alcohol (1.10 g, 5.137 mmol, 1.8 eq), DCC (1.18 g, 5.708 mmol, 2.0 eq) and DMAP (0.70 g, 5.708 mmol, 2.0 eq) were dissolved in dry CH_2Cl_2 (50 mL) and cooled to 0 ºC. A solution of 2-(*tert*-butoxycarbonylamino)acetic acid (500 mg, 2.854 mmol, 1.0 eq) in dry CH_2Cl_2 (10 mL) was transferred to the above solution *via* cannula. The reaction mixture was covered with foil and stirred at RT under N_2 for 5 h. After this time the reaction was adjudged complete by TLC analysis. The reaction mixture was filtered to remove the 1,3-dicyclohexylurea (DCU) side-product, quenched with water (200 mL) and the organic material extracted with CH_2Cl_2 (3 × 80 mL). The organic extracts were combined, dried over $MgSO_4$, filtered, and the solvent removed *in vacuo*. This residue was purified by silica gel column chromatography, eluting with EtOAc and hexane (1:9), to afford 4,5-dimethoxy-2-nitrobenzyl 2-(*tert*-butoxycarbonylamino)acetate (0.66 g, 63%) as a yellow solid: R_f 0.61 (EtOAc/hexane, 1:1); (Found C, 51.88; H, 5.90; N, 7.46. $C_{16}H_{22}N_2O_8$ requires C, 51.89; H, 5.99; N, 7.56); mp 152-154 °C (from EtOAc/petroleum ether); ν_{max}/cm^{-1} (KBr) 3327.3 (m)(N-H), 2928.5 (m)(C-H), 1626.3 (s)(C=O), 1576.2 (s)(NO_2), 1244.3 (m)(NO_2), 1088.6 (s)(C-O); δ_H (400 MHz; $CDCl_3$) 7.62 (1H, s, H_a), 6.97 (1H, s, H_b), 5.48 (2H, s, $ArCH_2$), 3.94 (2H,

s, CH_2N), 3.90 (6H, s, 2 × OMe), 1.35 (9H, s, $(CH_3)_3$); δ_C (100 MHz; $CDCl_3$) 170.1 (C=O), 155.9 (NC=O), 153.7 (C), 148.1 (C), 139.5 (C), 126.8 (C), 110.0 (C-H_b), 108.0 (C-H_a), 80.0 (*C*$(CH_3)_3$), 63.8 ($ArCH_2$), 56.5 (OMe), 56.3 (OMe), 42.5 (CH_2N), 28.2 ($(CH_3)_3$). ***m/z*** EI^+ [Found: $(M)^+$ 370.1375. $C_{16}H_{22}N_2O_8$ requires M^+ 370.1376]; ***m/z*** (EI^+) 370 ($[M]^+$, 100%).

9.8.4. 4,5-Dimethoxy-2-nitrobenzyl 2-aminoacetate hydrochloride **209**

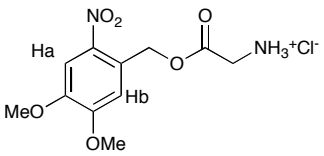

4,5-Dimethoxy-2-nitrobenzyl 2-(*tert*-butoxycarbonylamino)acetate (500 mg, 1.350 mmol, 1.0 eq) was dissolved in a solution of 1 M HCl in dioxane (25 mL) and stirred at RT for 24 h. The dioxane was removed *in vacuo* and the crude mixture precipitated in Et_2O to afford 4,5-dimethoxy-2-nitrobenzyl 2-aminoacetate hydrochloride (413 mg, 100%) as a yellow solid: mp 168-170 °C (from Et_2O); ν_{max}/cm^{-1} (KBr) 3442.1 (m)(N-H), 2959.9 (m)(C-H), 1741.6 (s)(C=O), 1529.5 (s)(NO_2), 1280.3 (s)(NO_2), 1066.6 (s)(C-O); δ_H (400 MHz; D_2O) 7.78 (1H, s, H_a), 7.15 (1H, s, H_b), 5.55 (2H, s, $ArCH_2$), 4.00 (2H, s, CH_2N), 3.93 (6H, s, 2 × OMe); δ_C (125 MHz; D_2O) 168.1 (C=O), 153.5 (C), 148.3 (C), 140.1 (C), 125.4 (C), 112.3 (C-H_b), 108.8 (C-H_a), 65.5 ($ArCH_2$), 56.6 (OMe), 56.4 (OMe), 40.3 (NCH_2). ***m/z*** (EI^+) [Found: $(M)^+$ 270.0847. $C_{11}H_{14}N_2O_6$ requires M^+ 270.0852]; ***m/z*** (EI^+) 270 ($[M]^+$, 100%).

9.8.5. 4,5-Dimethoxy-2-nitrobenzyl 4-(*tert*-butoxycarbonylamino)butanoate **215**

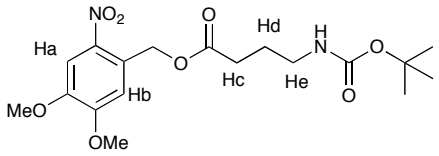

4,5-Dimethoxy-2-nitrobenzyl alcohol (1.26 g, 5.904 mmol, 1.2 eq), DCC (2.03 g, 9.840 mmol, 2.0 eq) and DMAP (1.20 g, 9.840 mmol, 2.0 eq) were dissolved in dry CH_2Cl_2 (50 mL) and cooled to 0 ºC. A solution of 4-(*tert*-butoxycarbonylamino)butanoic acid (1.0 g, 4.920 mmol, 1.0 eq) in dry CH_2Cl_2 (20 mL) was transferred to the above solution *via* cannula. The reaction mixture was covered with foil and stirred at RT under N_2 for 18 h. After this time the reaction was adjudged complete by TLC analysis. The reaction mixture was filtered to remove the DCU side-product, quenched with water (200 mL) and the organic material extracted with CH_2Cl_2 (3 × 80 mL). The organic extracts were combined, washed with brine (100 mL), dried over Na_2SO_4, filtered and the solvent removed *in vacuo*. This residue was purified by silica gel column chromatography, eluting with EtOAc and hexane (2:8), to afford 4,5-dimethoxy-2-nitrobenzyl 4-(*tert*-butoxycarbonylamino)butanoate (1.35 g, 69%) as a yellow solid: R_f 0.69 (EtOAc); (Found C, 54.31; H, 6.42; N, 6.97. $C_{18}H_{26}N_2O_8$ requires C, 54.26; H, 6.58; N, 7.03); mp 93-94 °C (from EtOAc/hexane) (Lit.[178] mp 96-97 °C); δ_H (400 MHz; $CDCl_3$) 7.72 (1H, s, H_a), 7.00 (1H, s, H_b), 5.51 (2H, s, $ArCH_2$), 3.98 (6H, s, 2 × OMe), 3.16-3.19 (2H, m,

H_e), 2.47 (2H, t, *J* 7.4, H_c), 1.87 (2H, tt, *J* 7.4, 7.1, H_d), 1.43 (9H, s, $(CH_3)_3$). *m/z* (ES^-) 433 (100%), 397 ($[M-H]^-$, 30%). These data are in accordance with the literature values.[178]

9.8.6. 4,5-Dimethoxy-2-nitrobenzyl 4-aminobutanoate hydrochloride **205**

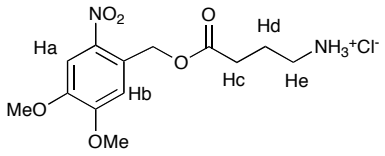

4,5-Dimethoxy-2-nitrobenzyl 4-(*tert*-butoxycarbonylamino)butanoate (230 mg, 0.577 mmol, 1.0 eq) was dissolved in a solution of 1 M HCl in dioxane (15 mL) and stirred at RT for 5 h. The dioxane was removed *in vacuo* and the crude mixture precipitated in Et_2O to afford 4,5-dimethoxy-2-nitrobenzyl 4-aminobutanoate hydrochloride (163 mg, 97%) as a yellow solid: mp 160-161 °C (from Et_2O) (Lit.[178] 168-169 °C); δ_H (500 MHz; D_2O) 7.64 (1H, s, H_a), 7.02 (1H, s, H_b), 5.33 (2H, s, $ArCH_2$), 3.87 (6H, s, 2 × OMe), 3.00 (2H, t, *J* 7.8, H_e), 2.57 (2H, dt, *J* 7.4, 1.7, H_c), 1.90-1.98 (2H, m, H_d); δ_C (125 MHz; D_2O) 174.5 (C=O), 153.1 (C), 147.9 (C), 140.0 (C), 126.0 (C), 112.0 (C-H_b), 108.6 (C-H_a), 64.2 ($ArCH_2$), 56.3 (OMe), 56.1 (OMe), 38.6 (C-H_e), 30.6 (C-H_c), 22.0 (C-H_d). *m/z* (ES^+) 299 ($[M-Cl]^+$, 100%). These data are in accordance with the literature values.[178]

9.8.7. (*S*)-1-*tert*-Butyl 5-(4,5-dimethoxy-2-nitrobenzyl) 2-(*tert*-butoxycarbonylamino)pentanedioate **216**

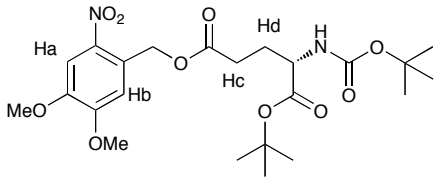

4,5-Dimethoxy-2-nitrobenzyl alcohol (309 mg, 1.450 mmol, 1.1 eq), 5-*tert*-butoxy-4-(*tert*-butoxycarbonylamino)-5-oxopentanoic acid (400 mg, 1.319 mmol, 1.0 eq) and DMAP (16 mg, 0.132 mmol, 0.1 eq) were dissolved in dry CH_2Cl_2 (50 mL). A solution of DCC (300 mg, 1.450 mmol, 1.1 eq) in dry CH_2Cl_2 (20 mL) was transferred to the above solution *via* cannula. The reaction mixture was covered with foil and stirred at RT under N_2 overnight. After this time the reaction was adjudged complete by TLC. The reaction mixture was filtered to remove the DCU side-product, quenched with water (100 mL) and the organic material extracted with CH_2Cl_2 (3 × 80 mL). The organic extracts were combined, washed with brine (100 mL), dried over Na_2SO_4, filtered and the solvent removed *in vacuo*. This residue was purified by silica gel column chromatography, eluting with EtOAc and petroleum ether (2:8), to afford 1-*tert*-butyl 5-(4,5-dimethoxy-2-nitrobenzyl) 2-(*tert*-butoxycarbonylamino)pentanedioate (570 mg, 69%) as a yellow solid: R_f 0.56 (EtOAc/hexane, 1:1); $[\alpha]_D^{25}$ -5.4 (*c* 1.0 in $CHCl_3$); (Found C, 55.51; H, 6.93; N, 5.51. $C_{23}H_{34}N_2O_{10}$ requires C, 55.41; H, 6.87; N, 5.62); mp 106-107 ° C (from EtOAc/petroleum ether); ν_{max}/cm^{-1} ($CHCl_3$) 3408.4 (m)(N-H), 2975.0

(m)(C-H), 1714.6 (s)(C=O), 1523.9 (s)(NO_2), 1278.5 (s)(NO_2), 1067.8 (s)(C-O); δ_H (400 MHz; $CDCl_3$) 7.71 (1H, s, H_a), 7.02 (1H, s, H_b), 5.52 (2H, 2 × d, *J* 15.0, 15.0, $ArCH_2$), 5.11 (1 H, d, *J* 7.8, NH), 4.19-4.24 (1 H, m, C*H*N), 3.99 (3H, s, OMe), 3.97 (3H, s, OMe), 2.43-2.59 (2H, m, H_c), 2.18-2.26 (1H, m, H_d), 1.91-2.00 (1H, m, H_d), 1.46 (9H, s, $(CH_3)_3$), 1.42 (9H, s, $(CH_3)_3$); δ_C (500 MHz; $CDCl_3$) 172.2 (C=O), 171.2 (C=O), 155.4 (NC=O), 153.5 (C), 148.2 (C), 139.9 (C), 126.9 (C), 110.4 (C-H_b), 108.2 (C-H_a), 82.3 (C), 79.8 (C), 63.4 (C-H benzylic), 56.43 (OMe), 56.38 (OMe), 53.3 (*C*HN), 30.3 (C-H_c), 28.1 (C-H_d), 28.3 ($(CH_3)_3$), 28.0 ($(CH_3)_3$). *m/z* (ESI^+) [Found: $(M+Na)^+$ 521.2106. $C_{23}H_{34}N_2O_{10}Na$ requires M^+ 521.2106]; *m/z* (ES^-) 497 ([M-H]$^-$, 100%).

9.8.8. (*S*)-2-Amino-5-(4,5-dimethoxy-2-nitrobenzyloxy)-5-oxopentanoic acid hydrochloride **207**

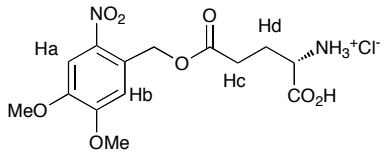

1-*tert*-Butyl 5-(4,5-dimethoxy-2-nitrobenzyl) 2-(*tert*-butoxycarbonylamino)pentanedioate (200 mg, 0.402 mmol, 1.0 eq) was dissolved in a solution of 1 M HCl in acetic acid (10 mL) and stirred at 45 °C for 6 h. An azeotrope of acetic acid and cyclohexane was removed *in vacuo* and the crude mixture precipitated in MeOH/Et_2O to afford 2-amino-5-(4,5-dimethoxy-2-nitrobenzyloxy)-5-oxopentanoic acid hydrochloride (69 mg, 50%) as a yellow solid: $[\alpha]_D^{25}$ -4.4 (*c* 0.25 in DMSO); mp 119-121 °C (from

MeOH/Et_2O); ν_{max}/cm^{-1} (KBr) 3440.6 (m)(N-H), 2951.6 (m)(C-H), 1736.4 (s)(C=O), 1523.5 (s)(NO_2), 1281.8 (s)(NO_2), 1069.7 (s)(C-O); δ_H (500 MHz; MeOD) 7.74 (1H, s, H_a), 7.16 (1H, s, H_b), 5.49 (2H, 2 × d, *J* 14.0, 14.0, $ArCH_2$), 4.05 (1H, br s, C*H*N), 3.96 (3H, s, OMe), 3.91 (3H, s, OMe), 2.69-2.74 (2H, m, H_c), 2.19-2.28 (2H, m, H_d); δ_C (125 MHz; MeOD) 173.2 (C=O), 155.1 (C), 150.1 (C), 141.7 (C), 127.5 (C), 112.7 (C-H_a), 109.5 (C-H_b), 64.9 ($ArCH_2$), 56.9 (OMe), 53.4 (CHN), 30.6 (C-H_c), 26.9 (C-H_d). *m/z* (ESI^+) [Found: $(M+Na)^+$ 365.0957. $C_{14}H_{18}N_2O_8Na$ requires M^+ 365.0955]; *m/z* (ES^-) 341 ([M-H]$^-$, 100%).

9.8.9. (R/*S*)- (3,5-Dimethoxyphenyl)(2-phenyl-1,3-dithian-2-yl)methanol **219**

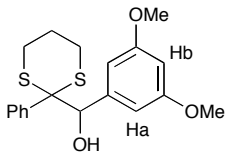

A solution of 2-phenyl-1,3-dithiane (1.0 g, 5.093 mmol, 1.0 eq) was dissolved in dry THF (20 mL) and cooled to 0 °C. *n*-BuLi (2.24 mL of a 2.5 M solution in hexanes, 5.603 mmol, 1.1 eq) was added dropwise under N_2. The solution was stirred at 0 °C for 30 min. A solution of 3,5-dimethoxybenzaldehyde (0.85 g, 5.093 mmol, 1.0 eq) in dry THF (10 mL) was added and the mixture stirred at 0 °C for 30 min. The mixture was then allowed to warm to RT over 1.5 h and quenched with a saturated aqueous NH_4Cl solution. The organic phase was collected, washed with brine, dried over Na_2SO_4, filtered and the solvent removed *in vacuo* to yield a viscous yellow oil. This oil was purified by

silica gel column chromatography, eluting with EtOAc and hexane (1:9 → 3:7), to afford (3,5-dimethoxyphenyl)(2-phenyl-1,3-dithian-2-yl)methanol (0.84 g, 45%) as a light-yellow oil: R_f 0.56 (EtOAc/hexane, 1:1); δ_H (300 MHz; $CDCl_3$) 7.72 (2H, dd, *J* 7.0, 1.6, 2 × ArH), 7.27-7.34 (3H, m, 3 × ArH), 6.29 (1H, dd, *J* 2.3, H_b), 5.99 (2H, d, *J* 2.3, H_a), 4.94 (1H, d, *J* 3.7, C*H*OH), 3.56 (6H, s, 2 × OMe), 2.96 (1H, d, *J* 3.7, OH), 2.62-2.77 (4H, m, SC*H*$_2$CH$_2$C*H*$_2$S), 1.89-1.96 (2H, m, SCH$_2$C*H*$_2$CH$_2$S). These data are in accordance with the literature values.[139]

9.8.10. (R/*S*)-2-(3,5-Dimethoxyphenyl)-2-hydroxy-1-phenylethanone **220**

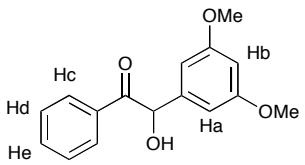

A solution of (3,5-dimethoxyphenyl)(2-phenyl-1,3-dithian-2-yl)methanol (5.40 g, 14.917 mmol, 1.0 eq) in CH_3CN (30 mL) and water (2.5 mL) was cooled to 0 ºC and stirred vigorously. A solution of bis(trifluoroacetoxy)iodobenzene (7.06 g, 16.409 mmol, 1.1 eq) in CH_3CN (20 mL) was slowly added to the above solution. After 25 min at 0 ºC, EtOAc (20 mL) was added. The organic phase was washed with a saturated aqueous $NaHCO_3$ solution (50 mL) and brine (50 mL), dried over Na_2SO_4, filtered and the solvent removed *in vacuo* to yield a viscous oil. This oil was purified by silica gel column chromatography, eluting with EtOAc and hexane (1:9 → 2:8 → 1:1). Crystallisation from EtOAc/hexane afforded 2-(3,5-

dimethoxyphenyl)-2-hydroxy-1-phenylethanone (1.76 g, 43%) as a colourless solid: R_f 0.51 (EtOAc/hexane, 1:1); mp 112-114 °C (from EtOAc/hexane) (Lit.[139] mp 113 °C); δ_H (300 MHz; $CDCl_3$) 7.93 (2H, dd, *J* 7.8, 1.3, H_c), 7.52-7.56 (1H, m, H_e), 7.41 (2H, dd, *J* 7.8, 7.4, H_d), 6.46 (2H, d, *J* 2.3, H_a), 6.35 (1H, dd, *J* 2.3, 2.3, H_b), 5.85 (1H, d, *J* 6.2, benzylic proton), 4.51 (1H, d, *J* 6.2, OH), 3.73 (6H, s, 2 × OMe). These data are in accordance with the literature values.[139]

9.8.11. (R/*S*)-1-(3,5-Dimethoxyphenyl)-2-oxo-2-phenylethyl 2-(*tert*-butoxycarbonylamino)acetate **221**

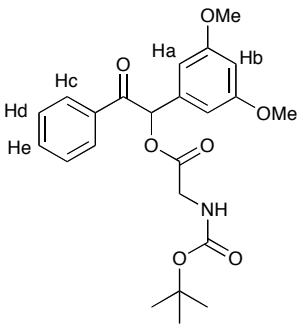

2-(3,5-Dimethoxyphenyl)-2-hydroxy-1-phenylethanone (300 mg, 1.102 mmol, 1.0 eq), 2-(*tert*-butoxycarbonylamino)acetic acid (212 mg, 1.212 mmol, 1.1 eq) and DMAP (5 mg, 0.044 mmol, 0.04 eq) were dissolved in dry CH_2Cl_2 (25 mL). A solution of DCC (250 mg, 1.212 mmol, 1.1 eq) in dry CH_2Cl_2 (10 mL) was transferred to the above solution *via* cannula. The reaction mixture was covered with foil and stirred at RT under N_2 overnight. After this time the reaction was adjudged complete by TLC. The reaction mixture was filtered to remove the DCU side-product, quenched with water (100 mL) and the organic

material extracted with CH_2Cl_2 (3 × 80 mL). The organic extracts were combined, washed with brine (100 mL), dried over Na_2SO_4, filtered and the solvent removed *in vacuo*. This residue was purified by silica gel column chromatography, eluting with EtOAc and petroleum ether (2:8), to afford 1-(3,5-dimethoxyphenyl)-2-oxo-2-phenylethyl 2-(*tert*-butoxycarbonylamino)acetate (448 mg, 95%) as a colourless gum: R_f 0.57 (EtOAc/hexane, 1:1); (Found C, 64.27; H, 6.41; N, 3.24. $C_{23}H_{27}NO_7$ requires C, 64.32; H, 6.34; N, 3.26); ν_{max}/cm^{-1} ($CHCl_3$) 3379.3 (m)(N-H), 2976.6 (m)(C-H), 1756.9 (m)(C=O), 1699.0 (m)(C=O), 1597.6 (s), 1160.4 (m)(C-O); δ_H (400 MHz; $CDCl_3$) 7.93 (2H, dd, *J* 7.8, 1.3, H_c), 7.52-7.55 (1H, m, H_e), 7.42 (2H, dd, *J* 7.8, 7.5, H_d), 6.80 (1H, s, benzylic proton), 6.58 (2H, d, *J* 2.3, H_a), 6.43 (1H, dd *J* 2.3, 2.3, H_b), 4.99 (1H, br s, NH), 4.03-4.19 (2H, m, CH_2), 3.77 (6H, s, 2 × OMe), 1.44 (9H, s, $(CH_3)_3$); δ_C (125 MHz; $CDCl_3$) 193.2 (C=O), 170.1 (C=O), 161.4 (C=O), 155.8 (C), 135.1 (C), 134.5 (C), 133.8 (C-H_e), 128.9 (C-H_c), 128.8 (C-H_d), 106.9 (C-H_a), 101.5 (C-H_b), 80.5 ($C(CH_3)_3$), 78.6 (C-H benzylic), 55.7 (OMe), 42.7 (CH_2), 28.4 ($C(CH_3)_3$). *m/z* (ES^+) [Found: $(M+Na)^+$ 452.1679. $C_{23}H_{27}NO_7Na$ requires M^+ 452.1680]; *m/z* (ES^-) 428 ($[M-H]^-$, 100%).

9.8.12. (R/*S*)-1-(3,5-Dimethoxyphenyl)-2-oxo-2-phenylethyl 2-aminoacetate hydrochloride **210**

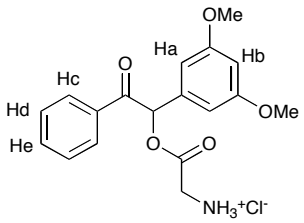

1-(3,5-Dimethoxyphenyl)-2-oxo-2-phenylethyl 2-(*tert*-butoxycarbonylamino)acetate (50 mg, 0.117 mmol, 1.0 eq) was dissolved in a solution of 1 M HCl in acetic acid (10 mL) and stirred at RT for 4 h. After this time, TLC analysis indicated that the reaction was complete. An azeotrope of acetic acid and cyclohexane was removed *in vacuo* and the crude mixture precipitated in MeOH/Et_2O to afford 1-(3,5-dimethoxyphenyl)-2-oxo-2-phenylethyl 2-aminoacetate hydrochloride (33 mg, 78%) as a yellow solid: mp 59-61 °C (from MeOH/Et_2O); δ_H (500 MHz; MeOD) 8.00 (2H, dd, *J* 8.0, 1.3, H_c), 7.61-7.64 (1H, m, H_e), 7.47 (2H, dd, *J* 8.0, 7.8, H_d), 7.08 (1H, s, benzylic proton), 6.63 (2H, d, *J* 2.3, H_a), 6.47 (1H, dd, *J* 2.3, 2.3, H_b), 4.04 (2H, 2 × d, *J* 17.5, 17.5, CH_2), 3.73 (6H, s, 2 × OMe); δ_C (125 MHz; MeOD) 194.5 (C=O), 168.2 (OC=O), 162.9 (C), 135.9 (C), 135.5 (C), 135.2 (C-H_e), 129.95 (C-H_d), 129.92 (C-H_c), 108.1 (C-H_a), 102.1 (C-H_b), 80.6 (C-H benzylic), 56.0 (OMe), 41.0 (CH_2). *m/z* (ESI^+) [Found: $(M)^+$ 330.1335. $C_{18}H_{20}NO_5$ requires M^+ 330.1336]; *m/z* (ES^+) 388 ($[M+(CH_3CN{\cdot}NH_4)]^+$, 100%). These data are in accordance with the literature values.[179]

9.8.13. (R/*S*)-1-(3,5-Dimethoxyphenyl)-2-oxo-2-phenylethyl 4-(*tert*-butoxycarbonylamino)butanoate **222**

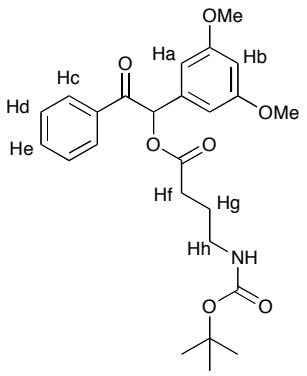

2-(3,5-Dimethoxyphenyl)-2-hydroxy-1-phenylethanone (360 mg, 1.322 mmol, 1.0 eq), 4-(*tert*-butoxycarbonylamino)butanoic acid (296 mg, 1.454 mmol, 1.1 eq) and DMAP (8 mg, 0.066 mmol, 0.05 eq) were dissolved in dry CH_2Cl_2 (25 mL). A solution of DCC (409 mg, 1.983 mmol, 1.5 eq) in dry CH_2Cl_2 (10 mL) was transferred to the above solution *via* cannula. The reaction mixture was covered with foil and stirred at RT under N_2 overnight. After this time the reaction was adjudged complete by TLC analysis. The reaction mixture was filtered to remove the DCU side-product, quenched with water (100 mL) and the organic material extracted with CH_2Cl_2 (3 × 80 mL). The organic extracts were combined, washed with brine (100 mL), dried over Na_2SO_4, filtered and the solvent removed *in vacuo*. This residue was purified by silica gel column chromatography, eluting with EtOAc and petroleum ether (2:8), to afford 1-(3,5-dimethoxyphenyl)-2-oxo-2-phenylethyl 4-(*tert*-butoxycarbonylamino)butanoate (510 mg, 85%) as a clear oil: R_f 0.49 (EtOAc/hexane, 1:1); (Found C, 65.77; H, 6.85; N, 2.91. $C_{25}H_{31}NO_7$ requires

C, 65.63; H, 6.83; N, 3.06); ν_{max}/cm^{-1} ($CHCl_3$) 3416.7 (m)(N-H), 2984.0 (m)(C-H), 1750.5 (m)(C=O), 1696.8 (m)(C=O), 1597.3 (s), 1160.5 (m)(C-O); δ_H (500 MHz; $CDCl_3$) 7.94 (2H, dd, *J* 7.9, 1.3, H_c), 7.51-7.55 (1H, m, H_e), 7.41 (2H, dd, *J* 7.9, 7.6, H_d), 6.76 (1H, s, benzylic proton), 6.59 (2H, d, *J* 2.2, H_a), 6.42 (1H, dd, *J* 2.2, 2.2, H_b), 4.72 (1H, s, NH), 3.77 (6H, s, 2 × OMe), 3.19-3.23 (2H, m, H_f), 2.47-2.61 (2H, m, H_h), 1.84-1.92 (2H, m, H_g), 1.44 (9H, s, $C(CH_3)_3$); δ_C (500 MHz; $CDCl_3$) 193.6 (C=O), 172.7 (OC=O), 161.2 (NC=O), 155.9 (C), 135.4 (C), 134.5 (C), 133.5 (C-H_e), 128.8 (C-H_d), 128.6 (C-H_c), 106.7 (C-H_a), 101.2 (C-H_b), 79.2 ($C(CH_3)_3$), 77.6 (C-H benzylic), 55.4 (OMe), 39.7 (C-H_f), 31.2 (C-H_h), 28.4 ($C(CH_3)_3$), 25.2 (C-H_g). *m/z* (ESI^+) [Found: $(M+Na)^+$ 480.1981. $C_{25}H_{31}NO_7Na$ requires M^+ 480.1993]; *m/z* (ES^+) 516 ($[M+(CH_3CN{\cdot}NH_4)]^+$, 100%).

9.8.14. (R/*S*)-1-(3,5-Dimethoxyphenyl)-2-oxo-2-phenylethyl 4-aminobutanoate hydrochloride **206**

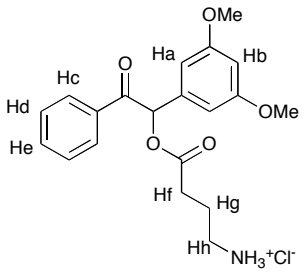

1-(3,5-Dimethoxyphenyl)-2-oxo-2-phenylethyl 4-(*tert*-butoxycarbonylamino)butanoate (500 mg, 1.093 mmol, 1.0 eq) was dissolved in a solution of 1 M HCl in acetic acid (10 mL) and stirred at RT for 4 h. An azeotrope of acetic acid and cyclohexane was removed *in vacuo* and the crude mixture precipitated in MeOH/Et_2O to afford 1-(3,5-dimethoxyphenyl)-2-oxo-2-phenylethyl 4-aminobutanoate hydrochloride (350 mg, 82%) as a yellow gum: ν_{max}/cm^{-1} (KBr) 3440.7 (s)(N-H), 2962.9 (m)(C-H), 1736.3 (m)(C=O), 1694.6 (m)(C=O), 1597.4 (s), 1160.3 (m)(C-O); δ_H (500 MHz; MeOD) 7.99 (2H, dd, *J* 7.9, 1.3, H_c), 7.57-7.60 (1H, m, H_e), 7.46 (2H, dd, *J* 7.9, 7.4, H_d), 6.93 (1H, s, benzylic proton), 6.61 (2H, d, *J* 2.2, H_a), 6.46 (1H, dd, *J* 2.2, 2.2, H_b), 3.73 (6H, s, 2 × OMe), 3.06 (2H, t, *J* 7.7, H_f), 2.58-2.72 (2H, m, H_h), 2.03 (2H, tt, *J* 7.7, 7.3, H_g); δ_C (125 MHz; MeOD) 195.9 (C=O), 173.5 (OC=O), 163.0 (C), 136.6 (C), 135.9 (C), 135.0 (C-H_e), 129.9 (C-H_d, C-H_c), 108.1 (C-H_a), 101.8 (C-H_b), 79.4 (C-H benzylic), 56.0 (OMe), 40.0 (C-H_f), 31.6 (C-H_h),

23.8 (C-H_g). *m/z* (ESI^+) [Found: $(M+H)^+$ 358.1657. $C_{20}H_{24}NO_5$ requires M^+ 358.1649]; *m/z* (ES^+) 358 ($[M+H]^+$, 100%).

9.8.15. (R/*S, S*)-1-*tert*-Butyl 5-(1-(3,5-dimethoxyphenyl)-2-oxo-2-phenylethyl) 2-(*tert*-butoxycarbonylamino)pentanedioate **227**

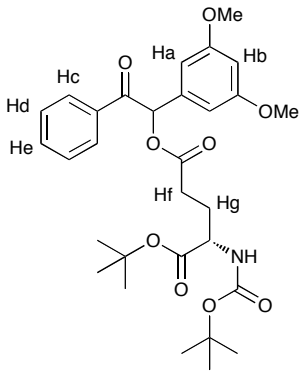

2-(3,5-Dimethoxyphenyl)-2-hydroxy-1-phenylethanone (100 mg, 0.367 mmol, 1.0 eq), 5-*tert*-butoxy-4-(*tert*-butoxycarbonylamino)-5-oxopentanoic acid (111 mg, 0.367 mmol, 1.0 eq) and DMAP (2 mg, 0.018 mmol, 0.05 eq) were dissolved in dry CH_2Cl_2 (10 mL). DCC (83 mg, 0.404 mmol, 1.1 eq) was added to the above solution. The reaction mixture was covered with foil and stirred at RT under N_2 for 72 h. After this time the reaction was adjudged complete by TLC analysis. The reaction mixture was filtered to remove the DCU side-product, quenched with water (50 mL) and the organic material extracted with CH_2Cl_2 (3 × 40 mL). The organic extracts were combined, washed with brine (50 mL), dried over Na_2SO_4, filtered and the solvent removed *in vacuo*. This residue was purified by silica gel column chromatography, eluting with EtOAc and petroleum ether (2:8), to afford 1-*tert*-butyl 5-(1-(3,5-dimethoxyphenyl)-2-oxo-2-phenylethyl) 2-(*tert*-

butoxycarbonylamino)pentanedioate (168 mg, 82%) as a mixture of diastereomers as a colourless solid: R_f 0.68 (EtOAc/hexane, 1:1); $[\alpha]_D^{25}$ +10.8 (*c* 0.5 in $CHCl_3$); (Found C, 64.57; H, 7.09; N, 2.62. $C_{30}H_{39}NO_9$ requires C, 64.62; H, 7.05; N, 2.51); mp 36-38 °C (from EtOAc/hexane); ν_{max}/cm^{-1} (CH_2Cl_2) 3357.0 (m)(N-H), 2934.1 (m)(C-H), 1700.8 (s)(C=O), 1059.6 (s)(C-O); δ_H (500 MHz; $CDCl_3$) 7.93 (2H, dd, *J* 7.9, 1.4, H_c), 7.51-7.54 (1H, m, H_e), 7.41 (2H, dd, *J* 7.9, 7.7, H_d), 6.75 (1H, d, *J* 1.9, benzylic proton), 6.59 (2H, dd, *J* 2.2, 1.9, H_a), 6.41 (1H, dd, *J* 2.2, 2.2, H_b), 5.11 (1H, 2 × d, *J* 7.9, 7.9, NH), 3.76 (6H, s, 2 × OMe), 2.51-2.57 (2H, m, H_f), 2.11-2.22 (1H, m, CH^*), 1.95-2.03 (2H, m, H_g), 1.47 (9H, s, $(CH_3)_3$), 1.46 (9H, s, $(CH_3)_3$); δ_C (100 MHz; $CDCl_3$) 193.4 (C=O), 172.3 (OC=O), 171.6 (OC=O), 171.3 (OC=O), 171.9 (C), 161.2 (C), 160.7 (C), 155.6 (C), 155.4 (C), 153.9 (C), 135.4 (C), 134.54 (C), 134.51 (C), 133.47 & 133.44 (C-H_e), 128.72 & 128.69 (C-H_c), 128.6 (C-H_d), 106.62 & 106.60 (C-H_a), 101.0 (C-H_b), 82.16 & 82.14 ($C(CH_3)_3$), 79.70 & 79.67 ($C(CH_3)_3$), 77.68 & 77.65 (C-H benzylic), 55.4 (OMe), 32.7 (CH_2), 31.9 (CH_2), 30.0 (CH_2), 28.27 & 28.24 ($(CH_3)_3$), 28.04 (CH_2), 28.02 (CH), 27.92 & 27.88 ($(CH_3)_3$). *m/z* (ESI^+) [Found: $(M+Na)^+$ 580.2523. $C_{30}H_{39}NO_9Na$ requires M^+ 580.2541]; *m/z* (ES^+) 616 ($[M+(CH_3CN{\cdot}NH_4)]^+$, 100%).

9.8.16. (R/S, *S*)-2-Amino-5-(1-(3,5-dimethoxyphenyl)-2-oxo-2-phenylethoxy)-5-oxopentanoic acid hydrochloride **208**

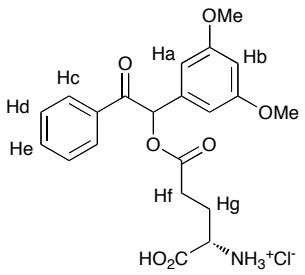

1-*tert*-Butyl 5-(1-(3,5-dimethoxyphenyl)-2-oxo-2-phenylethyl) 2-(*tert*-butoxycarbonylamino)pentanedioate (150 mg, 0.269 mmol, 1.0 eq) was dissolved in a solution of 1 M HCl in acetic acid (10 mL) and stirred at 45 °C for 3 h. An azeotrope of acetic acid and cyclohexane was removed *in vacuo* and the crude mixture purified by reverse phase silica gel chromatography, eluting with CH_3CN and water (1:3), to afford 2-amino-5-(1-(3,5-dimethoxyphenyl)-2-oxo-2-phenylethoxy)-5-oxopentanoic acid hydrochloride (73 mg, 62%) (mixture of diastereomers) as a colourless solid: $[\alpha]_D^{25}$ +9.0 (*c* 0.5 in DMSO); mp 85-87 °C (from MeOH/Et_2O); ν_{max}/cm^{-1} (KBr) 3441.3 (s)(N-H), 2926.6 (m)(C-H), 1751.0 (s)(C=O), 1697.8 (s)(C=O), 1598.1 (s)(C=O), 1160.6 (s)(C-O); δ_H (500 MHz; MeOD) 7.99 (2H, dd, *J* 7.8, 1.0, H_c), 7.56-7.59 (1H, m, H_e), 7.46 (2H, dd, *J* 7.8, 7.6, H_d), 6.91 (1H, d, *J* 1.8, benzylic proton), 6.61 (2H, dd, *J* 2.2, 1.8, H_a), 6.44 (1H, dd, *J* 2.2, 2.2, H_b), 3.73 (6H, s, 2 × OMe), 3.62-3.66 (1H, m, CH^*), 2.66-2.79 (2H, m, H_f), 2.10-2.27 (2H, m, H_g); δ_C (125 MHz; MeOD) 195.8 (C=O), 195.6 (C=O), 173.54 (OC=O), 173.46 (OC=O), 162.8 (C), 136.8 (C), 135.9 (C), 134.89 & 134.88 (C-H_e), 129.9 (C-

H_c), 129.8 (C-H_d), 107.1 (C-H_a), 101.86 & 101.85 (C-H_b), 79.33 & 79.29 (C-H benzylic), 55.3 (OMe), 55.4 & 55.3 (CH^*), 31.1 & 30.9 (C-H_f), 27.50 & 27.45 (C-H_g). *m/z* (ESI^+) [Found: $(M+H)^+$ 402.1536. $C_{21}H_{24}NO_7$ requires M^+ 402.1547]; *m/z* (ES^+) 402 ($[M+H]^+$, 100%).

9.8.17. 2-Bromo-1-(4-methoxyphenyl)ethanone **229**

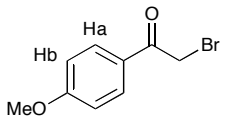

To a solution of 4-methoxyacetophenone (1.00 g, 6.659 mmol, 1.0 eq) and $AlCl_3$ (0.44 g, 3.330 mmol, 0.5 eq) in dry Et_2O (50 mL) at 0 ºC was added bromine (1.17 g, 4.995 mmol, 0.38 mL, 1.5 eq) dropwise. The reaction was left stirring at RT for 3 h. A saturated aqueous solution of $Na_2S_2O_3$ (100 mL) was added. The residue was partitioned between water (200 mL) and Et_2O (3 × 100 mL). The organic fractions were combined, dried over Na_2SO_4, filtered and concentrated *in vacuo*. Purification by silica gel column chromatography, eluting with EtOAc and petroleum ether (1.5:8.5) yielded 2-bromo-1-(4-methoxyphenyl)ethanone (0.46 g, 30%) as a colourless solid: R_f 0.80 (EtOAc/petroleum ether, 1:1); mp 70-73 °C (from EtOAc/petroleum ether) [lit.[180] mp 73 °C]; δ_H (400 MHz; $CDCl_3$) 7.98 (2H, d, *J* 8.9, H_a), 6.97 (2H, d, *J* 8.9, H_b), 4.41 (2H, s, CH_2), 3.89 (3H, s, OMe); δ_C (100 MHz; $CDCl_3$) 190.4 (C=O), 164.6 (C), 131.7 (C-H_a), 127.1 (C), 114.3 (C-H_b), 55.9 (OMe), 30.8 (CH_2). *m/z* (ES^+) 253 ($[^{81}M+Na]^+$, 97%), 251 ($[^{79}M+Na]^+$, 100%).

These data are in accordance with the literature values.[180]

9.8.18. 2-Hydroxy-1-(4-methoxyphenyl)ethanone **230**

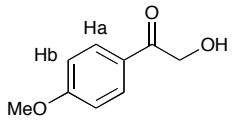

A solution of 2-bromo-1-(4-methoxyphenyl)ethanone (300 mg, 1.316 mmol, 1.0 eq) and sodium formate (540 mg, 7.896 mmol, 6.0 eq) in ethanol (85%, 10 mL) was heated under reflux for 4 h. After this time TLC analysis indicated that the reaction was complete. The ethanol was removed *in vacuo* and the residue partitioned between water (100 mL) and CH_2Cl_2 (2 × 100 mL). The organic fractions were combined, dried over Na_2SO_4, filtered and concentrated *in vacuo*. Purification of the residue by silica gel column chromatography, eluting with EtOAc and petroleum ether yielded 2-hydroxy-1-(4-methoxyphenyl)ethanone (168 mg, 77%) as a colourless solid: R_f 0.56 (EtOAc/petroleum ether, 1:1); mp 106-108 °C (from EtOAc/Et_2O) [lit.[181] mp 104-107 °C (from ethanol)]; δ_H (400 MHz; $CDCl_3$) 7.91 (2H, d, *J* 9.0, H_a), 6.97 (2H, d, *J* 9.0, H_b), 4.83 (2H, s, CH_2), 3.89 (3H, s, OMe); δ_C (100 MHz; $CDCl_3$) 197.0 (C=O), 164.7 (C), 130.3 (C-H_a), 126.6 (C), 114.5 (C-H_b), 65.3 (CH_2), 55.8 (OMe). *m/z* (ES^+) 189 ($[M+Na]^+$, 100%). These data are in accordance with the literature values.[181]

9.8.19. 2-(4-Methoxyphenyl)-2-oxoethyl 4-(*tert*-butoxycarbonylamino)butanoate **231**

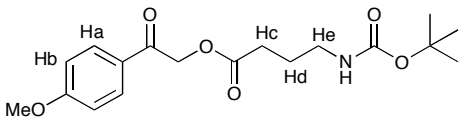

4-(*tert*-Butoxycarbonylamino)butanoic acid (257 mg, 1.264 mmol, 1.5 eq), EDC·HCl (194 mg, 1.010 mmol, 1.2 eq) and HBTU (319 mg, 0.842 mmol, 1.0 eq) were dissolved in dry CH_2Cl_2 (10 mL) and stirred at RT for 10 min. 2-Hydroxy-1-(4-methoxyphenyl)ethanone (140 mg, 0.842 mmol, 1.0 eq) and Hunig's base (218 mg, 293 μL, 1.684 mmol, 2.0 eq) were added to the above solution. The reaction mixture was covered with foil and stirred at RT under N_2 overnight. After this time the reaction was adjudged complete by TLC. The residue was partitioned between water (100 mL) and CH_2Cl_2 (2 × 100 mL). The organic extract was washed with aqueous 1 M HCl (100 mL), saturated aqueous Na_2CO_3 (100 mL) and water (100 mL). The organic extracts were combined, dried over Na_2SO_4, filtered and the solvent removed *in vacuo*. This residue was purified by silica gel column chromatography, eluting with EtOAc and petroleum ether (1.5:8.5), to afford 2-(4-methoxyphenyl)-2-oxoethyl 4-(*tert*-butoxycarbonylamino)butanoate (183 mg, 62%) as a light-yellow solid: R_f 0.78 (EtOAc/petroleum ether, 1:1); (Found C, 61.68; H, 7.06; N, 3.91. $C_{18}H_{25}NO_6$ requires C, 61.52; H, 7.17; N, 3.99); mp 83-85 °C (from EtOAc/petroleum ether); ν_{max}/cm^{-1} ($CHCl_3$) 3375.2 (m)(N-H), 2976.2 (s)(C-H), 2935.8 (s)(C-H), 1743.4 (s)(C=O), 1694.0 (vs)(C=O), 1602.2 (s)(C=O), 1244.5

(s)(C-O), 1165.2 (vs)(C-O); δ_H (500 MHz; $CDCl_3$) 7.89 (2H, d, *J* 9.0, H_a), 6.96 (2H, d, *J* 9.0, H_b), 5.32 (2H, s, OCH_2), 4.79 (1H, br s, NH), 3.88 (3H, s, OMe), 3.21-3.26 (2H, m, H_e), 2.55 (2H, t, *J* 7.2, H_c), 1.91 (2H, tt, *J* 7.2, 7.0, H_d), 1.44 (9H, s, $C(CH_3)_3$); δ_C (125 MHz; $CDCl_3$) 190.6 (C=O), 172.7 (OC=O), 164.1 (NC=O), 156.0 (C), 130.1 (C-H_a), 127.2 (C), 114.1 (C-H_b), 79.1 ($C(CH_3)_3$), 65.7 (OCH_2), 55.6 (OMe), 39.7 (C-H_e), 31.2 (C-H_c), 28.4 ($(CH_3)_3$), 25.3 (C-H_d). *m/z* (ESI^+) [Found: $(M+Na)^+$ 374.1568. $C_{18}H_{25}NO_6Na$ requires M^+ 374.1574]; *m/z* (ES^-) 386 ($[M+Cl]^-$, 100%).

9.8.20. 2-(4-Methoxyphenyl)-2-oxoethyl 4-aminobutanoate hydrochloride **232**

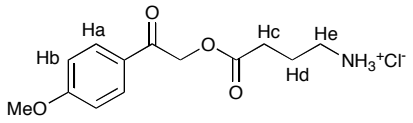

2-(4-Methoxyphenyl)-2-oxoethyl 4-(*tert*-butoxycarbonylamino)butanoate (150 mg, 0.427 mmol, 1.0 eq) was dissolved in a solution of 1 M HCl in acetic acid (10 mL) and stirred at RT for 2.5 h. After this time the reaction was adjudged complete by TLC. An azeotrope of acetic acid and cyclohexane was removed *in vacuo* to afford 2-(4-methoxyphenyl)-2-oxoethyl 4-aminobutanoate hydrochloride (96 mg, 79%) as a light-yellow solid: mp 154-156 °C (from $MeOH/Et_2O$); ν_{max}/cm^{-1} (KBr) 3439.5 (m)(N-H), 2977.0 (s)(C-H), 2923.8 (s)(C-H), 1739.7 (s)(C=O), 1691.5 (vs)(C=O), 1192.5 (s)(C-O), 1177.4 (s)(C-O); δ_H (500 MHz; MeOD) 7.99 (2H, d, *J* 8.9, H_a), 7.07 (2H, d, *J* 8.9, H_b), 5.47 (2H, s, OCH_2), 3.91 (3H, s, OMe), 3.09-3.12 (2H, m, H_e), 2.67 (2H, t, *J* 7.1, H_c), 2.05 (2H, tt, *J* 7.1, 7.6, H_d); δ_C (125 MHz; MeOD) 193.4 (C=O), 174.0 (OC=O),

166.4 (C), 131.3 (C-H_a), 128.2 (C), 115.3 (C-H_b), 67.5 (OCH_2), 56.2 (OMe), 40.1 (C-H_e), 31.5 (C-H_c), 23.9 (C-H_d). *m/z* (ESI^+) [Found: $(M+H)^+$ 252.1227. $C_{13}H_{18}NO_4$ requires M^+ 252.1230], *m/z* (ES^+) 252 ($[M+H]^+$, 100%).

9.8.21. (*S*)-1-*tert*-Butyl 5-(2-(4-methoxyphenyl)-2-oxoethyl) 2-(*tert*-butoxycarbonylamino)pentanedioate **233**

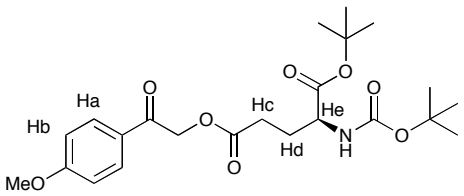

5-*tert*-Butoxy-4-(*tert*-butoxycarbonylamino)-5-oxopentanoic acid (1.04 g, 3.129 mmol, 1.0 eq), EDC·HCl (720 mg, 3.755 mmol, 1.2 eq) and HBTU (1.19 g, 3.129 mmol, 1.0 eq) were dissolved in dry CH_2Cl_2 (20 mL) and stirred at RT for 10 min. 2-Hydroxy-1-(4-methoxyphenyl)ethanone (520 mg, 3.129 mmol, 1.0 eq) and Hunig's base (809 mg, 1.1 mL, 6.258 mmol, 2.0 eq) were added to the above solution. The reaction mixture was covered with foil and stirred at RT under N_2 overnight. After this time the reaction was adjudged complete by TLC. The residue was partitioned between water (100 mL) and CH_2Cl_2 (2 × 100 mL). The organic extract was washed with aqueous 1M HCl (100 mL), saturated aqueous Na_2CO_3 (100 mL) and water (100 mL). The organic extracts were combined, dried over $MgSO_4$, filtered and the solvent removed *in vacuo*. This residue was purified by silica gel column chromatography, eluting with EtOAc and petroleum ether (2.5:7.5), to afford 1-*tert*-butyl 5-(2-(4-methoxyphenyl)-2-oxoethyl) 2-(*tert*-butoxycarbonylamino)pentanedioate

(942 mg, 67%) as a clear oil: R_f 0.47 (EtOAc/petroleum ether, 1:1); $[\alpha]_D^{25}$ +7.17 (*c* 0.6 in $CHCl_3$); (Found C, 61.06; H, 7.34; N, 3.02. $C_{23}H_{33}NO_8$ requires C, 61.18; H, 7.37; N, 3.10); ν_{max}/cm^{-1} ($CHCl_3$) 3370.5 (m)(N-H), 2978.4 (s)(C-H), 2935.6 (s)(C-H), 1839.2 (s)(C=O), 1697.8 (vs)(C=O), 1602.5 (s)(C=O), 1243.4 (s)(C-O), 1162.2 (vs)(C-O); δ_H (500 MHz; $CDCl_3$) 7.89 (2H, d, *J* 9.0, H_a), 6.95 (2H, d, *J* 9.0, H_b), 5.30 (2H, s, OCH_2), 5.16 (1H, d, *J* 8.1, NH), 4.18-4.29 (1H, m, H_e), 3.87 (3H, s, OMe), 2.53-2.63 (2H, m, H_c), 2.15-2.32 (1H, m, H_d), 1.89-2.07 (1H, m, H_d), 1.47 (9H, s, $C(CH_3)_3$), 1.43 (9H, s, $C(CH_3)_3$); δ_C (125 MHz; $CDCl_3$) 190.5 (C=O), 172.4 (OC=O), 171.1 (OC=O), 164.1 (NC=O), 155.5 (C), 130.1 (C-H_a), 127.2 (C), 114.1 (C-H_b), 82.2 ($C(CH_3)_3$), 79.7 ($C(CH_3)_3$), 65.8 (OCH_2), 55.4 (OMe), 53.3 (C-H_e), 30.1 (C-H_c), 28.3 (($CH_3)_3$), 28.08 (C-H_d), 27.98 (($CH_3)_3$). *m/z* (ESI^+) [Found: $(M+Na)^+$ 474.2078. $C_{23}H_{33}NO_8Na$ requires M^+ 474.2098]; *m/z* (ES^-) 486 ($[M+Cl]^-$, 100%).

9.8.22. (*S*)-2-Amino-5-(2-(4-methoxyphenyl)-2-oxoethoxy)-5-oxopentanoic acid hydrochloride **234**

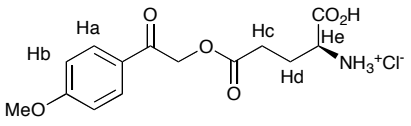

1-*tert*-Butyl 5-(2-(4-methoxyphenyl)-2-oxoethyl) 2-(*tert*-butoxycarbonylamino)pentanedioate (900 mg, 1.995 mmol, 1.0 eq) was dissolved in a solution of 1 M HCl in acetic acid (15 mL) and stirred at 45 °C for 4 h. An azeotrope of acetic acid and cyclohexane was removed *in vacuo* to afford 2-amino-5-(2-(4-methoxyphenyl)-2-oxoethoxy)-5-oxopentanoic acid hydrochloride (450 mg, 76%) as a light-yellow solid: $[\alpha]_D^{25}$ +10.2 (*c* 0.5 in DMSO); mp 174-176 °C (from MeOH); ν_{max}/cm^{-1} (KBr) 3437.3 (m)(N-H), 2930.7 (s)(C-H), 2344.4 (s), 1752.2 (s)(C=O), 1684.7 (s)(C=O), 1605.2 (s)(C=O), 1245.0 (s)(C-O), 1176.8 (s)(C-O); δ_H (500 MHz; DMSO) 7.95 (2H, d, *J* 8.9, H_a), 7.08 (2H, d, *J* 8.9, H_b), 5.45 (2H, s, OCH_2), 3.86 (3H, s, OMe), 3.72-3.76 (1H, m, H_e), 2.69-2.75 (1H, m, H_c), 2.57-2.64 (1H, m, H_c), 1.99-2.15 (2H, m, H_d); δ_C (125 MHz; DMSO) 190.9 (C=O), 171.6 (OC=O), 163.7 (C), 130.1 (C-H_a), 126.7 (C), 114.2 (C-H_b), 66.3 (OCH_2), 55.7 (OMe), 52.0 (C-H_e), 29.4 (C-H_c), 25.8 (C-H_d). *m/z* (ESI$^+$) [Found: $(M+H)^+$ 318.0947. $C_{14}H_{17}NO_6Na$ requires M^+ 318.0948]; *m/z* (ES$^+$) 296 ($[M+H]^+$, 100%).

9.8.23. 2-Bromo-1-(4-hydroxyphenyl)ethanone **236**

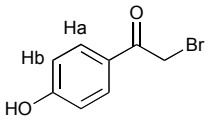

To a solution of 4-hydroxyacetophenone (1.00 g, 7.35 mmol, 1.0 eq) and $AlCl_3$ (0.49 g, 3.67 mmol, 0.5 eq) in dry Et_2O (50 mL) at 0 ºC was added bromine (1.29 g, 8.09 mmol, 0.41 mL, 1.1 eq) dropwise. The reaction mixture was left stirring at RT for 1.5 h. After this time TLC analysis indicated that the reaction was complete. A saturated aqueous solution of $Na_2S_2O_3$ was added. The residue was partitioned between water (200 mL) and Et_2O (3 × 100 mL). The organic fractions were combined, dried over Na_2SO_4, filtered and concentrated *in vacuo*. Purification by silica gel column chromatography, eluting with MeOH and CH_2Cl_2 (2:98) yielded 2-bromo-1-(4-hydroxyphenyl)ethanone (0.81 g, 51%) as a colourless solid: R_f 0.56 (EtOAc/petroleum ether, 1:1); mp 126-127 °C (from MeOH/petroleum ether) [Lit.[22] mp 129-131 °C]; δ_H (400 MHz; MeOD) 7.93 (2H, d, *J* 8.6, H_a), 6.87 (2H, d, *J* 8.6, H_b), 4.56 (2H, s, CH_2); δ_C (100 MHz; MeOD) 191.3 (C=O), 163.5 (C), 131.9 (C-H_a), 126.1 (C), 115.6 (C-H_b), 30.9 (CH_2). *m/z* (ES^-) 215 ($[^{81}M\text{-}H]^-$, 100%), 213 ($[^{79}M\text{-}H]^-$, 90%). These data are in accordance with the literature values.[22]

9.8.24. (*S*)-1-*tert*-Butyl 5-(2-(4-hydroxyphenyl)-2-oxoethyl) 2-((*tert*-butoxycarbonyl)amino)pentanedioate **237**

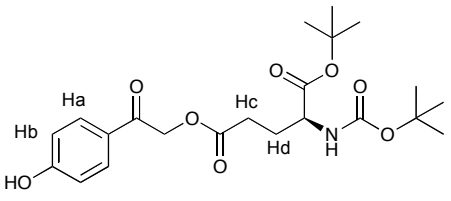

A solution of 2-bromo-1-(4-hydroxyphenyl)ethanone (200 mg, 0.930 eq, 1.0 eq) in THF (25 mL) was cooled to 0 °C. 5-*tert*-Butoxy-4-(*tert*-butoxycarbonylamino)-5-oxopentanoic acid (280 mg, 0.930 mmol, 1.0 eq) was added to this solution. DBU (156 mg, 153 μL, 1.023 mmol, 1.1 eq) was added dropwise. The reaction mixture was covered with foil and stirred at RT under N_2 overnight. After this time the reaction was adjudged complete by TLC. The reaction mixture was filtered to remove the DBU·HBr salts and the filtrate concentrated *in vacuo*. The residue was partitioned between water (100 mL) and CH_2Cl_2 (2 × 100 mL). The organic extracts were combined, dried over Na_2SO_4, filtered and the solvent removed *in vacuo*. This residue was purified by silica gel column chromatography, eluting with EtOAc and petroleum ether (3.5:7.5), to afford 1-*tert*-butyl 5-(2-(4-hydroxyphenyl)-2-oxoethyl) 2-((*tert*-butoxycarbonyl)amino)pentanedioate (260 mg, 64%) as a colourless solid: R_f 0.46 (EtOAc/petroleum ether, 1:1); $[\alpha]_D^{25}$ +6.30 (*c* 1.0 in $CHCl_3$); (Found C, 60.51; H, 7.12; N, 3.06. $C_{22}H_{31}NO_8$ requires C, 60.40; H, 7.14; N, 3.20); mp 109-111 °C (from EtOAc/Et_2O); ν_{max}/cm^{-1} ($CHCl_3$) 3351.8 (m)(N-H), 2980.2 (s)(C-H), 2935.6 (s)(C-H), 1732.1 (vs)(C=O), 1691.4 (vs)(C=O),

1230.2 (s)(C-O), 1163.6 (vs)(C-O); δ_H (500 MHz; $CDCl_3$) 7.79 (2H, d, *J* 8.4, H_a), 6.90 (2H, d, *J* 8.4, H_b), 5.28-5.30 (1H, m, NH), 5.27 (2H, 2 × d, *J* 16.5, 16.5, OCH_2), 4.25-4.29 (1H, m, CH^*), 2.52-2.66 (2H, m, H_c), 2.21-2.28 (1H, m, H_d), 1.97-2.04 (1H, m, H_d), 1.48 (9H, s, $(CH_3)_3$), 1.45 (9H, s, $(CH_3)_3$); δ_C (125 MHz; $CDCl_3$) 190.5 (C=O), 172.5 (OC=O), 171.4 (OC=O), 161.7 (NC=O), 155.8 (C), 130.4 (C-H_a), 126.5 (C), 115.8 (C-H_b), 82.5 (*C*$(CH_3)_3$), 80.2 (*C*$(CH_3)_3$), 65.8 (OCH_2), 53.4 (CH^*), 30.1 (C-H_c), 28.3 ($(CH_3)_3$), 28.03 (C-H_d), 27.96 ($(CH_3)_3$). *m/z* (ESI^+) [Found: $(M+Na)^+$ 460.1939. $C_{22}H_{31}NO_8Na$ requires M^+ 460.1942]; *m/z* (ES^+) 897 (100%), 460 ($[M+Na]^+$, 35%).

9.8.25. (*S*)-2-Amino-5-(2-(4-hydroxyphenyl)-2-oxoethoxy)-5-oxopentanoic acid hydrochloride **238**

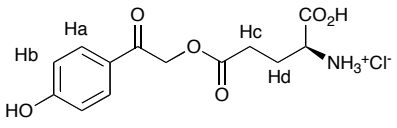

1-*tert*-Butyl 5-(2-(4-hydroxyphenyl)-2-oxoethyl) 2-((*tert*-butoxycarbonyl)amino)pentanedioate (68 mg, 0.156 mmol, 1.0 eq) was dissolved in a solution of 1 M HCl in acetic acid (5 mL) and stirred at 45 °C for 3 h. An azeotrope of acetic acid and cyclohexane was removed *in vacuo.* The residue was purified by reverse phase silica column chromatography eluting with CH_3CN and water (1:4) to afford 2-amino-5-(2-(4-hydroxyphenyl)-2-oxoethoxy)-5-oxopentanoic acid hydrochloride (37 mg, 74%) as a light-yellow solid: mp 180-183 °C (from MeOH/Et_2O); $[\alpha]_D^{25}$ -6.09 (*c* 0.12 in DMSO); ν_{max}/cm^{-1} (MeOH) 2939.1 (s)(C-H), 1738.1 (s)(C=O), 1680.7 (s)(C=O), 1603.6

(vs)(C=O), 1230.0 (s)(C-O), 1170.9 (vs)(C-O); δ_H (500 MHz; MeOD) 7.89 (2H, d, *J* 8.2, H_a), 6.90 (2H, d, *J* 8.2, H_b), 5.47 & 5.43 (2H, 2 × d, *J* 16.7, 16.7, OCH_2), 4.09-4.19 (1H, m, CH^*), 2.72-2.85 (2H, m, H_c), 2.18-2.43 (2H, m, H_d); δ_C (125 MHz; MeOD) 193.1 (C=O), 173.2 (OC=O), 171.6 (C), 164.6 (CO_2H), 131.6 (C-H_a), 127.1 (C), 116.6 (C-H_b), 67.4 (OCH_2), 53.5 (CH^*), 30.6 (C-H_c), 26.9 (C-H_d). *m/z* (ESI^+) [Found: $(M+Na)^+$ 304.0792. $C_{13}H_{15}NO_6Na$ requires M^+ 304.0792]; *m/z* (ES^-) 280 ($[M-H]^-$, 100%).

9.9. Synthesis of a Potential pH-Dependent Caging Group

9.9.1. Triisopropyl (3-methyl-4-nitrophenoxy)silane **251**

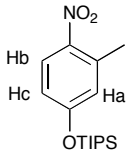

To a solution of 3-methyl-4-nitrophenol (5.00 g, 32.6 mmol, 1.0 eq) and imidazole (6.89 g, 101.2 mmol, 3.1 eq) in DMF (50 mL) at RT was added triisopropylchlorosilane (8.2 g, 10.6 mL, 42.4 mmol, 1.3 eq). The resulting solution was stirred at RT overnight, becoming dark brown in colour. TLC analysis indicated that the reaction was complete. The DMF was removed *in vacuo* to yield a thick, brown liquid. The residue was partitioned between CH_2Cl_2 (2 × 100 mL) and water (100 mL). The organic extracts were combined, dried over Na_2SO_4, filtered and the solvent removed *in vacuo*. The residue was purified by silica gel column chromatography, eluting with hexane followed by EtOAc and hexane (2:8), to afford triisopropyl (3-methyl-4-nitrophenoxy)silane (10.05 g, 99%) as a yellow oil: R_f 0.66 (EtOAc/hexane, 2:8); ν_{max}/cm^{-1} ($CHCl_3$) 2946.5 (s)(Ar-H), 2893.1 (m)(C-H), 2868.7 (s)(C-H), 1606.6 (s)(C=C, Ar), 1580.8 (s)(C=C, Ar), 1513.1 (s)(NO_2), 1486.9 (s), 1340.8 (s)(NO_2), 1284.2 (s), 1081.2 (m)(C-O), 996.9 (m)(Si-O), 882.4 (m)(two adj. Ar-H); δ_H (300 MHz; $CDCl_3$) 8.00 (1H, d, *J* 9.8, H_b), 6.76 (1H, dd, *J* 9.8, 2.5, H_c), 6.74 (1H, d, *J* 2.5, H_a), 2.59 (3H, s, CH_3), 1.32-1.23 (3H, sp, *J* 7.1, Si[C*H*(CH_3)$_2$]$_3$), 1.10 (18H, d, *J* 7.1, Si[CH(C*H*$_3$)$_2$]$_3$); δ_C (75.5 MHz; $CDCl_3$)

160.4 (CO), 142.4 (CNO_2), 136.8 (CCH_3), 127.4 (C-H_b), 123.3 (C-H_c), 117.7 (C-H_a), 21.4 (CH_3), 17.8 (Si[*CH*(CH_3)$_2$]$_3$), 12.7 (Si[CH(*CH_3*)$_2$]$_3$). ***m/z*** (EI) [Found: $(M)^+$ 309.1750. $C_{16}H_{27}NO_3Si$ requires M^+ 309.1755]; ***m/z*** (CI^+) 327 ($[M+NH_4]^+$, 17%), 280 (100%).

9.9.2. Triisopropyl (4-methyl-3-nitrophenoxy)silane

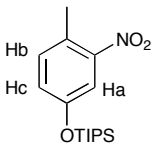

To a solution of 4-methyl-3-nitrophenol (1.50 g, 9.79 mmol, 1.0 eq) and imidazole (2.07 g, 30.4 mmol, 3.1 eq) in DMF (15 mL) at RT was added triisopropylchlorosilane (2.45 g, 3.17 mL, 12.7 mmol, 1.3 eq). The resulting solution was stirred at RT overnight. TLC analysis indicated that the reaction was complete. The DMF was removed *in vacuo* to yield a thick, brown liquid. The residue was partitioned between CH_2Cl_2 (2 × 100 mL) and water (100 mL). The organic extracts were combined, dried over Na_2SO_4, filtered and the solvent removed *in vacuo*. The residue was purified by silica gel column chromatography, eluting with hexane followed by EtOAc and hexane (2:8), to afford triisopropyl (4-methyl-3-nitrophenoxy)silane (2.70 g, 89%) as a light-yellow oil: R_f 0.66 (EtOAc/hexane, 2:8); ν_{max}/cm^{-1} ($CHCl_3$) 2946.7 (s)(C-H), 2893.1 (s)(C-H), 2868.6 (s)(C-H), 1622.3 (s)(C=C, Ar), 1533.6 (s)(NO_2), 1498.4 (s), 1464.5 (s), 1343.7 (s)(NO_2), 1296.3 (s), 1257.7 (s), 1066.1 (m)(C-O), 997.5 (m)(Si-O), 968.5 (s), 882.3 (s)(two adj. Ar-H); δ_H (300 MHz; $CDCl_3$) 7.49 (1H, d, *J* 2.5, H_a), 7.16 (1H, d, *J* 8.5, H_b), 7.02 (1H, dd, *J* 8.5, 2.5, H_c),

2.50 (3H, s, CH_3), 1.30-1.21 (3H, sp, *J* 7.1, Si[C*H*$(CH_3)_2]_3$), 1.09 (18H, d, *J* 7.1, Si[CH(C*H*$_3)_2]_3$); δ_C (100 MHz; $CDCl_3$) 154.8 (CO), 149.5 (CNO_2), 133.6 (C-H_b), 126.0 (CCH_3), 125.0 (C-H_c), 115.8 (C-H_a), 19.9 (CH_3), 17.9 (Si[*CH*$(CH_3)_2]_3$), 12.7 (Si[CH(*CH*$_3)_2]_3$). *m/z* (ES^+) [Found: $(M+NH_4)^+$ 327.2095. $C_{16}H_{31}N_2O_3Si$ requires M^+ 327.2098]; *m/z* (Cl^+) 327 ($[M+NH_4]^+$, 33%), 280 (100%).

9.9.3. *tert*-Butyldimethyl(3-methyl-4-nitrophenoxy)silane **253**

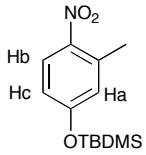

A suspension of 3-methyl-4-nitrophenol (2.00 g, 13.06 mmol, 1.0 eq) in dry CH_2Cl_2 (20 mL) was prepared. The suspension turned purple-red upon the addition of NEt_3 (4.54 mL, 3.30 g, 32.66 mmol, 2.5 eq). *tert*-Butyldimethylchlorosilane (TBSCl) (2.36 g, 15.68 mmol, 1.2 eq) was added to the reaction mixture, which was left stirring at RT overnight. The reaction was quenched with water (80 mL) and the organic material extracted with CH_2Cl_2 (3 × 80 mL). The organic extracts were combined, dried over Na_2SO_4, filtered and the solvent removed *in vacuo*. The residue was purified by silica gel column chromatography, eluting with hexane followed by EtOAc and hexane (1:9), to afford *tert*-butyldimethyl(3-methyl-4-nitrophenoxy)silane (2.80 g, 80%) as an orange oil: R_f 0.50 (EtOAc/hexane, 1:9); ν_{max}/cm^{-1} ($CHCl_3$) 2957.3 (s)(C-H), 2931.7 (s)(C-H), 2859.8 (s)(C-H), 1606.5 (s), 1581.3 (s), 1512.6 (s)(NO_2), 1487.1 (s), 1341.5 (s)(NO_2), 1284.3 (s), 1253.9 (s)(Si-CH_3), 1081.2 (s)(C-O),

1006.4 (m)(Si-O), 972.5 (s), 827.2 (s)(two adj. Ar-H), 784.6 (s)(Si-O); δ_H (300 MHz; $CDCl_3$) 8.02 (1H, d, *J* 9.6, H_b), 6.75 (1H, dd, *J* 9.6, 2.6, H_c), 6.74 (1H, d, *J* 2.6, H_a), 2.60 (3H, s, $ArCH_3$), 1.00 (9H, s, $SiC(CH_3)_3$), 0.26 (6H, s, $Si(CH_3)_2$); δ_C (75.5 MHz; $CDCl_3$) 160.0 (C), 142.7 (C), 136.9 (C), 127.3 (C-H_b), 123.6 (C-H_c), 117.9 (C-H_a), 25.5 ($SiC(\mathit{CH_3})_3$), 21.4 ($ArCH_3$), 18.2 ($Si\mathit{C}(CH_3)_3$), -4.4 ($Si(\mathit{C}H_3)_2$). *m/z* (ES^+) [Found: $(M+NH_4)^+$ 285.1629. $C_{13}H_{25}N_2O_3Si$ requires M^+ 285.1629]; *m/z* (CI^+) 285 ($[M+NH_4]^+$, 64%), 238 (100%).

9.9.4. (3-(Bromomethyl)-4-nitrophenoxy)(*tert*-butyl)dimethylsilane **254**

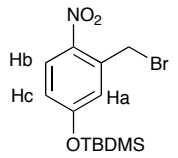

A solution of *tert*-butyldimethyl(3-methyl-4-nitrophenoxy)silane (2.00 g, 7.50 mmol, 1.0 eq) in dry CCl_4 (40 mL) was prepared. Recrystallised *N*-bromosuccinimide (2.00 g, 11.23 mmol, 1.5 eq) and recrystallised dibenzoyl peroxide (120 mg, 0.50 mmol, 7 mol%) were added to the solution. The reaction mixture was heated under reflux under N_2 for 120 h. TLC analysis indicated that the reaction was complete. The reaction mixture was allowed to cool to RT. After filtering the reaction mixture, the filtrate was collected and the solvent removed *in vacuo*. The crude residue was purified by silica gel column chromatography, eluting with CH_2Cl_2 and hexane (5:95) to afford (3-(bromomethyl)-4-nitrophenoxy)(*tert*-butyl)dimethylsilane (388 mg, 15%) as a brown oil: R_f 0.37 (EtOAc/hexane, 1:9); ν_{max}/cm^{-1} ($CHCl_3$) 2930.9 (s)(C-H), 1604.3 (s), 1580.9 (vs)(NO_2), 1518.4 (vs), 1339.7 (vs)(NO_2), 1260.4 (vs)(Si-

CH_3), 1077.9 (m)(C-O), 1006.9(w)(Si-O), 986.7 (s), 858.6 (s), 826.5 (vs)(two adj. Ar-H), 785.0 (s)(Si-O); δ_H (300 MHz; $CDCl_3$) 8.08 (1H, d, *J* 9.0, H_b), 6.99 (1H, d, *J* 2.7, H_a), 6.86 (1H, dd, *J* 9.0, 2.7, H_c), 4.83 (2H, s, CH_2Ar), 1.00 (9H, s, $SiC(CH_3)_3$), 0.28 (6H, s, $Si(CH_3)_2$); δ_C (75.5 MHz; $CDCl_3$) 160.5 (C), 141.6 (CNO_2), 135.6 (C), 128.2 (C-H_b), 123.5 (C-H_a), 120.1 (C-H_c), 29.7 (CH_2Ar), 25.5 ($SiC(\mathit{CH_3})_3$), 18.5 ($SiC(CH_3)_3$), -4.4 ($Si(\mathit{C}H_3)_2$). *m/z* (Cl^-) [Found: (^{79}M-H)$^-$ 344.0326. $C_{13}H_{19}NO_3Si^{79}Br$ requires M^- 344.0323]; *m/z* (Cl^-) 346 ([^{81}M-H]$^-$, 84%), 344 ([^{79}M-H]$^-$, 100%).

9.9.5. 5-Hydroxy-2-nitrobenzyl 4-fluorobenzoate **257**

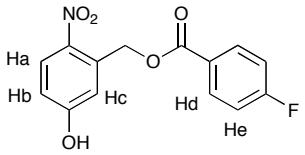

Method A

To a solution of 5-hydroxy-2-nitrobenzyl alcohol (0.80 g, 4.73 mmol, 1.0 eq) in dry CH_2Cl_2 (50 mL) at 0 °C was added 4-DMAP (29 mg, 0.24 mmol, 0.05 eq). Dry pyridine (0.56 g, 0.57 mL, 7.10 mmol, 1.5 eq) was added dropwise. After stirring for 45 min at 0 °C, 4-fluorobenzyl chloride (0.83 g, 0.62 mL, 5.20 mmol, 1.1 eq) was added dropwise. The reaction was left stirring at RT for 72 h before TLC analysis indicated that the reaction was complete. The reaction was quenched with water (200 mL) and the organic phase collected. The aqueous phase was extracted with CH_2Cl_2 (2 × 100 mL). The organic

layers were combined, dried over Na_2SO_4, filtered and the solvent removed *in vacuo*. The residue was purified by silica gel column chromatography, eluting with EtOAc and petroleum ether (2:8), to afford 5-hydroxy-2-nitrobenzyl 4-fluorobenzoate (0.73 g, 50%) as a light-yellow solid.

Method B

4-Fluorobenzoic acid (138 mg, 0.986 mmol, 1.0 eq), EDC·HCl (227 mg, 1.183 mmol, 1.2 eq) and HBTU (374 mg, 0.986 mmol, 1.0 eq) were dissolved in dry CH_2Cl_2 (7 mL) and stirred at RT for 10 min. 5-Hydroxy-2-nitrobenzyl alcohol (200 mg, 1.183 mmol, 1.2 eq) and Hunig's base (255 mg, 344 μL, 1.972 mmol, 2.0 eq) were added to the above solution. The reaction mixture was stirred at RT under N_2 overnight. After this time the reaction was adjudged complete by TLC analysis. The residue was partitioned between water (50 mL) and CH_2Cl_2 (2 × 50 mL). The organic extract was washed with aqueous 1 M HCl (50 mL), saturated aqueous Na_2CO_3 (50 mL) and water (50 mL). The organic extracts were combined, dried over $MgSO_4$, filtered and the solvent removed *in vacuo*. This residue was purified by silica gel column chromatography, eluting with EtOAc and petroleum ether (2:8) to afford 5-hydroxy-2-nitrobenzyl 4-fluorobenzoate (175 mg, 61%) as a light-yellow solid: R_f 0.59 (EtOAc/petroleum ether, 1:1); (Found C, 57.80; H, 3.52; N, 4.89. $C_{14}H_{10}FNO_5$ requires C, 57.74; H, 3.46; N, 4.81); mp 73-75 °C (from EtOAc/Et_2O); ν_{max}/cm^{-1} ($CHCl_3$) 3350.1 (br)(O-H), 1741.1 (s)(C=O), 1520.8 (s)(NO_2), 1344.7 (m)(NO_2), 1063.3 (s)(C-O); δ_H (400 MHz; $CDCl_3$) 8.25 (1H, d, *J* 8.9, H_a), 8.23 (2H, dd, ^3J H-F 14.1, ^3J H-H 8.7, H_e), 7.70 (1H, d, *J* 2.6, H_c),

7.35 (1H, dd, *J* 8.9, 2.6, H_b), 7.22 (2H, dd, ^4J H-F 8.7, ^3J H-H 8.7, H_d), 5.08 (2H, s, CH_2); δ_F (282 MHz; $CDCl_3$) -102.9 (F); δ_C (100 MHz; $CDCl_3$) 166.6 (d, ^1J 253.8, C-F), 163.4 (C=O), 155.1 (C), 144.3 (C), 140.1 (C), 133.0 (d, ^3J 9.8, C-H_d), 127.0 (C-H_a), 124.8 (C), 122.4 (C-H_c), 121.4 (C-H_b), 116.1 (d, ^2J 22.0, C-H_e), 62.2 (CH_2). *m/z* (ESI^+) [Found: $(M+Na)^+$ 314.0438. $C_{14}H_{10}FNO_5Na$ requires M^+ 314.0435]; *m/z* (ES^-) 290 ([M-H]$^-$, 90%), 168 (100%).

9.9.6. 2-(4-Hydroxyphenyl)-2-oxoethyl 4-fluorobenzoate

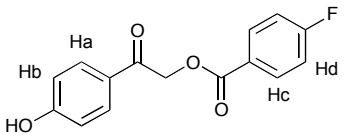

A solution of 2-bromo-1-(4-hydroxyphenyl)ethanone (600 mg, 2.789 mmol, 1.0 eq) in THF (50 mL) was cooled to 0 °C. 4-Fluorobenzoic acid (390 mg, 2.789 mmol, 1.0 eq) was added to this solution. DBU (467 mg, 460 μL, 3.068 mmol, 1.1 eq) was added dropwise. The reaction mixture was covered with foil and stirred at RT under N_2 overnight. After this time the reaction was adjudged complete by TLC. The reaction mixture was filtered to remove the DBU·HBr salts and the filtrate concentrated *in vacuo*. The residue was partitioned between water (100 mL) and CH_2Cl_2 (2 × 100 mL). The organic extracts were combined, dried over Na_2SO_4, filtered and the solvent removed *in vacuo*. This residue was purified by silica gel column chromatography, eluting with EtOAc and petroleum ether (2:8), to afford 2-(4-hydroxyphenyl)-2-oxoethyl 4-fluorobenzoate (530 mg, 69%) as a colourless solid: R_f 0.43 (EtOAc/petroleum ether, 1:1); (Found C, 65.83; H, 3.99. $C_{15}H_{11}FO_4$ requires

C, 65.69; H, 4.04); mp 158-160 °C (from EtOAc/Et_2O); ν_{max}/cm^{-1} (MeOH) 1720.8 (s)(C=O), 1673.4 (s)(C=O), 1376.0 (s)(C-O), 1244.7 (s)(C-O); δ_H (500 MHz; MeOD) 8.18 (2H, dd, ^3J H-F 14.3, ^3J H-H 8.9, H_d), 7.94 (2H, d, J 8.8, H_a), 7.27 (2H, dd, ^3J H-H 8.9, ^4J H-F 8.7, H_c), 6.91 (2H, d, J 8.8, H_b), 5.63 (2H, s, OCH_2); δ_F (282 MHz; MeOD) -107.6 (F); δ_C (125 MHz; MeOD) 192.8 (C=O), 167.5 (d, ^1J 253.6, C-F), 166.6 (OC=O), 164.5 (C), 133.1 (d, ^3J 9.6, C-H_c), 131.6 (C-H_a), 127.5 (d, ^4J 2.8, C), 127.3 (C), 116.6 (d, ^2J 21.9, C-H_d), 116.59 (C-H_b), 67.7 (CH_2). *m/z* (ESI^+) [Found: $(M+Na)^+$ 297.0535. $C_{15}H_{11}FO_4Na$ requires M^+ 297.0534]; *m/z* (ES^+) 297 ($[M+Na]^+$, 100%).

Bibliography

(1) Lee, H. M.; Larson, D. R.; Lawrence, D. S. *ACS Chem. Biol.* **2009**, *4*, 409-427.

(2) Barltrop, J. A.; Schofield, P. *Tetrahedron Lett.* **1962**, *3*, 697-699.

(3) Mayer, G.; Heckel, A. *Angew. Chem. Int. Ed.* **2006**, *45*, 4900-4921.

(4) Kao, J. P. Y.; University of Maryland Seminar: Baltimore, 2008, p 1-12.

(5) Kaplan, J. H.; Forbush, B.; Hoffman, J. F. *Biochemistry* **1978**, *17*, 1929-1935.

(6) Barton, D. H. R.; Chow, Y. L.; Cox, A.; Kirby, G. W. *Tetrahedron Lett.* **1962**, *3*, 1055-1057.

(7) Givens, R. S.; Conrad, P. G.; Yousef, A. L.; Lee, J.-I. In *CRC Handbook of Organic Photochemistry and Photobiology*; 2nd ed.; Horspooled, W. M., Ed.; CRC Press: 2003, p 69.1-69.46.

(8) Engels, J.; Schlaeger, E.-J. *J. Med. Chem.* **1977**, *20*, 907-911.

(9) Forbush, B. *Proc. Natl. Acad. Sci. USA* **1984**, *81*, 5310-5314.

(10) Givens, R. S.; Weber, J. F. W.; Jung, A. H.; Park, C.-H. *Methods Enzymol.* **1998**, *291*, 1-29.

(11) Pelliccioli, A. P.; Wirz, J. *Photochem. Photobiol. Sci.* **2002**, *1*, 441-458.

(12) Barltrop, J. A.; Plant, P. J.; Schofield, P. *J. Chem. Soc., Chem. Commun.* **1966**, 822-823.

(13) Bochet, C. G. *J. Chem. Soc., Perkin Trans. 1* **2002**, 125-142.

(14) Blanc, A.; Bochet, C. G. *J. Org. Chem.* **2003**, *68*, 1138-1141.

(15) Hasan, A.; Stengele, K. P.; Giegrich, H.; Cornwell, P.; Isham, K. R.; Sachleben, R. A.; Pfleiderer, W.; Foote, R. S. *Tetrahedron* **1997**, *53*, 4247-4264.

(16) Specht, A.; Thomann, J.-S.; Alarcon, K.; Wittayanan, W.; Ogden, D.; Furuta, T.; Kurakawa, Y.; Goeldner, M. *ChemBioChem* **2006**, *7*, 1690-1695.

(17) Walbert, S.; Pfleiderer, W.; Steiner, U. E. *Helv. Chim. Acta* **2001**, *84*, 1601-1611.

(18) Bamford, C. H.; Norrish, R. G. W. *J. Am. Chem. Soc.* **1935**, 1504-1511.

(19) Il'ichev, Y. V.; Schworer, M. A.; Wirz, J. *J. Am. Chem. Soc.* **2004**, *126*, 4581-4595.

(20) Gaplovsky, M.; Il'ichev, Y.; Kamdzhilov, Y.; Kombarova, S. V.; Mac, M.; Schworer, M. A.; Wirz, J. *Photochem. Photobiol. Sci.* **2005**, *4*, 33-42.

(21) Pirrung, M. C.; Lee, Y. R.; Park, K.; Springer, J. B. *J. Org. Chem.* **1999**, *64*, 5042-5047.

(22) Park, C.-H.; Givens, R. S. *J. Am. Chem. Soc.* **1997**, *119*, 2453-2463.

(23) Sheehan, J. C.; Wilson, R. M. *J. Am. Chem. Soc.* **1964**, *86*, 5277-5281.
(24) Sheehan, J. C.; Wilson, R. M.; Oxford, A. W. *J. Am. Chem. Soc.* **1971**, *93*, 7222-7228.
(25) Givens, R. S.; Matuszewski, B. *J. Am. Chem. Soc.* **1984**, *106*, 6860-6861.
(26) Givens, R. S.; Athey, P. S.; Matuszewski, B.; Kueper, L. W.; Xue, J.-Y.; Fister, T. *J. Am. Chem. Soc.* **1993**, *115*, 6001-6012.
(27) Pirrung, M. C.; Ye, T.; Zhou, Z.; Simon, J. D. *Photochem. Photobiol.* **2006**, *82*, 1258-1264.
(28) Zimmerman, H. E.; Sandel, V. R. *J. Am. Chem. Soc.* **1962**, *85*, 915-922.
(29) Sheehan, J. C.; Umezawa, K. *J. Org. Chem.* **1973**, *38*, 3771-3774.
(30) Epstein, W. W.; Garrossian, M. *J. Chem. Soc., Chem. Commun.* **1987**, 532-533.
(31) Givens, R. S.; Kueper, L. W. *Chem. Rev.* **1993**, *93*, 55-66.
(32) Anderson, J. C.; Reese, C. B. *Tetrahedron Lett.* **1962**, *3*, 1-4.
(33) Givens, R. S.; Park, C.-H. *Tetrahedron Lett.* **1996**, *37*, 6259-6262.
(34) Givens, R. S.; Jung, A.; Park, C.-H.; Weber, J.; Bartlett, W. *J. Am. Chem. Soc.* **1997**, *119*, 8369-8370.
(35) Zhang, K.; Corrie, J. E. T.; Munasinghe, V. R. N.; Wan, P. *J. Am. Chem. Soc.* **1999**, *121*, 5625-5632.
(36) Conrad, P. G.; Givens, R. S.; Hellrung, B.; Rajesh, C. S.; Ramseier, M.; Wirz, J. *J. Am. Chem. Soc.* **2000**, *122*, 9346-9347.
(37) Givens, R. S.; Heger, D.; Hellrung, B.; Kamdzhilov, Y.; Mac, M.; Conrad, P. G.; Cope, E.; Lee, J. I.; Mata-segreda, J. F.; Schowen, R. L.; Wirz, J. *J. Am. Chem. Soc.* **2008**, *130*, 3307-3309.
(38) Hagen, V.; Bendig, J.; Frings, S.; Wiesner, B.; Schade, B.; Helm, S.; Lorenz, D.; Kaupp, U. B. *J. Photochem. Photobiol. B* **1999**, *53*, 91-102.
(39) Hagen, V.; Kilic, F.; Schaal, J.; Dekowski, B.; Schmidt, R.; Kotzur, N. *J. Org. Chem.* **2010**, *75*, 2790-2797.
(40) Furuta, T.; Wang, S. S. H.; Dantzker, J. L.; Dore, T. M.; Bybee, W. J.; Callaway, E. M.; Denk, W.; Tsien, R. Y. *Proc. Natl. Acad. Sci. USA* **1999**, *96*, 1193-1200.
(41) Amit, B.; Ben-Efraim, D. A.; Patchornik, A. *J. Am. Chem. Soc.* **1976**, *98*, 843-844.
(42) Papageorgiou, G.; Ogden, D. C.; Barth, A.; Corrie, J. E. T. *J. Am. Chem. Soc.* **1999**, *121*, 6503-6504.
(43) Turner, A. D.; Pizzo, S. V.; Rozakis, G. W.; Porter, N. A. *J. Am. Chem. Soc.* **1987**, *109*, 1274-1275.
(44) Gagey, N.; Neveu, P.; Benbrahim, C.; Goetz, B.; Aujard, I.; Baudin, J.-B.; Jullien, L. *J. Am. Chem. Soc.* **2007**, *129*, 9986-9998.
(45) Fedoryak, O. D.; Dore, T. M. *Org. Lett.* **2002**, *4*, 3419-3422.
(46) Zhu, Y.; Pavlos, C. M.; Toscano, J. P.; Dore, T. M. *J. Am. Chem. Soc.* **2006**, *128*, 4267-4276.
(47) Denk, W.; Strickler, J. H.; Webb, W. W. *Science* **1990**, *248*, 73-76.

(48) Pawlicki, M.; Collins, H. A.; Denning, R. G.; Anderson, H. L. *Angew. Chem., Int. Ed. Engl.* **2009**, *48*, 3244-3266.

(49) Brown, C. T. A.; Stevenson, D. J.; Tsampoula, X.; McDougall, C.; Lagatsky, A. A.; Sibbett, W.; Gunn-Moore, F. J.; Dholakia, K. *J. Biophoton.* **2008**, *1*, 183-199.

(50) Aujard, I.; Benbrahim, C.; Gouget, M.; Ruel, O.; Baudin, J.-B.; Neveu, P.; Jullien, L. *Chem. Eur. J.* **2006**, *12*, 6865-6879.

(51) Gug, S.; Bolze, F.; Specht, A.; Bourgogne, C.; Goeldner, M.; Nicoud, J.-F. *Angew. Chem., Int. Ed. Engl.* **2008**, *47*, 9525-9529.

(52) Momotake, A.; Lindegger, N.; Niggli, E.; Barsotti, R. J.; Ellis-Davies, G. C. R. *Nature Methods* **2006**, *3*, 35-40.

(53) Gug, S.; Charon, S.; Specht, A.; Alarcon, K.; Ogden, D.; Zietz, B.; Leonard, J.; Haacke, S.; Bolze, F.; Nicoud, J.-F.; Goeldner, M. *ChemBioChem* **2008**, *9*, 1303-1307.

(54) Kaplan, J. H.; Ellis-Davies, G. C. R. *Proc. Natl. Acad. Sci. USA* **1988**, *85*, 6571-6575.

(55) Adams, S. R.; Kao, J. P. Y.; Tsien, R. Y. *J. Am. Chem. Soc.* **1989**, *111*, 7957-7968.

(56) Gomez, T. M.; Spitzer, N. C. *Nature* **1999**, *397*, 350-355.

(57) Matsuzaki, M.; Ellis-Davies, G. R.; Nemoto, T.; Miyashita, Y.; Iino, M.; Kasai, H. *Nat. Neurosci.* **2001**, *4*, 1086-1092.

(58) Yu, H.; Li, J.; Wu, D.; Qiu, Z.; Zhang, Y. *Chem. Soc. Rev.* **2010**, *39*, 464-473.

(59) Walker, J. W.; Somlyo, A. V.; Goldman, Y. E.; Somlyo, A. P.; Trentham, D. R. *Nature* **1987**, *327*, 249-252.

(60) Li, W.; Llopis, J.; Whitney, M.; Zlokarnik, G.; Tsien, R. Y. *Nature* **1998**, *392*, 936-941.

(61) Shestopalov, I. A.; Chen, J. K. *Chem. Soc. Rev.* **2008**, *37*, 1294-1307.

(62) Ando, H.; Furuta, T.; Tsien, R. Y.; Okamoto, H. *Nat. Genet.* **2001**, *28*, 317-325.

(63) Curley, K.; Lawrence, D. S. *Curr. Opinion in Chem. Biol.* **1999**, *3*, 84-88.

(64) Petersen, S.; Alonso, J. M.; Specht, A.; Duodu, P.; Goeldner, M.; Campo, A. d. *Angew. Chem., Int. Ed. Engl.* **2008**, *47*, 3192-3195.

(65) Wu, N.; Deiters, A.; Cropp, T. A.; King, D.; Schultz, P. G. *J. Am. Chem. Soc.* **2004**, *126*, 14306-14307.

(66) Endo, M.; Nakayama, K.; Majima, T. *J. Org. Chem.* **2004**, *69*, 4292-4298.

(67) Zou, K.; Cheley, S.; Givens, R. S.; Bayley, H. *J. Am. Chem. Soc.* **2002**, *124*, 8220-8229.

(68) Berridge, M. J.; Lipp, P.; Bootman, M. D. *Nat Rev. Mol. Cell Biol.* **2000**, *1*, 11-21.

(69) Berridge, M. J.; Bootman, M. D.; Roderick, H. L. *Nat. Rev. Mol. Cell Biol.* **2003**, *4*, 517-529.

(70) McCarron, J. G.; Chalmers, S.; Bradley, K. N.; MacMillan, D.; Muir, T. C. *Cell Calcium* **2006**, *40*, 461-493.

(71) Alonso, M. T.; Villalobos, C.; Chamero, P.; Alvarez, J.; Garcia-Sancho, J. *Cell Calcium* **2006**, *40*, 513-525.

(72) Chalmers, S.; Olson, M. L.; MacMillan, D.; Rainbow, R. D.; McCarron, J. G. *Cell Calcium* **2007**, *42*, 447-466.

(73) Poburko, D.; Lee, C.-H.; Breemen, C. v. *Cell Calcium* **2004**, *35*, 509-521.

(74) Rizzuto, R.; Bernardi, P.; Pozzan, T. *J. Physiol.* **2000**, *529*, 37-47.

(75) Soltoff, S. P. *J. Biol. Chem.* **2004**, *279*, 10910-10918.

(76) Katritzky, A. R.; Xu, Y.-J.; Vakulenko, A. V. *J. Org. Chem.* **2003**, *68*, 9100-9104.

(77) Chalmers, S.; McCarron, J. G. *J. Cell Sci.* **2008**, *121*, 75-85.

(78) Avlonitis, N.; Chalmers, S.; McDougall, C.; Stanton-Humphreys, M. N.; Brown, C. T. A.; McCarron, J. G.; Conway, S. J. *Mol. BioSyst.* **2009**, *5*, 450-457.

(79) Dasgupta, P.; Fowler, C. J. *Br. J. Urol.* **1997**, *80*, 845-852.

(80) Caterina, M. J.; Schumacher, M. A.; Tominaga, M.; Rosen, T. A.; Levine, J. D.; Julius, D. *Nature* **1997**, *389*, 816-824.

(81) Conway, S. J. *Chem. Soc. Rev.* **2008**, *37*, 1530-1545.

(82) Ferrer-Montiel, A.; Garcia-Martinez, C.; Morenilla-Palao, C.; Garcia-Sanz, N.; Fernandez-Carvajal, A.; Fernandez-Ballester, G.; Planells-Cases, R. *Eur. J. Biochem.* **2004**, *271*, 1820-1826.

(83) Bhave, G.; Hu, H.-J.; Glauner, K. S.; Zhu, W.; Wang, H.; Brasier, D. J.; Oxford, G. S. *Proc. Natl. Acad. Sci. USA* **2003**, *100*, 12480-12485.

(84) Jordt, S.-E.; Tominaga, M.; Julius, D. *Proc. Natl. Acad. Sci. USA* **2000**, *97*, 8134-8139.

(85) Olah, Z.; Szabo, T.; Karai, L.; Hough, C.; Fields, R. D.; Caudle, R. M.; Blumberg, P. M.; Iadarola, M. J. *J. Biol. Chem.* **2001**, *276*, 11021-11030.

(86) Szallasi, A.; Blumberg, P. M. *Pharmacol. Rev.* **1999**, *51*, 159-211.

(87) Jordt, S.-E.; Julius, D. *Cell* **2002**, *108*, 421-430.

(88) Walpole, C. S. J.; Wrigglesworth, R.; Bevan, S.; Campbell, E. A.; Dray, A.; James, I. F.; Masdin, K. J.; Perkins, M. N.; Winter, J. *J. Med. Chem.* **1993**, *36*, 2381-2389.

(89) Walpole, C. S. J.; Wrigglesworth, R.; Bevan, S.; Campbell, E. A.; Dray, A.; James, I. F.; Masdin, K. J.; Perkins, M. N.; Winter, J. *J. Med. Chem.* **1993**, *36*, 2373-2380.

(90) Walpole, C. S. J.; Wrigglesworth, R.; Bevan, S.; Campbell, E. A.; Dray, A.; James, I. F.; Perkins, M. N.; Reid, D. J.; Winter, J. *J. Med. Chem.* **1993**, *36*, 2362-2372.

(91) Szallasi, A.; Cortright, D. N.; Blum, C. A.; Eid, S. R. *Nat. Rev. Drug Dis.* **2007**, *6*, 357-.

(92) Szallasi, A.; Appendino, G. *J. Med. Chem.* **2004**, *47*, 2717-2723.

(93) Walpole, C. S. J.; Bevan, S.; Bovermann, G.; Boelsterli, J. J.; Breckenridge, R.; Davies, J. W.; Hughes, G. A.; James, I.; Oberer, L.; Winter, J.; Wigglesworth, R. *J. Med. Chem.* **1994**, *37*, 1942-1954.

(94) Gavva, N. R.; Treanor, J. J. S.; Garami, A.; Fang, L.; Surapaneni, S.; Akrami, A.; Alvarez, F.; Bak, A.; Darling, M.; Gore, A.; Jang, G. R.; Kesslak, J. P.; Ni, L.; Norman, M. H.; Palluconi, G.; Rose, M. J.; Salfi, M.; Tan, E.; Romanovsky, A. A.; Banfield, C.; Davar, G. *Pain* **2008**, *136*, 202-210.

(95) Gavva, N. R. *Trends in Pharmacol. Sci.* **2008**, *29*, 550-557.
(96) Kauer, J.; Gibson, H. E. *Trends in Neurosci.* **2009**, *32*, 215-224.
(97) Zemelman, B. V.; Nesnas, N.; Lee, G. A.; Miesenbock, G. *Proc. Natl. Acad. Sci. USA* **2003**, *100*, 1352-1357.
(98) Carr, J. L.; Wease, K. N.; Van Ryssen, M. P.; Paterson, S.; Agate, B.; Gallagher, K. A.; Brown, C. T. A.; Scott, R. H.; Conway, S. J. *Bioorg. Med. Chem. Lett.* **2006**, *16*, 208-212.
(99) Zhao, J.; Gover, T. D.; Muralidharan, S.; Auston, D. A.; Weinreich, D.; Kao, J. P. Y. *Biochem.* **2006**, *45*, 4915-4926.
(100) Gilbert, D.; Funk, K.; Dekowski, B.; Lechler, R.; Keller, S.; Mohrlen, F.; Frings, S.; Hagen, V. *ChemBioChem* **2007**, *8*, 89-97.
(101) Appendino, G.; Daddario, N.; Minassi, A.; Moriello, A. S.; Petrocellis, L. D.; Marzo, V. D. *J. Med. Chem.* **2005**, *48*, 4663-4669.
(102) Simonetti, M.; Fabbro, A.; D'Arco, M.; Zweyer, M.; Nistri, A.; Giniatullin, R.; Fabbretti, E. *Mol. Pain* **2006**, *2*, 11-25.
(103) Van Ryssen, M. P.; Avlonitis, N.; Giniatullin, R.; McDougall, C.; Carr, J. L.; Stanton-Humphreys, M. N.; Borgstrom, E. L. A.; Brown, C. T. A.; Fayuk, D.; Surin, A.; Niittykoski, M.; Khiroug, L.; Conway, S. J. *Org. Biomol. Chem.* **2009**, *7*, 4695-4707.
(104) Jung, J.; Hwang, S. W.; Kwak, J.; Lee, S.-Y.; Kang, C.-J.; Kim, W. B.; Kim, D.; Oh, U. *J. Neurosci.* **1999**, *19*, 529-538.
(105) Rami, H. K.; Thompson, M.; Wyman, P.; Jerman, J. C.; Egerton, J.; Brough, S.; Stevens, A. J.; Randall, A. D.; Smart, D.; Gunthorpe, M. J.; Davis, J. B. *Bioorg. Med. Chem. Lett.* **2004**, *14*, 3631-3634.
(106) Gavva, N. R.; Klionsky, L.; Qu, Y. S.; Shi, L. C.; Tamir, R.; Edenson, S.; Zhang, T. J.; Viswanadhan, V. N.; Toth, A.; Pearce, L. V.; Vanderah, T. W.; Porreca, F.; Blumberg, P. M.; Lile, J.; Sun, Y.; Wildt, K.; Louis, J. C.; Treanor, J. J. S. *J. Biol. Chem.* **2004**, *279*, 20283-20295.
(107) Trinchieri, G. *Annu. Rev. Immunol.* **1995**, *13*, 251-276.
(108) Miller, J. F.; Flavell, R. A. *Curr. Opinion in Immun.* **1994**, *6*, 892-899.
(109) Lindquist, R. L.; Shakhar, G.; Dudziak, D.; Wardemann, H.; Eisenreich, T.; Dustin, M. L.; Nussenzweig, M. C. *Nat. Immunol.* **2004**, *5*, 1243-1250.
(110) Cahalan, M. D.; Parker, I. *Semin. Immunol.* **2005**, *17*, 442-451.
(111) Milling, S.; Yrlid, U.; Cerovic, V.; MacPherson, G. *Immunol. Rev.* **2010**, *234*, 259-267.
(112) Zhu, J.; Yamane, H.; Paul, W. E. *Annu. Rev. Immunol.* **2010**, *28*, 445-489.
(113) DeMond, A. L.; Starr, T.; Dustin, M. L.; Groves, J. T. *J. Am. Chem. Soc.* **2006**, *128*, 15354-15355.
(114) Huse, M.; Klein, L. O.; Girvin, A. T.; Faraj, J. M.; Li, Q.-J.; Kuhns, M. S.; Davis, M. M. *Immunity* **2007**, *27*, 76-88.
(115) Sette, A.; Buus, S.; Colon, S.; Smith, J. A.; Miles, C.; Grey, H. M. *Nature* **1987**, *328*, 395-399.
(116) Terent'ev, A. P.; Preobrazhenskaya, M. N.; Sorokina, G. M. *J. Gen. Chem. USSR* **1959**, *29*, 2875-2881.
(117) Nadon, L.; Tardat, M.; Zador, M.; Fliszar, S. *Can. J. Chem.* **1973**, *51*, 2366-2374.

(118) Lyons, A. B.; Parish, C. R. *J. Immunol. Methods* **1994**, *171*, 131-137.
(119) Scholz, A. *Brit. J. Anaes.* **2002**, *89*, 52-61.
(120) Stuhmer, W.; Conti, F.; Suzuki, H.; Wang, X.; Noda, M.; Yahagi, N.; Kubo, H.; Numa, S. *Nature* **1989**, *339*, 597-603.
(121) Steinbach, A. B. *J. Gen. Physiol.* **1968**, *52*, 144-161.
(122) Nau, C.; Wang, G. K. *J. Membr. Biol.* **2004**, *201*, 1-8.
(123) Hille, B. *J. Gen. Physiol.* **1977**, *69*, 497-515.
(124) Sheets, M. F.; Hanck, D. A. *J. Gen. Physiol.* **2003**, *121*, 163-175.
(125) Sheets, M. F.; Hanck, D. A. *J. Physiol.* **2007**, *582*, 317-334.
(126) Yeh, J. Z. *Biophys. J.* **1978**, *24*, 569-574.
(127) Strichartz, G. R. *J. Gen. Physiol.* **1973**, *62*, 37-57.
(128) Binshtok, A. M.; Bean, B. P.; Woolf, C. J. *Nature* **2007**, *449*, 607-610.
(129) Kornblum, N.; Powers, J. W.; Anderson, G. J.; Jones, W. J.; Larson, H. O.; Levand, O.; Weaver, W. M. *J. Am. Chem. Soc.* **1957**, *79*, 6562.
(130) Clayden, J.; Greeves, N.; Warren, S.; Wothers, P. *Organic Chemistry*; Oxford University Press, 2001.
(131) Booij, L. H. D. J.; Broek, L. A. G. M. v. d.; Caulfield, W.; Dommerholt-Caris, B. M. G.; Clark, J. K.; Egmond, J. v.; McGuire, R.; Muir, A. W.; Ottenheijm, H. C. J.; Res, D. C. *J. Med. Chem.* **2000**, *43*, 4822-4833.
(132) Nerbonne, J. M. *Curr. Opinion in Neurobiol.* **1996**, *6*, 379-386.
(133) Nichols, C. G.; Niggli, E.; Lederer, W. J. *Pflugers Arch.* **1990**, *415*, 510-512.
(134) Ellis-Davies, G. C. R. *Tetrahedron Lett.* **1998**, *39*, 953-956.
(135) Kitani, S.; Sugawara, K.; Tsutsumi, K.; Morimoto, T.; Kakiuchi, K. *Chem. Commun.* **2008**, 2103-2105.
(136) Patchornik, A.; Amit, B.; Woodward, R. B. *J. Am. Chem. Soc.* **1970**, *92*, 6333-6335.
(137) Bochet, C. G. *Tetrahedron Lett.* **2000**, *41*, 6341-6346.
(138) Bochet, C. G. *Angew. Chem. Int. Ed.* **2001**, *40*, 2071-2073.
(139) Blanc, A.; Bochet, C. G. *J. Org. Chem.* **2002**, *67*, 5567-5577.
(140) Blanc, A.; Bochet, C. G. *J. Am. Chem. Soc.* **2004**, *126*, 7174-7175.
(141) Blanc, A.; Bochet, C. G. *Org. Lett.* **2007**, *9*, 2649-2651.
(142) Kessler, M.; Glatthar, R.; Giese, B.; Bochet, C. G. *Org. Lett.* **2003**, *5*, 1179-1181.
(143) Schelhaas, M.; Waldmann, H. *Angew. Chem., Int. Ed. Engl.* **1996**, *35*, 2056-2083.
(144) Bochet, C. G. *Synlett* **2004**, *13*, 2268-2274.
(145) Ladlow, M.; Legge, C. H.; Neudeck, T.; Pipe, A. J.; Sheppard, T.; Yang, L. L. *Chem. Commun.* **2003**, 2048-2049.
(146) Kammari, L.; Solomek, T.; Ngoy, B. P.; Heger, D.; Klan, P. *J. Am. Chem. Soc.* **2010**, *ASAP*.
(147) Campo, A. d.; Boos, D.; Spiess, H. W.; Jonas, U. *Angew. Chem., Int. Ed. Engl.* **2005**, *44*, 4707-4712.
(148) Stegmaier, P.; Alonso, J. M.; Campo, A. d. *Langmuir.* **2008**, *24*, 11872-11879.

(149) Kotzur, N.; Briand, B.; Beyermann, M.; Hagen, V. *J. Am. Chem. Soc.* **2009**, *131*, 16927-16931.

(150) Kantevari, S.; Matsuzaki, M.; Kanemoto, Y.; Kasai, H.; Ellis-Davies, G. C. R. *Nat. Methods* **2009**.

(151) Gundersen, R. Y.; Vaagenes, P.; Breivik, T.; Fonnum, F.; Opstad, P. K. *Acta Anaesthesiol. Scand.* **2005**, *49*, 1108-1116.

(152) Sjulson, L.; Miesenbock, G. *Chem. Rev.* **2008**, *108*, 1588-1602.

(153) Stowell, M. H. B.; Rock, R. S.; Rees, D. C.; Chan, S. I.; Noyes, A. A. *Tetrahedron Lett.* **1996**, *37*, 307-310.

(154) Thirlwell, H.; Corrie, J. E. T.; Reid, G. P.; Trentham, D. R.; Ferenczi, M. A. *Biophys. J.* **1994**, *67*, 2436-2447.

(155) Givens, R. S.; Athey, P. S.; Matuszewski, B.; Kueper, L. W.; Xue, J.-y.; Fister, T. *J. Am. Chem. Soc.* **1993**, *115*, 6001-6012.

(156) Strensrud, K.; Noh, J.; Kandler, K.; Wirz, J.; Heger, D.; Givens, R. S. *J. Org. Chem.* **2009**, *74*, 5219-5227.

(157) Conrad, P. G.; Givens, R. S.; Weber, J. F. W.; Kandler, K. *Org. Lett.* **2000**, *2*, 1545-1547.

(158) Hellrung, B.; Kamdzhilov, Y.; Schworer, M.; Wirz, J. *J. Am. Chem. Soc.* **2005**, *127*, 8934-8935.

(159) Corrie, J. E. T.; Barth, A.; Munasinghe, V. R. N.; Trentham, D. R.; Hutter, M. C. *J. Am. Chem. Soc.* **2003**, *125*, 8546-8554.

(160) Riguet, E.; Bochet, C. G. *Org. Lett.* **2007**, *9*, 5453-5456.

(161) Ando, R. A.; Borin, A. C.; Santos, P. S. *J. Phys. Chem. A* **2007**, *111*, 7194-7199.

(162) McCarron, J. G.; Muir, T. C. *J. Physiol.* **1999**, *516*, 149-161.

(163) Duchen, M. R.; Leyssens, A.; Crompton, M. *Journal of Cell Biology* **1998**, *142*, 975-988.

(164) Scaduto, R. C.; Grotyohann, L. W. *Biophysical Journal* **1999**, *76*, 469-477.

(165) Ward, M. W.; Rego, A. C.; Frenguelli, B. G.; Nicholls, D. G. *Journal of Neuroscience* **2000**, *20*, 7208-7219.

(166) McCarron, J. G.; MacMillan, D.; Bradley, K. N.; Chalmers, S.; Muir, T. C. *Journal of Biological Chemistry* **2004**, *279*, 8417-8427.

(167) Chalmers, S.; McCarron, J. G. *Journal of Cell Science* **2008**, *121*, 75-85.

(168) Armarego, W. L. F.; Chai, C. L. L. *Purification of Laboratory Chemicals*; 5th ed.; Elsevier Science (USA), 2003.

(169) Gazit, A.; Yaish, P.; Gilon, C.; Levitzki, A. *J. Med. Chem.* **1989**, *32*, 2344-2352.

(170) Nelson, E. K. *J. Am. Chem. Soc.* **1919**, *41*, 2121-2130.

(171) D'Aleo, A.; Pozzo, J.-L.; Heuze, K.; Vogtle, F.; Fages, F. *Tetrahedron* **2007**, *63*, 7482-7488.

(172) Bunce, N. J.; Stephenson, K. L. *Canadian J. of Chem.* **1988**, *67*, 220-226.

(173) Francisco, S.-V.; Berros, M. *Heterocycles* **2002**, *57*, 1869-1879.

(174) Ferdinandi, E. S. *J. Labelled Comp. Rad.* **1976**, *XII*, 357-364.

(175) MacDowell, D. W. H.; Greenwood, T. D. *J. Heterocyclic Chem.* **1965**, *2*, 44-48.

(176) Anderson, G. W.; McGregor, A. C. *J. Am. Chem. Soc.* **1957**, *79*, 6180-6183.

(177) Schnabel, v. E. *Liebigs Ann. Chem.* **1967**, *702*, 188-196.

(178) Wilcox, M.; Viola, R. W.; Johnson, K. W.; Billington, A. P.; Carpenter, B. K.; McCray, J. A.; Guzikowski, A. P.; Hess, G. P. *J. Org. Chem.* **1990**, *55*, 1585-1589.

(179) Pirrung, M. C.; Ye, T.; Zhou, Z.; Simon, J. D. *Photochemistry and Photobiology* **2006**, *82*, 1258-1264.

(180) Kajigaeshi, S.; Kakinami, T.; Okamoto, T.; Fujisaki, S. *Bull. Chem. Soc. Jpn.* **1987**, *60*, 1159.

(181) Chen, C.; Feng, X.; Zhang, G.; Zhao, Q.; Huang, G. *Synthesis* **2008**, *20*, 3205-3208.

Appendix -
Selected NMR Spectra